FACULDADE DE ENGENHARIA DA UNIVERSIDADE DO PORTO

μSmartScope - Development and optimization of a low-cost automated multi-axis microscopic stage for the accurate diagnosis of cervical cancer

Pedro Nuno Paulos Ferreira Brandão

Mestrado Integrado em Engenharia Mecânica

Supervisor at FEUP: Prof. Marco Parente, PhD

Supervisor at Fraunhofer AICOS: Paulo Torres da Silva, Msc

June 29, 2020

μSmartScope - Development and optimization of a low-cost automated multi-axis microscopic stage for the accurate diagnosis of cervical cancer

Pedro Nuno Paulos Ferreira Brandão

Mestrado Integrado em Engenharia Mecânica

June 29, 2020

Abstract

The exponential development of smartphones technology embraces medical science to precede to cure a wider array of patients with a more effective cost. Microscopy is a field that has evolved as well with this technology. With the addition of motorized stages in microscopes, it simplified the strenuous task of analysis of blood samples infected with parasites. These systems come with an expensive price tag and specialized staff. Thus, Fraunhofer AICOS proved possible the creation of a 3D-Printed intelligent Microscope that allowed for the autonomous acquisition of images using a smartphone at a very low cost that could be easily reproducible in developing countries. In this thesis, the goal is to show how a new solution that can achieve a broader field of view (FOV) and more stable behavior of the motors while maintaining a lean attitude and low cost.

To accomplish this goal, methodologies of design for manufacturing (DFM) and design for assembly (DFA) were used. Armed with these mindsets it is possible to create a device that is easy to assemble, which requires few tools and it is optimized for manufacturing. With the presence of additive manufacturing, technologies such as fused deposition modeling (FDM) and stereolithography (SLA) were used to prototype the device while it evolved in the typical development pipeline of a product. As such, it was also asked if a 3D printed prototype can accurately represent the final product that requires excellent precision and mechanical properties. This concept was explored with the design for additive manufacturing (DfAM) and tensile test to better have a design insight on the influence of infill density and wall count on cost and mechanical properties.

To optimize different parts and validate the structure, finite element analysis was used. ABAQUS was used to better understand the behavior of different structural parts. This software was also used to compare the behavior between Alucobond®, a novel sandwich solution, and an aluminum plate. Solidworks was used to better reproduce different case studies by using the topology optimization algorithm. The main goal is to use this algorithm as design insight to faster design optimize parts.

Finally, a cost analysis was proceeded to decide between the different presented solutions. It was observed that the solution that uses a PMI stage is the one worth exploring and advancing to the production stage. The total cost of this solution is 1050€, being this lower than the solutions presented in the market, and it is expected that different supply deals will greatly decrease the total cost of the device. It was concluded that 3D printing can be used to reproduce this device while saving significantly on development time. The assembly process was also improved greatly. However, it was also observed in some room for future improvement.

Keywords: Motorized Microscope Stage, Microscopy, DFM&A, DfAM, Topology Optimization

Resumo

O desenvolvimento exponencial dos *smartphones* abraça as ciências médicas com o objetivo de curar um leque maior de pacientes a um custo eficiente. O campo da microscopia encontrou nesta área uma oportunidade para se desenvolver. A adição de mesas motorizadas em microscópios, facilitou a extenuante tarefa de analisar amostras de sangue infetadas com parasitas. No entanto, estes sistemas apresentam um elevado custo de aquisição e a necessidade de trabalhadores especializados. A Fraunhofer AICOS provou superou ser possível com a criação de um microscópio inteligente, fabricado aditivamente. Permitiu assim, aquisição autónoma de imagens utilizando um *smartphone* a um custo extremamente baixo e de facilmente reprodução. O objetivo desta dissertação é desenvolver uma nova solução que consiga obter um campo de visão mais amplo e um comportamento mais estável mantendo uma atitude minimalista e de baixo custo.

De forma a atingir este objetivo, diferentes metodologias de *design* para fabrico e *design* para assemblagem foram utilizadas. Com esta corrente de pensamento é possível criar um dispositivo de fácil montagem, que necessita de poucas ferramentas e otimizado para o seu processo de fabrico. Com a presença de fabrico aditivo, de forma a prototipar o dispositivo durante a sua cronologia de desenvolvimento, foram utilizadas as tecnologias de estereolitografia e FDM. Assim sendo, levantou-se a possibilidade de fabricar um protótipo realizado em impressão 3D que representa-se de uma forma viável o produto final que necessita de excelentes propriedades mecânicas e precisão. Este conceito foi explorado aplicando *design* para fabrico aditivo. Realizou-se também testes de tração para se obter uma ideia geral da influência da densidade do enchimento e do número de paredes no custo e nas propriedades mecânicas.

Com o objetivo de otimizar diferentes peças e validar estruturalmente o produto, recorreu-se a uma análise de elementos finitos. O *software ABAQUS* foi usado para se compreender o comportamento de diferentes peças estruturais. Comparou-se também o comportamento do material Alucobond®, uma solução sandwich estado de arte, com uma comum chapa de alumínio. O *software Solidworks* foi utilizado para se reproduzir diferentes casos de estudo recorrendo ao algoritmo de otimização topológica. O principal objetivo ao utilizar esta rotina foi obter uma melhor orientação a nível de *design*, para se desenhar peças otimizadas mais rapidamente.

Para finalizar, procedeu-se a uma análise de custo para se decidir qual a solução económicamente mais viável. Observou-se que a solução que utiliza o equipamento da PMI é a mais interessante para se explorar futuramente e prosseguir-se para uma etapa de produção. O custo total desta solução ronda os 1050€ sendo este o valor mais baixo de todas as soluções observadas no mercado. Concluiu-se, por fim, que a solução impressa em 3D pode ser utilizada para se reproduzir este dispositivo, poupando tempo e custo significativo no desenvolvimento do produto.

Keywords: Microscopia motorizada, Optimização topológica, DFM&A, DfaM

Agradecimentos

Primeiramente, quero agradecer ao meu orientador, ao Professor Doutor Marco Parente pelo excelente acompanhamento, grande disponibilidade e por me motivar a explorar diferentes conceitos e soluções ao longo de todo o processo do porjecto.

Quero profundamente agradecer ao Eng. Paulo Torres por ser, não só um superbo mentor, mas também um bom amigo que me guiou sempre na direção certa. Todo o seu trabalho foi essencial ao desenvolvimento desta dissertação. Dedidico-lhe os frutos futuros que deste trabalho surgirem.

À Fraunhofer AICOS por me ter disponibilizado todo o equipamento e condições necessárias à realização deste trabalho. Levo comigo um elevado padrão no que respeita condições materiais e relacionais, com excelente ambiente de trabalho e cooperação entre todos. Dentro da Fraunhofer quero agradecer em particular aos elementos da minha equipa que tornaram esta dissertação possível, e ainda todo os meus colegas de trabalho.

Dedico uma menção honrosa ao Eng.Púria Stafardi pela disponibilidade e excelência nos conhecimentos que me transmitiu fundamentais à realização desta dissertação.

Realço o acompanhamento dos meus pais ao longo de toda a dissertação. Sem o seu apoio, sacrificios e amor incondicional nunca teria a possibilidade de realizar o sonho de me tornar Mestre em Engenharia Mecânica.

Quero agradecer à minha irmã, Eng. Ana Brandão, pelo seu espírito crítico e apoio, durante todo o tempo da quarentena, que se revelou fundamental para o desenvolvimento deste trabalho.

Por fim quero realçar os meus amigos que tornaram este trabalho possível.

Ao Pedro Duarte Menezes por ser uma fonte de motivação e alguém que tanto admiro.

Ao Pedro Moreira de Sousa por todo o conhecimento e apoios que me passou ao longo dos anos. Quero realçar-lhe a paciência, a quietude, lealdade e conhecimento exímio como as suas maiores virtudes.

Ao Afonso Jorge Ramos, Luís Guedes, João Gomes e Teresa Pina por me motivarem com camaradagem e ilustre cerveja artesanal.

Ao Jorge Wolfs por me corrigir e me orientar com conceitos essenciais ao desenvolvimento desta tese.

Ao João Bapatista, Miguel Dias, Filipa Martins, Marta Saraiva, Maria Pires, que comigo viajaram meio mundo e trazem o calor de Buenos Aires para tão perto.

Agradeço a todos os meus outros amigos e colegas que tornaram esta dissertação possível.

Por fim, quero agradecer aos meus gatos, em particular à minha gata Maíbi, que muitas noite me acompanhou lado a lado com leadade, carinho e admiração.

Pedro Brandão

"In the depth of winter,
I finally learned that within me there lay an invincible summer."

Albert Cammus

Contents

List of Figures

List of Tables

Abbreviations

FOV	Field of View
FN	Field Number
HTM	High-throughput microscopy
DFM	Design for assembly
DFM	Design for manufacturing
MVP	Minimum valuable product
PLA	Polylactic acid
PET	Polyethylene terephthalate
UTS	Ultimate Tensile Strength
EMPF	Effective mass participation factor
FFF	Fused filament fabrication
FDM	Fused deposition Modelling
SLA	Stereolithography
SLS	Selective Laser Sintering
SIMP	Solid Isotropic Micro structure with penalization
CAE	Computer assisted engineering
CAD	Computer assisted design
FEA	Finite element analysis
FDA	Food and Drugs Administration

Chapter 1

Introduction

Microscopic examination is the golden standard for the diagnostic of several neglected tropical diseases. However, its quality and availability in rural endemic areas is often limited by the lack of trained personnel and adequate equipment. These drawbacks are closely related with the increasing interest in the development of computer-aided diagnosis systems, particularly distributed solutions that provide access to complex diagnosis in rural areas. In this context Fraunhofer AICOS developed an automated 3D-printed smartphone based microscope with motorized stages, termed μSmartScope.

The developed prototype allows autonomous acquisition of a pre-defined number of images, by using a motorized automated stage fully powered and controlled by a smartphone, without the need of manual focus.

Project CLARE is a natural evolution of the μSmartScope which goal is to achieve wider array of pathologies available. The main focus of project CLARE is to use the μSmartScope to diagnose autonomously cervix cancer from pap smears. To achieve this goal it is required a redesign of the μSmartScope creating as well a sturdy platform for future iterations as well.

In 2018, more than half a million women suffered with cervical cancer. With that cervical cancer is the fourth most frequent type of cancer in women. The high rate of mortality due to cervical cancer can be reduced with prevention, early diagnosis and effective screening. It is estimated that 90% of the deaths occur in low- and middle-income countries. A fast and cheap solution to effective screening could lead to a decrease in the mortality rate of cervical rate [1].

Methodologies and mindsets of design for manufacturing and assembly will be used in this thesis to achieve a low cost and easy to assemble device. Additive manufacturing technologies such as FFF/FDM and SLA will be used to easily prototype different components. Different design pipelines and procedures will be created to simplify the engineering process. The current dissertation will finish with a fully developed engineering prototype ready to be manufactured or modified for large scale. Finite element analysis (FEA) and topology optimization procedures will be used as well to validate different load cases and create lightweight parts while maintaining a

high stiffness. Finally, in this thesis it will be asked if it is possible to develop an accurate device in additive manufacturing. To achieve this, different tensile studies where conducted to understand the effect of different parameters in cost and final mechanical properties.

1.1 Dissertation Framework

The current dissertation is under the μSmartScope project by Fraunhofer AICOS and FEUP's Master's dissertation.

The first prototypes of the μSmartScope started with the MalariaScope where the main goal was to solve the insufficiency of medical staff in Malaria affected countries. This project functioned by acquiring microscopic imagines with a 1000x magnification of malaria smears. Due to the success of the prof of concept, μSmartScope goal is to deepen the infection library. As such. the MalariaScope was adapted for the acquisition of samples of cytological, in a liquid environment, of cervical cancer with magnification up to 400x. This new project is under CLARE project where the goal of this thesis will focus.

As such, μSmartScope is to present a low cost and autonomous solution for a motorized microscope. This dissertation focus on solving and validating mechanical solutions that allows achieving the wider range necessary for other infections. This dissertation is under project CLARE.

1.2 Dissertation goals

The main goal of this master thesis is to design an improved micro-stage with better performance, resolution and working distances for the current μSmartScope. The main challenges of this thesis are:

- Re-design the micro-stage so that it achieves the required performance
- Create and embrace design methodologies that allow to achieve a low-cost easy to build device
- Explore the feasibility of additive manufacturing as prototyping technologies for extremely accurate devices.

The impact of achieving this goals will not only impact the future of project CLARE and the μSmartScope, but the prototyping pipeline of future medical devices. It is expected that future devices will be easily prototyped and designed with DFM&A in mind to achieve the lowest cost possible

1.3 Dissertation Structure

After the first the introduction chapter, the second chapter of this dissertation refers to a contextualization of concepts required to understand project CLARE and the μSmartScope.

Chapter 3 is a review of state of art where different solutions will be studied as well other novel concepts.

Chapter 4 constructs different metrics that will be used in the design of a new solution and explores the main flaws of the initial solution presented by Fraunhofer AICOS.

Chapter 5 explores the design process from a conceptual phase to a final engineering prototypes.

Chapter 6 creates FEA models for structural validation and explains the design process of different case studies.

Chapter 7 analysis the results of the different achieved solutions.

Chapter 8 reflects and creates conclusions of the work created as well leaving some advises for future works that can still be explored.

1.4 Acknowledgements

This work was done under the scope of "CLARE: Computer-Aided Cervical Cancer Screening", project with reference POCI-01-0145-FEDER-028857 and financially supported by FEDER through Operational Competitiveness Program – COMPETE 2020 and by National Funds through Fundation for Science and Tecnhology FCT/MCTES. The goal of this project is to provide automatic tools for cervical cancer screening based on cytology and colposcopy images.

Chapter 2

Contextualization

The aim of this chapter is to display different concepts and projects that might be required to understand the general scope of this dissertation. It will also be presented the predecessors to CLARE project.

The usage of optics laws is fundamental due to the diminutive nature of microscopic examinations. One of the main goals of the present dissertation is to develop the mechanism that can achieve the best optical metrics such as resolution and FOV, which allow for the wider examination of maladies. In this field, there will be also a small overview of optical validation exams. These concepts refer to section 2.2

Finally, some details over the different Infections and Illnesses and the different requirements that are needed to achieve can be found in 2.3.

2.1 μSmartScope Overview and μStage

The μSmartScope started as the Malaria Scope project. This project included Fraunhofer Portugal AICOS's ICT for developing competence center, in cooperation with Infectious diseases department of the Instituto Nacional de Saúde Dr. Ricardo Jorge. The main goal was to develop a light microscope that was mobile and effective in pre-diagnosing malaria in regions where there was few medical staff. This product would be powered and computed in a smartphone. Another important factor was the low cost and easy replicability.

The present section will present the older prototypes and concepts of the Malaria Scope and the more recent μSmartScope that appered as a more wider solution.

2.1.1 Protoype 1

The first prototype was still a very conceptual solution where almost all components were printed in 3D. In this prototype the hardware specification were:

- To be able to use a fixed magnification factor of 1000x
- To be able to use static layout for the illumination
- Decrease movement complexity in the XY axis or even completely automatize

The XY stage in this prototype uses only one screw and one string for each axis and allowed for 1 cm of displacement. The Z axis had the function of achieving the focus point.

It is possible to observe that this solution was still very infant with small use of components, strings and screws.

2.1.2 Prototype 2

The second prototype took 3D printing limitations understanding that tight tolerances would be a problem due to factors as: temperature, humidity and dust. In this prototype it was considered superficial humidity/dust in the filament, contraction during the cooling process. It was considered thath the μStage, the motorized and mechanical part the bottleneck of the project with the most needed place for improvement.

This is due mainly to the unpredictable behaviour of 3D printed parts that create many irregularities in the final product.

Therefore, some improvements were made to this system. The main goal was to improve a low cost solution by increasing efficiency of the image acquisition. In this prototypes the new requirements for the Z axis module was [2]:

- Allow the required focusing travel.
- Allow the required steps resolution.
- The Z module must be able to lift X and Y, the glass holder, the LED and the condenser.
- The Z axis movement must be fully decoupled from X and Y.
- The Z module must not be affected by the X and Y movement.
- The module must allow for the assembly of different sized steppers.
- The smallest step size must allow for a correct focus of the sample.

It was created three axis to support X and Y that created a stable platform. This system showed high friction ration between the the bottom part and the top part. Figure 2.1 shows the final solution of the μStage [2]. Figure 2.1 shows the printed solution of the second prototype.

2.1.3 Prototype 3

The third and last prototype before the most recent solution that changed from the Malaria Scope to the μSmartScope. In this prototype the μStage was the one that was mainly changed. In this prototype 3D printed parts were still a priority as way to minimize costs and easy replication.

Figure 2.1: Printed solution of the second prototype [2]

In the XY field, two bands were added to guarantee the movement in both ways, therefore the servo movement will not be linear. While this solution works well for blood smears analysis of Malaria and other neglected tropical diseases [2], for other cases its mandatory evolution. Hence, for the µSmartScope purposes, the new stage need to achieve high-precision and resolution for other magnifications.

In Z-Axis the two main changes were the M2 threaded rod and the buckling cover. The first allowed for a higher resolution in Z-Axis movement. This improves the resolution per revolution of 0.5 mm to 0.4 mm [2]. The latter, buckling cover, is know to improve the stability of sliding mechanism, The buckling cover consists on ensuring that each tubular stem should have more than the double of its diameter [2].

Figure 2.2 the new solutions of the XY axis and figure 2.3 the Z module. The main problem in this solution it is still the friction between the pillars and their dies. Thus, it is important to achieve the correct gap and tolerance between them. Filament Deposition Modeling works by depositing polymeric filament layer by layer. The size of the layer is dependent of the resolution of the printer system. This will affect surface roughness directly and increase friction between the sliding parts. In theory, with less layers, worse resolution, it is possible to achieve less contact are, which means less friction.

To test the Z-Axis and its behaviour and resolution, it was measured the displacement of the motor 100 times. It was achieved an $0.763 \pm 0.098 \mu$m. It is a major improvent compared second prototype of $0.98 \pm 0.18 \mu$m [2]

In the XY axis, it was achieved and median displacement of 330 μm and a deviation of 81μm. This results allowed for the correct analysis of malaria blood smears [2].

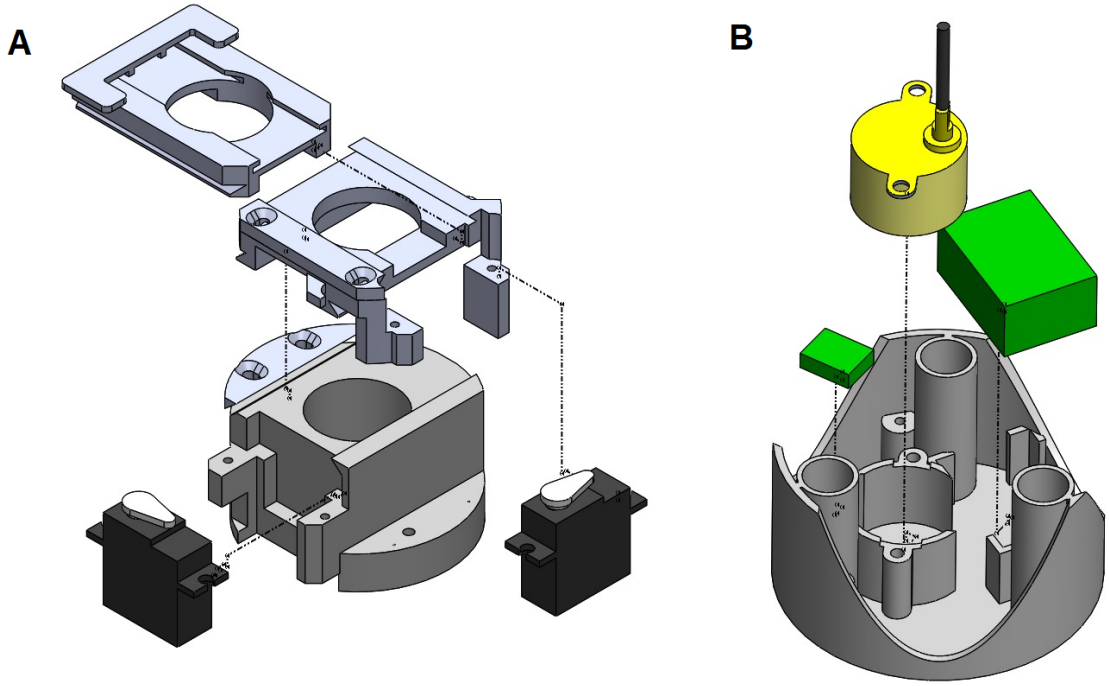

Figure 2.2: (A) XY system exploded view (B) stepper motor exploded view [2]

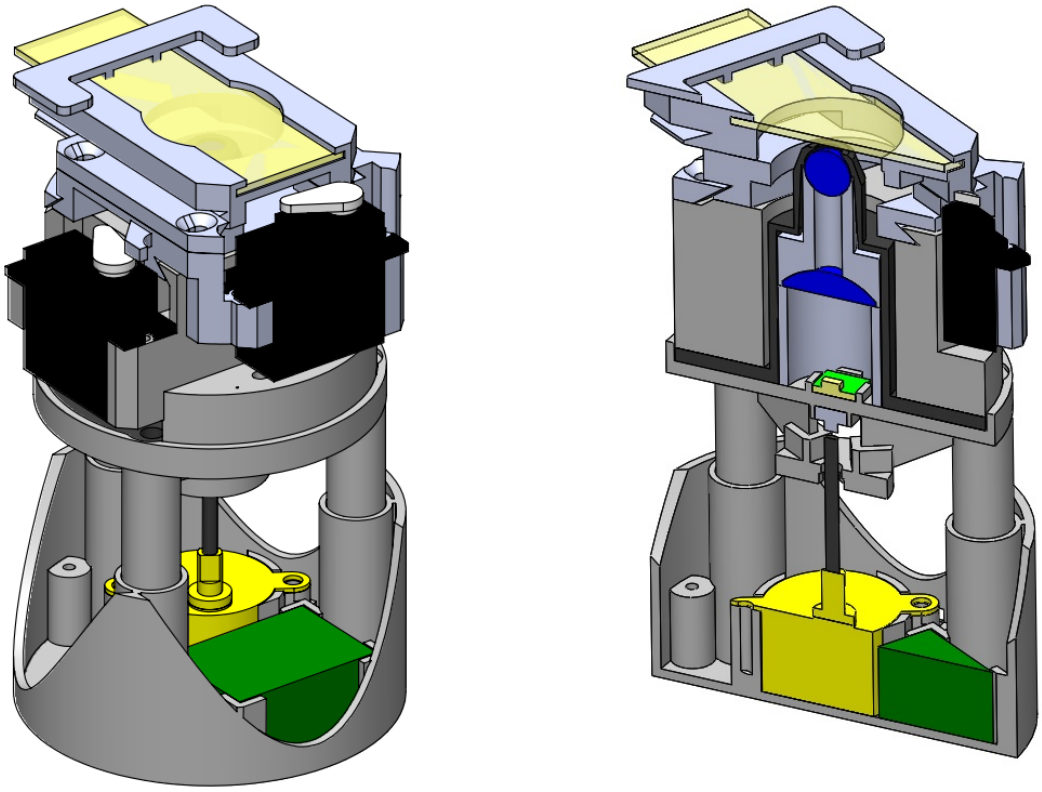

Figure 2.3: μStage solution [2]

2.2 Optics Metrics and System Validation

Microscopes allow perceiving information that is not current to the naked human eye. Therefore, it is currently the need for a device that allows the magnification of the micro world. Optics is the field of physics that uses glasses lenses that focus light to create a different view of the perceivable world. This classical physical field is dominated by different laws that make possible the examination of a microscopic world that it is necessary for the field of medicine, biology, pharmacy, and engineering.

One of the goals of the μSmartScope is to perform in a certain way under different magnifications. It is then important to study the different exams and concepts that will validate the results and proving the ability to achieve different results. These concepts will be very important as a metrical factor of performance for the mechanical solutions that will be developed in this project.

2.2.1 Optical Validation Test and Metrics

Before departing to the study of the validation test READY OPTICS USAF 1951, it is mandatory to comprehend the array of concepts: field of view - FOV -, resolution and magnification.

2.2.1.1 Optical Metrics and Concepts

Magnification This term is characterized by being the ration of the size of and object in a image created by the microscope and the real size of the object. Empty magnification occurs when the visual magnification is over the limit of the resolving power of the microscope. As a consequence, no additional details can be seen. Equation 2.1 represents the meaning of the ratio [3].

$$Magnification = \frac{dimension\ of\ the\ object\ in\ the\ image}{real\ dimension\ of\ the\ object} \tag{2.1}$$

Resolution In optical systems, the resolution is, simply put, the ability to identify details in an image. It can also be defined, as a measure of the limit of the smallest object that can be resolved. The resolution unit is expressed in line pairs per millimeter. This measures how different separated lines can be distinguished. The term of magnification relates to the resolution as subordinate. Empty magnification will occur if the optical system cannot create a distinction between two different details - **resolution** [3].

To achieve the maximum resolution in a microscope, all of the optical object must have the highest numerical aperture possible. This aperture depend on the refractive index of the objective and in half of the angular aperture of said objective. Another way to improve resolution is by using a shorter wavelength of light [4]. Resolution in a imagine can be divides as: pixel resolution, spatial resolution, spectral resolution, temporal resolution and radiometric resolution. In the case of microscopy spacial resolution is the most important. Spacial Resolution is characterized by the pixel density of an image, thus, the number of pixels per unit area [5].

FOV Field of View or Object Field is what it will be captured in the image created by the optical system. As consequence, objects will only be magnified with they are within the FOV. The FOV in the microscope is represent by a circular image. In the field of digital microscopy, the field of view is rectangular due to the shape of the image sensor [3]. The size of the field of view is given by equation 2.2.

$$FOV = \frac{FN}{M_0 * q} \tag{2.2}$$

Where **FN** is the field number expressed in mm. This factor is limited by the magnification and the field diaphragm size of the eyepiece. Modern field can exceed 28 mm. $M_0 * q$ is the total magnification before the eyepiece due to the objective being used, the considered zoom and any tube lenses [3]. Figure 2.4 show how the field of view changes with the variation in the field number [6].

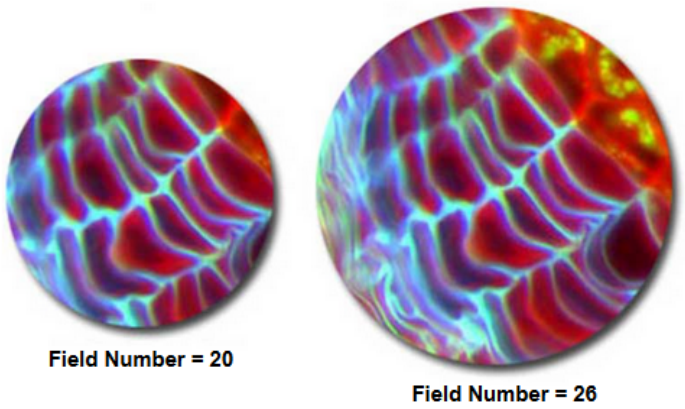

Figure 2.4: Variation of FOV with FN [6]

It is possible to conclude then, that FOV will be higher for lower magnifications and wider field diaphragm.

2.2.1.2 Optical Validation Test - USAF 1951

To study the performance of the micro stage, it is necessary to achieve standards of FOV, Resolution and Precision for different magnifications. The autonomous examination of medical microscopic images must have a minimum resolution for a certain area [2]. Therefore, have this optical validation, it is necessary to understand the purpose of an optical resolution test. It is necessary to obtain high-resolution images to achieve the best results. The selected test is the READY OPTICS 1951 USAF, under the standard MIL-STD-150A. It was standardized by the US AIR Force in 1951 [2]. This test is used to determine the value of spacial resolution. Firstly it is important to notice that special resolution is limited by the capabilities of the imaging sensor that capture the images [5].

The MIL-STD-150A it is still a widely accepted validation system for the resolution of optical systems in particular microscopes and cameras [7]. This analysis is a target test. This implies that

it utilises patterns to identify the visual sharpness of the image. The pattern uses assemblies of three bars each, with gradual different dimensions. Hence, the biggest bar is the limitation of the resolving power for said group. Each assortment of lines compounds an element. Each group has 6 different elements with gradually smaller dimensions [7]. The representation can be observed in figure 2.5 where red identifies the groups and blue represents the elements. Figure 2.5 also demonstrates how the pattern repeats. The higher the group that can be perceived, the greater the spatial resolution - the density of pixels in a specific unit area.

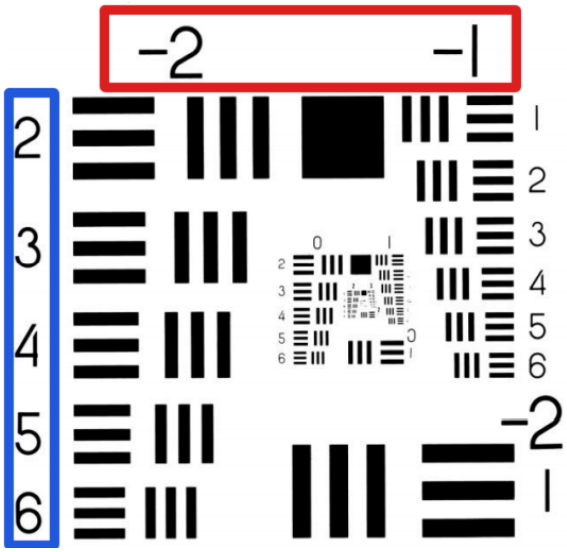

Figure 2.5: Targets used in USAF 1951 [7]

The separation between the lines is standardized with a certain relationship that also changes dimensions. Therefore, it is possible to obtain a measure of resolution dependent of the number of line pairs per each millimeter that can then be describes in micrometers. Equation 2.3 is the law that relates the measurements with the final result of resolution [7].

$$Resolution[lp/mm] = 2^{group+\frac{element-1}{6}} \tag{2.3}$$

This equation dictates that resolution evolves by the power of two, per element and group. The equation also weights the value of a certain group and element. Being the groups and elements discrete numbers, resolution by the test READY OPTICS 1951 USAF standard MIL-STD-150A are tabled and be consulted in a matrix dependent on the group and element. Table 2.1 shows the values of resolution in line pairs per millimeter.

2.3 Illnesses microscopic examination and the usage of cellphones

It is important to understand the different analysis methodologies and illnesses to understand the minimum requirements to achieve. As such,when designing the mechanism it is important to be integrated jointly with the cellphone system that will proceed the recognition of the infections.

Table 2.1: Values for Resolution Targets [7]

Number of Line Pairs / mm in 1951 USAF Resolution Test Target										
Element	Group Number									
	-2	-1	0	1	2	3	4	5	6	7
1	0.25	0.5	1	2	4	8	16	32	64	128
2	0.280	0.561	1.12	2.24	4.49	8.98	17.95	36.0	71.8	144
3	0.315	0.630	1.26	2.52	5.04	10.10	20.16	40.3	80.6	161.0
4	0.353	0.707	1.41	2.83	5.66	11.30	22.62	45.3	90.5	181.0
5	0.397	0.793	1.59	3.17	6.35	12.70	25.39	50.8	102.0	203.0
6	0.445	0.89	1.71	3.56	7.13	14.30	28.50	57.0	114.0	228.0

Light microscopy is related to low cost examination and, as such, is mainly used for identification pulmonary parasitic infections [8], blood smears for hematologic conditions, neglected tropical diseases [9], urinary and reproductive diseases. Thus it is possible to conclude the importance of an automated system, not only as a market success but as well in humanitarian and scientific matters.

2.3.1 Smear Analyses and Cervical Cancer

One of the end goals of the microscope is to be able to autonomously analyse different types of smears, blood, urine and even cervical. As such, the focus illness of this autonomous diagnosis device is cervical cancer [10].

It was expected that at least half a million women suffered from cervical cancer in 2003. Thus, in less developed countries, it is the most common type of death by cancer, making it 80% of cases worldwide. The human papilomavirus (HPV) is the main cervical cancer. This virus is acquired mainly through sexual activity. Early age sexual activity, high number of sexual partners, genital wards and cigarette smoking are other risk factors. Cervical cancer if detected in the first stages, it is curable and has a 5-year survival rate as high as 92% [10, 11].

The diagnosis of cervical cancer is passes by the analysis of a Pap smear. A sample is taken and if it shows the presence of micro-invasion it strongly suggest the presence of cervical cancer. Although in the presence of a patient who does appear to have invasive cancer, then a cone biopsy should proceed [10].

The Pap smear is created by brush of spatula that scrapes cellular material from the squamo-columnar junction in the cervix and then it is deposited into a glass of 25x50 mm. After, an cytotechnologist, goes examines the sample through a light microscope. After, maligancy is found in a specimen a medical doctor makes the final decision [11].

Cytotechnologist search for morphological changes such as larger nucleus and irreguarly shaped and smaller cytoplasm as show in figure 2.6. Due to the small size of 10 microns of diameter of

the nucleus, a lenses of 40x should be used. At a magnification of 10 times, it is need to analyse 1000 fields of view, and 10000 at a higher resolution of 40x. The specialized staff can only analyse 70 samples a day, or 7 hours, due to fatigue, giving an average to inspect three image fields per second. An automated system can surpass the average sample analysis time of a skilled human.

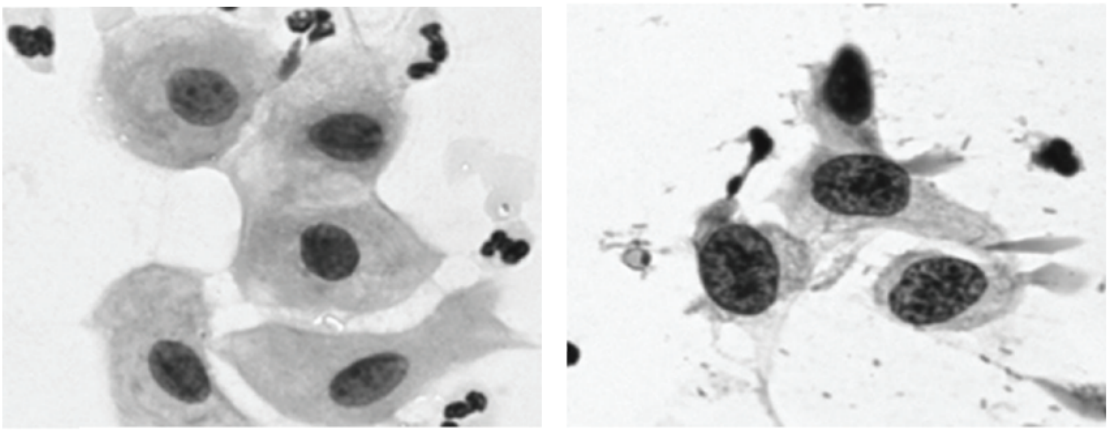

Figure 2.6: The difference between a normal papsmear (a), and an infected one (b) [11]

The main technical problems when screening of the sample is the large amount of information and focus accuracy and time. High quality auto-focus is important to have reliably extract texture information. It is very important to have a reliable and important auto-focus to reduce the time of the scanning [11].

Chapter 3

State of Art

Introduction

In this chapter general concepts will be exhibited. These will be necessary as a means to achieve the best result possible of the project.

Firstly, it is of utmost importance to understand the anatomy of a motorized microscope to have the ability to design one. As such, it is important to study the current market of motorized microscopes to understand what are the main design that the industry currently uses. Another remark about the current market study overstates the impact of a low cost motorized automated microscope in the current market. Although commercial accomplishment is important, another factor of success is the impact in society, mainly in developing ones. This concepts can be found in section 3.1.

3.1 Motorized Microscopes

Motorized microscopes came as a breakthrough in the microscopic examination field. This field, of microscopic medical imaging, works with a large number of images [12]. The motorization and the following automation of microscopes arrive to relieve the necessity of a large specialized staff. These devices are usually operated by trained medical laboratory technicians. The examination used to be done manually. As such, a microscopic examination was a strenuous and very time-consuming job. The trend of automated motorized microscopes reduce human errors by misreading results [13].

These microscopes work by autonomously examining the images taken of the blood samples by the specialist or allowing a remote specialist to analyze the sample. As a consequence, this concept reduces the amount of work and training that a certain specialist needs to endure. Another advantage is the ability to use these devices in impoverished and rural areas where a meticulous examination is harder to accomplish [2].

3.1.1 The Anatomy of a Motorized and Autonomous Microscopes

3.1.1.1 Types of Microscopes

Before studying the motorization of microscopes it is important to understand the different classes of microscopes and their uses. Each type of microscope will have distinct objectives as well capabilities and resolving power [14].

Conventional microscope In conventional microscopy a large area incoherent source is focused by the condenser lens illuminating a large area in the specimen corresponding to the field of view of the objective. After that, the objective lens forms the primary image.

The image in this microscopes is created by and objective and it is an inverted image. Compound microscopes add and eye piece that creates a virtual image [14].

Scanning Microscope In a scanning system a probe of light is creating by demagnificating the source and it is scanned over the object. This light is then detected by a photo-dectetor that build the image [14].

Confocal microscope In this type of microscopes, a point source illuminates a small area of the object. After that a detector detects light from this area. The unison work between the point source and detector creates a 2D image. The behavior of confocal microscopes allow for a significant improvement in resolution [14].

3.1.1.2 Contrast Mechanism

Phase Contrast Phase contrast relates to the surface height variation and optical material properties of the sample. This contrast is used when object are weakly scattering to be visible [14].

Polarization In this contrast mechanism, changes in light are detected , that changes the polarization state of the light transmitted. Birefringence is detected from the form or material. As a consequence this mechanism is used in biology and mineralogy. [14]

Fluorescence In this mechanism electrons that were exited by illumination decay to the ground state and, as a consequence, emits photos of light. This type of contrast is used in a confocal microscope. [14]

3.1.1.3 Light Microscopy

The μSmartScope fits in the category of light microscopy. This type of microscope magnifies object by transmitting and reflecting light and it is one of the most important tools in scientific research.

Simply put, a compound microscope is created by four main components: a light source, condenser lens, objective lens and eyepiece. A condenser lens goal is to collect the light from the source. The objective lens creates the magnified aerial image of the specimen [15].

Light microscopes can also be defined by the way they use light. These can be by transmission, where light goes through the sample or by reflection where the image is created from the light the reflects from the sample.

Commonly, microscopes come with a low tension tungsten-halogen lamp, 6 to 12V and this lamps usually stay in an external house for heat dissipation. The light-alignment is of utmost importance and the shape of the filament can come in place to achieve the best result possible. In the case of fluorescence microscopy it is also needed to align gas discharges sources. [16]

Following illumination, it comes the lamp collector that captures the light of the source and sends it to the condenser. The focal length, the aperture, and the degree of the optical correction of the collector lens influences the flux of light and uniformity of illumination of the specimen [16].

The condenser works with the lamp light collector to provide the brightest illumination of the specimen for the different magnification array. Resolution, contrast and depth of field are influenced by the numerical aperture or cone angle of illumination [16].

Filter and diffusers can also be used to achieve a more even distribution of the light without compromising light intensity. On the other hand, filters serve as correction of color balance, contrast enhancement, neutral light attenuation and aiding in the selection of specific spectral regions for fluorescence excitation.

The objective is the most important component of light microscopy. This component defines magnification, resolution, contrast, image brightness, depth of focus, sharpness and color rendition [16]. Figure 3.1b and 3.1a show the two different solutions of microscopes.

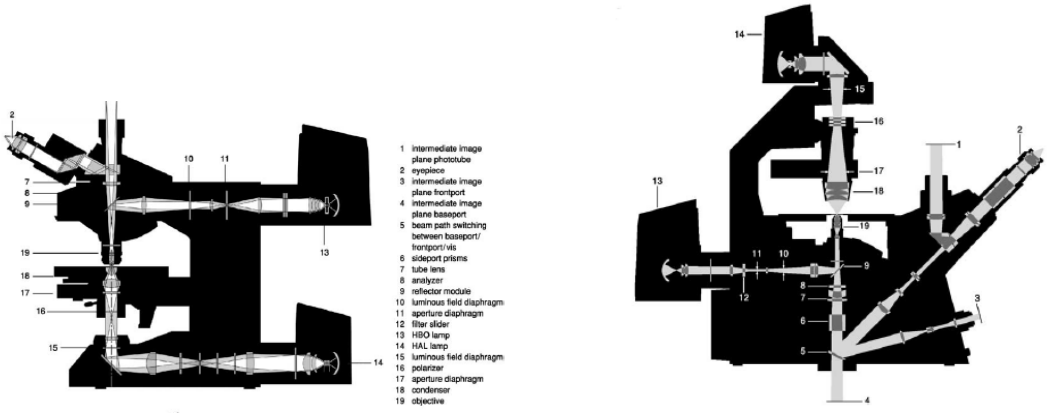

(a) upright microscope **(b)** inverted microscope

Figure 3.1: Different types of microscopes and their components [16]

3.1.1.4 Automation and Motorization

Firstly, an autonomous and motorized microscope magnifies on the studied sample, a camera captures the image and it is sent to a repository for storage. Computer software controls each step and it can proceed for the automated analysis [17].

The flowchart in figure 3.2 explains how automated microscope works and it divides in two colors the different function: blue color means that it is computer controlled and red color indicates the function of the motorized feature.

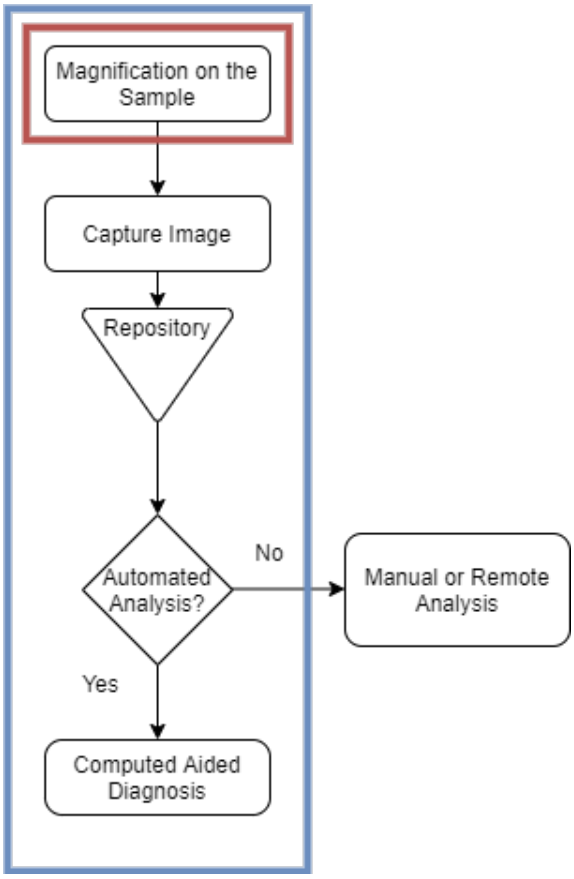

Figure 3.2: Automated and Motorized microscope function flowchart

In microscopy, multidimensional is the ability to use different axis (spatial, time, or others) to obtain the highest amount of information possible. As such, well-know manufacturers replaced all manual controls for ones that are motor driven with encoders that allow for precise automated positioning. This important change adds features like autofocus, scanning stages and illumination and detection multiplexing [18].

The usage of a stepper in the z-axis allow for high-resolution and micro-positioning. The usage of encoders, in a close-loop system is mandatory to achieve the desired results and never losing the focal point. It is important to notice that some optical systems still allow for manual focus if desired [17]. To achieve the best results with automated microscopy, it is necessary to automate as many steps as possible, even trivial tasks [19].

Anatomically, the main mechanism in a motorized microscope is the focus and stage. The stage is usually divided in two distinct components: the x-y stage and z-stage. These stages correspond to the different dimensions that allow the focus and capture of images. This focus system, controls very precisely the stepper motor of the z-stage that translates the stage in the axial direction allowing for image stacks.

The latter, x/y stage, houses the imaging chamber, where the sample is placed. The stages eliminate lateral drifting by being controlled by DC stepper or servomotors. Usually this systems travel range, goes from 50.8 to 101.6 milimiters in both directions and can achieve resolutions of 300 to 750 nanometers in a repetitive function. This motorized stages can also be controlled by a human player through the use of joysticks [20]. Figure 3.3 show the different components of a typical X/Y stage.

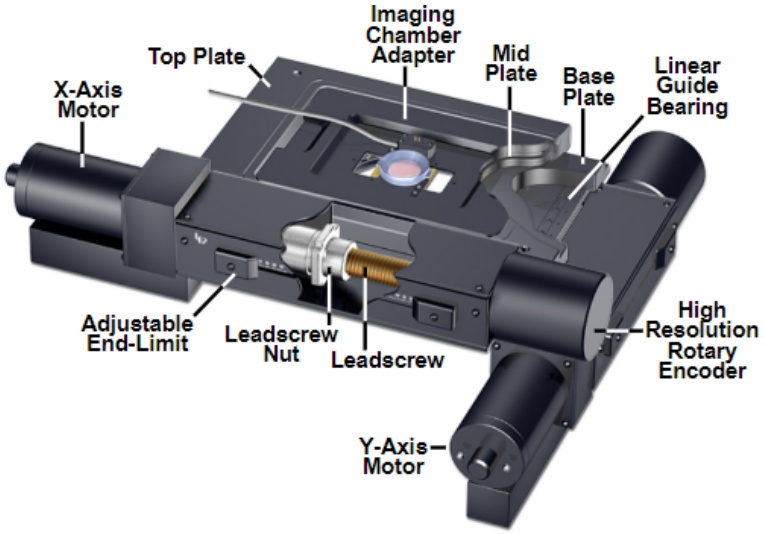

Figure 3.3: Typical components of a X/Y stage [20]

An XY stage, works with the same principle as a XY table of a, i.e, a CNC machine table. The actuation of the motor rotates a leadscrew, that, in its turn translate a table. The precision of the X/Y depends on the step of the motor and the pitch of the road. Both this factor will dictate accuracy, repeatability and speed.

3.2 Contemporary Solutions

The current solution in the market are usually related to autonomous X/Y stages. Well known companies with successful product are: Prior®, Thorlabs, Leica, Olympus, Zeiss. Other solutions that were theorically developed will also be talked in this section as well as a small resume in the end.

3.2.1 Market Solutions Research

Prior® Prior® is a well know company that creates different optical solutions. In the world of automation, this enterprise focuses on the creation of the motorized stages and sell them as upgrades of normal microscopes. It also sells robots that handle and load samples. The packages comes with a motorized stage, piezo fine focus stage, a focus motor, a controller and a joystick for manual focus.

Prior® sells a vast array of series of motorized stages. The main differences between series is mainly precision and size. Every stage uses step motor, except series HLD17, that uses a linear DC servo motor for ultra high precision. This is also the only series that comes with an integrated encoder.

The use of linear motor allow for superior repeatability in the values of 0.15 μm, faster scanning speed, up until 300 mm/s with ultra quiet operation [21]. Figure 3.4 shows the XY stage HLD117NN of ultra precision from Prior®

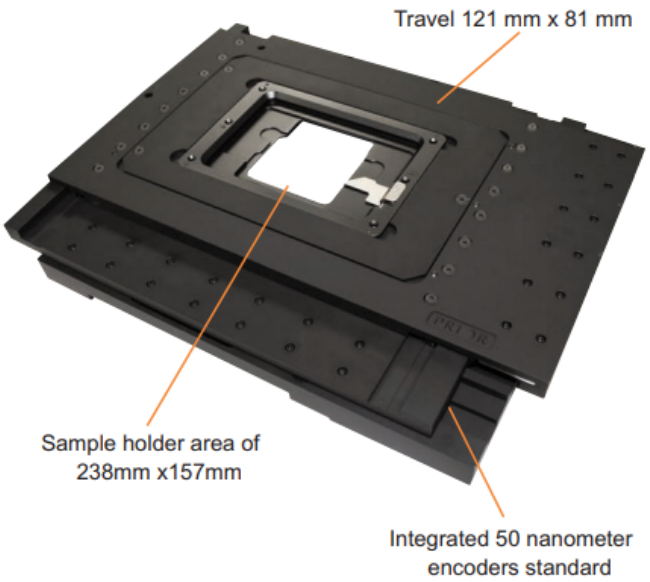

Figure 3.4: Prior® HLD117NN XY stage [21]

Thorlabs Thorlabs enterprise also sells all type of components in separated. This process allows for a cheaper solution to upgrade and already existent microscope. Thorlabs is reference name when buying optical systems components and as expected it al sells motorized microscope stages. These components can be bought depending specially for a certain brand of microscopes. They sell Z stages with piezo actuators, high-speed XY stages and XYZ. The latter are a combination of the posterior two.

XYZ stages are made by a fast XY scanning stage MLS203-1. This stage uses brushless DC servo motors with optical linear encoders. This solution can achieve a bidirectional repeatability

of 0.25 μm with a max speed of 250 mm/s. The estimated price of the stage is of 6846,18€ with the necessity to buy a BBD202 2-Channel Benchtop 3-Phase Brushless DC Servo Controller with the price of 2976,51€. In total the XY stage bundle costs 9824,69 [22].

The addition of a Z-Axis stage, allows for 3D imaging and confocal microscopy. This adds the bundle MAZS500-E, single channel controller and z-axis piezo stage. Figure 3.5 the mounting of the z stage in the xy stage.

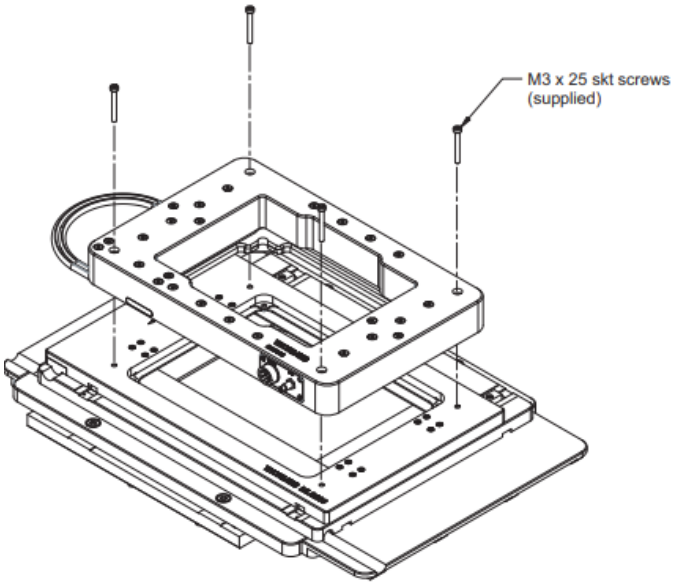

Figure 3.5: Mounting the Z stage to the XY stage [22]

The piezoelectric actuator allows for a resolution of 25 nm with a minimum step size of 250 nm. This bundle costs an extra 10574,19. Another extras need to be add such as joysticks for the Z-Axis and XY-axis - if manual adjustment is necessary - and mouting brackets [22].

The sum cost of all components can achieve a grand total of approximately **23K** euros.

Leica Leica is well know, international renown brand of optical systems. Leica sells flagship final products and solutions with patented in-house technology. Leica has a large array of motorized microscopes. The main features are automated contrast and illumination manager. It is important to observe that most of the solutions present a motorized Z axis that main function is to rapidly focus the system.It exists other more complex solution that present XY motorized stages, objective motorized changer [23].

Olympus A respected brand in the market. Olympus offers an inverted automates microscope and an automated cell counter. The first, offers both bright-field and fluorescence observation. Olympus claims low thermal drift and high accuracy, that come from a ultrasonic stage. In the latter product, the automates cell counter, focus is made in an autonomous way by Z-axis, using liquid lens technology. This allows for accurate and more reproducible results. This allows for a portable with a small footprint device [24].

Nikon Nikon is a very well know giant in the imaging and optical market. Well know in the photography world as well in the microscopy one. This enterprise focus on selling full products and software. It also sells some components related to optics.

Nikon has the upright microscope line called Eclipse Ni/Ci. In this class it is presented the model Ni-E that it is fully motorized. The focus on this model is made by the Z axis as well. This model also offers a typical motorized XY stage that can be controlled by a joystick [25].

Mitutoyo Mitutoyo is well know for they ability in producing accurate systems and mechanisms. The mitutoyo MF-U3017D is a brightfield microscope, that is fully motorized. This model offers a motorized Z axis, that translates the optical system. As a consequence it can achieve speeds of 20 mm/s. This model also present an motorized XY stage [26].

Autoscope Malaria The Autoscope Malaria, made by students of the University of Washington comes as a similar solution to the problem of the smart, automated, low-cost microscopes for rural and impoverish areas. It is reported that the Autoscope is made mainly in aluminium with 37 cm in height, 17 in width and 19 in depth. It is reported that this solution can cost between 1500$ USD to 4000 $ USD.

Parts were not design but bought. This systems is and XY-Z stage. That means that the sample travels between the X and Y and the Z movement that allows the focus, is made by a piezoelectric motor that thrusts the optic tube plus the camera. Figure 3.6 shows the different components used in the creation of this chassis [27].

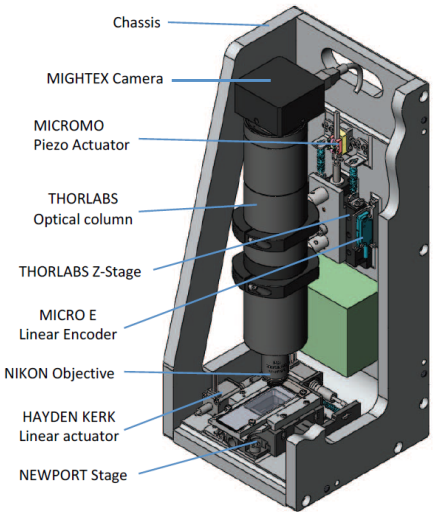

Figure 3.6: The autoscope components [27]

OpenLabTools Cambridge University is the patrons the OpenLabTools initiative that aims to the development of low cost and open acess scientific tools. Undergraduates and graduated used tools as data acquisition, actuating and 3D manufacturing to design and automated microscope.

The structure is based in aluminium profiles and the 3D printed partes are mostly mounts for other mechanical pieces. There is no 3D printed functional mechanical part. This systems it is still incomplete, although the stage function similar to a 3D printer where the bed (in this case the sample holder) travels along the Z-Axis. It is not clear how the motorized XY stage was performed. Project stalled Figure 3.7 shows the microscope created by this5 project [28].

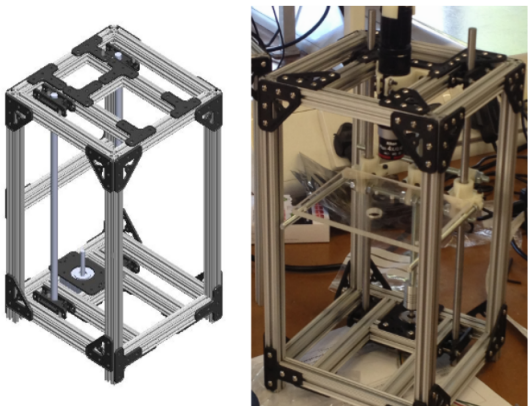

Figure 3.7: Open Lab Tools open source microscope [28]

OpenStage This proposal promises to deliver a 1000$ USD motorized microscope controlled by an Arduino. Achieving a price 10 times lower than the normal price. The control of the stage can be done by a PC port or an hand-held game pad. This microscope claims that it allows a minimum incremental motion of 0.04 μm in the Z direction and 0.1 μm in the X/Y direction. The repeatability is 1 μm and 0.10μm in the X/Y and Z axis, respectively. In terms of speed the system can achieve 1.2 mm/s in the Z axis and 1.8 mm/s in the X/Y [29].

In this system, the objective is mounted in a single linear translator, that allows for focusing. The X/Y stage is made by four pair of linear translator that allow the air-table to be moved with the objective. It is interesting to notice, that the stepper motors are connected to the micrometers by a a flexible shaft. It was used a Thorlabs PT1 linear translator with micrometer for the X/Y stage. The usage of the flexible shaft can be seen in the figure 3.8. The stage is large and heavy - approximately 17 kg [29].

OpenStage is one more system that uses the Z-Stage as linear translator for the objective. This objective is hold by the ThorLabs XT95 optical rails in the middle of the gantry. Once again, a stepper motor with a flexible shaft was use, where one full revolution corresponds to a translation of 250 μm [29].

It is noted that both resolution and speed of the drive system is affected by the choice of stepper motor. Resolution is dictated by the size and torque. Steppers can have common sizes of 1.8º and 0.9º. To achieve better resolutions, it can be used micro-stepping. This techniques allow to use fractional step sizes. With micro-stepping there exists a decrease in torque of the engine. Thus a motor with a higher torque may achieve better resolutions [29].

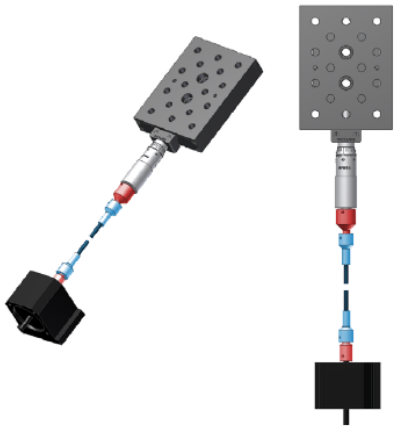

Figure 3.8: The usage of the flex shaft for driving the guiding system [29]

3.3 XYZ stages

XY stages are very well know for their versatility. It is possible to describe an wide array of application for this type of system, going from medical devices, to 3D printers and even automated industries. An XY stage is a well known mechanism that allows for the translation of a certain load in the X and Y direction with a certain resolution. The addition of the Z axis, allows also for the vertical translation of the load. This stages can even become XYZθ stages, that also allow for rotation. All six degrees of freedom (DOF) can be controlled if desired as it can be seen in figure 3.9 [30, 31].

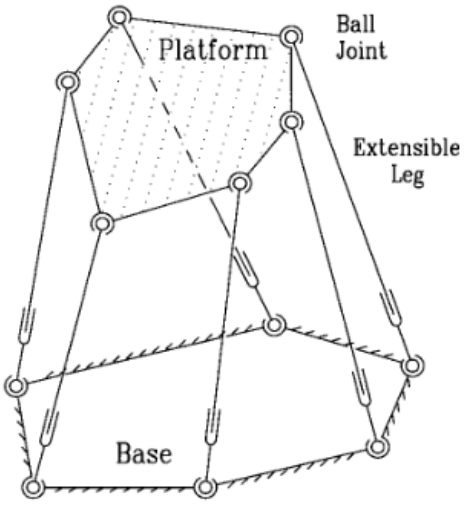

Figure 3.9: The Stewart mechanism is a famous example of a compact six DOF mechanism [31]

XYZ stages can difference themselves in a great amount. Size, accuracy, resolution, load are the main factor that will influence what solution should be chosen for the mechanism. Normally, and XY mechanism, and as a consequence the XYZ mechanism as well, is a combination of linear

actuators as it can be portrait it figure 3.10. XY stages have two type of configuration, cartesian and

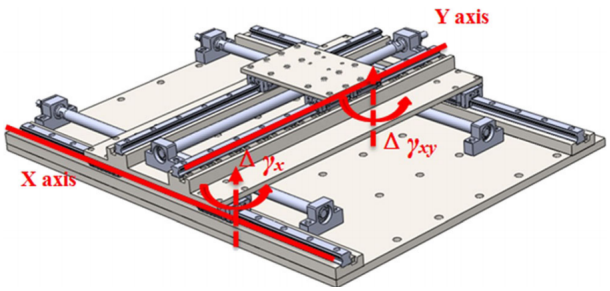

Figure 3.10: In a typical XY table, one axis is dependent of the other, but both can be controlled independently [32]

with parallel drives. Cartesian configuration is the most common, where one linear system drives the other linear guide. Parallel drives, commonly know for CoreXY systems or H-Frame, use parallel motors where both are use for the independent translation in XY of the load. As such, due to lower inertia and higher torque due to the combine efforts of the motors, this systems are used to achieve light-weight, low-cost compact positioning systems [33, 34]. The main disadvantages of this systems is related to size, accuracy and the existence of non-linear factors [33]. Due to the usage of time belts and pulleys, the accuracy and repitability can be compromised in this systems. The main non-linear factors of this systems are the elastic transmission and non-linear friction [33].

In the case of microscopes, high precision tables are the most common usage of the XYZ stage, to correctly align or position the sample in another field of view. In the case of the μSmartScope, the XY stage creates another camp of view and the Z stage helps to focus on the system. In the world of microscopic precision, systems are usually divided into the following mechanical solutions: air bearings, mechanical bearings and stages with flexural guides [35].

All of these solutions offer different features and prices. It is then important to understand that all of these three solutions can be combined and have a different type of actuators. For example, an XY stage with flexural guides can be combined with an XY stage with mechanical bearings to achieve nanometric resolutions and millimetric travel distances. For actuators, there are typically three different solutions: steppers, servomotors and piezoelectric devices. Stepper motors have many advantages such as having a lower cost and allowing for a wider range of travel distance. Piezoelectric devices are faster and have a smaller hysteresis. However the added precision comes with higher cost and limited travel distance [20,35]. Magnetic motor can also be used in air bearing systems [36].

It is important to understand that each mechanism has a different accuracy and repeatability. Figure 3.11 represents the difference between repeatability and accuracy. These are the metrics of performance in the mechanical system for the microscope. Repeatability is the measured from the deviation of the positioning and accuracy is the deviation from a certain standard [37].

Figure 3.11: Difference between accuracy and repeatability [37]

3.3.1 Compliant Mechanisms

It is important to understand compliant mechanisms and how they relate to microscopic systems. It has been observed many solution with nanometric resolution that use the physics behind compliant mechanism to achieve such feat [38–40]. Thus, to be able to implement it is necessary to understand the concept behind a flexural mechanism.

Compliant mechanism is a mechanism that bends to achieve its goal. Pragmatically, designers use rigid body's to achieve the desired solutions. Compliant Mechanisms do come with many advantages: [41]

- Lower cost due to a monolithic design, fewer components and simplified manufacturing;
- Better performance, with higher precision, reduced wear and no backlash;
- This mechanisms are also low weight and also eliminates the need of lubrication.

These advantages are well welcome in the microscopic industry with the high precision it is possible to achieve better resolutions. Lower weight will optimize performance with reduced vibrations, noise, more efficiency and smaller drivers. Components are also cheap and the lack of lubrication and fluids makes it easier to be medically certified [41].

In opposition to these mechanisms, it is necessary to undertake simulation to correctly understand motion and the load behavior of the system. This is due to the non linear range and classical linear equation might not be accurate to describe the system. Fatigue of compliant mechanism and respective life it is necessary to be well studied. The flexural joints present points where rupture can begin, leading to system failure. Another problem is that motion of this mechanism is still a very big problem such has material selection for load conditions. It is possible to conclude that compliant mechanisms goal is to not replace contemporary mechanism with rigid link, but to complement and to improve designs [41].

Before understanding the physics behind compliant mechanism it is necessary to enhance the comprehension on some easily mistaken concepts. Firstly, stiffness is not a synonym of strength. Stiffness is the ability not to bend while strength can be consider the ability to not breaking. There might be the need of system to be resilient to failure while being able to deflect in considerable ways. To achieve desired flexibility one must design it system based on material properties, geometry and loading conditions. In terms of materials, they should have high strength and a low Young's modulus [41].

In the focus of this dissertation, it is useful to understand how linear motion compliant mechanisms work and behave and how they are implemented in a microscope. Figure 3.12 show and example of an XY linear motion compliant stage, whre Δe is the parisitic error [42].

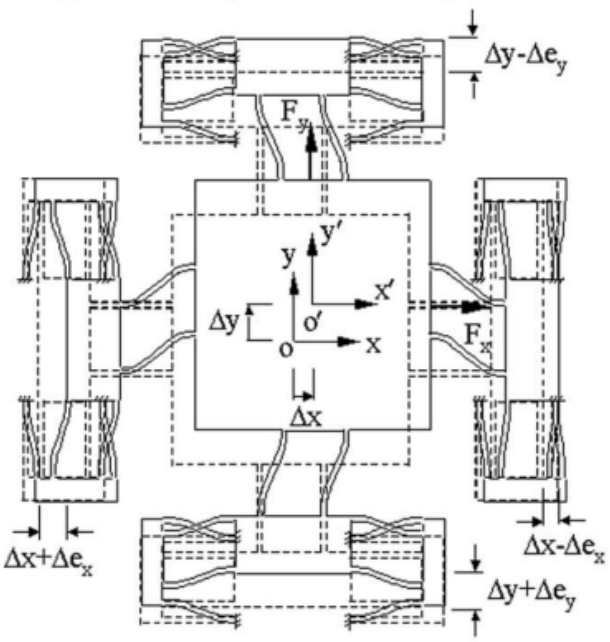

Figure 3.12: Working principal of an XY compliant stage [42]

To better understand the physic behind a compliant mechanism, it being by drawing the displacement between to rigid bodies, as it can be seen in figure 3.13.

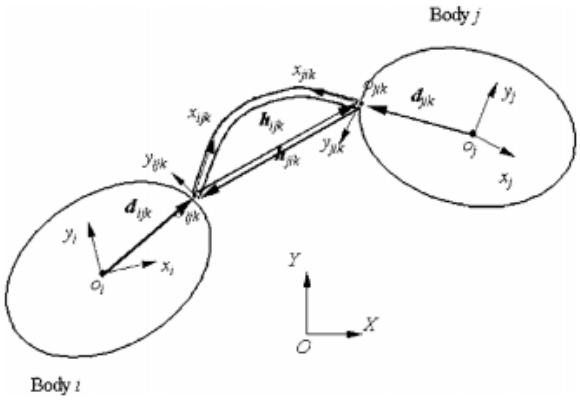

Figure 3.13: Rigid bodies with a flexural joint [42]

The displacement of two rigid bodies with a flexural joint in the middle can be giver by:

$$d_{ijk} = \begin{bmatrix} d_{x_{ijk}} & d_{y_{ijk}} \end{bmatrix}^T \tag{3.1}$$

Lets assume that h_{ijk} is the displacement of a certain k flexural between the starting point o_{ijk} and

the end point o_{jik} as: [42]

$$h_{ijk} = \begin{bmatrix} h_{x_{ijk}} & h_{y_{ijk}} \end{bmatrix}^T \tag{3.2}$$

Then, if the mass of the flexural joint is not computed, due to the small area related to the mass of the rigid bodies, then, second law of Newton can be writen as

$$\tilde{M}\Delta\ddot{q} + \tilde{K}\Delta q = Q \tag{3.3}$$

Where $\tilde{M}$ is the equivalent mass matrix, $\tilde{K}$ is the equivelent stiffness matrix, Δq is the displacement vector and finally Q is the force vector [42] It is important to notice that the element of the equivelent mass matrix is given by:

$$M_i = \begin{bmatrix} m_i & 0 \\ 0 & J_z \end{bmatrix} \tag{3.4}$$

Where, m_i is 2X2 mass matrix of the rigid body and J_z is the mass inertia of the rigid body. To complement the elements of the equivalent stiffness matrix are given by the multiplication between displacement and stiffness of the joint or the rigid body [42]. As such it is then possible to define the compliance matrix, as the inverse of the stiffness matrix as:

$$C^0 = \begin{bmatrix} \frac{a}{Ebc} & 0 & 0 \\ 0 & \frac{4a^2}{Eb^3c} & \frac{6a^2}{Eb^3c} \\ 0 & \frac{6a^2}{Eb^3c} & \frac{4a^2}{Eb^3c} \end{bmatrix} \tag{3.5}$$

Where E is the elastic modulus of the material, and a,b,c are geometric dimensions of the prismatic beam. There it is now possible to define the characteristic equation as

$$\left|\lambda I - \tilde{M}^{-1}\tilde{K}\right| = 0 \tag{3.6}$$

Thus, is it possible to conclude that the resonances frequencies of the system will be

$$f_i = \frac{1}{2\pi}\sqrt{\lambda_i} \tag{3.7}$$

f_i and λ_i define the modal frequencies of a certain characteristic root. Finally, when the acceleration of the system is null, then displacement can be given by:

$$\Delta q = \tilde{K}^{-1}Q \tag{3.8}$$

After understanding the working physics behind an XY parallel compliant system, it is necessary to create some design constrains. The first should be that the translation resonance frequency of the system should be: [42]

$$f_0 - \Delta f \leqslant f_T \leqslant f_0 + \Delta f \tag{3.9}$$

Where f_0 is the desired frequency and Δf is the maximum allowable deviation. Then, it is necessary to guarantee that the rotational frequency is greater than the translational frequency, to avoid unwated parasitic rotational movements. Thus:

$$f_R \geqslant c_f f_T \tag{3.10}$$

Where c_f is a constant over 2. In terms of stress and displacement, it is necessary to achieve that maximum stress is lower than the yield stress of the material considering a certain safety factor [42].

$$\sigma_{max} \leqslant \frac{\sigma_Y}{N_f} \tag{3.11}$$

The maximum stress occurs, as expected, in the end of the flexrues and it is given by

$$\sigma_{max} = 3K_t E \frac{b}{a^2} \delta_{max} \tag{3.12}$$

Where K_t is the stress concentration coefficient and δ_{max} is the maximum displacement of the translating system [42].

3.3.2 Actuators and Solutions

3.3.2.1 Guiding Systems

The system of guiding constrains the motion to a certain direction. This component is of utmost importance since it determines the trajectory accuracy, stiffness and load capacity. Trajectory accuracy is characterized by straightness, flatness, maximum angular deviation [37]. Load capacity is also important for design of this systems since it will dictate the service life and robustness. It will also influence how smooth the motion is due to friction [37].

Air Bearings Air bearings XY systems proposes the usage of air fluid mechanics combined with electromagnetic motors. This systems tend to be expensive due to the difficulty of controling position and levitation of the stage. Air bearings allow for small motion error achieving high precision while maintaining high speed due to the lack of friction. Therefore they present a very high guide stiffness This systems require laser feedback to make the most of the system.This systems can achieve nanometers-range noise in straightness and flatness [36, 37].

Air bearings works by the usage of compressed air, that creates and air cushion under the plate levitating it. The air gap is usually of 5 to 10 μm. Load capacity is dependent on surface area and pressure distribution. Pressure is usually 0.4 MPa what allows for the necessary lift. Figure 3.14 shows how an air bearing works [43, 44].

Linear ball bearings This systems allow for precision down to micrometers. The work principle of this systems, is that when moving, the balls are, generally maintained at a given position with a linear ball cage that prevents the movement of the platform. While moving along the drive or

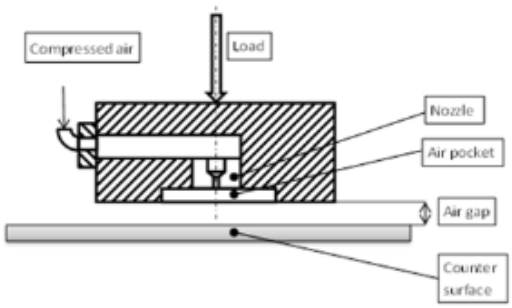

Figure 3.14: Scheme of an air bearing [43]

guide shaft/ beam. Balls move at the same speed to achieve less resistance and friction with the elements. It is important to notice that the larger contact area the better the load capacity but as well the resistive load.

Figure 3.15 shows the common actual system of position of the balls, a recirculating system. Other similar systems is the usage of linear roller bearings that present a better load capacity and stiffness while not increasing by much friction forces.

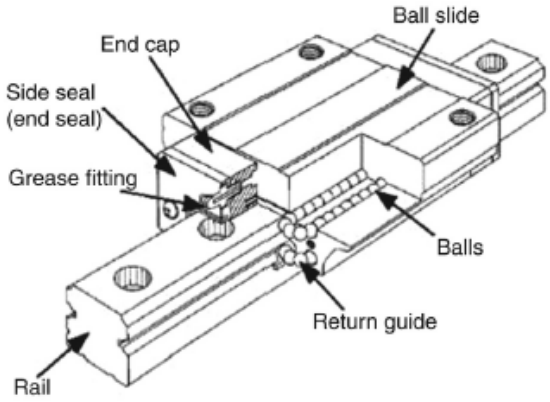

Figure 3.15: Scheme of an "truck and rails" ball bearing system [37]

Other solutions that are presented in the IGUS® drylin® that is a class of maintenance an lubrication free linear bearings. This creates a maintenance free, wear resistant, with low friction and weight reduction systems. Thus, it can achieve high-speed while maintaining a very quiet operation. Due to the higher area of contact for better load distribution, it is possible to use cheaper shafts. Due to the lack of need of lubrication and chemical resistance it is easier to apply this systems for medical certification [45].

Flexural Guides Based on compliant mechanisms refereed in 3.3.1, this type of guides are used for limited travel and are based in the deflection of blades and beams. This system provides

excellent stiffness and it is usually actuated by piezo actuators that can achieve the necessary load to maintain the small travel [37].

3.3.2.2 Drive Systems

Lead Screw The usage of lead screw is the most common way to transform a rotational movement into translation. Cost effective equipment that present good axial stiffness and smooth small displacements. Due to friction issues, a lead-screw is limited in velocity. Figure 3.16 shows the principal of work of a lead screw.

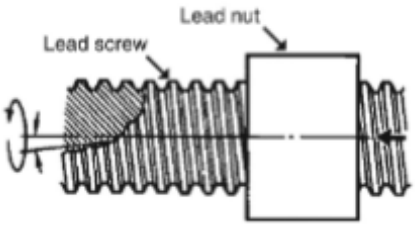

Figure 3.16: Scheme of an leadscrew [37]

Due, that lead screw will be very used as linear actuators it will be presented important concepts when designing the driving system. Certain linear actuator might not have the leadscrew in the exterior, but are still actuated with a lead screw and a stepper motor but present a more robust and efficient solution. This configuration can be seen in figure 3.17.

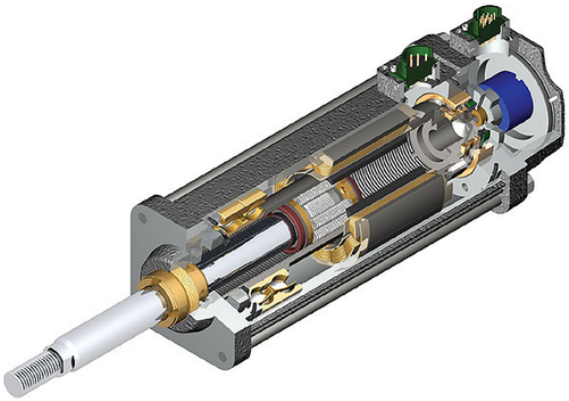

Figure 3.17: Anatomy of a linear actuator [46]

To correctly design a power screw, first it is necessary to imagine an unrolled thread and to a force balance where the load is applied. This system will be similar to a falling mass on a steep inclination. Where the height of the slope is the pitch and the length is the mean diameter perimeter (πd_m). The forces acting in this system are all axial forces, the driving force and a frictional force [47].

Thus the maximum torque required to overcome friction and pull the load is given by two expression: one to raise the load and another to lower. It will be presented the equation of the

raising torque, since this is the maximum torque the actuator must be able to withstand:

$$T_r = \frac{F d_m}{2}\left(\frac{l + \pi \mu d_m}{\pi d_m - \mu l}\right) \tag{3.13}$$

It is important that the screw are self-locking. This means that the load does not lowers itself. Thus the following condition must be followed:

$$\pi \mu d_m > l \tag{3.14}$$

Thread efficiency is the ratio between the the torque considering friction and not considering friction, given by:

$$e = \frac{Fl}{2\pi T_r} \tag{3.15}$$

It is common to use a thrust collar bearing in this applications as a way to reduce the necessary torque required as it is possible to reckon in figure 3.18. Torque is given by

$$Tc = \frac{F \mu d_c}{2} \tag{3.16}$$

In terms of buckling, for power screw J.B Johnshon buckling formula applies very well and it is

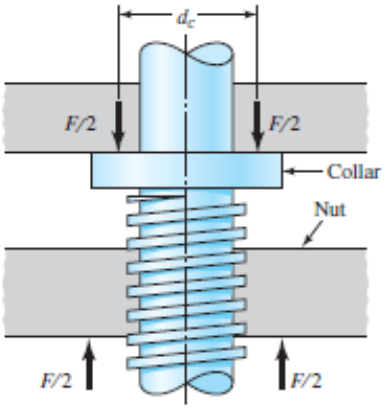

Figure 3.18: Collar being used in lead screw drive [47]

given by [47]:

$$\left(\frac{F}{A}\right)_{crit} = S_y - \left(\frac{Syl}{2\pi k}\right)^2 \frac{1}{CE} \tag{3.17}$$

Where C is a constant give by the end conditions, E is the Young Modulus and S_y is the Yield Proof of the material. Stress wise, axial stress is given by:

$$\sigma = \frac{4F}{\pi d_r^2} \tag{3.18}$$

The maximum nominal shear stress due to torsion is given by:

$$\tau = \frac{16T}{\pi d_r^3} \tag{3.19}$$

Ball Screws This type of screws present high efficiency and low heating, low wear which is proportional to a high service life [37, 48]. A screw supported by thrust bearings and a nut wit recirculating balls drive the system. On one side it is attached a rotary motor directly or through a gear/belt. Pitch typically varies between 5 and 40 mm. Figure 3.19 show the working principles of this type of systems [48].

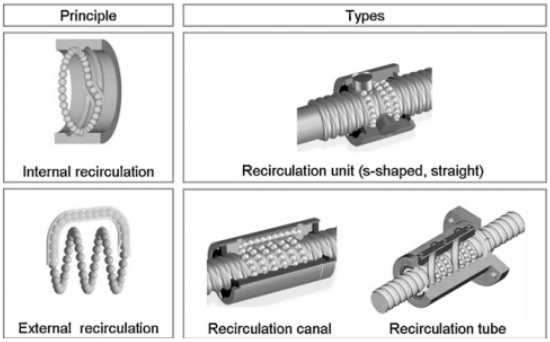

Figure 3.19: Ball screw mechanism [48]

Iron Core Linear Motor Iron core motor come with the goal to solve problems that mechanical elements have such has backlash and deadzones. This type of motor relates as a rotary motor, with a rotor, a stator and air gap. With a three-phase current, and electromagnetic field is created. With the variation of the three phase current, and electromagnetic force is created that will thrust the carrier along a linear rail [49]. This system can be seen in figure 3.20. Iron core linear motor

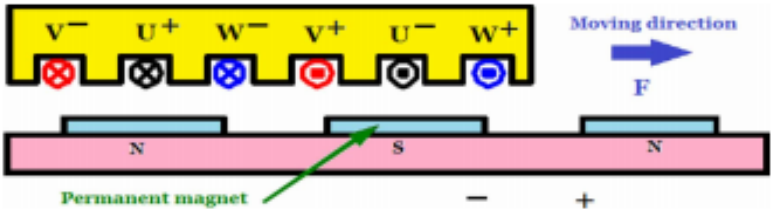

Figure 3.20: Iron Core mechanism [49]

can achieve high speed combined with high accuracy. This systems usually use air bearings. It is possible to use rolling element bearings, that are preferable for lower cost. The main disadvantage of that is that it can cause situations that will end in premature failure [50].

Iron less Linear Motor Iron less also use electromagnetic forces that depend of the flux to achieve linear motion. In this solution tracks are in U shape [37,51]. This allow for better precision control. Figure 3.21 is a scheme of this system [51].

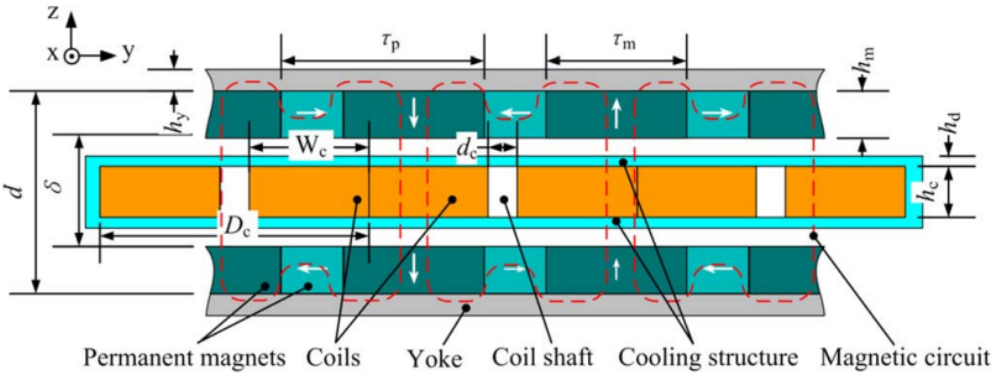

Figure 3.21: Ironless mechanism [52]

This system compared to the iron core is that it present a linear relationship between thrust and current, lack of detent force and little armature reaction. Some of this systems can be water cooled to help not reaching high temperatures that can damage the mechanism [52].

Piezoelectric Actuator A piezoelectric element can work both as a generator and a motor. Applications of this actuator range between mainly positioners, motors and vibrations suppressors [53, 54]. When applied a current there is a piezoelectric actuator converts electrical energy into a mechanical displacement or stress through the piezoelectric effect [55]. Short control displacement and be given an actual stroke that works for micro robotic [53]. Piezoelectric actuators is the combination between structural ceramics and electronics. This stacks of ceramic sheet present the advantages of a low driving voltage, quick response, high generative force and high electomechanical coupling with very small displacement [56]. While not being best for most application, due to the typically short travel range, this systems can be used with others to achieve resolutions in the range of the nanometers. The most common piezoelectric actuators are the multilayer, moonie and bimorph as it can be seen in figure 3.22.

3.3.3 Summary

Table 3.1 shows a comparison between the different guiding mechanisms and table 3.2 shows a comparison between the different driving mechanisms.

3.3.4 High Throughput Microscopy Market

Autonomous and Motorized Microscopy comes as revolution in the fields of image diagnosis. The need for motorized microscopes appeared in the field of genomics, proteomics, biochemistry and molecular biology. The usage of robotics allowed for new experiments to be followed and to handle samples in shorter time [18].

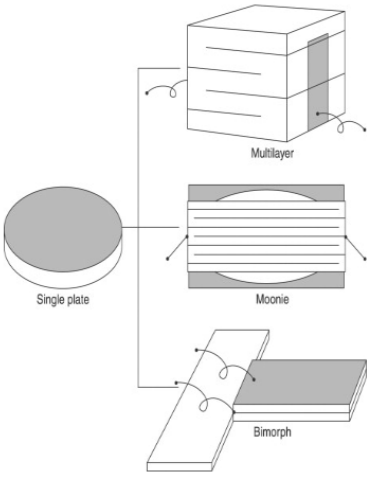

Figure 3.22: Different piezoelectric actuators designs [56]

Parameter	Linear Ball Bearings	Recirculating	Crossed Rollers	Air	Flexures	Kinematics
Travel range	<400 mm	No limit	<400 mm	No limit	<10 mm	<25 mm
Load capacity	OK	Good	Good	Good	Good	OK
Trajectory accuracy	Good	Good	Very Good	Excellent	OK	OK
Motion, sensivity	Good	Good	Very Good	Excellent	Excellent	Good
Speed, acceleration	Good	Excellent	Good	Excellent	Excellent	OK
Stiffness	Good	Very Good	Very Good	OK	Very Good	Good
Damping	Very Good	Good	OK	Very Good	OK	OK
Robustness	Good	Very Good	OK	Very Good	Excellent	OK-excellent
Wear	Low	Low	Low	Very low	Very low	Fair
Cost range	$	$$	$$	$$$$	$	$-$$$$

Table 3.1: Comparison between guiding systems [37]

Parameter	Lead Screw	Ball Screw	Ironless Linear Motor	Ironcore Linear Motor	Piezo Linear Motor
Vertical Use	Excellent	Good	OK	OK	Good
Position stability	Very good	Very good	Excellent	Excellent	Very good
Speed stability	OK	OK	Excellent	Very good	Good
Motion sensitivity	Very good	Good	Excellent	Excellent	Excellent
Low heat generation	Good	Very good	OK	OK	Excellent
Robustness	Good	OK	Excellent	Excellent	OK
Low wear	OK	Very good	Excellent	Excellent	Good
Cost	$	$$	$$$$	$$$	$$$

Table 3.2: Comparison between driving systems [37]

Autonomous and Motorized Microscopy are the tools of High-throughput microscopy (HTM). Advances in biology and bioinformatics where possible due to this technologies breakthroughs in computing ability.

The most important usage of this technology is to relieve staff intensive work. Even thought technology is not yet perfect to the point to completely replace human factor, this systems do not

fatigue when in touch with a large array of images. For the correct analysis of the human genome-wide it is necessary to collect approximately 1,000,000 images. Assuming perfect condition a robot can capture this images in the space of 2 week or less. The hardest task is to analyze all 1,000,000 images. In this stage, computer aided analysis is mandatory to achieve results in feasible time not only due to fatigue related problems but also repetitive and bias factors [19]. It is possible to conclude that automated and motorized optical systems allow to use less trained staff and achieve results in a shorter amount of time with more accuracy.

Smear microscopy is the standard type of examination of many illness in particular tuberculosis. The technique used for tuberculosis analysis, Sputum smear microscopy (SSM) suffers with low sensitivity and inability to detect drug-resistance. It was predicted that 36,6 million test per year, in 22 high burden countries by 2020. This value corresponds to a value of US$137 million in 42827 microscopy centres in 2012. Replacing the test for a more expensive one could have a potential one of US$154 million per year [57]. It is possible to conclude that high throughput microscopy allows to significantly to diminish cost margins and allow for profit.

3.3.5 Smartphone as an identification device

Smartphones are daily tools with an exponential technologies advances. The evolution in smartphone hardware and software allows for capturing images, when coupled with microscopy components, that are in pair with those from optical systems. In 2010, 90% of the world achieved mobile cellular network. The usage of cellphones keeps a double digit growth, therefore, it is an opportunity application of telemedicine improving healthcare in impoverish areas [58].

3.3.5.1 Hardware

When creating and optical system for a smartphone system, there are three different solutions have been developed: on-chip analysis, off chip clip-on methodology and on-lens approach [58]. Figure 3.23 represents a schematic with the different approaches.

On-chip analysis This is the approach that requires more modification of the hardware of the smartphone [59]. This solution controls the spatial coherence of the illumination that comes from the source, that allows for the recording of the holographic diffraction pattern of each cell [60]. After the capture of the holographic diffraction pattern an algorithm processes the 2D image and builds a 3D one. The light is created by a LED that is then scattered from each micro-object to a interface that then creates a hologram of an object in a detector array on the cellphone [61]. Figure 3.24 demonstrates how this optical system.

The main disadvantages of this system is the high modification in hardware and the fact that even though it can achieve an high FOV and no optical external attachments, it can only achieve acceptable resolutions for 40x magnifications with NA=0.65. Adding to this, a lot of processing power is necessary to reconstruct the image [2]. Figure 3.25 shows the comparison between a normal light microscope and an on-chip analysis system.

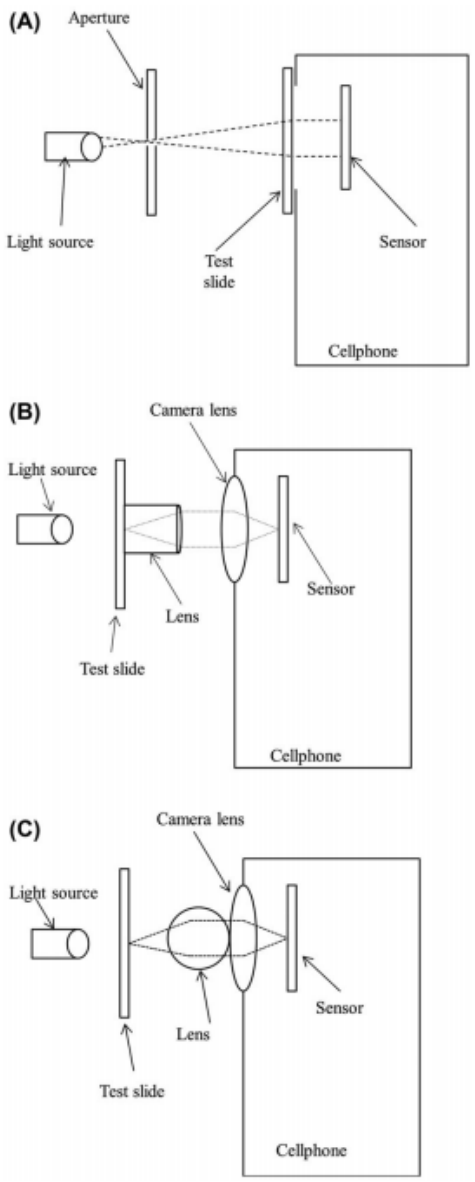

Figure 3.23: (A) On-chip, (B) off-chip, (C) on-lens [58]

Off-chip clip on This approach requires solution exterior to the cell phone that come as attachments to be mounted on the cellphone [59]. This type of system is very common due to the lower price and non evasive hardware. Most solution in literature use this solution with some modifications [2]. This type of system allows for the usage of inexpensive commercial grade optical equipment and even fluorescent filtering [62]. Figure 3.26 shows a scheme of a typical attachment based approach.

This system proved reliable to capture images of infected blood cells [62]. As such, malaria scope concept followed this approach as well. The main disadvantages of this system are: the ability to use high magnification limits FOV and the unique cellphone model design. With first problem emerges the need to create a mechanical system the samples to be able to cover a large

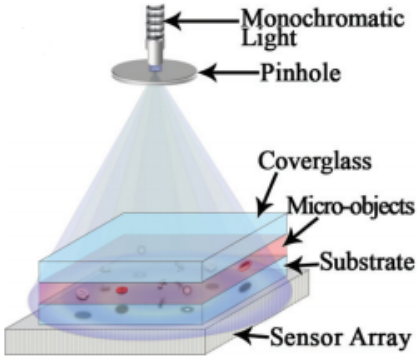

Figure 3.24: Diagram of lensfree system [60]

enough area. This will be mandatory in the μSmartscope due to the need to use a x1000 magnification to correctly analyse malaria blood smears [2].

On-lens This approach considers the application of the optical system directly attached to the camera lens [59]. This type of systems is attached to the smartphone camera [2] and uses light field microscopy to enhance the allow the view point to change after the reconstruction from a single photograph. Figure 3.27 shows a schematic of the optical layout of this type of solutions [59].

In this system magnification only depends on the ratio of the focal lengths, so its independent of the proximity between camera and sample. This systems present chromatic aberrations and radial distortion [2, 59]. The main advantage of this system is the easy application in any type of model of smartphone. Another factor is the ability to move the camera and take panoramic images of the sample [58].

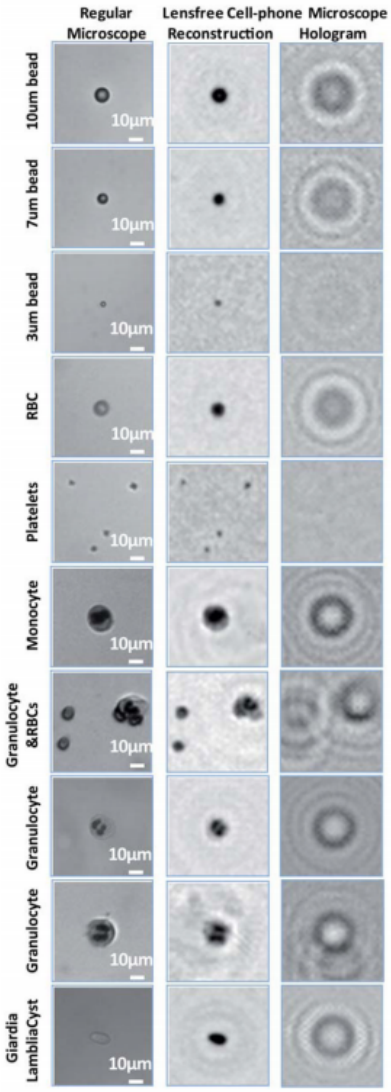

Figure 3.25: Comparison between a regular microscope and a lensless system [61]

3.4 Additive Manufacturing

When designing a product, prototyping and validation comes in as natural part of the process. Additive manufacturing, in the scope of this dissertation comes as a tool of design validation and part creation. Thus, 3D printing is used not only for metrical purposes but as component design that suffer from complex geometries.

Additive Manufacturing or 3D printing, comes has a revolution to the industry as way to create impossible shapes, accelerate product development and optimize material waste [63]. 3D printing generates from the idea of the addition of material to a certain object instead of the typical approach of subtracting material as it is possible to observe in the diagram of figure 3.28. The main well known processes in additive manufacturing are Stereolithography (SLA), Selective Laser Sintering (SLS) and Fused Deposition Modeling (FDM). In the scope of the thesis, the fabrication process

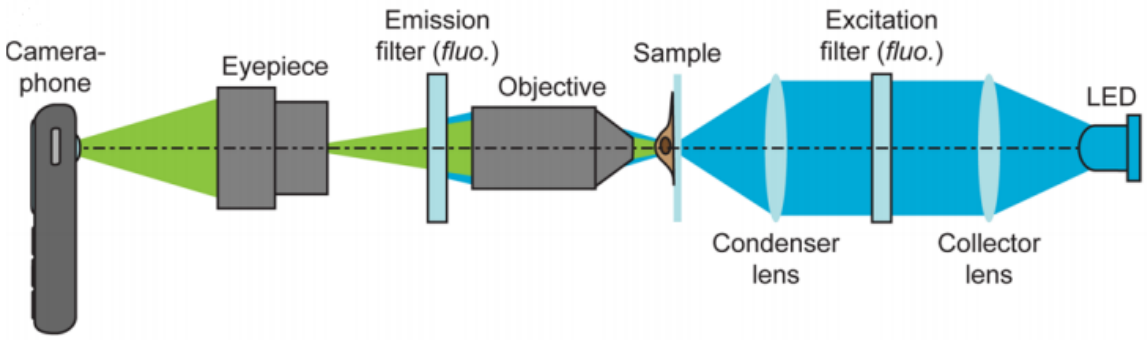

Figure 3.26: Optical layout of an off-lens ad-dons. With the optional addition of fluorescent filtering [62]

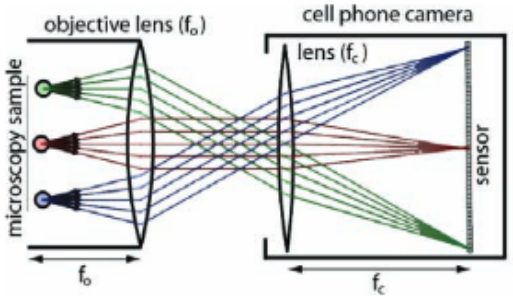

Figure 3.27: Optical Layout of On-Lens solution with the respective focal lengths [59]

that will be used are FDM and SLA. In FDM it was used an Prusa Mini, Ultimaker 3 and a customized Ender 3 Pro with a SKR mini e3 and a 3Dtouch probe. Formlabs 3 were used for SLA solutions.

3.4.1 3D printing in medical environment

The revolution of additive manufacturing touched many fields of science. Medical and Pharmaceutical sciences were also infected with the possibility to use technologies of the easy to customize features typical of 3D printing.

In the field of medical devices additive manufacturing is view upon mainly in customized prosthetic and patient specific drugs. It is proven that with the advances of image-based designs with bio-material structures can create an biomechanical behavior in a certain period of time. The main advantage of 3D-printed implants in medicine is to be able to create a product that is customized to the patient's anatomy [64]. Another strong example of the usage of 3D printing in the medical science field is, for example, the creation of mouth guards, where after having the printer parameters optimized, the entire workflow from the intraoral scan to the final wearing of

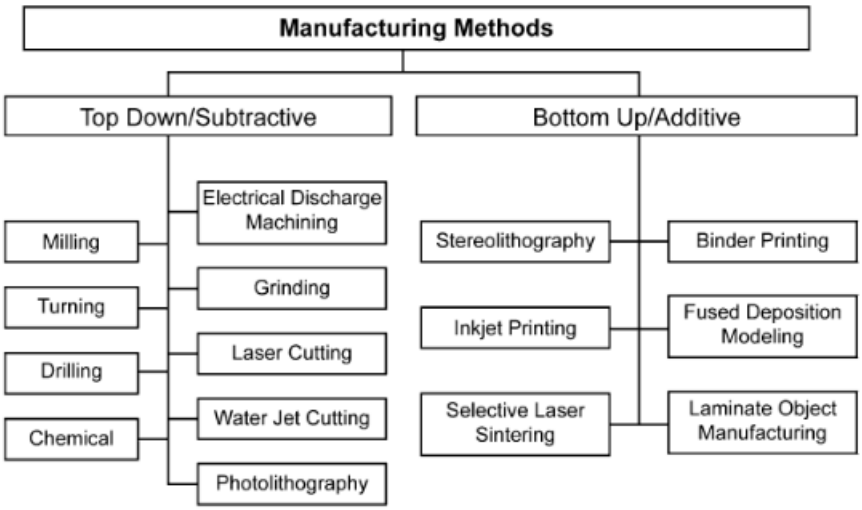

Figure 3.28: Additive Manufacturing Process [63]

the device took less than 2 hours that is a big advantage compared to the traditional process [65]. Dentist use rapid fabrication for the creation of molds of the implant. 3D printing in this field of science can extend to the creation of accurate models for education of new professionals [66].

This trend only keeps growing, with estimation of 20 years to be able to print a fully function printable heart. 3D printing of bio-printing, cell and biomaterials are still a matter of study for the correct existence of customised implants [65].

The field of medical sciences, it is involves in regulation due to the high risk and responsibility of the field. As such, regulation of these 3D printed devices it is a field of study and evolution. For example, 3D printers of drugs need to be legally defined as manufacturing or compounding equipment so that it is possible to apply laws [67].

During the recent outbreak of COVID19 many manufacturers employed additive manufacturing process in the creation of parts for medical equipment, mainly ventilators and valves. The industry, laboratories and individuals rose up to the situation and responded to the distress call. In the UK more than 60 industries produced 20,000 ventilators in two weeks. Airbus and Vauxhall distinguish by producing large number of 3D printed parts [68].

The quality of the final product will be affect mainly by: placement, orientation and packing density. When choosing orientation and placement, it is important to understand where are the most optimal print areas and if there and pieces nearby with similar or different design. As an example, creating parts near the edges have less that optimal print quality than those printed in the center. Orientation is also important to achieve the less anisotropic properties of the parts [69].

Certain features might require support materials such as: overhangs, high aspect ration features that protrude from the main body of the device or component, internal features and thing features that can warp. This support materials can be removed physically or by chemical means. It is important to guarantee that this support is removed without impacting the safety or effectiveness

of the product.

When choosing the layer thickness, depending on the additive manufacturing process, it depends on the device, bonding between layers and sensitivity to power fluctuation. If energy density is changed to reduce layer thickness, layers may not cure or bond together completely. Finally, the last main point is the choice of the build paths. This parameter can affect quality of the finished product, by changing the amount of melting and re-melting. It is important to maintain consistency of the build path and build speed. When using a non-solid fill, it is important to understand if the part needs to be fully sealed and allows for internal voids. It may also need to be necessary to address the type of gas that might fill the voids and compromise the part [69].

To achieve the best properties it is important to maintain procedures and therefore to adequately control environmental conditions in the room where build volume is found. On the other hand, the main printing parameters that the device manufacturer should report and that have a major impact on the part are:

- Instantaneous power of the energy delivery system;
- Build speed;
- Build path;
- Total energy density;
- Focal point or nozzle diameter.

3.4.1.1 Medical Devices Regulations

When designing a medical device it is important to understand the special regulations that come with the field of science. Medicine is a high risk and very complex science that it is responsible for the well being and life of the patients. Therefore everything related to such need to be well regulated as way to sum extra health problems to the patient. In 2015, it was approved the first medication pill made by 3D printing methods. The U.S Food and Drug Administration (FDA), release a guidance document due to the non massive fabrication related to this type of manufacturing. This allows hospitals operating rooms and university laboratory to create and design quality products [70].

Devices in medicine belong to a very big array of complexity that can start from pacemakers and descend to gloves and bedpans. All of these devices fall under three different classes (I , II and III). The first one, class I, is a low-risk device. There is almost no potential for harm. The second class is moderate-risk devices. These are devices where general controls fall short to guarantee safety. In the last class, is where high risk devices fall. Figure 3.29 demonstrates the process that the U.S Food and Drug Administration use for the different classes of products [71].

When designing medical devices with additive manufacturing processes, one should follow the guidance from FDA to achieve the best quality possible as well working parts with the ability to be used in the medical environment. It is important when designing for medical devices to

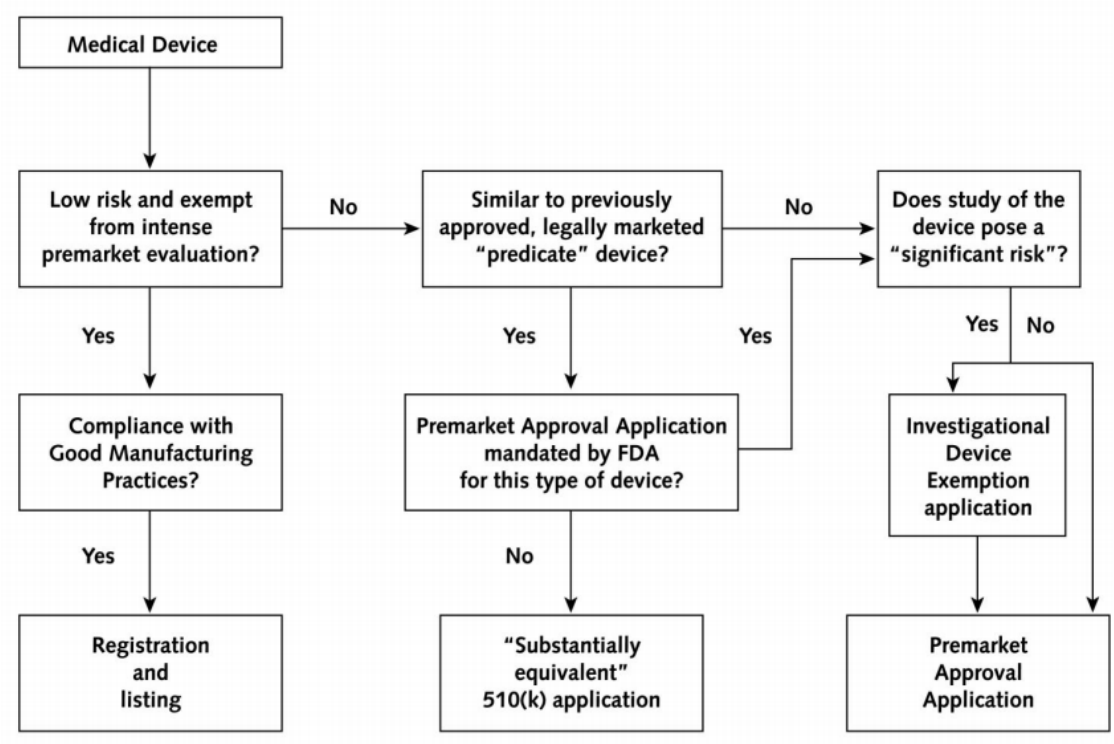

Figure 3.29: Diagram with the different procedures to approve different devices [71]

understand the minimum possible size of a certain feature, for certain build parameters. This will ensure that all parts have the desired dimensional specifications and tolerances. It is important to understand that certain features can suffer from the stepping effect and can lead to rougher surface finishes [69].

3.4.2 Topology Optimization

Topology Optimization is a novel technique that was mainly developed with the appearance of additive manufacturing as way to produce final products. Due to the ability of 3D printing to create complex geometries that are considered impossible in traditional manufacturing processes, topology and shape optimization.

This field, looks to structures and products in an objective way. The main goal might be reducing mass, cost, minimizing stress or maximizing stiffness. The topology optimization software will run the simulation, to achieve a certain goal while being constrained by technical considerations.

Many methods can be use as an approach to an algorithm to achieve the most accurate topology optimization, the most common one is Solid Isotropic Micro structure with penalization (SIMP) [72]. This method creates a power law to relate material properties and design ones, in terms of material density. As such this method replaces integer variables with continuous variables that allow the creation of gray areas with densities between 0 and 1. It follows then a penalty system that eliminates this grays areas and give a discrete solution eliminating middle densities.

SIMP works by meshing the body into a fixed grid of **n** finite elements. All these elements have a certain density that act as a design variable. Achieving the goal will create a new design space. The most common goal is to minimizing the compliance of the structure while subjected to a certain, limited amount of material.

$$\begin{cases} \text{Minimize :} & C(X) = F^T U \\ \text{Subjected to} & \begin{cases} V^T X \leq V^* \\ 0 \leq x_{min} \leq x_i \leq 1 (i = Ln) \\ F = [K]U \end{cases} \end{cases} \tag{3.20}$$

Where X is the design variable, C is the compliance of the structure, V^T is a vector of the volume of the elements, V^* is the volume constrain, F is the load vector, U is the displacement vector, K is the stiffness matrix [73]. It is important to notice that minimizing compliance, or stain energy, is to maximize stiffness.

The commercial tool for topological optimization is called *TOSCA* offer two different algorithms: a controller based one and a sensitivity based one. *TOSCA* also allows for the usage of not only technical constrains, but also manufacturing and design constrains such as demold constrains and member size constrains [74]. This allows to apply the principle to pieces that can be manufactured not only by additive manufacturing. *TOSCA* is the tool used by *Solidworks* and other finite element analysis softwares such as Abaqus, ANSYS and MSC Nastran [75].

Normally, product optimized with this process have the tendency to create complex parts that do not suffer from simplification constrains that able to manufacture for traditional processes. AM allows to create the topology independently of the complexity. Another factor is the production cost, wich does not increase with complexity. Thus topology optimization works hand in hand with additive manufacturing processes. The main limitation of AM in this type of process is the minimum feature size [76].

It is possible to conclude from topology optimization algorithm the following:

- Topology Optimization has the tendency to create designs where material is accumulates in the outer boarder areas;
- This tendency increases with increasing size of the design space;
- It is important to create feasible proposals to achieve the best weight-optimized topology;
- The bigger the size of the part the further way is the infeasible design from the optimal one.

It is normal that after the optimization process one should redesign the part to achieve low weight and easy manufacturability as it can be presented in the figure 3.30. With this comes thickness control, that allow to restrain a certain minimum thickness to the part by blocking the element and remaining solid. Thus, the minimum thickness is maintained parallel to the border. This feature also guaranties that all the walls in propose have a certain minimum thickness and there are no

holes created. As a consequence this means that topology does not change during the optimization process.

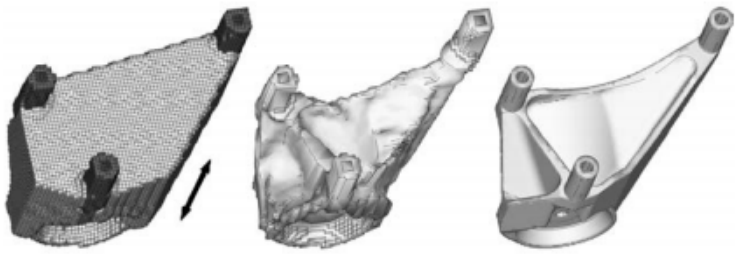

Figure 3.30: Pipeline of creating a piece with the topology optimization algorithm [76].

Topology optimization comes as a reference to improve the first design and preparing the design for machining or other process, achieving cost effective parts. Figure 3.31 show the pipeline when doing optimization for different types of manufacturing [77].

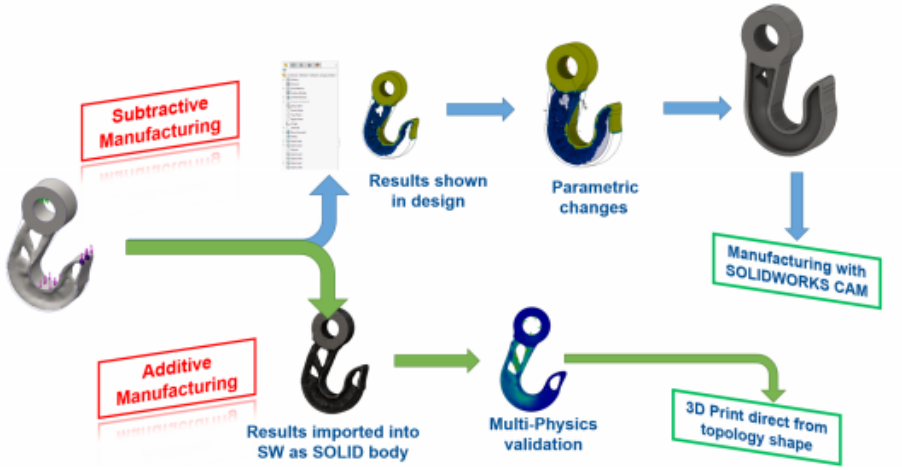

Figure 3.31: Pipeline to follow in different process for topology optimization [77]

3.5 Design for Manufacturing and Assembly

When designing a product the main concern of the engineer should be final cost and performance. The mindset of designing a system with the manufacturing in mind from the beginning is the main tool to achieve the lowest production cost. It is important to collect different concepts and understand design for manufacturing to achieve one of the main goals of this dissertation - low cost and easiness of fabrication. Quoting David M. Enderson: [78]

> *"Cost is designed into the product, especially by early concept decisions, and is difficult to remove later."*

It is now important to observe that design for a low cost is divided into two main concepts: design for manufacturing (DFM) and design for assembly (DFA). DFM is the tool that design teams use

to correctly select the most cost effective material and process. This mindset is to also produce pieces with the goal to ease manufacturing. Following DFM, is DFA. This tool main goal is to produce products with a small number of parts, ease of handling and assembly.

As such, DFM and DFA, both seek to reduce cost and shorten production time with less material and labor [79]. This tools should be used from the beginning of design. It has been shown that 80% os the cost of a product is determine after design and the later the stage in a the life cycle of a product the more expensive it is to reduce cost. Figure 3.32 shows how cost behaves with the life cycle of a product. DFM can be the difference of success in very competitive markets [78].

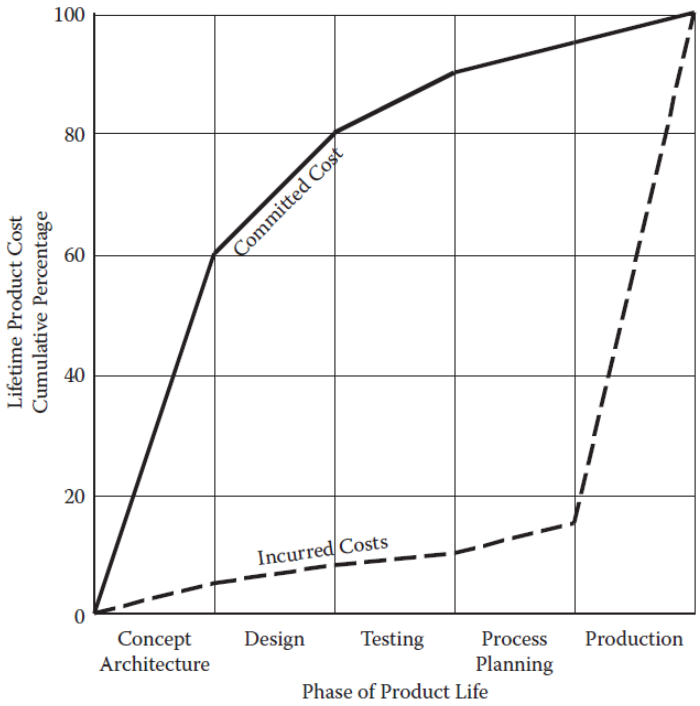

Figure 3.32: Cost behavior in the product life cycle [78]

It has been shown that designing a product focused on easy of assembly and fabrication has lower cost and better productivity than automating assembly. Efficient designs allow manual assembly to achieve cost effective prices against automated parts. It is estimated that for large volumes, automation can reduce cost in 86% and with DFA, manual assembly can reduce costs in 92% [80]. Figure 3.33 show how the upgrade in assembly simplicity affected production.

Thus, the sequence of design should be firstly concept design, followed by design for assembly with the goal of minimizing part count. The next step is the design for manufacturing and finally detailed design [79].

3.5.1 Design for Assembly

DFA, analyzes the design of the part and product to reduce cost during the process cycle. The main goal is easy and low cost assembly [81]. This can be achieved mainly by reducing the number of

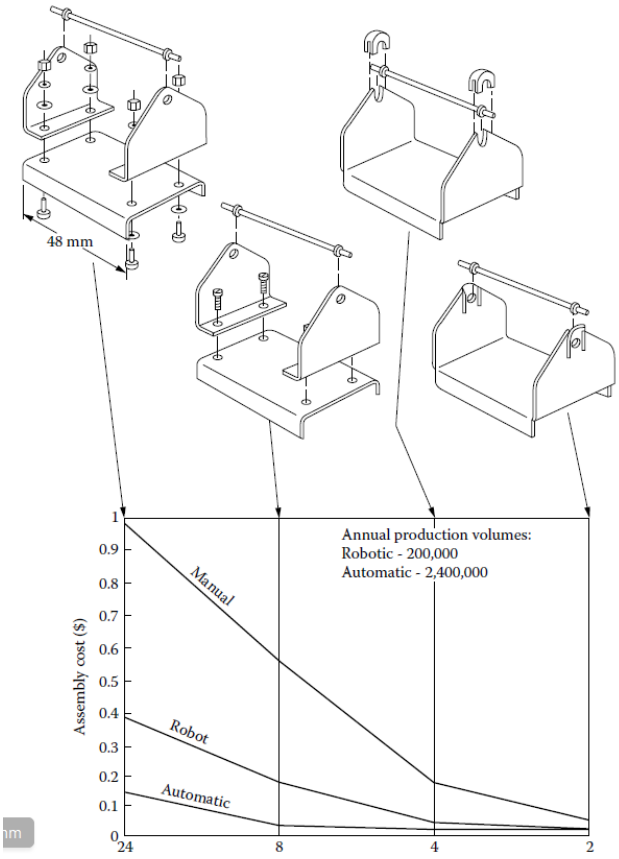

Figure 3.33: DFA as effective cost reduction tool [80]

parts necessary and the easy of handling parts: orientation, transport and how they are placed and fastened. This can be achieved for example by replacing screws and washers and use snap-fit mechanisms placed in a single part [82].

When designing for assembly, the process should be the following [79]:

1. Understand functional requirement, identify parts that can be standardized and determine part count efficiencies;
2. Determine practical part count;
3. Identify quality opportunities (mistake proofing);
4. Identify handling opportunities;
5. Identify insertion opportunities;
6. Identify opportunities to reduce secondary operations;
7. Analyse data for new design;
8. Benchmark when possible;

Figure 3.34 represents how the pipeline should follow to understand if the part is essential or it can be replaced or even suppressed.

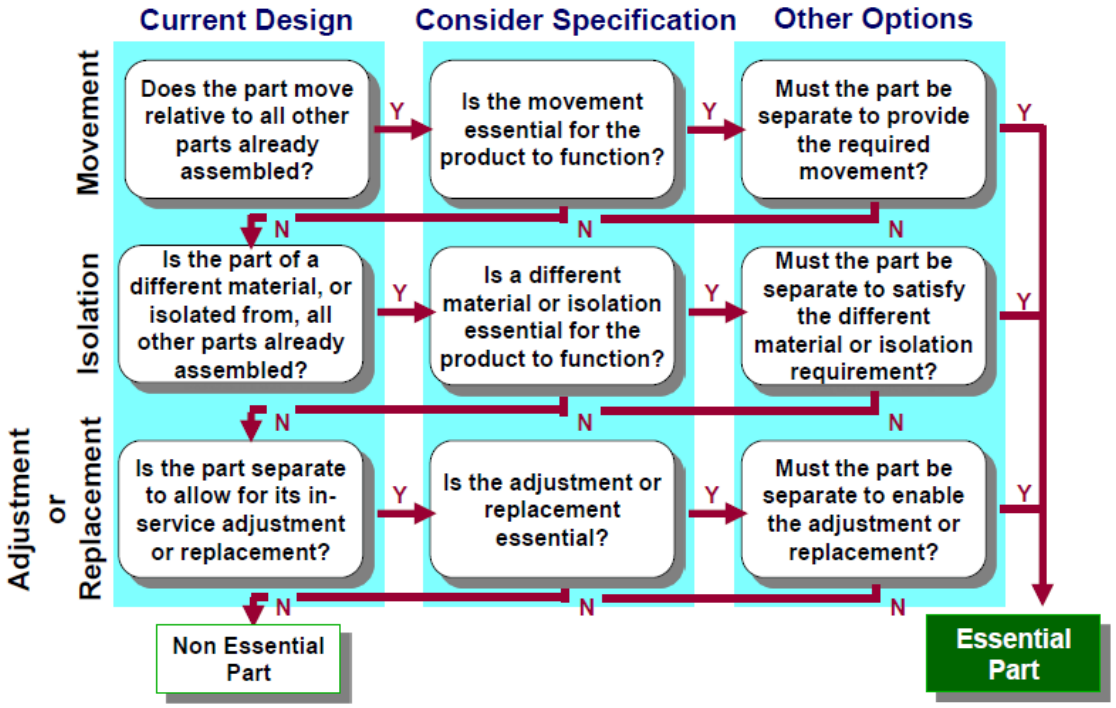

Figure 3.34: Pipeline of decision between a non essential part and an essential part [79]

As such it is possible to understand the part efficiency:

$$Part\ Count\ Efficiency = \frac{TheoreticalMin.No.Parts}{TotalNumberofparts} * 100 \tag{3.21}$$

It is therefore the percentage of essential parts that the project presents. A good efficiency goals is 60% or more. Another good metric for complexity is [79]:

$$DCF = \sqrt{\sum N_p \cdot \sum N_i} \tag{3.22}$$

Where N_p is the number of parts and N_i is the number of par-to-part interfaces and DCF is the design for assembly complexity factor.

Following this, it will be presented some important design guidelines for a good part handling and fastening.

3.5.1.1 Handling

- Parts should have maximum possible symmetry;
- If not symmetrical, than they should be obviously asymmetric;
- Avoid features that allow for tangling of parts;

- Avoid parts that stick together, slippery, delicate, flexible, very small or very large.

Some metrics used in handling parts are: size, thickness, weight, nesting, tangling, fragility, flexibility, slipperiness, stickiness, necessity for using two hand, necessity of grasping tools, necessity of optical magnification or mechanical assistance. It is possible to develop a scoring methodologies with this metrics [83].

As a goal to better understand and quantify part orientation, to help alignment and rotation two kinds of symmetry were created:

1. Alpha symmetry is the angle a part must be rotated about an axis perpendicular.

2. Beta symmetry that depend on the angle a part must be rotated about the axis of insertion.

Figure 3.35 represents this concept. It is possible, by using the methods time measurement system,

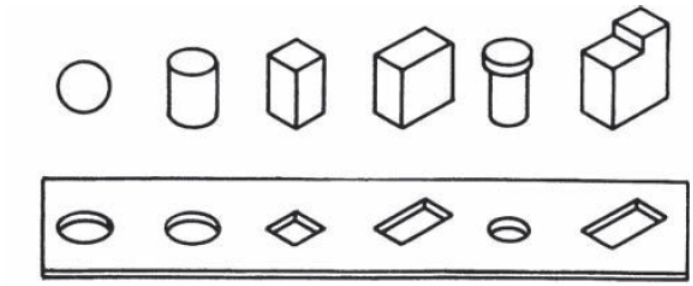

α	0	180	180	90	360	360
β	0	0	90	180	0	360

Figure 3.35: Examples of part and how alpha and beta symmetries work [80]

to divide parts into three different groups: symmetric, semisymmetric, nonsymmetric. The most useful parameter was the total angle of symmetry [80]:

$$Total\ angle\ of\ symmetry = \alpha + \beta \tag{3.23}$$

This value can describe the total handling time based on symmetry as it can be seen in figure 3.36. Another important factor that effect handling time is the part thickness and size. In the Work Factor system defines very well this concepts. Thickness in a cylindrical part is its radius and in non-cylindrical parts is the maximum height of the part measured from a flat surface. It has been shown that parts with 2 mm present no handling problems. Figure 3.37 (a) and (b) show how handling time relates to the thickness and major dimension of the part, respectively [80, 83]. Finally weight is also and important consideration when minimizing handling time. The total handling time is given by [83]:

$$t_{pw} = 0.0125W + 0.011Wt_h \tag{3.24}$$

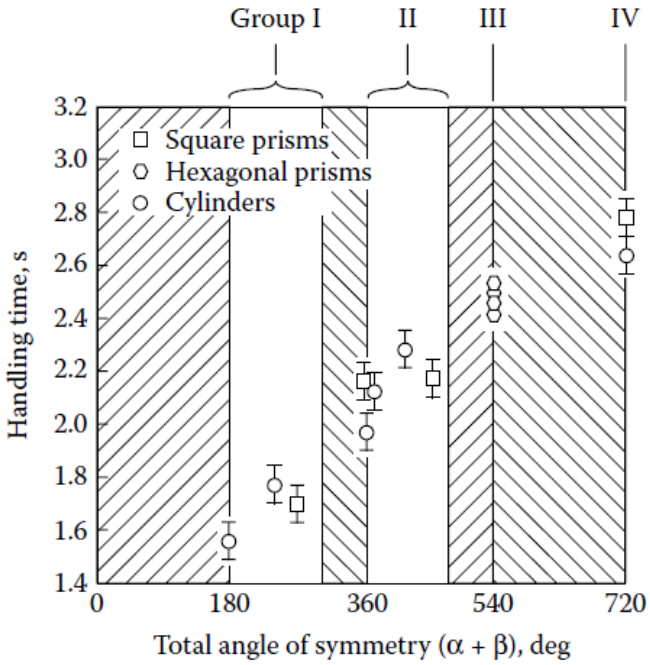

Figure 3.36: Relation between symmetry and time to handle the part. Shaded areas represent non existing values [80]

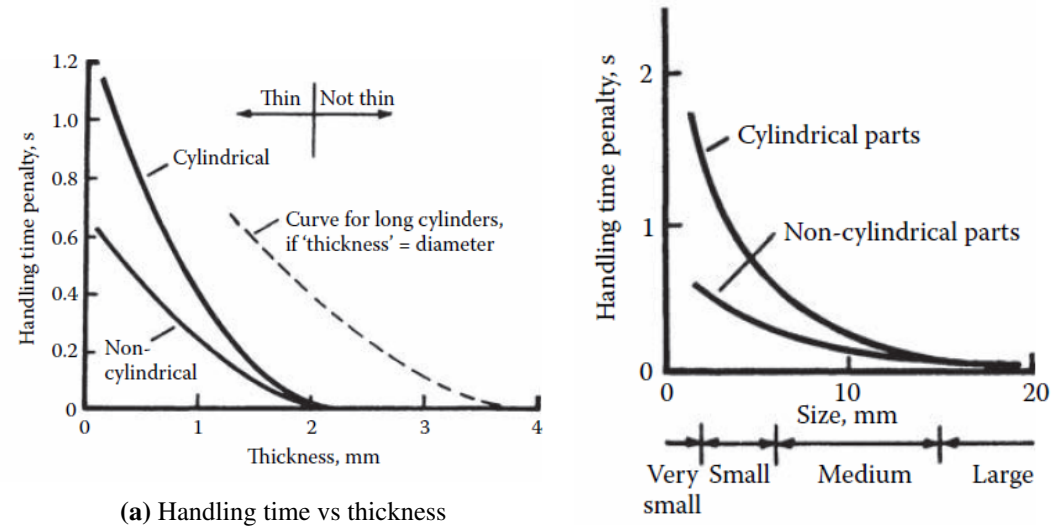

(a) Handling time vs thickness

Figure 3.37: Handling time vs major dimension [80]

Where W is the weight of the part and t_h is the basic time for handling a light parts with no orientation. The average value of t_h is 1.13 seconds. Finally other factors can be handling with two hand that can add a penalty factor.

3.5.1.2 Fastening

For ease insertion and good fastenings, some guidelines are [80]:

- Provide chamfers to guide insertions and use generous clearances;
- Use standardize and common parts;
- Use pyramid assembly to allow for progressive assembly over on axis of reference;
- Design for self locating parts, this means that a part is located before it is released;
- Understand the cost of different fasteners. In general from less to more expensive: snap , twist tab, river and then screws.

The main factors and metrics in fasteners are: accessibility of assembly location, ease of operation of assembly tool, visibility of assembly location, ease of alignment and positioning during assembly, depth of insertion.

It has been shown that clearance over 16 mm, will not affect engagement time, but the geometry and type of the screw will. Recessed holes are the best tool to achieve the best time, depending on the clearance.

Another factor is the tool used to fasten the screw. Allen screw proved to be the least time consuming, non power tool for an increasing number of threads. This can be seen in figure 3.38

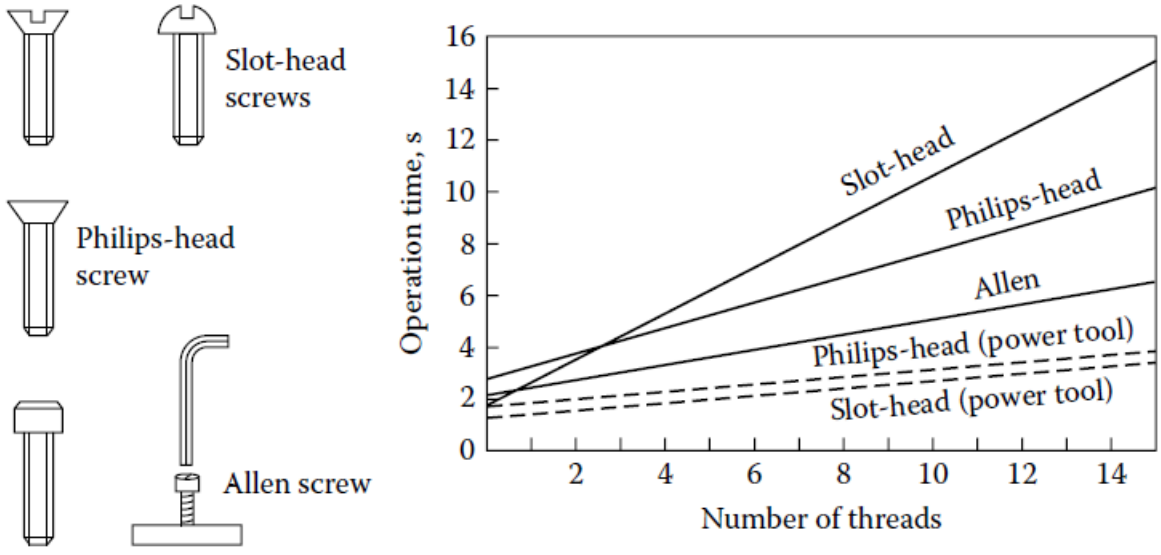

Figure 3.38: Operation time for different types of screws [80]

3.5.1.3 General Design DFA guidelines

Other guidelines can be used to increase efficiency are [80]:

- Avoid connections;
- Design so that access for assembly operations is not restricted;
- Avoid adjustments;

- Avoid over-constraints.

3.5.2 Design for Manufacturing

The counterpart of DFA is the Design for manufacturing. This methodology is used to improve the easiness of manufacturing reducing complexity and total cost. The main goal is to develop an clean and optimized product focused on manufacturability, quality and delivery [78].

When creating a product, standard parts should be prioritized and adopted. Using standard parts is important. This mentality can save money and availability. As such, another similar rule is to use as many off-the-shelf parts possible. This will improve cost and quality [78].

Overconstraining and tolerances are another important aspects of creating design for manufacturing. It is important to use the minimum possible constrains. They are expensive and well creating problems with quality control. Another important over-constrain is designing for unrealistic tight tolerances and dimensions. Tolerances should also be optimized and be chosen not relying on block tolerances or arbitrary assumptions. The designer should be aware of the wort-case tolerance situations. Taguchi Methods can be used to understand the relation between improving a tolerance faced with cost [78].

When using sheet metal as a main process for part fabrication, some special considerations are needed. It is important to design the piece considering the skill needed. This means that it is important to minimize demands on sheet metal manufacturing. Standardize sheet metal should be use to minimize supply chain cost and delays.

The different number of sizes used should also be minimized so that all can be made by the same stock and bought directly from the mill. This mentality reduces metal waste. When using shit metal tolerances should be too tight. Normally tolerances are between ± 0.5 mm and ± 0.2 mm and 0.127 mm for flatness. Warpage can be minimized by using annealed sheet metal [78].

3.5.3 Laser Cutting

To create a cheap functional prototype that is able to perform to the requirements laser cutting was mainly used for sheet shaping. As the nature of the microscope, being a non mass production product, and the scope of the project to upgrade prior solutions, this process came in handy as way to reduce cost. Laser material processing is a cheap way to create low volume series, such as proof of concepts and work alike engineering solutions. This is an high-speed and local process with a very high precision and low waste [84].

The laser process is non contact what eliminates part distortion, tool set-up costs are low to non existent. A small kerf allows for the maximization of usage of the metal sheet. This process also produces little or no thermal affects neither, generally, need machining operations [85].

Laser cutting and laser machining works by optical energy being absorbed by the interaction of electric field with electromagnetic radiation. Thus, the electron, if inside a solid body, will transfer the force of the interaction to the structure. When the flux of photons increase that will

cause the structure to vibrate enough to break it. Firstly it melt and then evaporates. The vapour is ionized, which forms a plasma what introduces Coulomb forces that will remove the material [86].

In sum, an high intensity laser beam is focused and heat a small interaction zone. This forms a kerf and high-pressure gas is injected in the slot to help removing material melted by the laser. The size of the kerf, the quality of the cut edges and the appearance of the cut determines the laser that will be used as well, the quality of the beam, delivered power and type of motion. In a mild steel, 2 mm of thickness, the normal kerf diameter is of 0.1 mm. The usage of Nitrogen gas has been shown to reduce roughness in 2 mm thick applications. Figure 3.39 show the different quality factor oh this process [85].

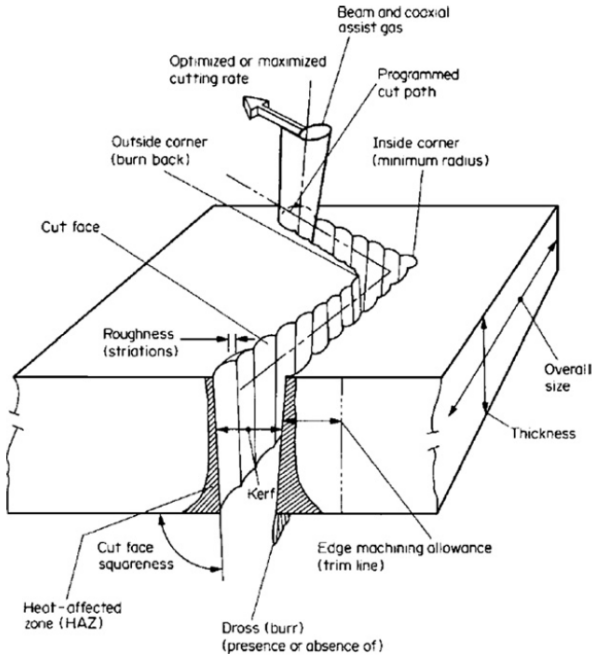

Figure 3.39: Laser sheet cutting quality factors [85]

The main limitations of this process are the maximum cut thickness and the nature of the material. Difficult materials for laser cutting are: [87]

- Metallic materials with high reflectively and conductive materials;
- Thick structural ceramics;
- Composite materials.

Aluminium is under the array of a widely used and difficult to cut material. Aluminium present high reflectively to the laser radiation and high electrical conductivity as well. This are the main factors that creates difficulties in cutting aluminium sheets by CO_2 laser. Another problem is the high thermal conductivity, that allows for rapid dissipation of the absorbed energy. This creates a large heat-affected zone in the material surrounding. It is also shown that during the process a film

of Al_2O_3 is formed that prevents the oxidation of the material underneath. This oxidation creates an uneven profile due to a behaviour to recast formation, that will promote fatigue cracking [87].

The best parameters found to cut sheets of aluminium are in Pulse mode due to efficient laser radiation and reduced heat input and thickness between 2 and 4 millimeters. It is possible to reduce thickness until 0.9 mm by controlling the cutting speed that relates directly to pulse frequency.

Chapter 4

Benchmark of the initial prototype

To be able to create a compelling product with quality it is necessary to prototype it. With this mindset it is possible to analyse mistakes, features improvements and run metrical test. This chapter exposes the prototyping and validation of the initial system created for CLARE by Fraunhofer AICOS. It is important to understand the main features of this system so that it can be improved upon and to redesign it without leaning over similar mistakes. A prototype was manufactured, tested and improvement opportunities were searched for: assembly, price, weight, size and performance.

In this same chapter, it will also be exposed the design iterations that were created as such some mechanical design validations. Thus, simulations and topology analysis will be shown as way to create a lighter end product. Considerations and metrics will also be explored.

4.1 Metrics, constrains and design considerations

To create focus while designing a product it is important to have constrains and metrics. This way it will be possible to have a guiding line when iterating the design with the goal to optimize all factors in play. The main objective would be to have the best metrics possibles while using the maximum of the constrains possible. To achieve a good design it is also necessary what type of system it is being developed. For example, the current microscope being developed has many small and lightweight components embedded in the XY stage. It is expected that this XY stage will be designing differently comparing to an industrial high payload XY crane present in many cargo docks or warehouses around the world.

The design considerations are some details that are useful to understand. In the case of the system that it is being developed is:

- All loads are very lightweight, therefore mechanical design considerations will only be addressed when seen necessary;
- A safety coefficient higher than two will be used in most situations.

- All components and parts are very extremely small;
- The main goal of the project is to create an engineering prototype, with manufacturing and assembly also in mind;
- It is very important the low cost of the device. It is expected that the actuators will be the most expensive part of the build;
- As way to be easy and inexpensive to prototype, laser cutting and 3D printing were the main manufacturing processes used.

Design constrains are the minimums that are needed to achieve and to consider that cannot be changed. The constrains of this project were:

- At least a linear translation in one axis of the XY stage of 40 mm;
- At least a linear translation in the the other axis of the XY stage of 20 mm;
- At least a linear translation of the Z axis of 5 mm;
- The distance between the objective lens and the sample surface should be a fixed distance;
- The distance between the condenser lens and the sample surface should be a fixed distance;
- Accuracy in the XY and Z axis should be maximum of 10 μm.

Finally, metrics were tough upon as goals. It is important to note that these metric will conflict between themselves. As a consequence, decision situations will arise making necessary more weight the different in the final design. For example, deciding between different actuators with very distinct weights. Using the heavier actuator will achieve better performance, but it will also increase overall weight of the system. In this case for example, performance is prioritize compared to weight. The selected metrics were:

- Mass in the XY stage. The lower the weight in this component, the faster the translation of each axis;
- General mass of the product. The lower the mass of the product, then less material is used, achieving a lower the cost. Being this product designed as a field microscope, as well, it is expected that it will also improve mobility;
- The footprint of the product. A smaller product will increase mobility, practicality and lower the total cost;
- Stability of the XY stage. The more stable this system is, the less prone to parasitic errors it is, such as stage drifting. This will increase accuracy and repeatability;
- Mass in the Z Axis. The lower the mass, the faster achievable focus. This is critical to reduce the time to analyse the sample;

- Stability in the Z axis. High stability of the Z axis it is very important for a fast and accurate system;
- Rigid structure. A rigid structure will guarantee that the product can survive in harsher environments, cheaper packing, shipment and misusage;
- Easy to assemble. As seem in chapter 3, a faster and easy to assemble product means a lower cost;
- Easy to manufacture;
- Part Count. The less number of parts used, in particular, non-standard parts, the lower the cost.

In sum, the main goals is to use less parts, improve performance without increasing overall price, compared to more expensive market solutions.

4.2 Initial System validation

This section will characterize the initial system that it was review upon. Fraunhofer AICOS team developed this first solution. The review of this system will be focusing on upgrading it and develop a new solution with better performance. It also creates a starting point to understand what are the main bottlenecks and failures. These opportunities will be exploited as a way to greatly increase the system performance and feasibility. This system was prototyped which was possible to accurately measure the metrics chosen and clearly see the bottlenecks.

4.2.1 Initial System characterization

This system is based on a XYZ stage. This means that all the axis will move one single module of the system. As such, in this mechanism, the Z-Axis servo pushed in the vertical direction a platform. This platform, in its turn will carry the XY table and illumination block. The illumination block consists on the LED, the condenser lens that goes underneath the sample.

On the other hand, the XY table main function is to guarantee the translation of the samples. This will allow for the smartphone control the table and take as many pictures necessary as the amount of minimum field of views needed to correctly analyse the sample. Figure 4.1 shows a general overview of this solution.

It is possible to observe that this solution uses an all aluminium approach. All components are made with aluminium sheets which thickness varys between 3 and 4 mm. The enclosure elements use a 4 mm thickness sheet while other elements use 3 mm. This solution measures 144 mm * 155 mm as base dimension and 354 mm in the Z direction. Due to the height, and the box-like structure, extra elements were added to give more structural rigidity. In this solution the optic tube is fixed and it is the sample that reaches to the objective as a way to focus. The condenser lens is put at a fixed position of the sample.

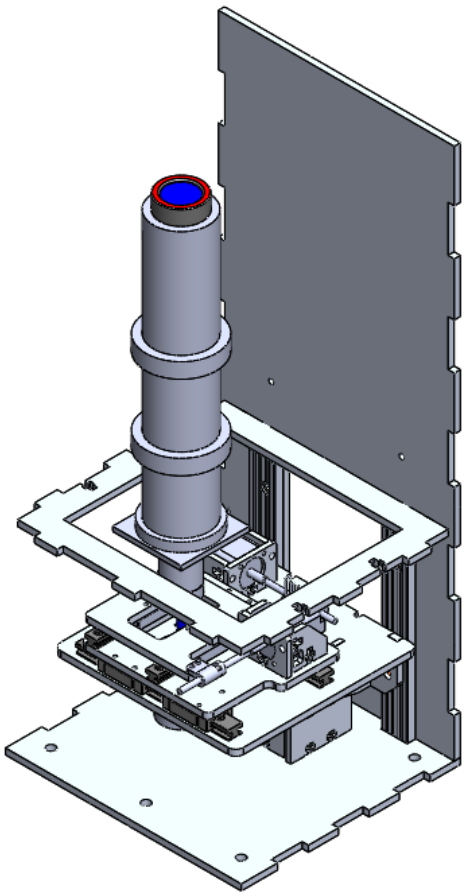

Figure 4.1: Computer assisted designed (CAD) representation of the initial system

4.2.1.1 The μmodule

In this systems, the μmodule is the most important mechanical part. This module condenses all the main movements in to one, the focus by translating the platform and the XY table. This system consists 3 on a linear actuator and 2 stepper motor with lead screw drive. The XY stage, uses IGUS® linear carriages series 07 and 09. The 09 series is used for the 40 mm movement and the 07 for the 20 mm movement. The latter movement has only two carriages being used instead of four. The XY table is over a platform. The thickness of the plates of the XY table and platform is 4 mm. The stepper motors being used are of low quality and are quite inexpensive, however they lack proper accuracy and can't reach high velocities, affecting the overall performance.

The following Z-axis is controlled by a non-captive linear actuator that it is fixed with by a box support. This linear actuator allow for better accuracy and high speeds. The non-cylindrical axis add another constrain to a DOF by not allowing rotation of the platform. The platform is guided by the low-profile IGUS® carriages. These carriages are connected to piece that on it's turn is fixed to the platform and to two triangular plates that serve as support. Figure 4.2 shows an isometric (4.2a) and side view of the module (4.2b).

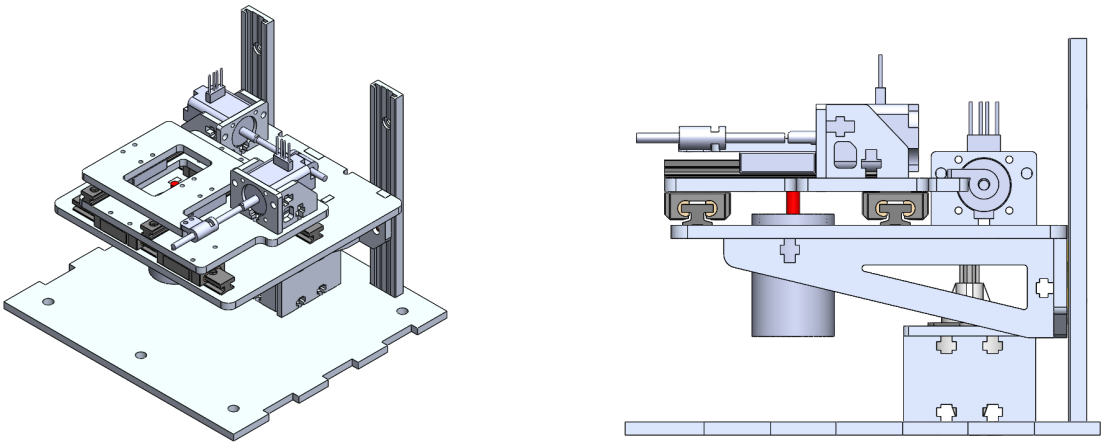

(a) Isometric view of the module

(b) Side view of the module

Figure 4.2: μmodule

4.2.1.2 System Flaws

Before manufacturing a prototype it was possible to notice major flaws that might compromise quality and performance. These flaws will serve as a starting point for redesigning a new system. Firstly, this design is not optimized for laser cutting. As seen in chapter 3, when using sheet metal, thickness variations should be optimized so that only the minimum size possible is used. In this system, many sizes are used. Due to the light nature of the system, this can be optimized. Slimmer sheet metals will also reduce general weight. Heavier plates and stage will also increase the moment of inertia, this will lead to a higher stage drift.

The usage of a platform bounds the utilization of different thickness sheet metals. It is possible approaching the platform to a cantilever beam,that due to the loads, it will generate moment that, on it's term it will create parasitic deflection where the XY stage is positioned. This will significantly increase the complexity of calibration and focusing, leading to a possible longer focusing time. Dynamic effort need also to be taken in consideration, with the fast vertical movement, this flaws will also become more prominent. The high amount of components and, in consequence, mass that the Z-axis has to push and pull will lead to low speeds, increasing further the time necessary to focus the sample.

IGUS® guides are selected due to their low price, good quality and the usage of non-lubricated and self maintaining bearings. As seen in chapter 3 the usage of polymers for mechanical pars in medical devices are strongly suggested. IGUS® parts present themselves as good choices for this systems.However, the main flaw observe is the usage of compact series in the Z axis. Even tough, this series is more compact saving fundamental space, it is a less robust solution, which means that it will handle worse, have a shorter life and prsent looser tolerances. The Z-Axis needs to be extremely accurate so tolerances need to be as thigh as possible to a sliding system. This compact guides are also prone to suffer from other manufacturing flaws. In the XY table, more sturdy version was used that guarantees tighter tolerances and heavier loads. It is expected higher quality

in this version as well higher work life. It is recommended to use if possible, always two carriages instead of one. This way it is possible to design the system while taking into account the drive force and the load.

The layout of the actuators are the most used in the industry as way to save space and create a better usage of space. The main problem of this layout is the creation of an eccentric driving force will, in its turn, create momentum that combined with low cost parts and motors can create serious accuracy problems.

Finally, it is important to observe that this system will create a lot of free space under the platform, that it is being badly used and it can be optimized so that will decrease footprint, weight and size. In this part one can notice the support for the linear actuator is very sturdy and unnecessary complicated and over-constrained.

4.2.2 Assembly of the Prototype

After buying, laser cutting and 3D manufacturing all the necessary pieces to build the solution, the assembly of the prototype began. During the assembly process, it was possible to observe many different problems and features that could be improved, that during the conceptual phase was harder to understand. These problems are typically due to quality process control and unexpected flaws from the manufacturer or pieces. It is common that when designing the product in CAD to forget about easiness to assembly and manufacturing limitations. In this prototype, not only that was observed as well other flaws. Figure 4.3 show the system opened, with the μmodule already assembly, missing only some few structural parts.

It was possible to notice that the "puzzle" fixation system is a good idea as an added constrain, but it was the part that most suffered with the laser cutting, creating rough edges and surfaces. This was considered that it was due the bad calibration of the cutting machine for the presented aluminium. As seen in chapter 3 aluminium is considered a complex material to cut under laser cutting and the cutting speed relates directly with the final result. Being this a prototype, it was used a faster speed to reduce cost. As such it is important to have a special attention to smaller details and try to avoid them if possible.

During the assembly, it was difficult to understand the correct place of which plate. This problem was observed in particular in the structural elements. The main plates were hard to discover the correct orientation and position. This problem was solved by creating some marks indicating the order of assembly and the side that it is in contact with the base. Other parts suffered from similar problems. This indicates that this product does no have interchangeable pieces and a symmetrical footprint. Adding to that, the non symmetrical parts are not very distinct leading to easy confusion. The assembly of the support for the Z axis actuator reinforced this symptom strongly. This support is composed by three different plates each one with two nut and bolt fixture. This is clearly a case where it exists over-constraining. Remembering chapter 3 it is only needed 3 points to fix a plane. Figure 4.4, show the different between larger features (4.4a) and smaller ones (4.4b). Figure 4.4b also shows an interesting fixation system between perpendicular plates so that brackets aren't used as much.

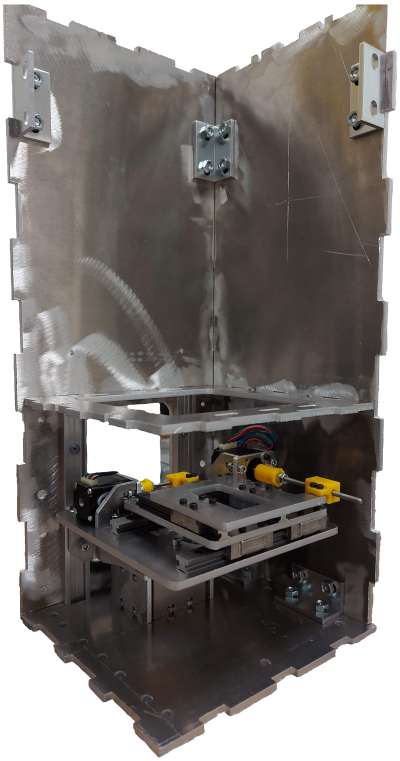

Figure 4.3: Assembled solution

(a) Larger detail plate

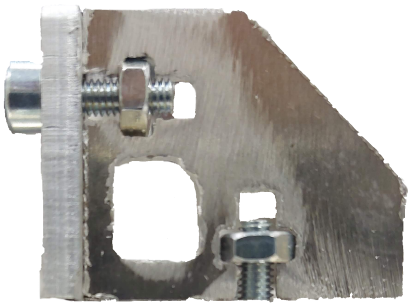

(b) Smaller details finish and fixation between perpendicular plates

Figure 4.4: μmodule

Finally, it was seen that the stock tolerances from the IGUS® carriages, were very loose. It was observed and by previous experiences, that IGUS® parts present the same sliding tolerance of about 0.1 mm. As such, series 09 had a better sliding that the 07 series. This factor can also be due that the 07 series only has two carriages. Rigorous design in the guide that carries the samples

is of utmost importance so that no reading mistakes happen. Another general problem was the location of the many standards parts of the system. This ultimately led to a high assembly time.

4.3 Summary

To conclude it is possible to observe that this system has many flaws and does not respond accurately to the proposed metrics. The flaws observed were:

- The usage of a XYZ platform creates displacement due to the cantilever approximation. This displacement will affect greatly performance, assembly and focus time;
- The solution uses many different thickness aluminium plates;
- Only two carriages are used for the translation of the sample;
- Loose tolerances;
- Non-accurate actuators;
- To many parts;
- Features that are hard to manufacture;
- Heavy mechanism that will lead to a slower system response and higher stage drift;
- Complex assembly that it is prone to errors;
- Confusion in the assembly due to the small difference between parts;
- Low stability and robustness of the overall mechanism;

Chapter 5

New design proposal

In this chapter it will be presented the new solution proposal. It will be explored the thinking process as well mechanical design considerations. Mainly conclusions will be shown, as such calculations will be presented if relevant or other certificated calculator results. For example, to determine the life of the linear bearings IGUS® online calculator will be used.

This chapter orients itself by presenting the *mockups* that were done, the reason for that solution and why they were discarded or improved. Parts that went under a topology optimization process, will be presented in chapter 8. This chapter will also try to predict cost, easy of assembly and other possible flaws of the general solution. Figure 5.1 shows some of the generations that will be explained under this chapter and how the evolution of product went from a conceptual stage to a final one.

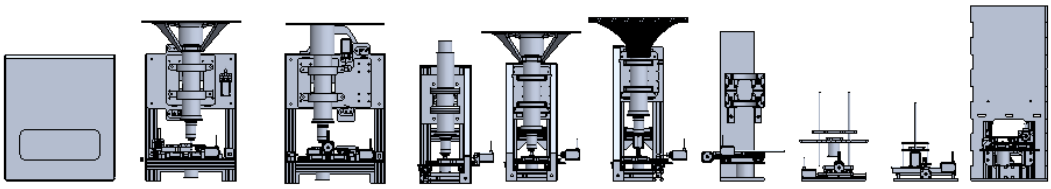

Figure 5.1: Different generations that will be explored under the current chapter

5.1 Design Methodology

When creating a product it is important to understand the different phases of product development. In this section a design methodology will be created as well explaining the different stages.

First, it is necessary to distinguish the difference between work-alike prototype and look-alike prototype. The first one is the typical engineering prototype whose goal is to achieve the required performance. In this prototype aesthetics, looks, feel and usability of the product is not a concern. This prototype is normally created by engineers and applies techniques of machine design to achieve the necessary performance of the product. The look-alike prototype is the prototype that takes in consideration the aesthetic, feel and how a user will approach the product. The culmination of both of this prototypes is the engineering prototype. This is the final prototype and the closest one to the final product.

The manufacturing process and material are usually selected in the end stages of the prototype not allowing for a correct design for manufacturing and assembly. As seen in chapter 3 DFM and DFA mentalities should be present since the beginning of the product development process. It is then fundamental to select materials and manufacturing process while making the mechanical design as way to improve cost.

The first stages of the design methodology developed are the market review, creation of metrics and constrains and the conceptualization. The first stage is the most common stage between all design methodologies. After having an idea of a product it is important to research what it has already been done, what can be improved and where not to fail. For example, if it was necessary to create a chair, a simple object, with a fast market research it would be an easy conclusion that using four legs instead of three is a better design practice. Three legs would minimize the cost, but using four legs would achieve a better performance and more comfortable design. Thus, conceptualization time would be save. Knowing beforehand what to avoid when creating a product creates time for further innovation and developing unique features to the iteration in study.

The second stage observed as observed in figure 5.2 is **Creation of Metrics and Constrains List**. This the first true step of creating the desired products. In this stage de developers create metrics and constrains to understand the performance and design goals of the product. The importance of this stage should not be undermined. To achieve good results is important the creation of goals and plan in accordance on how to achieve them. In addition, this stage is where prioritization happens. In many product is impossible to achieve all goals simply because they can contradict themselves. For example, trying to achieve the lowest cost possible while trying to have the best flexural properties on a specific part by using an extremely expensive material can lead to contradiction. Thus, it is important to create metrics, performance constrains, plan how to achieve them and prioritize them.

The final stage of this initial subsystem of the developed design methodology is the conceptualization. In this final stage designers and engineers usually work in symbiosis trying to conceptualize and sketch different ideas of an minimum viable product (MVP). This stage is characterized by the creation of different mockup up designs, having initial ideas on how to tackle machine

design, rough dimensions. It is normal in this stage to interact with out-of-box or novel concepts since conceptual design modifications can get expensive down the path of product development, as seen by the rule of ten seen in chapter 3.

Figure 5.2: First three stages of the created design methodology

The next subsystem that should be followed to achieve an theoretical MVP has three different stages: proof of concept, design and finally the creation of a theoretical MVP. This is the stage where a first product will come to life. This theoretical MVP will be a unrealistic idea of the project that the main goal is to achieve most of the constrains as optimized as possible.

The subset starts with the proof of concept. The proof of concept stage ask the question: will it work? As such, small prototypes can be done to test different systems and mechanism to prove that the final product has a strong possibility to work as expected. The proof of concept can be taken as well as a more market driven stage where queries can be provided to a general public to understand the desirability of the product and to attract investors and partnerships as well.

As observed in 5.3 the second stage of this subsystem consists in a multitude of different paths to take. If the proof of concept stage is passed with success thnn the conceptualized product can begin the transformation to a working device. In this stage is where the machine design is taken in consideration and all of the important mechanisms are design according to the settled constrains. Many enterprises in the development of a product do not consider DFM and DFA in their process. Introducing these mindsets early on in the product development process is fundamental to achieve a low-cost, low material usage and help saving capital in future development stages. Thus, material design and selecting the manufacturing technology of different parts are important to be inserted in this stage as well. In the eventuality of these factors be iterated in the future, parts will already be designed with a low-cost, low waste mindset.

Finally the culmination of all of these factors result into a theoretical MVP. This is the ideal product that is incredibly complex to assemble or to manufacture. In the case of DFA and DFM have already been applied in a large extend in the design process then this theoretical MVP will be closer to a work-alike prototype.

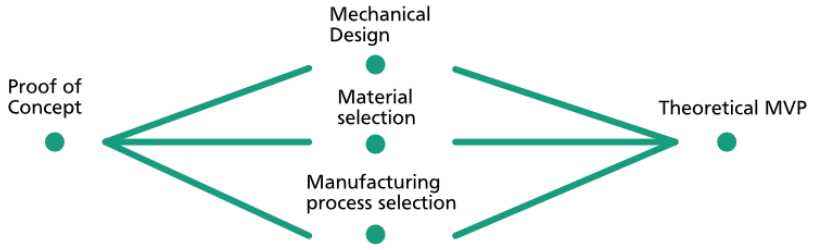

Figure 5.3: Second three stages of the created design methodology

Following this subsystem the product development current is divided into two important rivers: the work-alike prototype and the look-alike prototype.

The first will improve the mechanical part of the theoretical MVP and the second will create the design of the product that consist on aesthetics, usability, total weight, portability and the feel of the product. Even thought two different paths were created, it is important that exists cross communication between the both. This is the peak of the product development where all type of professional are working together on the creation of a final product.

Starting by the mechanical and manufacturing design, the stages observed in figure 5.4 are the the detailing of the mechanism. This stages serve to apply better and in depth DFM and DFA methodologies as ways to reduce cost and improve assembly. The main goal is to create a product that work and it is also easy to assemble and manufacturing. Finally, some parts are looked over again as case studies to improve manufacturability and performance. This parts can be suffer a FEA process to simulate the behaviour in the work conditions. It is typical to iterate on this specific parts as ways to reduce weight, cost, improve performance and optimize for the metrics created. Finally the culmination of all of this sub-stages is in a work-alike prototype. This is the prototype that resembles to the closest the functioning of the final product.

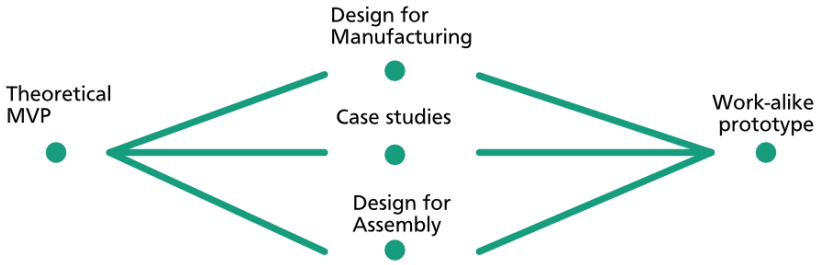

Figure 5.4: The work-alike path

The second path focus on product design and usability. From a theoretical MVP is it normal the realization of the look-alike prototype. Some of the stages that this path takes are: Improving usability, branding, improving aesthetics as seen in figure 5.5.

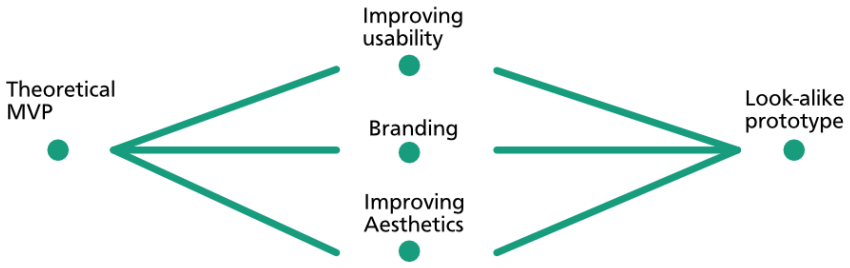

Figure 5.5: The look-alike path

Finally, the combination of the look-alike prototype with the work-alike prototype creates an engineering-prototype. This prototype is the closed to a final product possible. Few iteration can still be made to better perform with the manufacturing regulations, but this prototype will be very

similar to the final one. For an example, this stage is where it is custom to create small series to test the market once more. It is also common to use this engineering prototypes to showcase in industry conferences or to be used by the marketing department.

5.2 First Mockup & Second Mockup

The first and second mockups are conceptual evaluations of different ideas. These mockups serve as representation of different features that should be added, edited or modified. The main difference between the first mockup and the second is the usage of standardize parts and refinement in concepts.

The first concept brainstorming ideas appeared due to the necessity to bring the XY stage to a more stable, static position. The main goal with this is to be able to achieve great repeatilibity, accuracy and resolution. Occurring that focusing time is the bottleneck of the overall system performance, then the main dogma that this thesis defends is that the XY stage should not move the Z axis.

The XY table is of extreme importance and the module that carries the most of the weight and parts that directly influences the performance and velocity of analysis. In the position where the XY is carried over the Z-axis, not only it will be hard to achieve higher resolution required for the focusing system, misalignment will suffer with inertia as well. Higher inertia due to a high number of components moving at once will create more load strain in the carriages. As such keeping the XY stage in a fixed base would improve all kinds of performance metric, leaving to the Z-axis only one function.

Focusing the Z axis on only one function will present many valuable improvements that will be explored in further chapters. In this conceptual mockup, the XY table would shift the illumination module around under a fixed samples. Then the second step would be the translation of the illumination module over the Z-axis. The concept of translating the illumination module would achieve great velocities and repeatability over any other conceptual choice. Figure 5.6 shows the CAD representation of the different concepts. This Z-axis will be defined by three different point, two shaft linear guides and a linear step driver motor.

This concept created space for the creation of many more ideas. The usage of piezoelectric chips and stacks were explored ins this phase to increase resolution. The main problem with using piezoelectric chips and the complemantary compliant mechanism is the addition of complex non-linear behaviour that would requires expensive electronics to correctly function. Non-linear behaviour is also prone to possible unnecessary flaws. For example, suffering from the piezoelectric hysteresis effect.

The main advantage of this concept is the high reduction in weight, part count and size. It is expected that this stage would be extremely fast and stable. This system also allows for easy assembly by mounting all parts in a simple base and assemble it with the rest of the structure. Due to the stability of being on a base, it is also expected better vibration support as it can transmit it to the base. This way dynamic factors can be minimized as well due the lower inertia. The

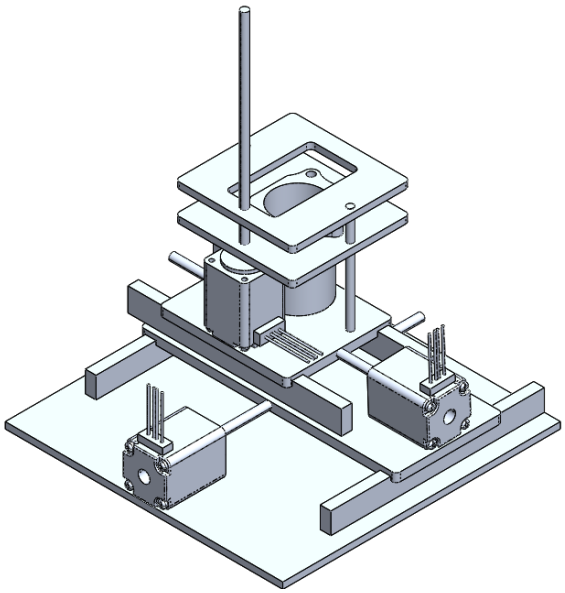

Figure 5.6: CAD representation of the first version of the product

comparison in size between the original XYZ table and the first mockup stage can be found in figure 5.7. The second mockup is an evolution in this concept, but it can be considered conceptual

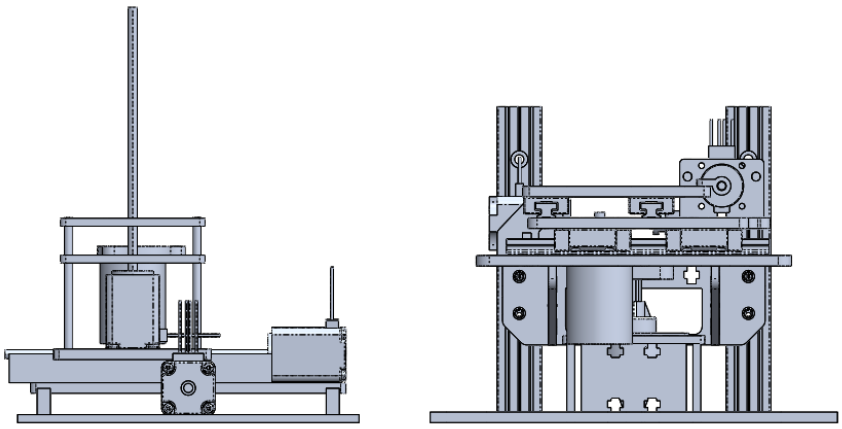

Figure 5.7: Size comparison with the original stage

as well. In this second mockup, early conceptual prototypes were created. The principal evolution in this mockup was the deepening of past explored ideas. The idea of having the illumination module translating during the Z-Axis, with haste was proven containing many conceptual flaws. The main problem to the translation of the Z-Axis is the need to allow the independent movement of the illumination module with the sample. Thus, in the XY direction only the sample should move. The main problem presented when only the illumination module needed to translate and the samples should be fixed in the vertical direction. The challenge present is due the layout of having the sample holder above the illumination module.

Even tough these two initial mockups present major conceptual flaws, both display fundamental ideas and dogmas that were explored in future version of the product. To solve the presented problem, the solution was to create space in the the plate that holds the illumination module to allow the translation in the XY direction of the vertical guides that support the sample. A forklift-like plate was also created. The goal of the forklift part is to be actuated, when needed, by the the lead screw and translate in the vertical direction the illumination module without moving the sample holder. To allow a correct translation in the vertical direction of the sheet that holds the illumination module extra features were added. These features will translate in the wall of the structure. The mockup in consideration can be observed in figure 5.8.

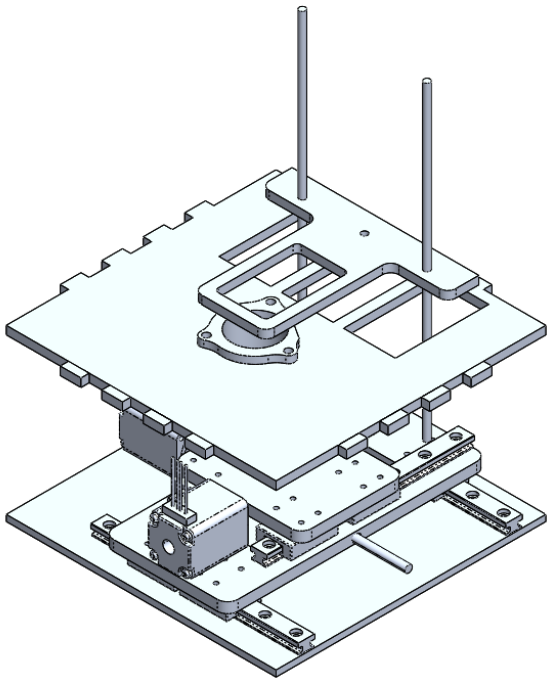

Figure 5.8: Second iteration of the conceptual mockup

This solution presented more problems than answers. The layout problem was fixed but now new problems arise from the solution. The first major flaw observed with this solution layout is the number of extra parts needed to hold this solution. For example, the plate that holds the illumination module is heavy and unnecessarily spacious with the only goal of holding the illumination module. Thus, making this solution less attractive that the original one. The usage of a forklift part to lift the plate that holds the illumination module creates weight leading to a not so faster vertical focus movement. This slow movement would be also affected by the high friction between the guiding features and the adjacent space in the wall where they would slide. To observe test this concept a small scale polylactic acid (PLA) model was created as it is possible to observe in figure 5.9. It was concluded that this concept layout needed to be discarded due to the high friction and difficult assembly.

In the end, the main flaw of this system is the fact that the translation of the guides uses unnecessary space and it will also suffer considerable dynamical loads. Shaft guides are precision

devices that need to be correctly mounted and suffer minimum displacement as possible. This concept would lead to flexural and bending, leading to an eventual unpredictable parasitic error of the sample.

Figure 5.9: Proof of concept of the second mockup

5.2.0.1 Summary

To sum up, this layout was discarded due to many flaws. However, it presented an extreme important dogma to follow: the weight in Z axis should be minimum and the respective translation should be constrained only to one function. Aiming to achieve a fast and repeatible translation, then the Z axis should only be designed for the focusing mechanism. Another important factor is the usage of a base for the XY axis to give a sturdy and rigid place that allows for a faster and safer movement. The idea of adding low cost piezoelectric actuators with 3D manufactured compliant mechanism were swiftly discarded because it introduced non-linear behaviour to the mechanism.

5.3 Third Iteration

With this version is the version where the layout of the final product was finalized. This version works more as a proof of concept version where it is shown the final layout, how the mechanism is predicted to work and some final conceptual features. This iteration is the middle term between conceptual versions and work-alike version.

Observing the first two mockups it is required that the illumination module is fixed at a certain distance from the sample. Thus, the new base layout would have a static base at a certain height and fixed at the side walls while having the illumination module under it. The empty space created by the illumination module would prove valuable space for the fixation of all the required electronic components. Thus, this space would not be empty space. In addition, having this space in the base allows for faster disassembly of the electronics if needed maintenance. One problem of the

original product observed in the last chapter is the complex disassembly in case of need to change parts.

It is not expected that having the XY stage fixed at a certain height will interfere in the performance and precision. If correctly designed flexural displacement can be minimized as well vibrations, leading to a similar performance just as it would supported in the base. In this layout, only the sample has to suffer X-Y translation, leading to a very fast stage. It is important fast X-Y stage since this parts will translate 40 mm in one direction and 20 mm in the other. Since dimensions are not equal, it is important to decide which direction will carry an higher load. It was decided that the 20 mm direction will carry higher load (the weight of the other axis above and the sample), so that an higher inertia moves less creating smaller dynamic efforts.

From the initial mockups it was transmitted the idea that the Z-Axis should be fast and focused on one movement only. Making the XY stage independent of the Z stage is a good design practice that allows an independent focusing mechanism from the mechanism that translate the sample. Since both require different velocities and precision, then if they are separated it is easier to design and guarantee better performance. Another factor is that, it is easier to assemble, by using different modules. In this layout, XY-Z, it is possible to design the mechanisms for the different necessities of each module.

As such, the proposed system has the optic tube to be the driven as the focusing system. Inspired by the Autoscope UW project and other products studied in chapter 3. It is common to use the Z axis as only auto-focusing system. Having this change will lead to excellent accuracy, better assembly and a more stable and repeatable results. In terms of velocity it depends on two factor: the actuator used and the amount of mass being translated. Independently of higher mass, the actuator can be upgraded, if required, to achieve the desired speed. The higher cost of a better actuator comes with the exponential better performance of the focusing system, allowing the best performance possible. Another challenge will be to move the cellphone. It is important to remember that Z-axis will have a maximum displacement of 5 mm. Moving the the optic tube also allows for the creation of a platform for future products. Furthermore, having the axis in the optic tube allows for the creation of the most compact and accurate product possible. Figure 5.10 shows the third version before evolving for the fourth version.

The main flaw observed in this product was the usage of two different feature: every part is made of sheet metal and the linear actuators used present vibrations that are difficult to damped in a low cost system.

The usage of a complete sheet metal enclosure can be something typical in many machine design. In the correct situations and product it can be great way to create an sturdy enclosure that can withstand rough environments. In this situation, sheet metal is being used as a structural part. In this particular low cost situation, sheet metal was presented as an cost effective solution. While cost effective, it is not the best part to use as structural chassis due to the section rigidity. It will lead to a heavy body. While compact, sheet metal does not guarantees perpendicularity between the optic tube and the sample. This problem would be solved by increasing the thickness of the sheet metal that would leave to higher weight and higher cost due to the use of different sheet metal sizes

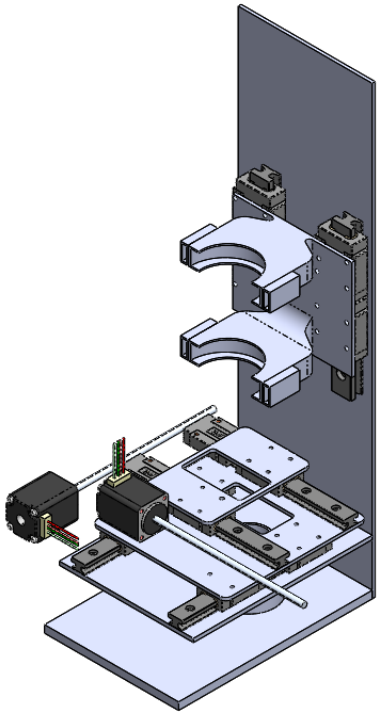

Figure 5.10: Third iteration of the product

and the use of more material. The number of part required to mount correctly of the sheet metal (in case it was used bending) is incredibly high. As a fail safe, it is important that this structure is extremely rigid so that no misalignment happens during assembly and functioning. Therefore, using a sheet metal body would prove inefficient and costly in the long run. The solution that will be explored will see the creation of a sturdy chassis with extruded aluminium profiles. These profiles are used in all types of machines, presenting a very cost effective solution for the rigidity required. The usage of aluminium profiles will also allow and easier assembly. Standard parts should be prioritize as seen in chapter 3.

The final problem observed was the usage of lead screw actuators. Many solution in the market present the usage of lead screw actuators due to their effectiveness compared to the total cost. It was observed that using lead screws in an lateral position as seen in figure 5.10 can lead to seriously problematic misalignment. Another observed effect was the major displacement caused in the screw shaft due to the vibration. Normally, manufacturers don't observe this problems due to the usage of expensive guides that do not suffer with misalignment and other parts that mitigate all the problems that come with the usage of lead screws. In this solution, where most of the parts are made by sheet metal to keep the cost down, it is required to change the orientation as well the actuator type. In chapter 5.4 the solution to this problem will be explored further.

5.4 Fourth Iteration

This iteration of the product design is considered a middle phase of the work-alike prototype where concepts are defined and mechanical design starts to ensure the quality of the device. Due to the iterative nature of machine and product design, this step of the process is the one that suffered the most iterations. In this dissertation only major steps will be presented with the final results for each mockup as well.

This iteration can be considered the most important one. In this stage conceptual will be transformed in reality. Many features will be added that will guarantee the best performance of the device. This is the phase where the guides being used will be decided, the product chassis designed and the actuator chosen. To design the linear guides, an online calculator provided by IGUS® will be used.

5.4.1 Linear guides

Choosing the system for the linear guides and projecting it is not an easy task. Before being able to decide which enterprise to have as supplier of these parts, it was necessary to decide which driving and guiding mechanism would the system use.

5.4.1.1 Deciding the driving and guiding systems

Referring to the tables in the chapter 3.3.3, they will be a good deciding matrix. Firstly it is necessary to concern economic reasons. Therefore, it is necessary to decide a driving mechanism that will achieve great performance without compromising the price. Low cost is a priority. As such Ironless and Ironcore linear motors were immediately off the table. These type of mechanism have incredible performance, outperforming the minimum needed for the system. Even tough, greatly outperforming is not a bad parameter, this would come with a colossal increment in cost. Thus, reinforcing the idea that it is necessary to achieve the minimum performance metrics required with the lowest cost possible.

Piezo linear motor or actuators can range widely in price and the main ability of these systems is the ability of great resolutions due to the piezo effect. The biggest problem is the fact that the travel range of this type of mechanism are very small, normally under 1 mm. Larger travel ranges require amplified piezo actuators, still only ranging 5-10 mm and with astronomical prices. As such this solution might be interesting to apply in compliance with another driving mechanism to achieve, in a cost-effective manner, long range and nanometric precision. Nanometric precision could be useful as way to achieve the most accurate focus possible, with the down side that might injure focus time.

Finally, the two biggest contenders, and the most common ones, are the Lead Screw or the Ball Screw Screw. Both driving mechanism are very similar in terms of error performance and stability. Ball Screws present less backlash and have less wear. Ball screws are usually used in industrial 3D printers or CNC machines that also requires better load capability. On the other

hand, ball screws are more expensive and are not, in general, as precise as lead-screws due to the nature of the system.

After deciding the driving mechanism it is possible to quickly decide how the guiding will be done. Flexural and Kinematics guiding are left out due to the low range they present. Air guides are very expensive and require extra equipment to have pneumatic compressed air system. All other three guiding systems are very similar. The main advantage of using linear ball bearings or plain bearings is that they are more common and less expensive. The main downside is that with higher loads, working life is greatly decreased. This will not be a problem with the low loads that will be considered. To sum up, lead screws were used as the driving mechanism and ball bearings with a rail will be used.

5.4.1.2 Actuator choice

Choosing the right actuator is the most important decision of the project. The actuator is the most expensive part of the project, therefore it is important to decide the correct one. When choosing the actuator, performance is the decisive factor. It is of utmost importance that it can achieve a timing lower of 10 minutes. The second most important factor is precision, resolution and repeatability and finally cost. The engine need to be extremely precise. Other XYZ stages in the marked use screw drives and piezoelectric actuators. There are some more expansive solutions as for example ironless motors.

As seen in chapter 3 piezoelectric actuator, due to the small travel distance are used in combination with other long range actuators such as screw drives. As a way to reduce costs, complexity and non-linear effects, piezoelectric actuators were left out. Thus, to achieve the required resolution, it was chosen an actuator the presents a vey fine resolution and over that, *microstepping* was applied. By default, stepper motors are divided or in 1.8º steps or 200 steps per revolution or in 0.9º steps or 400 steps per revolution [88]. *Microstepping* is a feature that certain drives allow that divide the normal step of a stepper motor in to hundreds or thousands of steps. this feature allow for better resolution with the cost of available torque [88].

Haydon Kerk is a well know supplier of actuators used in medical devices. They produce and sell actuators of a small fototage, with high rated torque and that can achieve great resolution. Their smallest size is NEMA 8, where the footprint is really small. Some actuators of this series can achieve maximum recommend thrust of 45 N for the maximum load recommended and resolutions of 1.5 μm. This type of actuator is more than ideal for our system. In addition to this, with *microstepping* then, it is expected that, very refine resolutions can be achieved [89].

Screw drives actuators can be captive, external and non-captive. Each of these build solutions present different pros and cons. Non-captive actuator allow the screw to move linearly through the actuator. This class allows for wide lengths of strokes and can tolerate misalignment. Another advantage of this motor is the possibility to slide attached to the carriage while having the screw is fixed in position. Another advantage is that this type of actuator allow for multiple actuators in the same screw. This is the cheapest solution [89].

The most common solution is the external actuator. They allow for wide strokes with precision due to the locked motor. An anti-backlash nut rides the shaft supporting and carrying the load. The main disadvantage of this system is that long screws will, at some length experience a resonance point. In some cases, vibration and noise will be enough to cause lost steps.

Finally, captive linear actuators is available for short strokes and it is a very sturdy solution. This mechanism is simple and present no rotation mechanism. This systems are extremely powerful and precise and combine the best of external actuators and non-captive actuators. The main downsides are cost, short stroke, up to 50 mm and large assembly set-up.

The decision was made between external and captive actuators. Those were the only that could achieve the necessary resolution and repeatability required for the system. In the end, the captive actuator was chosen to be able to achieve the best resolution possible while keeping the repeatibility high. This solution presents better dampening of vibrations as well.

5.4.2 Mechanical Design

In terms of mechanical design, guiding systems have many different parameters to consider: assembly accuracy, life of the bearings, lubrication, load capability, tolerances, layout and preloading. Notice that, not all solutions present high tolerances, pre-loading and lubrication and dust free features.

The main factors that decide which guides and correspondent series to use are the work life (static and dynamic) and the load capability. Layout is also very important, it will influence every other factor. As such this decision should be first to do.

Guides can divide and multiply. The layout can be one rail and one carriage, one rail and two carriages, two rails and two carriages, two rails and four carriages, two rails and six carriages and so on [90]. The most optimized layout is using only two rails and four carriages, more can be used if needed to carry higher loads without increasing in size and series of the carriages. Using less four carts are not recommend due to the influence of rolling, pitching and yawing moment in the dynamic equivalent load. Therefore, when using four carriages, moments cancel each other, achieving a more stable, durable and robust system. The present of other moments will also create unnecessary oscillations that will lead to errors and uneven wear of the bearings. Thus, only radial rigidity is needed to be taken in consideration. Leaving this layout the most common and recommended one, when designing an accurate guiding system [90].

The following step is to consider basic static load rating and determine rating life. This will be and important factor to decide the series that will be used. In general, bigger ball bearings can undergo larger compressing stresses and have better durability. When designing for life, it is normal to consider 100 km or 50 km, that it the most common for most applications. Larger and heavy applications would be expected the necessary maintenance. Bearing life depends on many factors: on the hardness of the rail, the basic dynamic load rating and other coefficients that can be used for safety and operational condition. Thus, rating fatigue life is given (L) , in kilometers

by [90]:

$$L = \left(\frac{f_h \cdot C}{f_w \cdot Fm} \right)^3 \tag{5.1}$$

Where, f_h is a coefficient that depends on the hardness of the rail and f_w is a coefficient related to the load. Rails must have at least an harness of HRC58 to 62, otherwise it will effect the general rating life of the bearings. It is normal to observe anodized aluminium shafts or martensite steel being used [90].

Another rating of life is basic static load rating. This rating is used as safety factor to observe f the linear bearing can withstand the load situation. It can be expressed as:

$$fs = \frac{C_0}{P_0} \tag{5.2}$$

Where C_0 is the basic static load rating and P_0 is the load combination rating. This expression can also be written in the terms of moments.

In terms of displacements, load and moment in the carriages, it can be perceived by the free body diagram represented in figure 5.11. The equation for the normal force in each carriage is

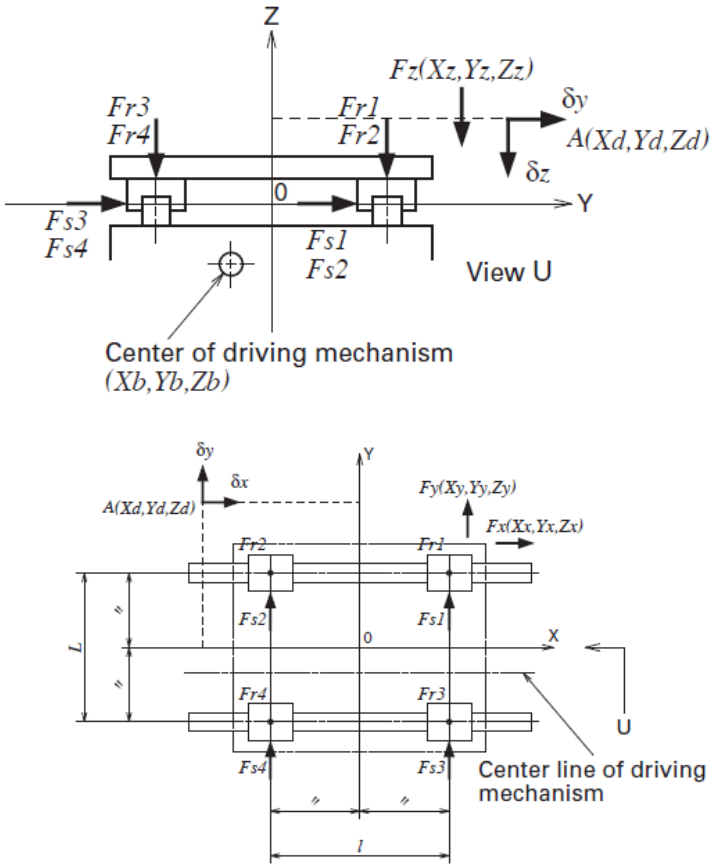

Figure 5.11: Free body diagram of the chosen layout [90]

given by, the total load divided by four carriages and a combination of moments, one related to the moment created by the driving and axial forces (yawing moment) and the other for rolling

moment [90]. The expression of the first carriage is given by (other carriages follow a similar combination):

$$Fr_1 = \frac{\sum_{k=1}^{n} Fz_k}{4} + \frac{M1}{2L} + \frac{M2}{2l} \tag{5.3}$$

Where $M1$ is the yawing moment and $M2$ is rolling moments. It is possible to conclude that the distance L and l are of extreme importance. As a general rule of thumb, the distance of the driving force to the reference fixed rail should be maximum twice of the distance between carriages in said rail [45, 90]. This rule is confirmed by equation 5.3.

Lateral forces even if not present, can be created due to pitching moment:

$$Fs_1 = \frac{\sum_{j=1}^{n} Fy_j}{4} + \frac{M3}{2l} \tag{5.4}$$

As seen this also depends on the distance between carriages. Rolling moment is giver by:

$$M1 = \sum_{j=1}^{n} (Fy_j \cdot Zy_j) + \sum_{k=1}^{n} (Fz_k \cdot Yz_k) \tag{5.5}$$

It is possible to conclude that rolling moment is created by lateral forces in each cart and non centered loads. Yawning moment is given by:

$$M2 = \sum_{i=1}^{n} \{Fx_i(Zx_i - Zb)\} + \sum_{k=1}^{n} (Fz_k \cdot Xz_k) \tag{5.6}$$

Yawning moment is given by the difference created by driving force and other axial forces plus moment created by a non centered normal force. It is important to notice that in a situation of vertical carriage, this moment would be extremely important due to the significant presence of gravity [90]. Finally, pitching moment if given by:

$$M3 = \sum_{j=1}^{n} (Fy_j \cdot Xy_j) - \sum_{i=1}^{n} \{Fx_i(Yx_i - Yb)\} \tag{5.7}$$

Pitching moment is created by a non centered driving force and lateral forces that migh be present in the system.

Displacement in the normal direction of the plate is given by:

$$\delta z = \frac{\sum_{k=1}^{n} Fz_k}{4 \cdot Kr} + Xd \cdot \frac{Fr1 - Fr2}{l \cdot Kr} + Yd \cdot \frac{Fr1 - Fr3}{L \cdot Kr} \tag{5.8}$$

Where (Xd, Yd, Zd) are the coordinates of the measured point and Kr is the radial rigidity. This expression creates even more value in the span of the rail and of the carriages, as way to improve vertical displacement without having to increase the thickness of the sliding plate [90].

Tolerances in sliding systems can be complex to control and to achieve a nice and smooth movement. Generally, as tolerances are tighter and exact, cost increases exponentially. Achieving very exact tolerances required more fabrication steps, better equipment and skilled staff. Thus, it

is normal that many manufacturers don't present many tolerances options. In common manners, as pieces are usually bought of the rack to lower product cost, then it is necessary to use the given tolerances. Manufacturers normally use their own specific class tolerances, as way to simplify manufacturing and reduce cost. ISO norms for sliding mechanism of basic hole are H6/g5 for exact mechanics, H7/g6 for a careful precision and H8/h8 for a normal one [91]. For the microscopic system it is important to guarantee tight tolerances. Due to the high resolution the minimum drifting flaw can be observe in the final result. The main challenge is to achieve good tolerances without having an astronomical increase in cost. More expensive systems offer the option of pre-loading. This is an elimination of clearance between the rail and the rolling elements. This way the deformation due to vertical load is improved increasing overall stiffness. Other important tolerances is the parallelism between rails [90].

Finally, assembly comes in the last step but still of major importance. A correct assembly will guarantee that no other flaws will occurs and the correct performance of the linear guides. The main factor that will suffer from mounting error are: life, friction and accuracy. The latter one will effect in particular straightness in yawning and pitching direction. Assembly error can be a quality factor, understanding why some product will focus faster than others. Straightness is a very important tolerance to achieve in the sample plate so that is does not create focus errors or other types of revolving flaws. To help installation many manufacturers use shoulders to simplify the fixation of the rail. This shoulders can be added or they can be embedded in the mounting plate. The main consideration when mounting is to fix on rail and have it as reference and measure parallelism in the floating rail before fixing it in the right place [90].

5.4.2.1 Market Review

After understanding all the requirements that come to designing a linear actuator, one can search for the best solution in the market. Different manufacturers will have different array of features, patented solutions and in particular cost and quality.

Analysing the market, will also be needed to study the different solutions that available by distinct manufacturers. It is important to not forget the metrics taken in consideration: searching the best for the lowest possible price. Weight and size will also be taken in consideration as well tolerances. Heavier carts will have better performance, but will increase the weight of the overall XY stage and Z stage leading to a worse performance in terms of velocity.

The large array of possibilities, not all manufacturers and solutions, that were searched, will be presented, only some that present the best products. The first manufacturer is NSK, a very well know Japanese company of machine parts. They present excellent quality product and have a wide array of solutions and tolerances. NSK has a miniature series and a self-lubrication series [90].

IGUS®, is another contender in this decision. They are a well known company for presenting good, low cost products. They mainly focus on polymer based parts with a special type of PTFE that doesn't require maintenance and lubrication. They have miniature series and a low profile one. As seen in chapter 4 low profile series do not present a stable and precise solution, so they won't analysed. All of their products use the self lubricating solution. Their property plain bearings and

material have a better load distribution compared to normal linear bearings systems. This way it is possible to use non-hardened rails. This type of materials are great to use in situations where there is dirt, dust and other hard environmental conditions [45].

Rexroth is a Bosch company that sells high quality machine part components. They have a miniature series with tight parallelism tolerances and preload features. The miniatures have three distinct accuracy classes: P, H and N. These parts present high values of basic dynamic load rating and seals can also be added for extra protection [92].

Finally, Scheenberger is another company that creates high quality linear guides and rails. They have a mini series that are normally used in microscopes. They can also have some self-lubricated parts, with the LUBE-S system, that will run smoothly over a long time. The have different accuracy classes and sturdy solutions [93].

Thus, in a prototyping case is was decided to use IGUS® components for the followings reason:

1. Lowest Cost;

2. Even though tolerances are not great, if the system works with theses parts, they will work even better with better quality ones;

3. The Self Lubrication bearings offer a free maintenance system that works; greats in the all type of conditions. One of the goals of project CLARE is to be able to works in all types of complex realities and environments;

4. Easy availability.

While using IGUS® parts to simplify design, the online calculator by IGUS® will be used to confirm the life and the mechanical behaviour. Thus the design process is simplified. If needed the before observed considerations will be applied. When designing linear guides for the precision required for this product, the main goals is to guarantee rigidity and lightweight. Due to the low loads, it is expected that rated life will not be a problem.

5.4.3 Chassis

In this product to minimize cost and weight the profile used was an extruded aluminium 20x20 mm profile. This slim profile presents excellent relation between rigidity and density, creating an affordable, *off-the-rack* part. The chassis design was inspired in different 3D printers, since it is common to observe similar mechanisms. It is believed that this configuration of chassis will able to withstand with safety the loads being considered for design. There are two main different important parts of this chassis design: the box that serves as base for the product and the XY table and the Z axis. The main function of the pillars that hold the Z axis is to support and transmit to the base all the effort created by gravity and those created by the fast displacement of the load that will travel in the vertical direction. In addition to this, another important function of the Z axis

is to guarantee perpendicularity to where the sample stands. It also serves as a way to guarantee parallelism between the chassis.

On the other hand, the chassis box serves as a rigid base that hold the illumination module and the XY table. Having a rigid box close to the ground helps creating a dampener in vibrations created by the XY stage mechanism. It should not go understated the importance of having a very rigid base so that no misalignment is created by flexural displacement. Remembering the main dogma of this project is to remove weight from where speed is necessary, and add mass where stiffness is needed. Figure 5.12 shows the designed chassis with the XY stage above it.

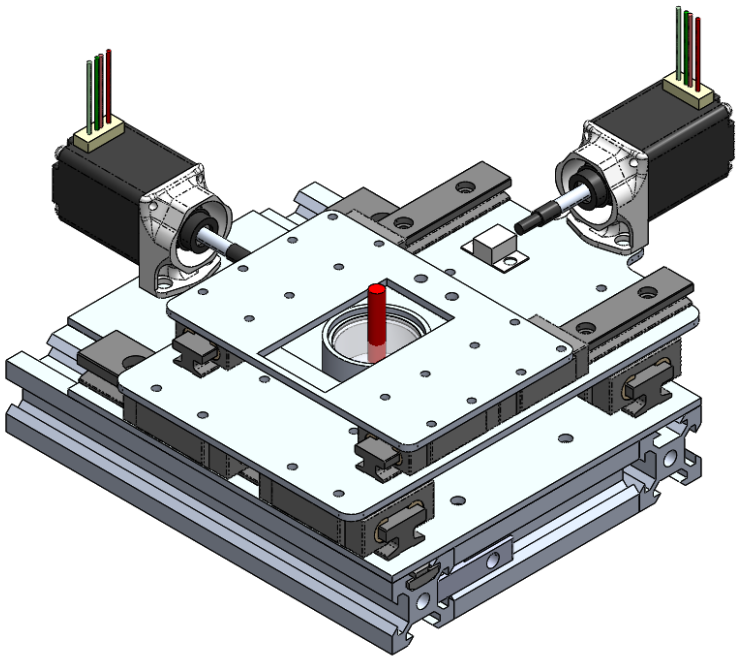

Figure 5.12: Designed chassis with the XY stage above it

Another important factor to work with common extruded aluminium profiles is the easy availability and wide community support behind them. It is easy to find fasteners or parts that hold the chassis together without needing an extra manufacturing process. In the particular case of this dissertation, the load that this profile will have to endure are less than a kilogram, then normal, standard parts can be used to create this joints. This will reduce cost, assembly steps and product complexity.

The chassis evolved from not only using extruded profiles but sheet metal as well. With the addition of the profiles, the sheet metal parts can be cropped extensively, saving on considerable weight. The main function of these parts is to mitigate any small bending and buckling effects. The created parts would be manufactured by bending. It was observer that creating this part would be very complex to near impossible. Thus, it was quickly replaced by another, less complex part that will mitigate the load as well. Figure 5.13 shows the chassis with the extra parts that we added.

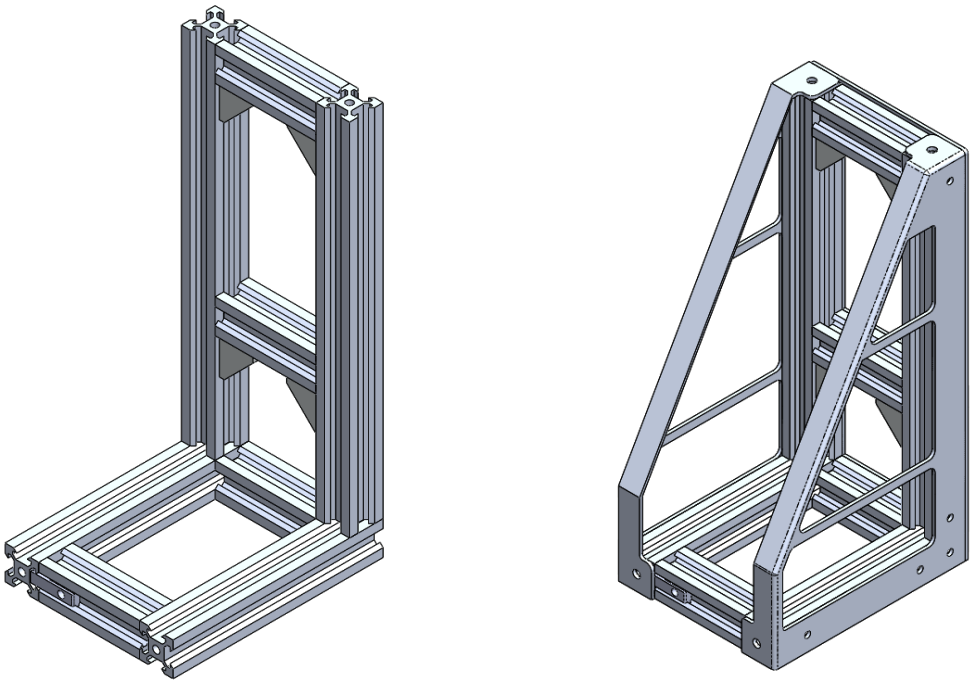

(a) Chassis skeleton **(b)** Chassis skeleton with added parts

Figure 5.13: Chassis skeleton (a) with added parts (b)

This configuration is the most stable and the smallest possible. It is suggested as well to ensure that there are no considerable efforts due to buckling and bending the creation of 3D parts that hold between them a threaded rod. This idea was later discarded due to addition of unnecessary parts that would not affect considerably the final performance of the product.

This iteration present an extremely compact and low waste solution. This led to many different flaws, such as, the actuators not being inside the the chassis. This will require a more complex enclosure. Structural parts and fasteners parts are missing and do not have the required clearence to be assembled. The small size of the whole product adds an extra level of complexity on assembly. Easiness of calibration and mistake proofing is not present in this iteration. Thus, this iteration is the theoretical ideal version of the project. Another flaw is that having the base in the presented position, it does not allow for the required distance between the condenser lens and the sample. Figure 5.14 shows the final iteration of the ideal product.

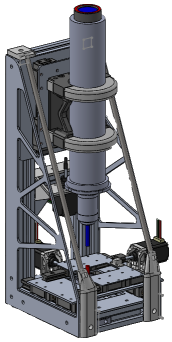

Figure 5.14: Final iteration of the ideal product

5.5 Sixth Iteration

The fifth iteration was jumped as it rethinked the guiding system to be used. Instead of using linear guides, it was suggested to use a typical gantry system with rubber wheels. This system would be a cheaper option and with a better usage of free space. This idea was drafted due to the lack of precision and loose tolerances tah comes with the usage of rubber wheels. The life of this wheels if not lubricated would significantly diminished which would lead to bad performance over a short period of time.

In this iteration it is presented a working and easy to assemble prototype. In the sixth iteration different changes were done to guarantee an easier assembly and manufacturing. This is the iteration closer to a final working product, the work-alike prototype. Features were added and space sacrificed to guarantee that the device would maintain a low cost and could easily be assembled allowing space for mounting mistakes. Some final mechanical considerations were done to understand in an analytical manner the behaviour of the flexion of the base plate. Dynamic models were created to understand the effect of inertial factors in that certain bodies will be under. For example, in the top plate of the XY stage, drift can occur due to inertia, if not corrected. This can lead to a loss of performance.

5.5.1 Design

As expected in this iteration different flaws were correct as well improving the design to error proof. It is typical when assembling an accurate device that it might need calibration or a complex mounting process. For example, a parallelism error between linear guides can lead to significant life decrease, as well to jamming the sliding motion. It is important to give tools and mechanism that allows for correction of this error in a manual or autonomously way. Other errors from manufacturing are common and not all parts are trully equal. This should also be taken in consideration as well.

To guarantee the distance between the condenser lens, the illumination module, and the sample, a flange was created to hold the illumination module at the correct position. Being this distance wider than the profile size, it was now necessary to lift the XY base up. For that two legs were

added. The existence of free space under the table was also seen as a good opportunity as it created space for the required electronics. Having a larger product is also a good solution for a stable platform for future products or models of the μSmartScope.

The feet that were created from extruded profile were a bit larger than the minimum required to take in consideration flaws during the cutting of the profile. It also allows for easy translation of the XY table in the Z direction for calibration. This mechanism creates an array of values that the table can translate to calibrate for the optimal focusing time.

This iteration has general dimensions of 200 mm x 200 mm making it the larger iteration of all that were presented. The large base for the XY table guarantees that the actuators are kept inside the model. In this base it was also added a hole so that all electrical cable can pass through, helping cable management. This will help achieving a faster assembly. In terms of layout, the optic tube and the micro-stage were swiped to the side to use the better optimize space usage. An iteration with the optic tube in the center was tested and it was observed that it used unnecessary space. Having a non aligened center of gravity with the driving force is not advised for the best performance of the guides. In particular in situations where massive loads create a strong momentum that can lead to an uneven degradation of the linear bearings. Due the light nature of the loads considered in this project, this was not a problem.

Coplers and end stops were added as well. This parts were designed once again with flexibility of assembly in mind. The parts that hold the endstops allow for the displacement in a few millimeters to guarantee that it contacts correctly with the end plate.

Finally, the chassis was modified to remove parts that were over-constraining the system. Some very light structural plates were updated to guarantee the perpendicularity and parallelism. Figure 5.15 shows the final result of this iteration.

5.5.2 Mechanical considerations

To ensure the correct performance of the design some analytical mechanical considerations were made. This analytical models will be simplifications to classical conditions, this way it is possible to simplify the problems and have a more conservative vision on the problem. The flexion of the XY extruded profiles considerations will not be presented since the purposed chassis is incredbly more rigid compared to the loads in consideration. As a consequence, it can be dismissed.

5.5.2.1 Plate thickness

One of the main flaws of the first model was the incorrect misusage of the plates used for structural and stage gantries. It is expected that with the introduction of the chassis, minimum thickness plates can be used. Thus as it was defined before in chapter 3, the difficulty of laser cutting plates with thickness under 2 mm increases exponentially. Increased complexity means increased cost. Thus, all plates will be replaced with 2 mm thickness aluminium to simplify production and weight.

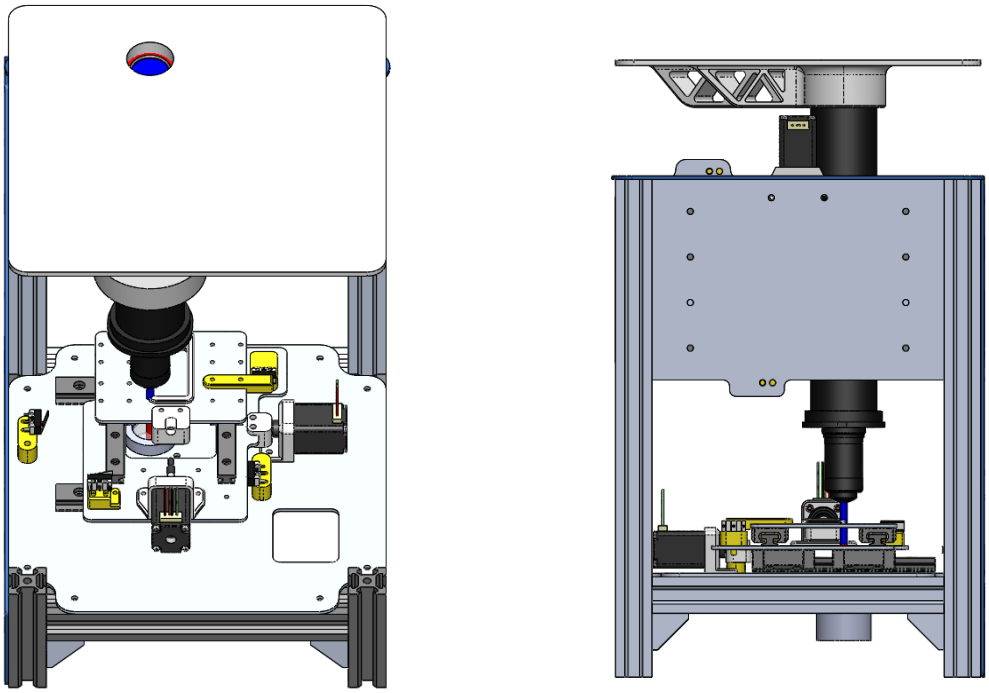

(a) Sixth iteration **(b)** Back of the sixth iteration

Figure 5.15: Sixth iteration (a) and the back of the Sixth iteration (b)

The main plate that need to be ensured the correct function is the base plate that holds the XY stage. To determine maximum deflection of the base plate it will be used plate theory of a clamped rectangular plate in 4 edges.

In the base plate four clamped edges was considered. Even tough, screws are applied, they still allow for deformation. Their goal is to do normal force that allow the fixation. The load considered was a normal force equally distributed in area of the plate. It is important to notice that, the stage is not well centered.

Firstly, it is possible necessary to review the simplification to a pure bending case and neglect shear effects. This way, Kirchhoff classical plate theory [94] can be applied.

$$u(x,y,z) = -z\frac{\partial w_0}{\partial y} \tag{5.9}$$

$$v(x,y,z) = -z\frac{\partial w_0}{\partial y} \tag{5.10}$$

$$w(x,y,z) = w_0(x,y) \tag{5.11}$$

Where (u,v,w) are the displacement components along the (x,y,z) directions and w_0 is the transverse deflection of a point on a mid-plane.

Althought this case can be considered pure bending, it is important to notice that some shear

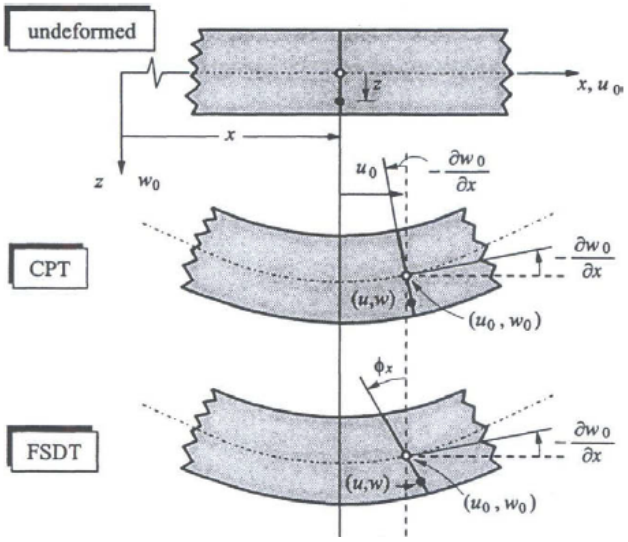

Figure 5.16: Difference between the different plate models [95]

deformation might happen, other more expansive models can be use, such as the Mindlin plate theory. This model as an increased accuracy [94]. Due to the low weight it is not expected deformation through the thickness of the plate, therefore higher polynomial models are not needed to be used. The Mindlin model can be represented as:

$$u(x,y,z) = z\phi_x(x,y) \tag{5.12}$$

$$v(x,y,z) = z\phi_y(x,y) \tag{5.13}$$

$$w(x,y,z) = w_0(x,y) \tag{5.14}$$

Where ϕ_x and ϕ_y are rotations in the x and y axes, respectively. Figure 5.16 shows the difference between the two models [95]. Displacement is the most important factor to study and guarantee that is it not critical. Thus, the governing equations for plate displacement after being applied the Laplace operator to simply are:

$$-\frac{K_s E h}{2(1+\nu)}\left(\nabla^2 w_0 + \frac{M}{D}\right) = q(x,y) \tag{5.15}$$

$$-D(1-\nu)\nabla^2\phi_x - (1+\nu)\frac{\partial M}{\partial x} + \frac{K_s E h}{1+\nu}\left(\frac{\partial w_0}{\partial x} + \phi_x\right) = 0 \tag{5.16}$$

$$-D(1-\nu)\nabla^2\phi_y - (1+\nu)\frac{\partial M}{\partial y} + \frac{K_s E h}{1+\nu}\left(\frac{\partial w_0}{\partial y} + \phi_y\right) = 0 \tag{5.17}$$

Where D is the flexural rigidity of the **isotropic material**, that it is given by [96]:

$$D = \frac{Eh^3}{12(1-\nu^2)} \tag{5.18}$$

The factor K_s is determined such that the strain energy due to the transverse shear stress of the FSDT is equal to the three dimensional elasticity theory. On the other hand M is the sum of moments:

$$M = \frac{M_{xx}+M_{yy}}{1+\nu} = D\left(\frac{\partial \phi_x}{\partial x}+\frac{\partial \phi_y}{\partial y}\right) \tag{5.19}$$

Now it is needed to apply the boundary conditions. For clamped plates these are [96]:

$$w_0 = 0, \phi_n = 0, \phi_s = 0 \tag{5.20}$$

For simplification reasons the classical theory will be used as well considering clamped in 4 edges as way to easily compute problem. Due to the geometry of the plate, it will be used the Ritz Method applied to bending of rectangular plates [96].

The boundaries conditions for this method and fixture condition are:

$$w = 0, \frac{\partial w}{\partial x} = 0, (x = 0, x = a) \tag{5.21}$$

$$w = 0, \frac{\partial w}{\partial x} = 0, (y = 0, y = b) \tag{5.22}$$

Were a and b are the dimensions of the rectangular plate. Thus, by the Ritz method, it is possible to simplify and have deflection as:

$$w = \sum_{m=1}^{\infty}\sum_{n=1}^{\infty} a_{mn}\left(1-cos\frac{2m\pi x}{a}\right)\left(1-cos\frac{2n\pi y}{b}\right) \tag{5.23}$$

In the case of a square plate, the maximum deflection takes place in the center of the plate and is given by [96]:

$$w_{max} = 0.00128\frac{p_0 a^4}{D} \tag{5.24}$$

Where in equation 5.23 should be replaces by a_{11} that it is given by:

$$a_{11} = \frac{p_0 a^4}{4\pi^4 D}\frac{1}{3+3(a/b)^4+2(a/b)^2} \tag{5.25}$$

In a square plate is:

$$a_{11} = \frac{p_0 a^4}{32\pi^4 D} \tag{5.26}$$

For a square plate the other a_{mn} factors are given by:

$$\begin{bmatrix} 0.11774p_1 & 0.01184p_1 & 0.00268p_1 \\ 0.01184p_1 & 0.00189p_1 & 0 \\ 0.00268p_1 & 0 & 0.00020p_1 \end{bmatrix} \tag{5.27}$$

Where p_1 is given by:

$$p_1 = \frac{p_0 * a^4}{4D\pi^4} \tag{5.28}$$

Thus material properties for a 2 mm aluminium 6061 sheet is given are:

$$E = 70GPa, v = 0.334, h = 2mm \tag{5.29}$$

Flexural Rigidity was determined as $D = 52.526$. The sizer of the square plate is a = 200 mm and b= 200 mm. Thus the square hypothesis can be applied. The considered load will be 5 N with a security coefficient of 2, as such, 10 Newtons will be considered.

$$p_0 = \frac{10}{0.04} = 250Pa \tag{5.30}$$

Then p_1 is given by

$$p_1 = \frac{0.8 \cdot 0.2^4}{4 \cdot 52.526\pi^4} = 1.954 * e^{-5} \tag{5.31}$$

Thus a_{mn} matrix is

$$\begin{bmatrix} 2.301e^{-6} & 2.314e^{-7} & 5.238e^{-8} \\ 2.314e^{-7} & 3.694e^{-8} & 0 \\ 5.238e^{-8} & 0 & 3.909e^{-9} \end{bmatrix} \tag{5.32}$$

w_{max} along the length of the plate is show in the figure 5.17. The maximum expected deformation will be about 12 μm. This value is more than ideal for the correct performance of the part. It is expected that a more accurate representation of this problem is considering only the area where the XY stage will be present. Thus, an higher displacement can be expected, having the Ritz-Method has a design insight on the behaviour of the 2 mm thickness. As such, 2 mm thickness will optimize the decided requirements.

5.5.2.2 Dynamic Model

Creating a dynamic model will help understand the performance of the system under inertial efforts. There will be two different models, for the XY stage and another one for the Z axis.

As it is an XY system, it is possible to simplify the system to 2D approximations. The model will put the sample as the center of gravity of both bodies in the their geometric center if it the gantries were considered perfectly rectangular.

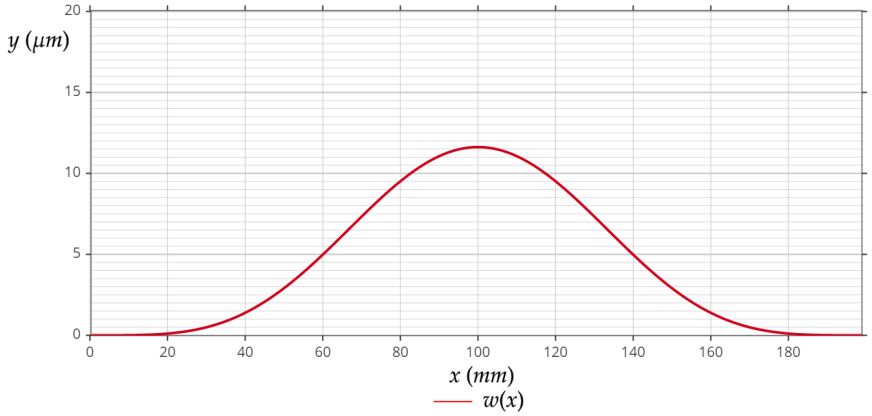

Figure 5.17: w_{max} along the length of the plate

This system will be modeled in a fixed referential. Body 1 will be the lower stage and body 2 will be the stage that carries the sample. The free body diagram in consideration dynamical effects can be seen in figure 5.18. Where $r(t)$ is the position of the body in any given moment.

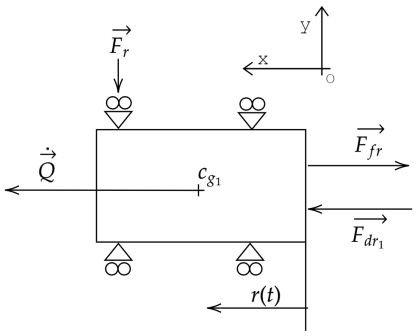

Figure 5.18: Free body diagram for Body 1

The dynamic equilibrium is presented by:

$$\begin{aligned} \sum \vec{F_{ext}} &= \dot{\vec{Q}} \\ \sum \vec{M_{ext}} &= \vec{K_{gc1}} \end{aligned} \tag{5.33}$$

Where $\dot{\vec{Q}}$ are the inertia effects and $\vec{K}_1$ is the dynamic moment. Thus, inertia is given by:

$$\dot{\vec{Q}} = m_1 \vec{a}_1 = m_1 \begin{Bmatrix} \ddot{r} \\ 0 \\ 0 \end{Bmatrix} \tag{5.34}$$

The dynamic moment is given by:

$$\vec{K_{gc1}} = \dot{\vec{H}} + \vec{OG}_{c1} \times \dot{\vec{Q}} \tag{5.35}$$

Cinematic moment is not accounted as there is few to none angular movement. This effect will be considered null. Thus:

$$\vec{K_{gc1}} = \begin{Bmatrix} r(t) \\ 0 \\ 0 \end{Bmatrix} \times m_1 \begin{Bmatrix} \ddot{r} \\ 0 \\ 0 \end{Bmatrix} = 0 \tag{5.36}$$

This means that the movement does not create moment due to dynamic efforts, this can be achieved due to correct position of the driving force. If the driving forces was eccentric then dynamic moment would be seen that would be critical to the correct functioning of such precise mechanism. Thus, replacing in the initial equation 5.33 it is determined:

$$\begin{aligned} \begin{Bmatrix} 0 \\ F_r \\ 0 \end{Bmatrix} + \begin{Bmatrix} F_d 1 \\ 0 \\ 0 \end{Bmatrix} - \begin{Bmatrix} \mu m_1 g \\ 0 \\ 0 \end{Bmatrix} &= m_1 \begin{Bmatrix} \ddot{r} \\ 0 \\ 0 \end{Bmatrix} \\ \sum \vec{M_{ext}} &= 0 \end{aligned} \tag{5.37}$$

In this system, the reaction forces where simplified because they are all null. In the body 1 there is only reaction forces in the vertical component due to the load of the cart, that will not create a problem in dynamic motion, only on the life of the bearings and sliding friction. As such, due to the non existence of reaction force in the X and Y direction, the moment created by the reaction forces will be null as well. Which makes sense as the dynamic moment is also null. The drive force is given by the manufacturer and it as 45 N. The friction coefficient can vary between considering steel-steel friction (0.2) or steel-PTFE around 0.15 [97]. The final equations for the body 1 are:

$$\begin{cases} \ddot{r} = \frac{45}{m_1} - 0.2 \cdot 9.81 \\ Fr_y = 0 \\ \sum \vec{M_{ext}} = 0 \end{cases} \tag{5.38}$$

After that the second body can be analysed. This body travels with body 1 and also has independent travel as well. Free body diagram of body 2 is seen in figure 5.19. The inertia of this system is given by:

$$\dot{\vec{Q}}_2 = \dot{\vec{Q}_2} 1 + \dot{\vec{Q}}_1 \tag{5.39}$$

$$\dot{\vec{Q}}_2 = m_2 \begin{Bmatrix} 0 \\ \ddot{z} \\ 0 \end{Bmatrix} + m_1 \begin{Bmatrix} \ddot{r} \\ 0 \\ 0 \end{Bmatrix} \tag{5.40}$$

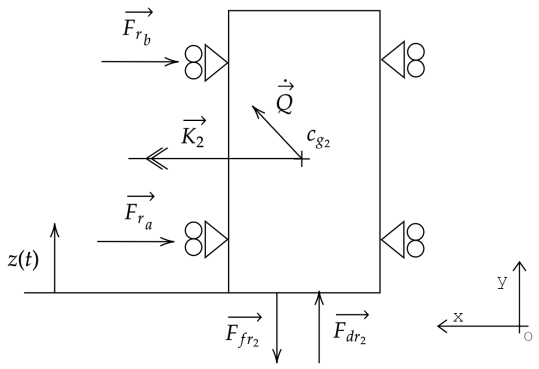

Figure 5.19: Free body diagram of body 2

Thus:

$$\dot{\vec{Q}}_2 = \begin{Bmatrix} m_1\ddot{r} \\ m_2\ddot{z} \\ 0 \end{Bmatrix} \tag{5.41}$$

Dynamic moment in this system is given by the second Koening theorem where:

$$\vec{K_{gc2}} = \vec{K_{gc1}} + \vec{G_1G_2} \times \dot{\vec{Q}}_2 \tag{5.42}$$

Thus:

$$\vec{K_{gc2}} = \begin{Bmatrix} 0 \\ z \\ 0 \end{Bmatrix} \times \begin{Bmatrix} m_1\ddot{r} \\ m_2\ddot{z} \\ 0 \end{Bmatrix} \tag{5.43}$$

$$\vec{K_{gc2}} = \begin{Bmatrix} 0 \\ 0 \\ -m_1\ddot{r}z \end{Bmatrix} \tag{5.44}$$

This means that when there is movement in the body 1 and in the second body as well, if the two plates are not centered then the upper body will suffer a dynamic moment that will crate drift. This moment will be refuted by the moment created of the reaction forces in the carts. This creates another reason why it is important using 2 carts, instead of one, this way they can stop the stage drifting. Good tolerances and good capability to withstand this moment is important as well. There will be reactions forces in the 0x in the carts that are in direction of the acceleration. This means that at a given moment, only the left carts stop the stage drifting or the right carts.

As such, it is possible to simplify this problem as 3 point simply supported beam bending. Thus, the goal of the carts and, as a consequence, lateral reaction forces is to stop the moment created by the acceleration of the body 2 together with body 1. Figure 5.20 shows this approximation. As seen, once again, the distance between carts it is extremely important for stage drift. Thus the

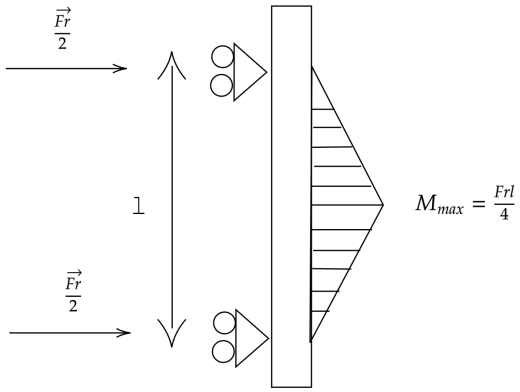

Figure 5.20: 3-Point bending approximation

equilibrium equation for the second body are:

$$\begin{Bmatrix} Fr_x \\ 0 \\ 0 \end{Bmatrix} = \begin{Bmatrix} m_1\ddot{r} \\ m_2\ddot{z} \\ 0 \end{Bmatrix} + \begin{Bmatrix} 0 \\ \mu m_2 g \\ 0 \end{Bmatrix} - \begin{Bmatrix} 0 \\ 45 \\ 0 \end{Bmatrix}$$
$$\begin{Bmatrix} 0 \\ 0 \\ -\frac{Frl}{4} \end{Bmatrix} = \begin{Bmatrix} 0 \\ 0 \\ -m_1\ddot{r}z \end{Bmatrix} \tag{5.45}$$

Then, the model equations are:

$$\begin{cases} Fr_x = m_1\ddot{r} \\ 45 = m_2\ddot{z} + \mu m_2 g \\ -\frac{Frl}{4} = -m_1\ddot{r}z \end{cases} \tag{5.46}$$

The system final equation are, considering maximum acceleration, for maximum thrust force of $45N$:

$$\begin{cases} Fr_x = 43.038N \\ \frac{45}{m_2} - 0.2 * 9.81 = \ddot{z} \\ -\frac{Fr_x l}{4*43.038} = -z \end{cases} \tag{5.47}$$

It is important to notice that the minimum reaction force that the each cart needs to hold is approximately 22 N, but the carts can hold much higher loads, thus the distance between the carts can be smaller.

Finally the Z-stage model can be done. This model will be done in a similar fashion as the first body, but gravity plays an important role. In some cases it will help the focus and in other it will retard it. It will be considered that the gravity center is linear to driving force, due to the very small distance between the two. The moment created by this small displacement will be easily damped by the carts. The free body diagram of this situation is presented in the figure 5.21. The

center of gravity is not in the center of the cart because of the weight of the optical tube. Since distance between the center of gravity and the driving force is small, then the moment created will not be considered. Friction will not be considered, as well, due to the vertical nature of the case. It may exist in the case of bad mounting errors. The inertia in this system (in the case of the gravity

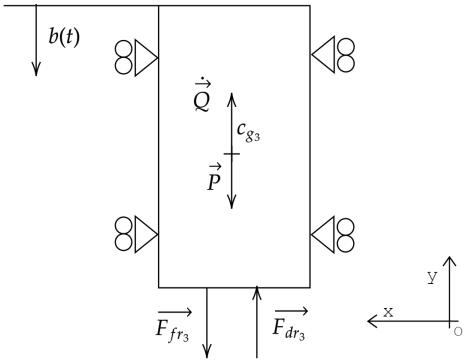

Figure 5.21: Free body diagram of the Z-Stage

is retarding movement) is given by:

$$\dot{\vec{Q}} = m\vec{a} = m \begin{Bmatrix} \ddot{b} - g \\ 0 \\ 0 \end{Bmatrix} \tag{5.48}$$

As we seen in the first body, the $\vec{K}$ will be zero. This means that no moment due to dynamic effects will be created. Thus the equilibrium equation are given as:

$$\begin{Bmatrix} 0 \\ 45 \\ 0 \end{Bmatrix} = m \begin{Bmatrix} 0 \\ \ddot{b} - g \\ 0 \end{Bmatrix} \tag{5.49}$$

Thus:

$$\begin{cases} \frac{45}{m} = \ddot{b} - g \end{cases} \tag{5.50}$$

As expected, the system will be faster when having gravity helping. With this models it is possible to correctly understand how long a system needs to achieve another field of view. The maximum pitch moment created on the carts to an eccentric load is given by:

$$Mr = \frac{4Bm(a+g)}{l} \tag{5.51}$$

Where B is the distance between the center of mass of the load to the carts plane and l is the distance between carts. One again, the bigger the distance, the better the system can withstand pitch moment.

Finally, it is interesting to study the rotation and efforts that the vertical beams that have the efforts will endure. Thus, the maximum moment created by the load will be:

$$M_b = \frac{(B+D)[m(a+g)]}{2} \tag{5.52}$$

Where B is the arm that goes from the center of gravity to the plane of the carts and D is the the distance between said place and the center of beams. This load translates 5 mm in the vertical direction changing the application point with the translation. This will not be taken in consideration, as the change of the application point in a long beam is very small creating a small gradient of rotation and deformation. Thus, the presented system is seen in figure 5.22. Before considering

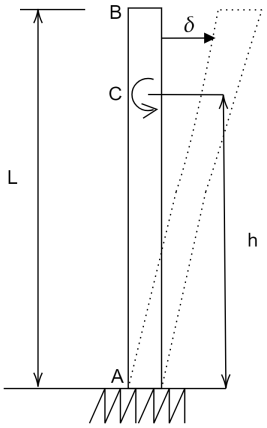

Figure 5.22: Deformation on the beam due to deformation

the textbook example of beam deformation, it is needed to observe if buckling might occur. Thus:

$$i = \sqrt{\frac{A}{I_z}} = \sqrt{\frac{10342.07}{187.6}} = 7.42 \tag{5.53}$$

Thus, slenderness is :

$$\lambda = \frac{300}{7.42} = 40.43 \tag{5.54}$$

Long columns, have a slenderness typical between 30 and 150. As 40 is a value close to 30, then buckling effect will only occur for really high loads, therefore this effects can be discarded [98]. Thus is a typical textbook example where beam there can be used. Thus:

$$\frac{\mathrm{d}^2\delta}{\mathrm{d}h^2} = -\frac{M}{EI} \tag{5.55}$$

$$\frac{\mathrm{d}\delta}{\mathrm{d}h} = -\frac{Mh}{EI} + A \tag{5.56}$$

$$\delta = -\frac{Mh^2}{2EI} + Ah + B \tag{5.57}$$

Where A and B are integration constants that can be solves with the boundary conditions. This conditions are:

$$\begin{cases} \frac{\mathrm{d}\delta}{\mathrm{d}h} = 0, \text{ if h = 0} \\ \delta = 0, \text{ if h = 0} \end{cases} \tag{5.58}$$

Then $A = 0$ and $B = 0$. Thus:

$$\delta = -\frac{Mh^2}{2EI} \tag{5.59}$$

Replacing the moment in the equation, deformation is given by:

$$\delta = -\frac{(B+D)[m(a+g)]h^2}{4EI} \tag{5.60}$$

The difference between the top position and the lowest position due to translation is given by:

$$\Delta\delta = -\frac{(B+D)[m(a+g)]}{4EI} \cdot [-10h + 25], \text{ if h = max value} \tag{5.61}$$

5.5.3 Composite Panel

With the objective of reducing weight and improving flexural properties it was suggested the usage of sandwich panel. Alucobond® is a commercial solution of a composite panel that uses two films of aluminium and a Polyethylene terephthalate (PET) core. The increased price on using this type of panel can be outweighed due to significant less weight by using Alucobond®. Certain critical parts from the XY and Z stage will be replaced by this material to understand the effect on velocity [99].

Another great characteristic of using Alucobond® is the fact that, this solution, can be manually bent. This material is perfect to be used for in an enclosure situation, not requiring extra manufacturing processes. It is only require to create grooving features in the CNC cutting that allow for the easy bending in 90º or 135º. This material also presents great environmental resistance as it is typically used in facades of buildings and warehouses [100] .

It is important when using typical fasteners with this material due to the compression on the the core material. This compression will degrade mechanical properties of the material overtime. Thus it is required to use extra parts, such as, brass inserts. This will avoid the application of compression effort directly on the core of the panel [100].

5.6 PMI guides solution

It was observed that IGUS® guides would present many flaws even when using larger series. Tolerances and uneven performance would not be satisfying for repeatability. The larger series sizes would also dominate the weight of a certain axis of the stages. In terms of cost, due to the necessity of using larger sizes, cost increased significantly. As such, other solutions were searched with the objective of improving weight, size and tolerances.

PMI is a Taiwanese brand that sells mid range guiding solutions. MSC is their miniatures series. These guides use ball-bearings as rolling solution which is expected to increase strength and work life.

Observing the catalogue of this series it is possible to compare that series 7 - the smallest one - has increasingly better performance than the IGUS® counterparts. The higher performance is due to the usage of ball bearing that will increase static and dynamic load rating.

Using these guides will solve loose tolerances due to the the more careful manufacturing. PMI presents three distinct series with their MSC guides: N, H, P. As expected, the higher the tolerances chosen the higher the cost. Class N is a significant increase from the IGUS® counterparts. It is expected that N class will be sufficient for the required solution. This effect can be optimized by using a slight preload. Preloading the guides will exponetially increase rigidity at hte cost of tighter parallelism clearances as well. Another drawbacks of using preloading are increased cost and being less prone to mounting errors.

Other features of using MSC PMI series instead of the IGUS® counterparts are the the gothic-arch groove that is designed for a contact angle of 45º that creates and equal load in radial, reversed radial and lateral direction. Better costumer service, extensive documentation and stainless steel rails. The difference in size between the guides can be seen in figure 5.23. The difference in price is around 60 euros. In addition, the difference in weight from a IGUS® series 12 cart to a PMI series 7 cart is 27 g. The difference in weight between 100 mm of rail and two carts between both solutions is 52 g. It is possible to observe that PMI will give a better value per gram, making this solution very appealing.

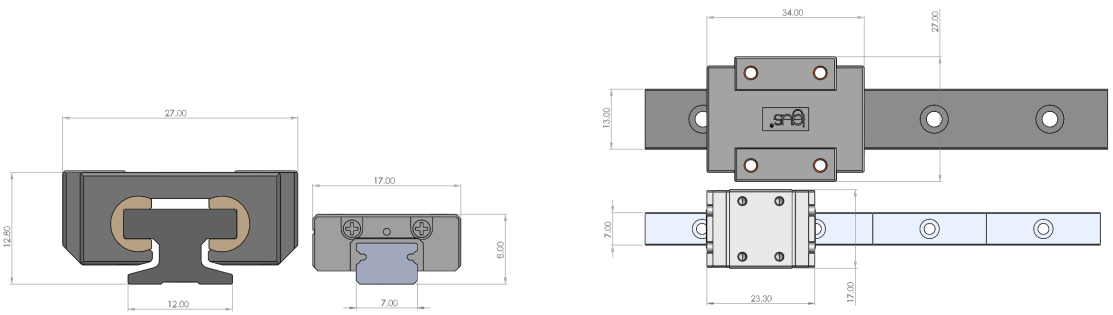

(a) Front view size comparison between carts **(b)** Above view size comparison between carts

Figure 5.23: Front (a) and the above (b) views of the two different carts

The final product is very similar to the one observed in the sixth iteration. The main difference is that by using smaller parts its was possible to save 15 mm in the X direction and 10 mm in the Y direction.

5.7 3D Printed solution

Prototyping in house is the most inexpensive and fastest way to test a product before doing major design modifications. Using traditional manufacturing technologies for prototyping requires, most of the times, the usage of third parties. Thus, main advantages are having a prototype close to the final product and the possibility of using a similar material. The main drawback of using third parties suppliers are many. The drawbacks are the increased cost in raw material, skilled work and machine time. This cost can be increased by considering the time of manufacturing and the bureaucratic process that companies create to proceed with a purchase. As a consequence, a part that a desktop 3D printer can create in 10 hours, can take weeks. The only solution to pass these drawbacks would be having a capable workshop near where the conception of the product happens. This solution is not bearable by small or medium companies that can't afford the required machinery or skilled workers. One final drawback of using third parties is property security. The usage of extra companies creates wider fronts where leaks of information can occur.

In these situations, 3D manufacturing become very appealing. The main problem of technologies such as FFF / FDM or SLA are the final piece properties, build size, mechanical properties and the mainly usage of only polymers. During the pandemic of COVID19, 3D manufacturing of a prototype mostly the only way to evolve the different iterations in product development. As such is was asked: is it possible to create this prototype while using 3D manufacturing? FDM is not well know for the dimensional accuracy and roughness. It is also a process that suffers from many flaws that can lead to a considerable material waste. As such, different parts were redesign with 3D manufacturing in mind [101, 102]. Structural parts we redesigned as well considering the fact that now there would be a polymeric lattice structure instead of a metallic sheet.

After running the Ritz method for PLA it was observed that the thickness of the base needed to be, at least, 6 mm, with a maximum displacement of 22 μm as it is possible to observe in figure 5.24.

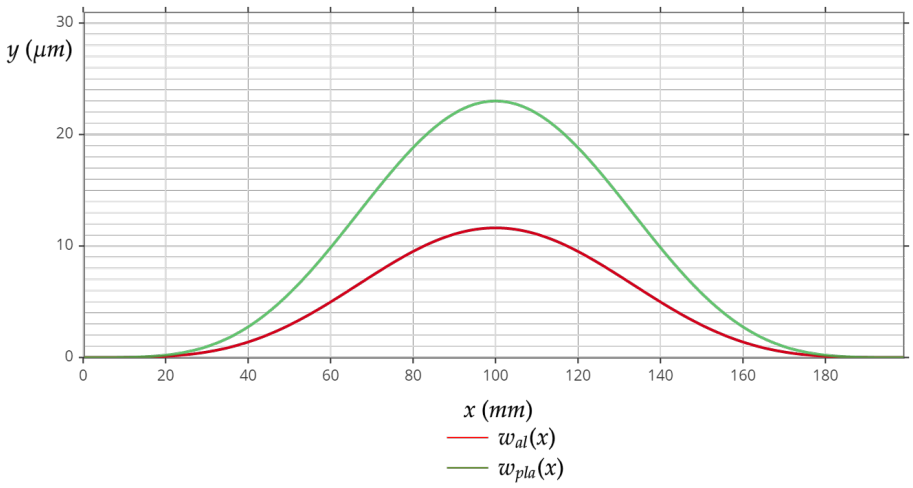

Figure 5.24: Comparison between Ritz Method for the aluminium base plate for the 6 mm PLA base

Figure 5.25 shows the simulation and the comparison of displacement between a PLA part with 2 mm and one with 6 mm. It is important to notice that this simulations are similar to an injection moulded part. Thus, the real final properties will also be dependent of the parameters used, wall count, infill density and type of infill [103]. As such for a 2 mm part the maximum displacement is close to a 1.056 mm and for a 6 mm thickness part is similar for an aluminium sheet metal as it will be observed in chapter 6.

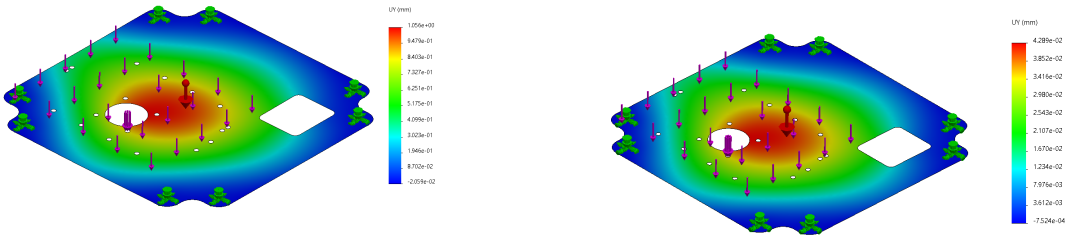

(a) Displacement for a 2 mm thickness

(b) Displacement for a 6 mm thickness

Figure 5.25: Displacement for 2 mm thickness (a) and 6 mm thickness (b)

The thickness of other parts were modified accordingly. Using 3D manufacturing allows for the creation of more complex parts. As such extra features were added to improve performance and assembly. For example, in the base it was added a small hole that simulates the addition of shoulders a typical feature in machined micro-stage. The addition of this shoulders will conferee extra stability and easy of assembly. Having an easier reference geometry for the mounting of the railing can save a considerable amount of time.

Fillets and chanfers were used to diminished thermal effects such as warping. The usage of fillets will diminished the concentration of thermal loads in a corner creating that could lead to a bad end result and the possibility or warping. The build orientation and the feasible minimum feature size were considered. It is important to understand that some features will take extra time to build. As such, time consuming features were eliminated. In more complex parts, self-supporting angles were used to avoid using support structures. To improve adhesion the parts were printed at a nozzle temperature of 220ºC. This temperature with the addition of a binding agent is a very effective combination to avoid warping [103]. Layer height of 0.2 mm was chosen taking in consideration the material usage and time consumption. Figure 5.26 shows different parts that were modified having 3D manufacturing in mind.

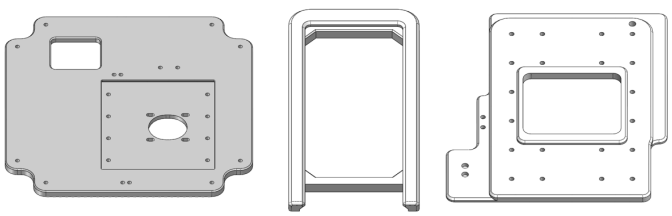

Figure 5.26: Modified parts after passing through a DfAM process

5.8 Look-alike Prototype

An engineering prototype combines the work-alike prototype with the look-alike prototype. The look-alike prototype gives a glimpse of the possible final future creating a very similar idea how it is expected for this product to feel and look. Figure 5.27 show different views of the final engineering prototype.

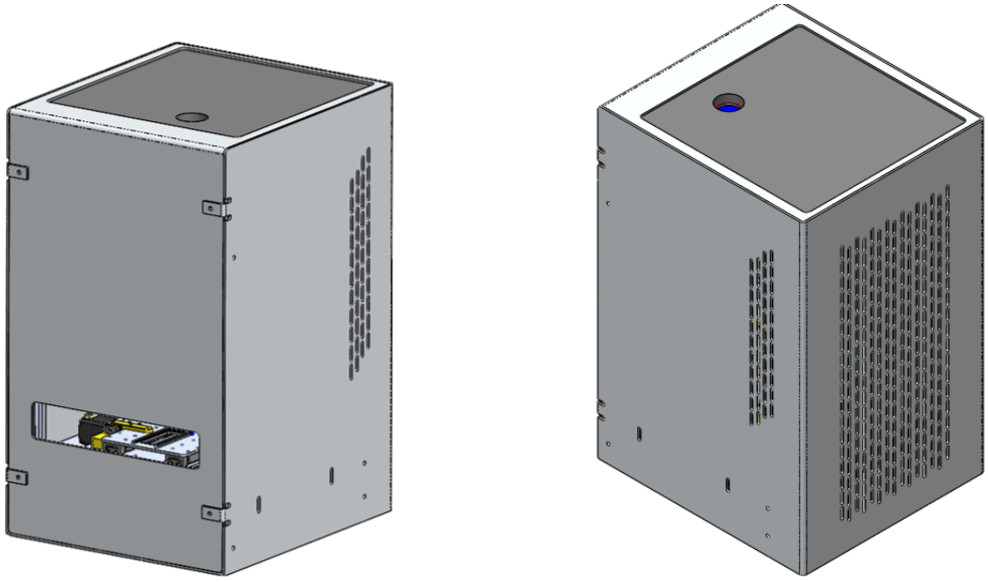

(a) Front of the engineering prototype **(b)** Back of the engineering prototype

Figure 5.27: Front (a) and the back (b) of the engineering prototype

Different iterations of the same look-alike prototype were developed to create an enclosure that will be easy to manufacture, allow fast assembly and disassembly, while maintaining all the products secure. The enclosure was envision to use sheet metal and metal bending manufacturing technologies, so that it is cheap, sturdy and light.

Metallic bending can be considered a fairly complex manufacturing process. As such, all holes were design to take in consideration the bending factor as well the addition of bending radius to the total dimension of the flat sheet. Other techniques such as cut outs were used to guarantee the corrective bending of important features. In the case of using the composite panel as the material, it would simplify the process and assembly time time while reducing total weight as well. In addition, the device would have a panel that resists environment issues and would be easily portable as well. It is expected that for the enclosure, the extra cost of using Alucobond would be out-weighted by the positive factors and the reduce of assembly and manufacturing cost. The structural sheet metal will be replaced with the enclosure as way to reduce weight and not creating unnecessary redundancy.

The enclosure is constituted by three different parts: and L shape, an U shape and the base. The first L shaped part would close the enclosure and fit the platform that holds the smartphone as well. The U shaped part is the main structural component of the enclosure that replaces the back

wall and the ones on the side. Finally there is a square base that allows for fast disassembly so that maintenance on electronics it's not complex to reach.

Extra features were added in this prototype to take to the limits the possibilities of the enclosure. Firstly calibration mechanism were added so that the table XY module can be easily fixed in the required position. Other features such as ventilation holes were added to cool down electronics and actuators. The ventilation features due to the machining/cutting per hour of cost can added up to the total sum. As such this ventilation should be minimized and better thought upon.

Chapter 6

Case studies and finite element analysis of structural components

Finite element analysis is a powerful computational tool that gives the ability to engineers to correctly design complex and critical parts. The numerical models are increasingly more present in validation and decision in engineering. These powerful tools save time and capital by allowing a less conservative mindset as well reducing the need for prototyping. There are large multitude of software of finite element analysis. With the ascending presence of additive manufacturing, FEA relevance grew allowing to build impossible parts, that, by traditional methods, were otherwise considered impossible.

The main goal of this chapter is to present different case studies that were taken under finite element analysis. These parts are characterized by the need of extreme accuracy and precision when design it. Analytical analysis have it's limitations and, even tough classic load cases can achieve a very accurate representation of the reality, FEA allows to understand the true behaviour of a component under the boundary conditions and different load cases. FEA will also grant for a more correct approach of the analysis of critical structural components.

In this chapter it will also be presented different case studies of certain parts that in a normal, non-optimized state would be very heavy. Thus, resorting to additive manufacturing and topology optimization, it was possible to create a guideline that maximizes stiffness and minimizes weight. The parts that will be shown are: the holder of the smartphone, the engine mounts and the optic tube mounts. These are piece that are fundamentally done in additive manufacturing and that require more complex shapes. Due to their weight, it will effect drastically performance.

6.1 Structural Analysis

FEA main purpose was to analyze with certainty three dimensional structures. Thus, in the different cases presented here, due to their structural importance *ABAQUS* will be used. The main advantage of using *ABAQUS* software over *Solidworks* simulation embedded plug-in is due to accuracy and mesh limitations reasons. *ABAQUS* allows for more extensive in-depth mesh and interaction features. For example, in chapter 6.1.1.3 it is explored the case of sandwich structure. Accurate analysis of this example would be incredibly complex to achieve in *SolidWorks* Simulation.

6.1.1 Plate Study

The base plate is expected to be the part that will suffer the most with the load case. Due to the span of the plate and higher loads, if this plate is well designed, then all of the similar mechanisms above will as well. The main goals is to observe and confirm that an 2 mm aluminium sheet is able to withstand the load without substantial displacement. In this study it will be presented three different situations. The aluminium sheet will be compared between the results in *ABAQUS* and *SolidWorks*. Finally, Alucobond® will be simulated and compared to the sheet metal.

6.1.1.1 ABAQUS Case

To correctly test the geometry, the sketch was imported to *ABAQUS* through an .dxf file of the part in question. After defining the properties of the material with consistent unit, boundary and load conditions were given. It was necessary to create a partition in the shell model to correctly represent the load case. The model and the load case can be observed in figure 6.1.

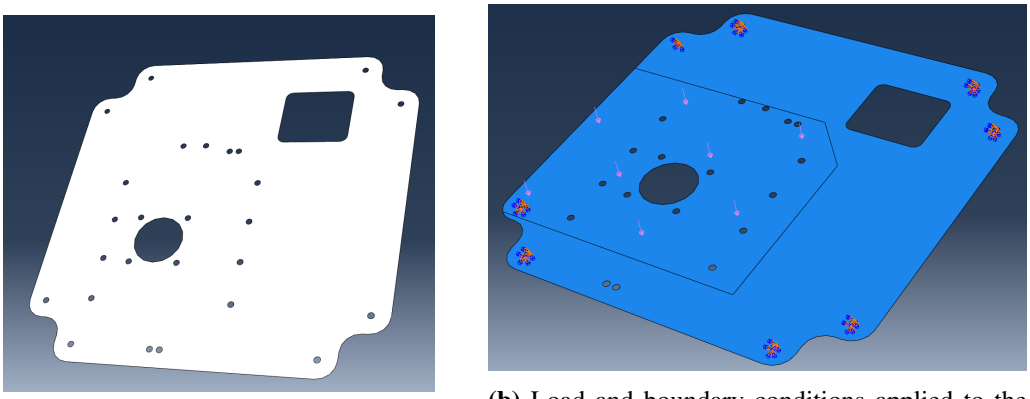

(a) Shell model of the part

(b) Load and boundary conditions applied to the body

Figure 6.1: Shell model (a) and load and boundary conditions applied to the body (b)

The next step was to create the mesh. In this case study it was used shell elements. The usage of shell elements allow for faster results with similar accuracy to the 3D elements. Quadratic elements over a free mesh were selected due to the higher number of Gauss points compared to a triangular element. Thus, the type of element used was a linear S4 element, that *ABAQUS*

describes as a "4 nod doubly curved general purpose shell, infinite". The information about this mesh can be observed in table 6.1. Figure 6.2 shows the obtained results [104].

Element shape	Element type	Number of Elements	Number of Nodes	Element Order
Quad Free	S4	45619	46240	First order

Table 6.1: Mesh used wit S4 shell elements for the plate Model

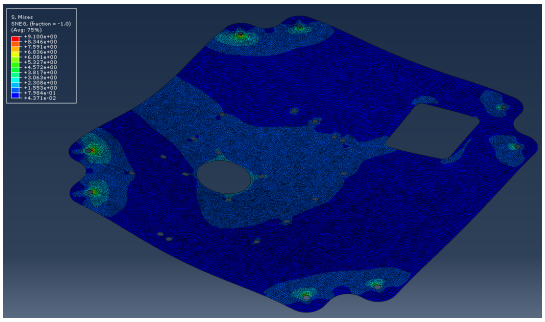

(a) Determined stress

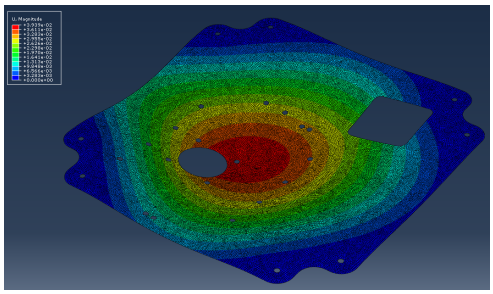

(b) Determined displacement

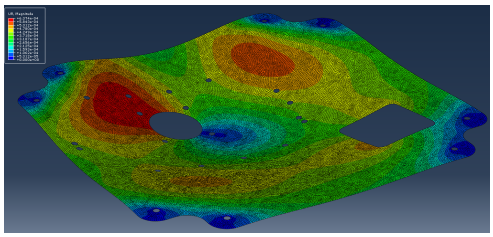

(c) Determined strain

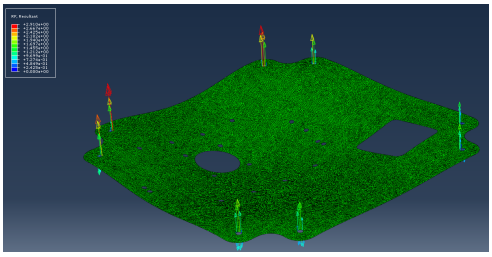

(d) Determined reaction forces

Figure 6.2: Determined strass (a), displacement (b), strain (c) and reaction forces (d)

Observing figure 6.2 it is possible to determine that the results obtained in figure 5.17 have some error. The small difference between maximum values obtained between the simulation and the Ritz method can be explained due to the consideration of a constant pressure over the surface, while in *ABAQUS*, the load is only applied in the partition are as seen in 6.1. The maximum displacement obtain was of 40 μm and the maximum stress is $9,1$ MPa. This values were inside the expected. A small displacement around 40 μm is not problematic on the focus of the system. The maximum stress is not above the yield stress of aluminium. It is possible to observe that the maximum stress will occur in section where the M3 bolts are fixing the plate. A typical low-cost M3 of material class 6.8 can withstand a proof tensilse strengh of 440 MPa [105]. As such, the maximum stress will not be a problem for the plate and the bolts fixing it.

6.1.1.2 *SolidWorks* embedded simulation

Solidworks Simulation allows to use shell elements as well. The same finite element analysis pipeline was used. Due to the limitations of *Solidworks*, the mesh used was blended curvature based mesh with a very refined element. The mesh obtained as well the load cases can be observed

in figure 6.3. The obtain results can be observed in figures 6.3b, 6.3c, 6.3d. The difference in values can be explained due to the mesh formulation of *Solidworks* by using triangular elements.

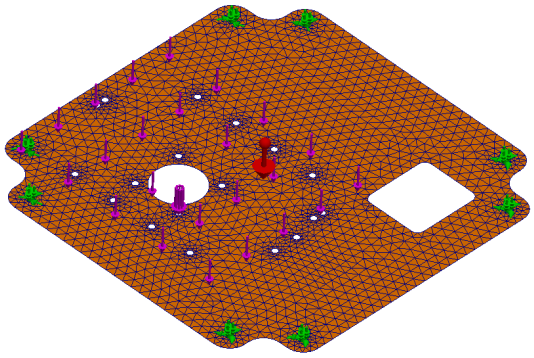

(a) Mesh and load case

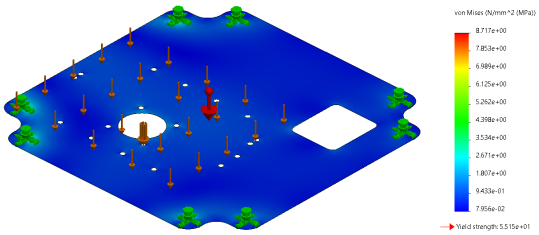

(b) Determined stress

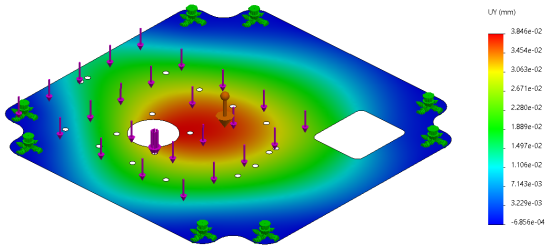

(c) Determined displacement

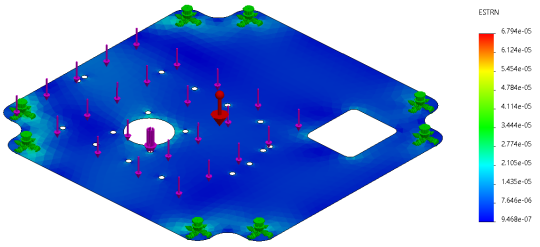

(d) Determined strain

Figure 6.3: Design space (a) and , determined stress (b), displacement (c), strain (d)

Thus the maximum stress by *Solidworks* formulation is 8,17 MPa and the maximum displacement is 38,6 μm. Therefore, *Solidworks* presents excellent results compared to *ABAQUS*. This presents a good advantage to*Solidworks* software, that without having to leave the CAD program, it is possible to run accurate static simulations with ease.

6.1.1.3 Sandwich structure

In this chapter, only *ABAQUS* was used due to the increased complexity that only an computer assisted engineering (CAE) Software can correctly replicate. To avoid using interaction and other factor that would increase the model complexity, the sandwich plate was built in *ABAQUS* from the initial mesh itself.

Studying Alucobond® technical data it is possible to observe that in their inventory plates have either 3 or 4 mm thickness, where the aluminium film as a thickness of 0.5 mm. It was used the 3 mm plate. Thus 4 elements were used to describe the core material and 2 for the aluminium films. It is expected that a 3 mm plate has less displacement that what it was observed in chapter 5 due to the higher flexural stiffness and lesser weight.

The aluminium properties were used as the outside film material. As for the foam material that composes the core, it was considered fully dense 100% PET [99]. Alucobond® adds solid minerals

in the core foam to help retarding fire and make it more durable. This effect will not be considered as it doesn't affect structural properties. Load were applied over one surface only as way to be similar to the real case and boundary conditions were considered in the area where the bolts will be fixed. The model created can be seen in figure 6.4a and the load cases in figure 6.4b. The The elements used in the creation of mesh model were for general cased of 3D stress. These are

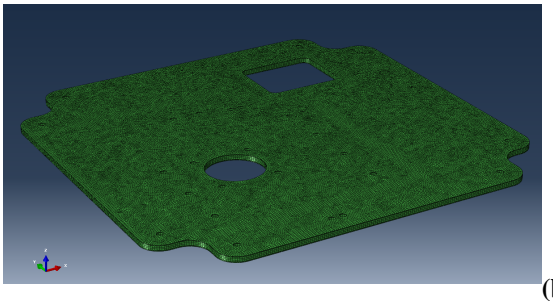

(a) 3D model of the part

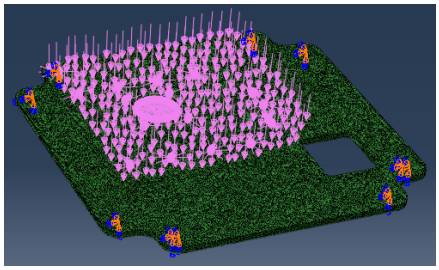

(b) Load and boundary conditions applied to the model

Figure 6.4: Model of the part (a) and the applied load and boundary conditions (b)

linear hexahedral elements with 8 nodes with reduced integration for better computer efficiency - C3D8R. The mesh used in this model can be consulted in table 6.2. The stress distribution in

Element shape	Element type	Number of Elements	Number of Nodes	Element Order
Hexahedral Free	C3D8R	319333	369920	First order

Table 6.2: Mesh used for the composite panel using solid elements - C3D8R

this plate can be seen in figure 6.5a, the displacement in figure 6.5b and the strain in the ε_{31} in the figure 6.5c As it is possible to observe, the expected was achieved. The 3 mm plate weights less that the 2 mm aluminium plate with better performance. The maximum displacement is half of the aluminium plate at 21,44 μm and the maximum stress is around $7,911MPa$. Performance wise, Alucobond® presents itself as good option to the sheet metal. It is possible to observe, in figure 6.5c, that the maximum strain happens at compression in the core material. Due to the fact that the core is less resistant that the film, crushing will subject the core to an extreme compressive load that in the long term the core material loses their mechanical properties leading to an eventual pull-through failure [106]. This problem can be solve using for example another material in the region where it the bolt will be fixed.

6.1.1.4 Summary

To sum up, it was possible to observe that 2 mm aluminium sheet can withstand the load and the performance required. Another important factor that it was observed is that *SolidWorks* and *ABAQUS* for simple cases both present accurate results. Finally the Alucobond® sandwich solution was analyzed presenting itself as a good solution to reduce weight in a significant while maintaining a good performance. Table 6.3 shows the obtained values for the different situations.

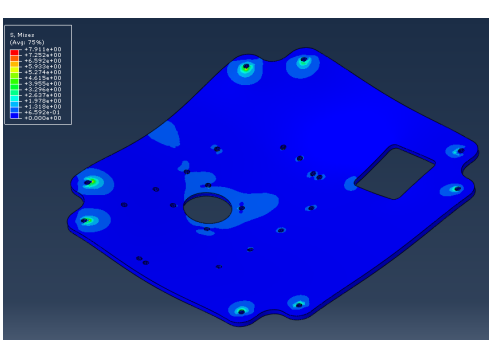

(a) Stress of the model

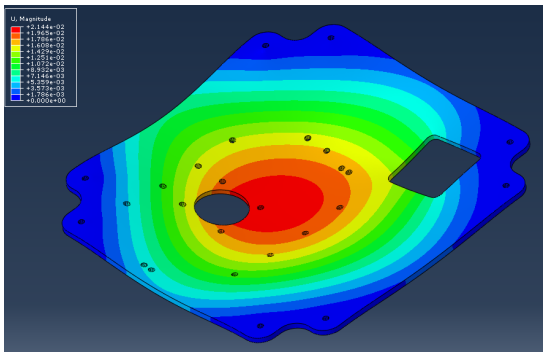

(b) Displacement of the model

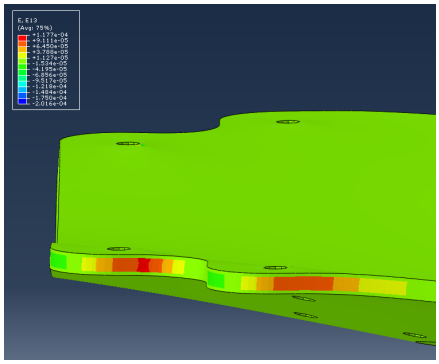

(c) Strain in the ε_{31}

Figure 6.5: Determined stress (a), displacement (b) and strain (c) in the model

The weight of both XY was measured. The aluminium plate weighted 190g and the Alucobond® weighted 134g. This is a difference of 56g, a reduction of 30%. The displacement of Alucobond® is 18 μm lower, a reduction of 46%.

Case Study	Max Stress [MPa]	Displacement [mm]	Strain
ABAQUS	9,1	0,03939	$6{,}374e^{-4}$
SolidWorks	8,717	0,03846	$6{,}794e^{-5}$
Alucobond®	7,911	0,02144	$1{,}309e^{-4}$

Table 6.3: Summary of the study of the base plate

6.1.2 Beam Case

The last structural case that it is of utmost importance to confirm is the possibility of bending and buckling of the main 20x20 aluminium profiles that are holding the optic tube. This way it will be possible to predict possible errors in the perpendicularity of the optic tube when focusing. The mesh used can be observed in table 6.4.

To design the model, the section of the profile was imported to *ABAQUS* and then extruded to the desired height. Firstly, the tested load case consists only on an encastrated beam with torque in the top region. To correctly simulate this moment, it was created an binary on the edges of the

Element shape	Element type	Number of Elements	Number of Nodes	Element Order
Hexahedral Free	C3D8	77532	106038	First order

Table 6.4: Mesh used for the beam model using solid elements C3D8

section with two opposing forces of 100 N. These forces combined will create an bending moment of 1 Nm in the top surface in the desired direction. The maximum displacement observes was 50 μm as it is possible to observe in figure 6.6.

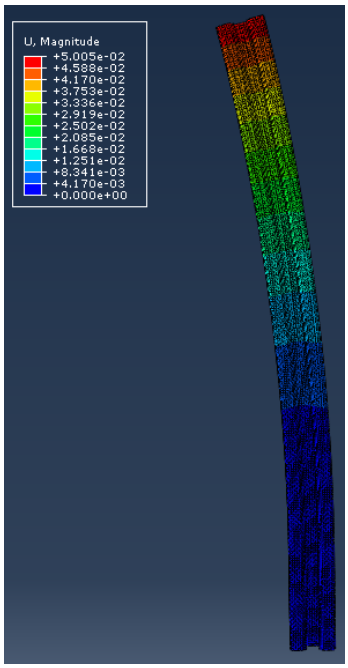

Figure 6.6: Determined displacement

50 μ m is not a critical displacement that might compromise the sampling process. Although, it might, lead to a higher focusing time due to the unnecessary parasitic displacement. Thus, it was added side walls and other beam to help this factor. The new load case takes this factors in considerations as demonstrated in figure 6.7.

Thus, with this new load cases the results were as expected, confirming the sturdiness of the structure. The maximum deflection is of $3,68e^{-8}mm$ as it is displayed in figure 6.7.

In conclusion, with the addition of the side walls and the extra support from the beam of the XY stage, the optic tube perpendicularity is achieved in the nanometric field. This fact ensures the correct and best performance of the focusing mechanism.

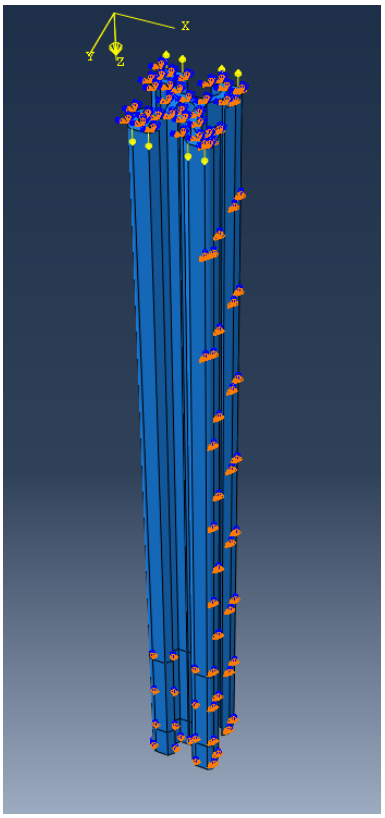

(a) Realistic load case

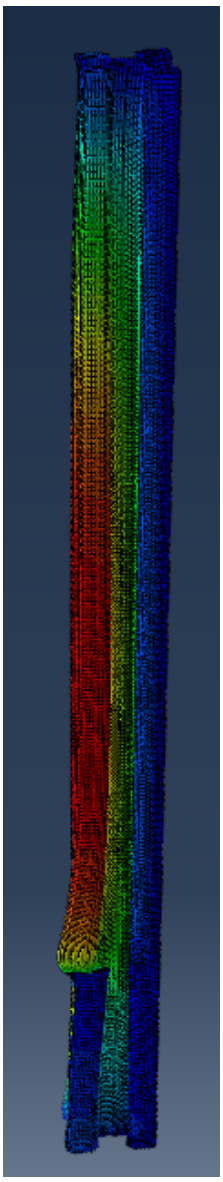

(b) Final displacement of the model

Figure 6.7: Realistic restrains (a) and computed displacement (b)

6.2 Case Studies

In this section, different critical parts will be studied. These pieces are in a situation where they need to, fundamentally, be 3D dimensional. Thus, in the final product these parts will be done by manufacturing processes that are not based in sheet metal. Therefore, these parts will be considered the most expensive as well keeping an high importance for the correct performance of the microscope.

Finite element analysis will be used in the correspondent load conditions to understand the behaviour of the pieces to the load cases. Topology optimization will also be used as way to reduce as much mass possible and still maintain the necessary stiffness to resist displacement. The main goal is to reduce mass as possible, while keeping the part easy to manufacture.

Due to the possibility to use additive manufacturing processes, topology optimization can be used without limits. The part design pipeline can be seen in picture 6.8. Firstly, from a rough CAD model, an static FEA verification is done to observe if the initial model can withstand the load conditions. After this stage, if positive, the topology optimization algorithm is run. Models originated from this routine are usually a non-parametric model leaving it hard to redesign. These models also present sections and geometries that are impossible to create in traditional manufacturing process. The complex geometries are also pron to high concentration factors that will lead to residual stress and locations where fracture will occurs. After the redesign theses pieces can be submitted again for the topology optimization, if needed. The final digital stage is to validate again by FEA the mechanical results. Finally, a prototype of the parts is created to observe the final piece and the geometry, allowing to validate the part and the mechanical behaviour [107, 108].

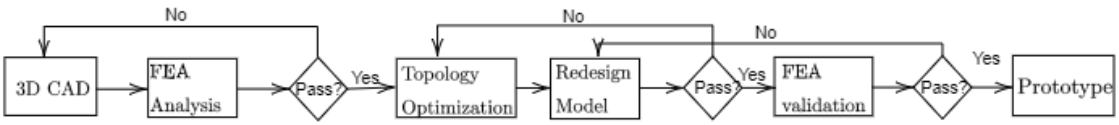

Figure 6.8: Part design sequence

The parts that were submitted to this design process were: the smartphone holder, the optic tube holder and the engine mount. The smartphone holder is a typical textbook example of a part that can be optimized. The performance of this design space is characterized by the displacement that occurs between the hole for the smartphone camera. The only function of this part is to hold the smartphone and guarantee that there is no enough deflection that might affect the results and the perpendicularity between the camera and the hole. The part that holds the optic tube main goal is to allow for the translation without considerable radial misalignment. This piece is also a low cost solution to the one that exist in the market and can easily be applied to different prototype solutions. The last case study is the engine holder, that can be replaced easily by a market engine mount. The main goal to use this part is to reduce weight and increase flexibility in the assembly stage as well making the prototypes more compact.

6.2.1 smartphone Holder

With the evolution of the prototype to move the Z-axis, it comes the challenge of creating a piece that can correctly hold the smartphone without major displacement. High displacement might compromise results due to the loss of resolution in the correct position. The major problem of this part is to guarantee the necessary stiffness with the lightest weight possible. The heavier this part is, the more it will influence the performance of the focusing mechanism.

Before starting the development of the part, different smartphone sizes and weight were searched and the position of the back camera as well. This results can be consulted in table 6.5. This way it is possible over dimension in a way to understand to predict future tendencies of bigger smartphones. Another factor to consider is the general weight of the smartphone as well the position of the camera module. Most smartphone have their camera on the left. As such, that detail was considered to create an piece that has non symmetrical support. As it is possible to observe weight

SmartPhone	Year of Release	Weight [g]	Size [mm]	Camera Module
Samsung A71	2020	179	163.6 x 76	Left
Samsung s20 Ultra	2020	220	166.9 x 76	Left
Iphone 11s Pro Max	2020	226	158 x 77.8	Left
Iphone 6s	2015	143	138.3 x 67.1	Left
One Plus 6T	2018	185	157.5 x 74.8	Center
Xiaomi Mi 6	2017	168	145.2 x 70.5	Left

Table 6.5: Different smartphone models

and general dimensions haven't increased considerably. Thus, the size of this piece will be 200 x 200 mm and design to withstand a load of 1 kg. This indicates that the device will, structurally, support future iterations and possible bigger smartphone sizes. To start the design process, this part started as a block with 200x200x23 mm. It was chosen 23 mm as thickness because it is the maximum value that allow for enough mounting clearance of the engine.

6.2.1.1 CAE model creation and initial verification

Before departing to the different load cases and fixtures, it is important to define the material. As this part will be 3D printed in the most common material in PLA. It will be used the 2.85 mm Ultimaker PLA. Thus the properties of this material can be seen in table 6.6. It is expected that by designing for PLA then it will also be correctly designed for other stronger polymers such as ABS or Nylon 6 and metallic materials as well.

Tensile Modulus	Tensilse stress at yield	Elongation at yield	Flexural strength	Flexural Modulus
2347 MPa	45,6 MPa	3.3 %	103 MPa	3150 MPa

Table 6.6: Ultimaker's PLA mechanical properties [109]

Firstly, an static load case to the normal part was done, while using very refined blended curvature-based mesh. Table 6.7 displays the mesh used. Cylindrical restrains were used as well

Type of Mesh	Number of Nodes	Number of Elements	Element type	Element order
Blended Curvature based	42402	27887	Tetrahedron	Second Order

Table 6.7: Mesh used for the static simulation of the smartphone holder

an uniform pressure on the top surface. These factors can be observed in figure 6.9a and figure 6.9b and the stress distribution in figure 6.9c and the displacement in study in figure 6.9d. Displacement

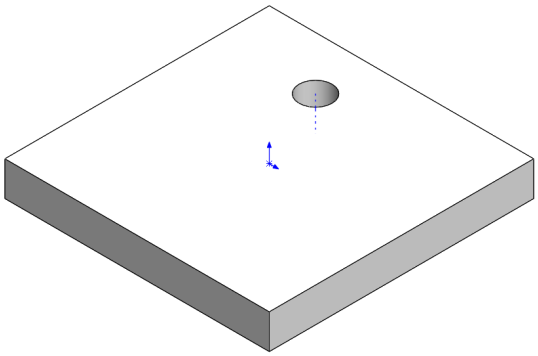

(a) Design space

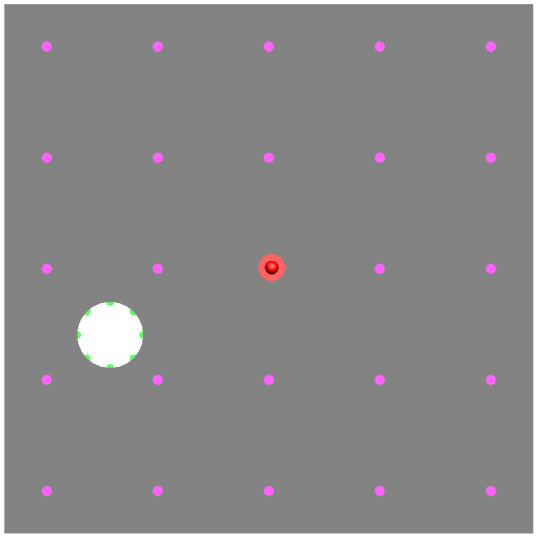

(b) Determined stress

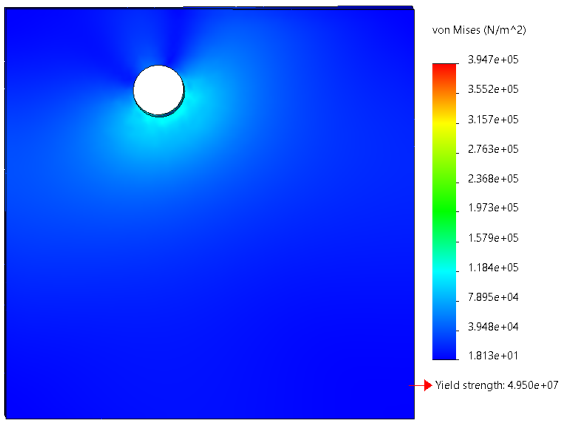

(c) Determined stress

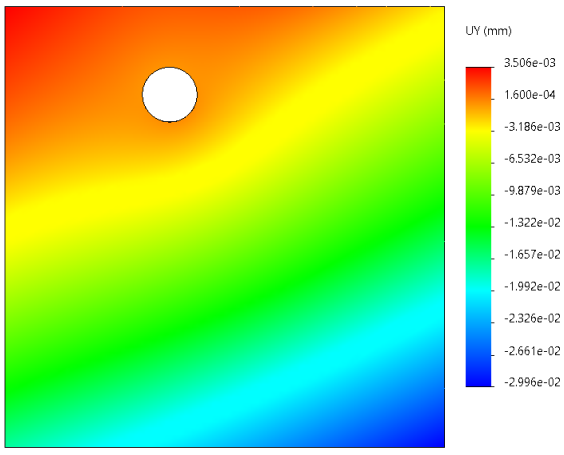

(d) Determined displacement in the Y direction

and stress are really small, therefore it is not expected any performance flaw with this thickness. The main problem is now to reduce weight while maintaining an excellent behaviour. The current weight according to *SolidWorks* is 1227.46 grams. This weight is not only very heavy as it is time consuming and expensive to prototype.

It was noticed that considering only the static load of the weight can be further away from the reality. It was considered that all of the thrust that the engine of the body is applied in this part. Thus, there are two different load cases, the first when it is according gravity acceleration and the second when it's against gravity. It is expect that the first load case is the one that will provoke the highest deflection due to existence of an higher load.

It was considered that this forces are being applied in the same surface where the weight of the smartphone is being applied since this is the most important surface. Furthermore, this study is only observing the effect of deflection in the vertical direction. As a consequence applying said force in the center of gravity of the body or in the surface would not create moments in the direction in study. Another important factor to take in consideration is that the thrust is being created as a force and not as a given displacement. This force is the sum of the first case with the thrust force in the direction of gravity, with the magnitude of 55 N. The correspondent stress and displacement can be seen in figures 6.10b and 6.10a, respectively. The last load case considered this force on the opposite direction, partaking a total of -35 N. The results of this second case can be observed in figure 6.10c and 6.10d. The maximum results of each load case can be observed in table 6.8.

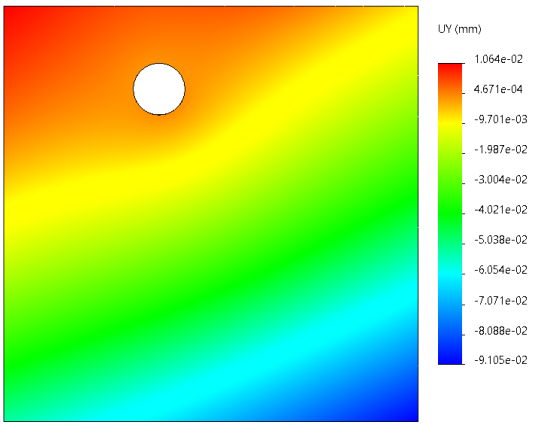

(a) Determined displacement for the higher load case

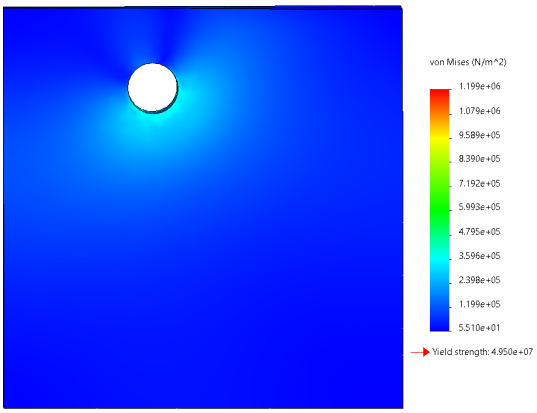

(b) Determined stress for the higher load case

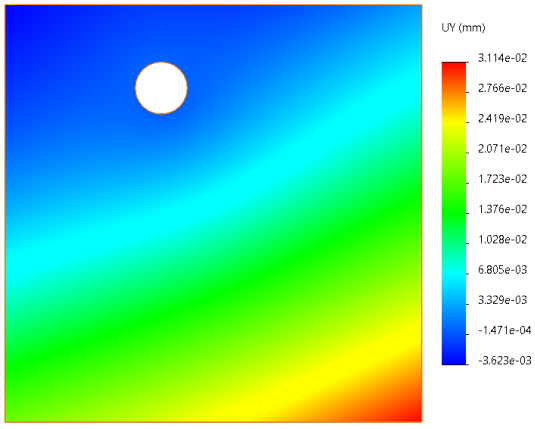

(c) Determined displacement for the lower load case

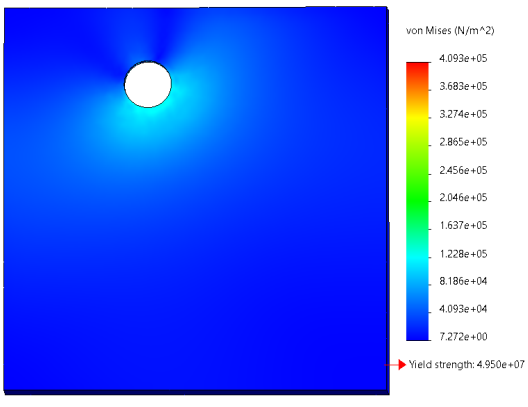

(d) Determined stress for the lower load case

	Max Tension [MPa]	Max displacement [mm]
Max load case	1,199 MPa	0,016
Min. load case	0,409 MPa	0,036

Table 6.8: Results for the different load cases

As expected the maximum load case has the highest displacement and stress. The highest displacement happens in near the edge, not affecting in a significant manner the performance of this part. It is important to remember that an smartphone will never fully spread over the entire area. It is possible to observe that the maximum stress happens in the interaction between the part and the optic tube. It is important to observe that there is some tilting happening in another edge. This factor will be corrected with the fact that the smartphone does not cover all of the surface. Another, more extreme solution, is the addition of a fastener feature to better hold the part.

As a consequence, it is important to observe the same two load cases while interacting with the optic tube. In this model there are two different distinct formulations: considering the optic tube infinitely rigid or considering it deformable with remaining parts. The first formulation will save computational power while possibly sacrificing accuracy. In this model cylindrical fixtures were considered where the optic tube in the part that hold the optic tube in place. Thrust force was still considered in the top surface as a conservative design formulation. In addition, due to the considerable weight of the part, the center of gravity it is still close to surface. This way, it is expected that real displacement will be smaller that the calculated. Mesh and fixtures can be seen in figure 6.11.

The mesh considered for this case was a very refined blended curvature based mesh. The values used for this model can be observed in table 6.9. Interacting surfaces were found using

Type of Mesh	Number of Nodes	Number of Elements	Element type	Element order
Blended Curvature based	98480	65017	Tetrahedron	Second Order

Table 6.9: Mesh used for the assembly formulation

the automatic interaction finder of *Solidworks*. Although, it was considered that the interaction between the optic tube and the part is non-penetrative to allow possible rotation. This will present a more real behaviour of both parts. The results where the optic tube as an deformable body can be seen in figure 6.12. As it is possible to observe results are considerable different from the case with non interaction. The highest resultant displacement for the highest load case is $0,529mm$. Once again this extreme value is only present on an extreme edge. Maximum stress, although a little bit higher, it is very similar, in a design insight standpoint, with the value of $2,044MPa$. The main difference is that now, this stress is distributed in a larger area ant it is the optic tube dealing with most of it.

The next model, is considering the optic tube infinitely rigid compared to the part in study. This is a valid hypothesis, the rigidity of the optic tube can be also considered the rigidity of

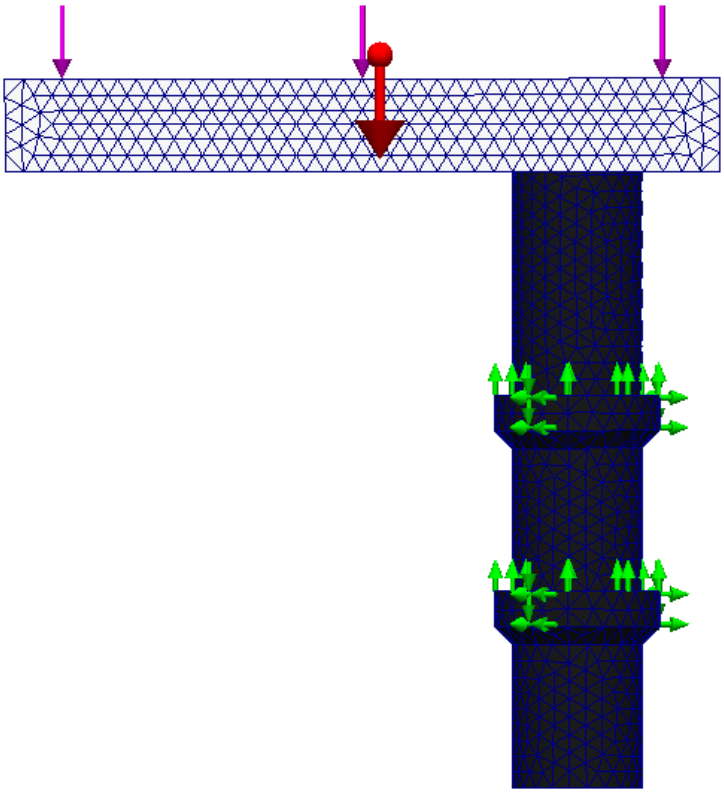

Figure 6.11: Mesh and fixtures with interaction with the optic tube

the piece that holds it, and the chassis of product. This consideration can be done since this parts are "bonded" together. Thus the total rigidity will be higher than the rigidity of the part in study. Another factor that adds to this conclusion is the fact that PLA under the glass transition temperature is extremely brittle, not allowing for a plastic behaviour. Thus, the obtained results can be seen in picture 6.13. It is possible to observe that this results are closer to the model where the body is simulated without interactions with the exterior. Maximum resultant displacement is $0,093mm$ and the maximum stress is $1,301MPa$. The results of the different models for the maximum load situation can be observed in table 6.10.

	Max Tension [MPa]	Max displacement [mm]
Rigid Model	1,301	-0,093
Non interactive	1,341	-0,092
Deformable	2,044	-0,529

Table 6.10: Results for the different models

To conclude, the non-interactive model presents as the lest conservative option that requires few computational power. Due to the need of needing less computational efforts this model will be used in the different case studies and topology optimization study. Another interesting observation is that the static model will have very similar results to the model that considers the optic tube

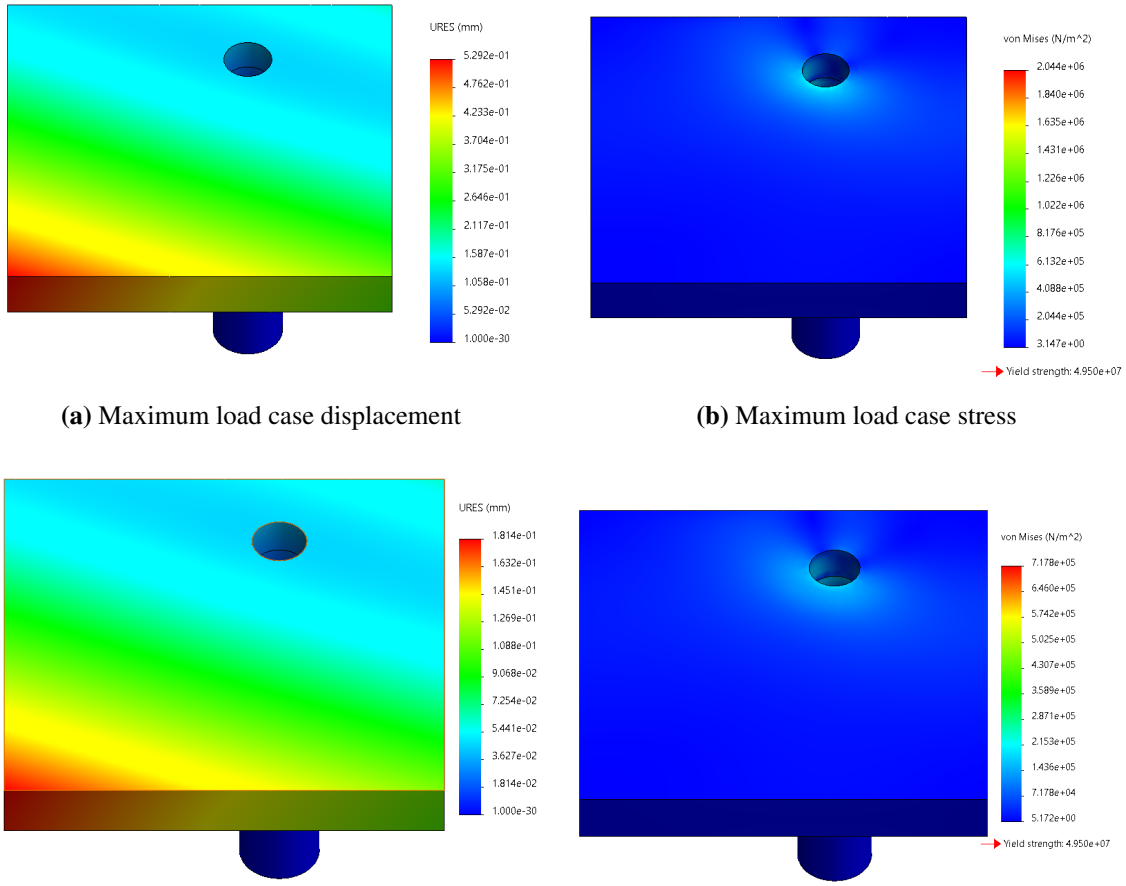

(a) Maximum load case displacement

(b) Maximum load case stress

(c) Minimum load case displacement

(d) Minimum load case stress

Figure 6.12: Computed result for the deformable body hypothesis

extremely rigid. It is important to notice that the most correct approach to this simulation would be by using multi body dynamics, that would come with the increased accuracy and computational complexity.In this solution, considers the thrust force as the maximum force that will be produced by inertial efforts. Considering the maximum thrust force is a simplification that implies that the maximum acceleration is applied to the body in the initial instant matter. Thus, it is important the usage of high security coefficients and use all the values obtained as design considerations and approximation to a simplified version. The real part is expected to be slower as the engine will never achieve the maximum acceleration in such a short displacement. Thus ,the effects of inertia and linear momentum are expected to be lower of those considered in the simplification, making the presented values good conservative approximations.

6.2.1.2 Topology Optimization

After deciding the CAE model to use, it is now possible to proceed to the topology optimization of the part in question. Normally, topology optimization is exclusively for a specific load case creating the best part for that situation. It is expected that different load cases will require a different

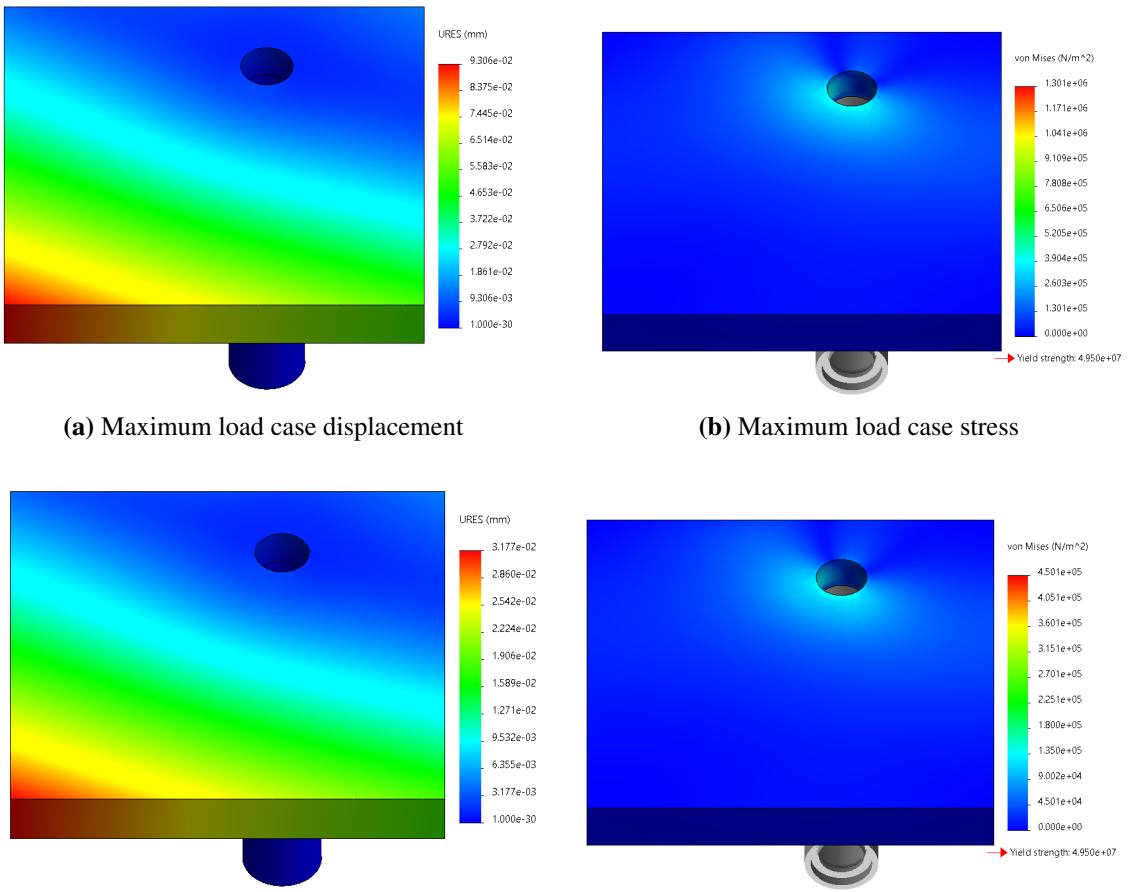

(a) Maximum load case displacement

(b) Maximum load case stress

(c) Minimum load case displacement

(d) Minimum load case stress

Figure 6.13: Computed result for the rigid body hypothesis

behaviour from the part. As such, *SolidWorks* topology optimization plug-in allows for multiple load cases optimization. Due to the geometry of the body in study it was used a refined standard mesh as it is possible to observed in table 6.11. Thus, the part created will be the optimized for all

Type of Mesh	Number of Nodes	Number of Elements	Element type	Element order
Standard	44453	217798	Tetrahedron	First Order

Table 6.11: Mesh used for the cellholder for the topology optimization algorithm

the load cases in simultaneous. The decided goal in the first iteration was to achieve the best stiffness to weight ratio while reducing mass. The smoothed mesh body and the respective redesigned part, can be seen in figure 6.14. This first iteration has a weight of approximately 610 g. It has been reduced 613g. Even thought that is a lot of weight reduced, it is of utmost importance to be able to make this part even lighter or it will be hard to create an competitive focusing system. Before heading for a second iteration and maximum load case simulation was undertaken. The goal of this study is to understand if the performance of the part is already in it's limit and if there is still room to better enhance performance. The maximum stress observed by this part was $1,610MPa$

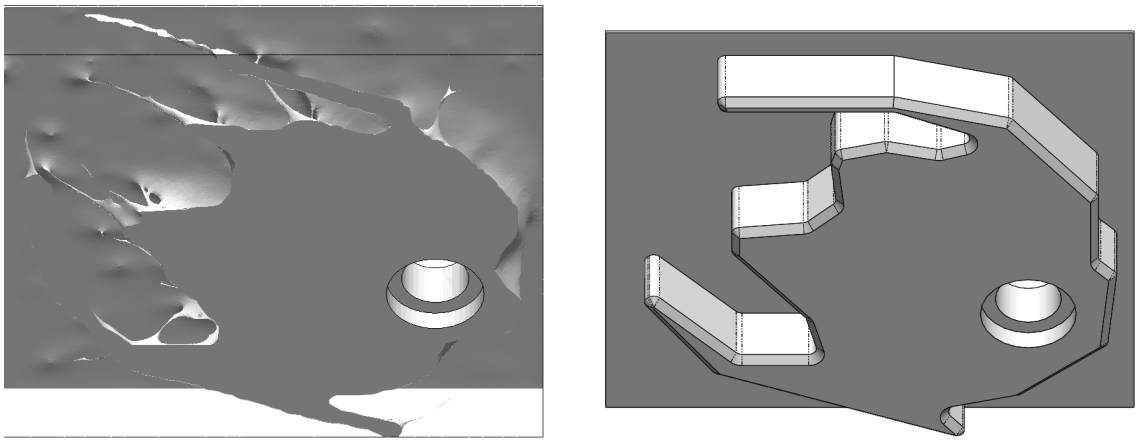

(a) Smoothed mesh body of the first iteration

(b) Redesigned part first iteration

Figure 6.14: Smoothed mesh body (a) and Redesigned part (b)

and the maximum resultant displacement was $-0,2813mm$. This value only appears on the edges of the body and most of part that will actually be covered by the smartphone will have a maximum resultant displacement of 80 microns.

After analyzing the results obtained, it is viable to undertake the part in a second iteration with the same objective: maximize stiffness per gram while reducing mass. The final mass obtained was 282 g, a reduction of 331g from the previous iteration and 941g from the initial part. The new model obtained was redesigned and tested. After different iterations on the design on the second topology optimization iteration, the final part was created. Another feature that was edited was the base thickness. Increasing thickness will increase directly rigidity. The final simulation results can be seen in figure 6.15. The final part has 245 g. The maximum stress observed was

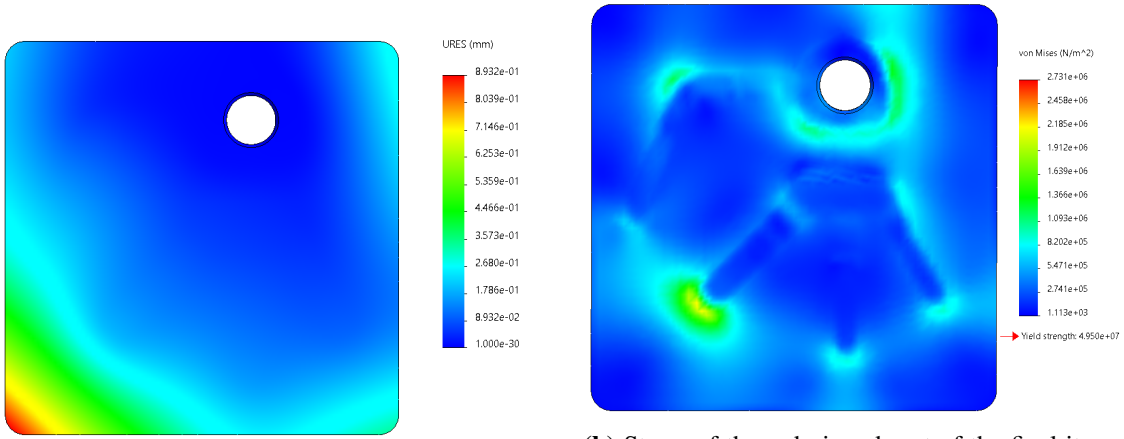

(a) Displacement of the redesigned

(b) Stress of the redesigned part of the final iteration

Figure 6.15: Displacement (a) and Stress (b) of the redesign part of the final iteration

$2,731MPa$ and the maximum displacement $-0,893mm$. It is extremely important to analyse that the part of the body where the smartphone will actually be, have a maximum a medium value of

150 micrometers. As such, it is expected that will not affect severely the perpendicularity of the body.

The final weight of the part can be improved by the usage of cellular structures typical of additive manufacturing. By reducing the % of infill density is possible to reduce exponentially without sacrificing to much mechanical behaviour. The slicer simulates for a 30% cubic infill a total of 165 g. The final part obtained can be seen in picture 6.16

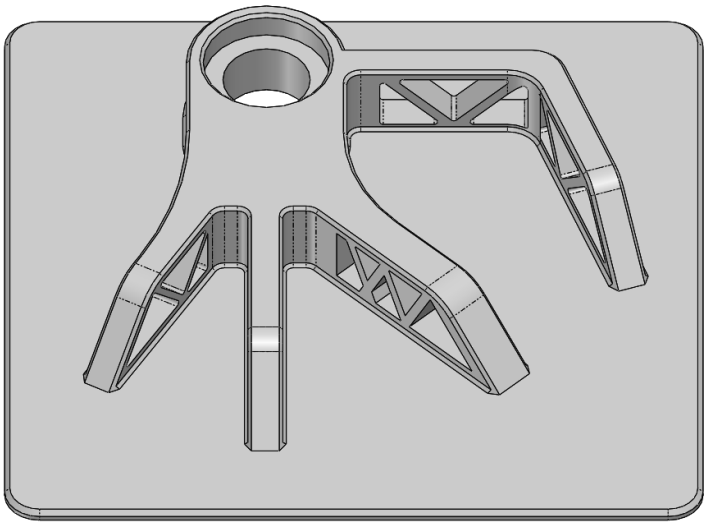

Figure 6.16: Final part obtained

6.2.2 Optic Tube Holder

With the decision to translate the optic tube vertically, it was now required an part that would mount the optic tube to the linear guiding system. This part requires high strength and lightweight. The high stiffness is necessary so that the optic tube doesn't suffer any misalignment due to inertial efforts. To achieve this, the topology of the optic tube was changes to allow non-invasive fastening. Two cylindrical features were added with the goal to be cover by two parts that hold the optic tube in tube. One point of fixation is more than enough to bond the optic tube with the rest of the mechanism. Some aftermarket products do present this geometry [22].

Thus, to mitigate this problem and use polymers based products that are extensively lighter that the metallic counter part and FDA approved, two support points were used. This way it is possible to correctly define a line and guarantee that there are no parasitic motions that can lead to misalignment. In both these two cylindrical feature, 45º degrees chanfers were added to help the manufacturing of the optical tube without the addition of supports. As such, less time and less material is required while achieving better results.

6.2.2.1 Static simulations

The optic tube mount starts as a block that can hold the required part. Before proceeding with the topology optimization verification, an first static analysis was made. The load cases are similar as the ones seen in chapter 6.2.1 but one kilogram in total weight was added to consider the weight of the optic tube and respective optic. In this part the total weight is divided in two different surfaces where the loads will be divided equally. It is expected that the smaller surface will achieve higher displacements and stress. In the case where thrust is opposing gravity, the resultant force is applied in the top surface. To have in consideration harder geometries to mesh, a very fine blended based curvature mesh used. The final mesh used can be observed in table 6.12. Fixation was considered

Type of Mesh	Number of Nodes	Number of Elements	Element type	Element order
Blended curvature based	14608	8759	Tetrahedron	Second Order

Table 6.12: Mesh used for the static analysis of the optic tube holder

two different situation: a simple support in the back wall due to the sheet plate and cylindrical fixation in the place where the brass inserts will be. The maximum load case and fixtures are represented in figure 6.17.

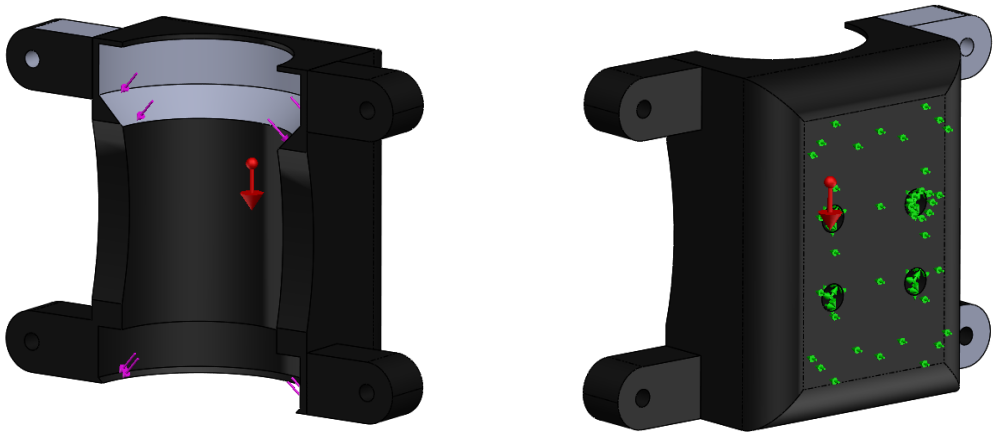

(a) Considered loads for the maximum situation **(b)** Fixtures used in the model

Figure 6.17: Considered loads for the maximum situation (a) and fixtures (b) used in the model

After analyzing both static cases, it was concluded that displacement would not be an issue in this part. Due to the high rigidity of the model, displacement was in a sub-micron magnitude. It was observed that stress can be problematic. Even though magnitude is low, it is concentrated in places where area and thickness are very small. Both load cases stress can be observed in figure 6.18. These features need extra improvement an attention to guarantee a more evenly stress distribution over the body. However, stress the maximum stress that the body achieves in a given

moment is $0,9199MPa$, that is safely under the yield stress of PLA. The maximum resultant displacement observed in the body at a given moment is $0,012mm$.

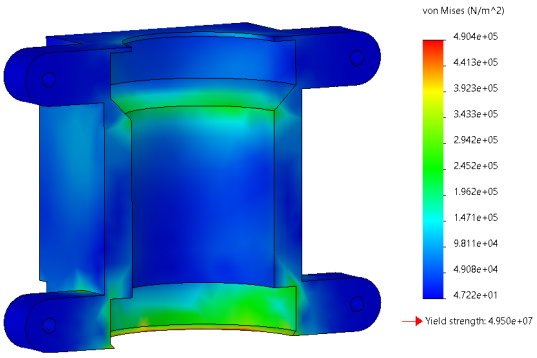

(a) Maximum load case stress behaviour

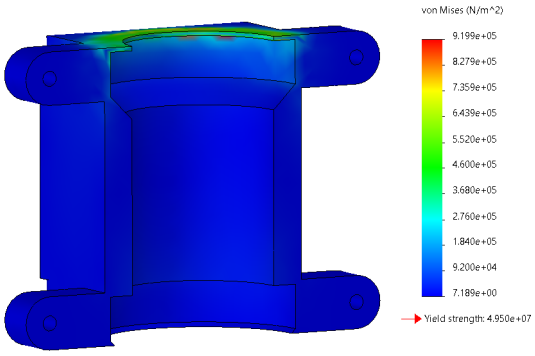

(b) Minimum load case stress behaviour

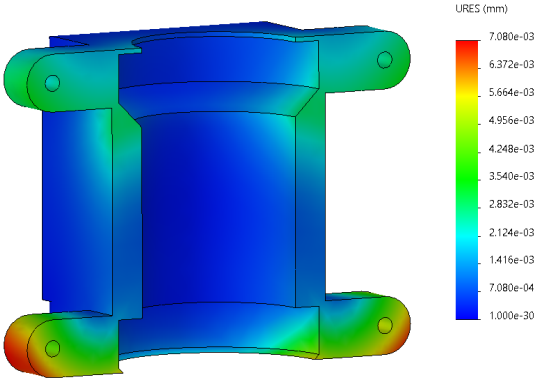

(c) Maximum load case displacement

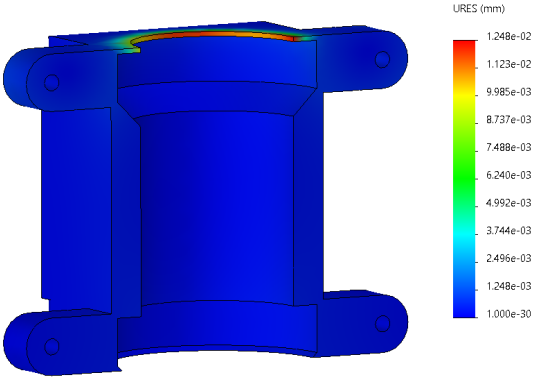

(d) Minimum load case stress

Figure 6.18: Maximum load case stress (a) and minimum load case stress (b) behaviour

6.2.2.2 Topology Optimization

Once the part is validated to undertaken the topology optimization algorithm, it can advance with the creation of goals. The initial part started with and initial mass of 80g. The main goal of this algorithm is to optimize stiffness per gram as it is necessary the maximum stiffness possible. It is expected to remove a minimum of 50% of mass, to a more tolerable 40 g. This weight guarantees a faster and cost effective performance. The main advantage of topology optimization, is that it also optimizes the amount of material used. This factor, in particular with additive manufacturing is vital as the main driver of cost is the price of filament.

In this case of topology optimization, it was used once again a table of cases, optimizing the part for different situations. In this case manufacturing controls were added to guarantee that the algorithm removes features. For example the place where brass inserts will be. Once again a very fine blended curvature based mesh was used to achieve accurate results. The description for this mesh can be observed in table 6.13. Figure 6.19 shows the final mesh body obtained and the

Type of Mesh	Number of Nodes	Number of Elements	Element type	Element order
Blended curvature based	28112	136820	Tetrahedron	First Order

Table 6.13: Mesh used for the topology optimization of the optic tube holder

redesigned part.

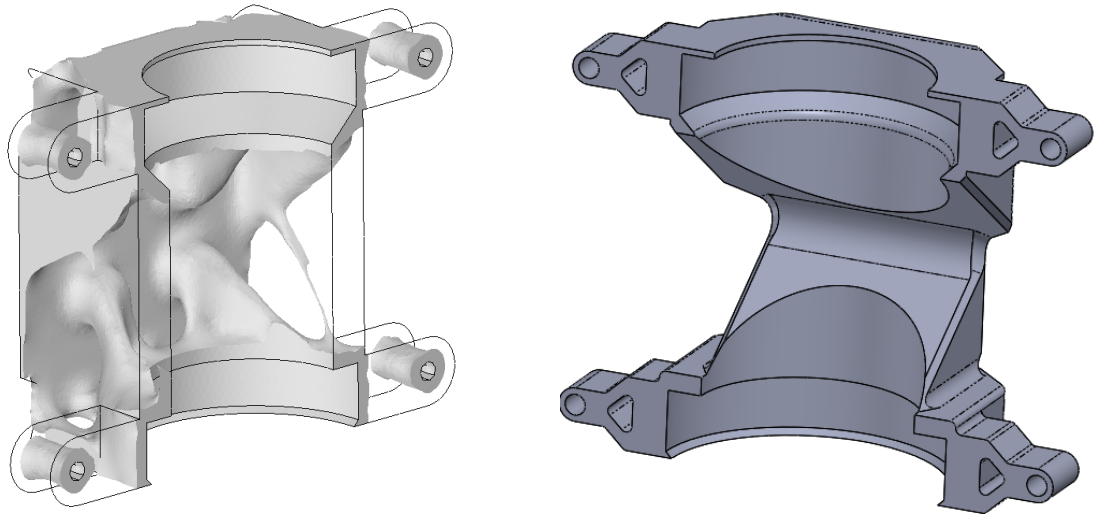

(a) Final mesh body **(b)** Final redesigned part

Figure 6.19: Smoothed body mesh (a) re-designed part (b)

The obtained mesh body is certainly interesting. The prominent feature is the creation of triangle shapes from the cylindrical features to the back of the body. This triangle shapes will work as a truss structure leading efforts in a fast way to the connection with the exterior. Another interesting feature is the truss structure near the place where correspondent bolts will be added to ensure a complete fixation of the optic tube. The final part after being redesigned weights 42g. It is important to notice that this weight can be reduced tragically with the use of lattice structures such as different infill densities.

It proceeded a static analysis to the part to understand the behaviour of the part to the load cases in question. this way it is possible to validate the part. Once again the maximum displacement achieved is in the decimal units of the micron. The maximum resultant displacement observed was $0,029mm$. Thus, it is expected that misalignment will not be a problem. The stress and displacement distribution in both cases can be seen in figure 6.20. The maximum stress is not problematic with the maximum values of $1,128MPa$. It is expected that this part will work under the load conditions without any type of problems.

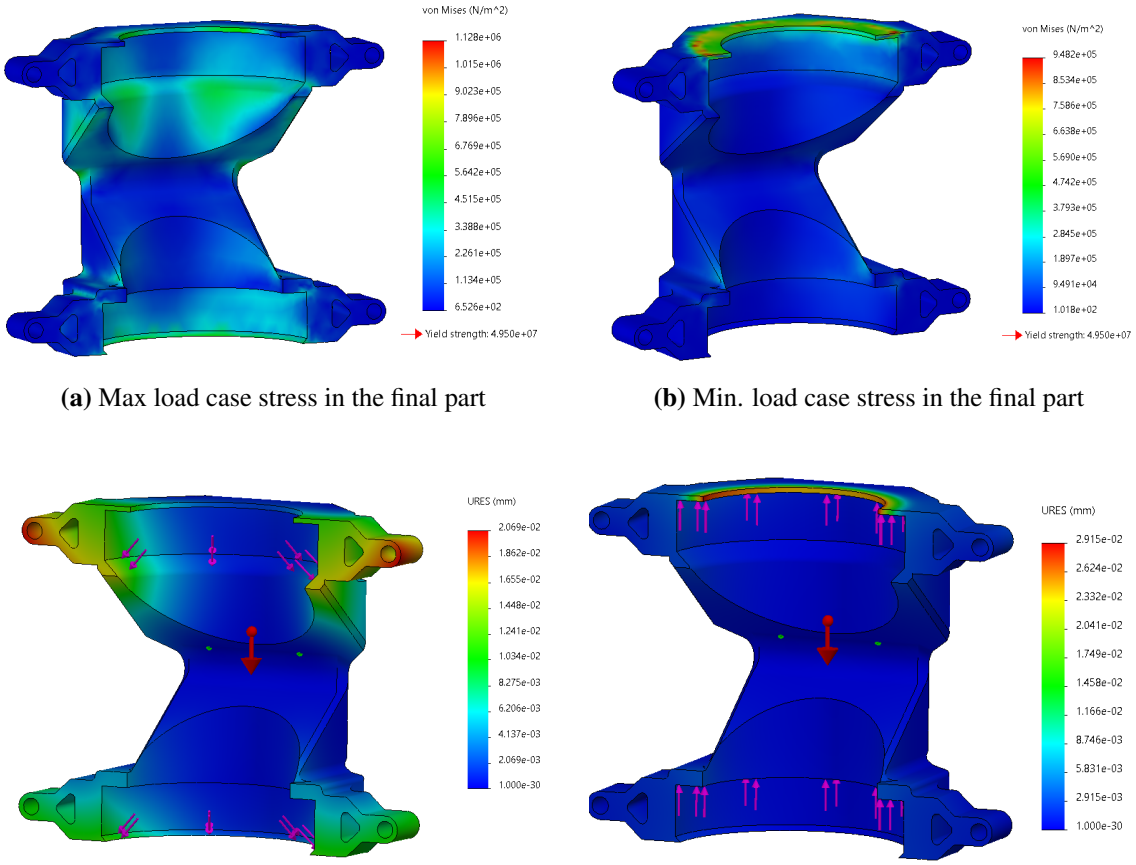

(a) Max load case stress in the final part

(b) Min. load case stress in the final part

(c) Maximum load case displacement

(d) Minimum load case stress

Figure 6.20: Stress behaviour for max load case (a) and min. load case (b)

6.2.3 Engine Mount

The final part that suffered the topology optimization design process was the engine holder. The goal of this part is to hold the engine in a lightweight and sturdy fashion. Normal engine holders are made of aluminium. It is important to notice that the original holder is already a light part and the study of this piece should be considered to understand the limitations of the topology optimization design process.

This part is the most complex part observed in the prototype. The main reason for this is that, this part is submitted to different load cases situations. The main goal is to hold correctly with minimum displacement of the engine. Thus maximizing stiffness while reducing weight as much as possible.

The created model considers the mass of the engine as a remote mass of 50g. This is applied by using the center of gravity of the engine and the weight of the engine. There are three different load situations on this parts: the first one only has to hold the engine, the second has to the the same function while withstanding inertial efforts due to the acceleration of stage. Finally, the last case is a static one where is has to withstand the mass of the engine in the vertical direction.

6.2.3.1 Static Simulations

The different load cases were test while using a high quality blended mesh. Table 6.14 shows the information considering the mesh used.

Type of Mesh	Number of Nodes	Number of Elements	Element type	Element order
Blended curvature based	88088	58219	Tetrahedron	Second Order

Table 6.14: Mesh used for the static analysis of the engine mounts

The maximum displacements of each load case situation can be observed in figure 6.21 and the maximum stress can be observed in figure 6.22. Being this a small part, high stress are expected.

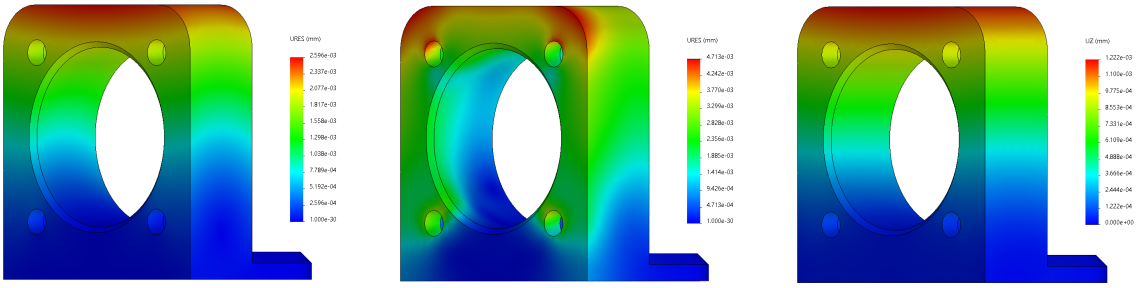

(a) Resultant displacement in the 25 mm load case

(b) Resultant displacement in the 40 mm load case

(c) Resultant displacement in the Z load case

Figure 6.21: Stress behaviour for max load case (a) and min. load case (b)

As expected the observed displacements are very small. Most of the displacement happen only in one direction while in the other directions were just parasitic movement. Most of the displacement occurred further from the places where the restrains are. The maximum observed displacement in the 3 load cases was in the 40 mm load case with a displacement of 4.713 μm. This is the critical load case due the presence of inertial efforts created by the movement in one specific direction while carrying the remote mass as well. It is expected that this efforts will be noticed in particular in the fasteners between the engine mount and the engine itself. As expected the maximum displacement is very small and does not presents as problematic for the correct performance of the mechanism.

In terms of stress the 40 mm load case is the one that it is expected to occur higher stresses due to dynamical efforts. As expected the maximum stress will occur in the interface where the engines will be mounted. The maximum stress observed is $6,463MPa$. As a consequence, stress will not be a problem when designing this part. It is possible to conclude that this part is ready to undergo the topology optimization algorithm.

6.2.3.2 Topology Optimization

Being this a complex part with different load cases a multiple load case situation will be used to correctly prepare this part. It was noticed that *Soliworks* uses a first order elements as a default for

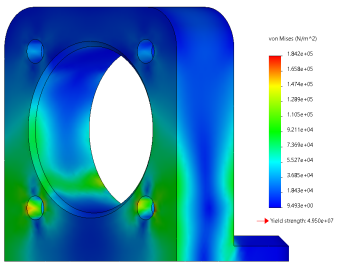

(a) Von Mises stress in the 25 mm axis load case

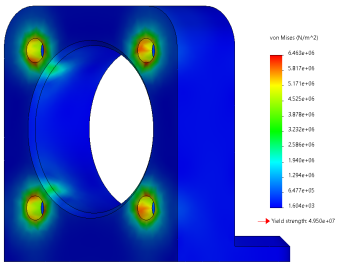

(b) Von Mises stress in the 40 mm axis load case

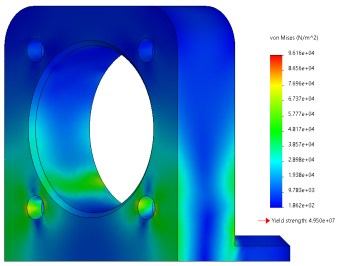

(c) Von Mises stress in the Z stage load case

Figure 6.22: Stress behaviour for max load case (a) and min. load case (b)

topology optimization cases. The main difference between a mesh with second order elements and a mesh with first order elements is the addition of 4 extra nodes and the order of the polynomial. A mesh with first order elements uses a linear polynomial approximation and less nodes [110]. Both meshes use a tetrahedral elements. As expected the mesh with second order elements will approximate better circular features with the main drawback of extra computational time [110]. The difference of the two elements can be observed in figure 6.23.

(a) Second order elements

(b) First order elements

Figure 6.23: Second order elements (a) and first order elements (b) [110]

It is important to also add that the type of mesh being used is a Blended Curvature-Based mesh. This mesh not only uses the surface algorithm to better fit the mesh in round features, but it also creates the same for internal elements. The main result of this is a more even aspect-ratio of elements [111].

Using a mesh with first order elements will save exponentially more time. The design process being used for topology optimization is also fool proof. The FEA static validations use as standard a mesh with second order elements. Thus, the parts after being redesign will be validated with a more accurate mesh. The main drawback that can be expected is the added difficult of reducing mass is regions of the part where the geometry is complex. To observe the difference between

using a mesh with first order elements and a second order quality one in the topology optimization algorithm, both were conducted on this parts with a blended curvature-based mesh with the smallest feature size as the element size. For reference the mesh with second order elements took 2 hours and 15 minutes to complete while the mesh with first order elements took 20 minutes. For the mesh with second order elements 201945 nodes and 137479 elements were created. For the mesh with first order elements 27549 and 137479 elements were created. It is possible to observe, that, as expected the number of nodes increased, but not the number of elements. The results of both can be observed in figure 6.24

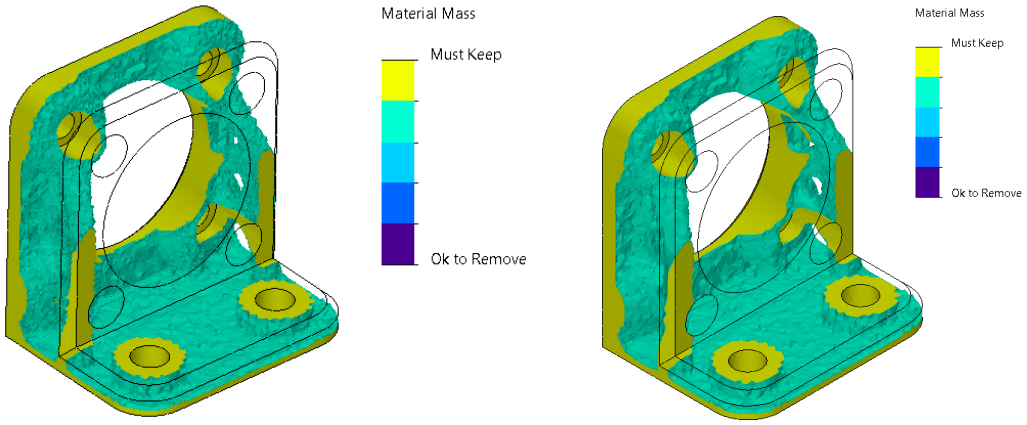

(a) Mass plot for the mesh with second order elements

(b) Mass plot for the mesh with first order elementsf)

Figure 6.24: Mass plots of the mesh with second order elements (a) and the mesh with first order elements (b)

As is possible to conclude, the mesh with first order elements and the mesh with second order elements had almost no influence in the final result of the topology optimization process. Thus, using a mesh with first order elements will be favorable to reduce the time due to computational efforts.

Different iterations were created from the final part. As a reference the initial part is expected to have about 3.7 grams. With a multiple iterative process it was possible to reduce the part to about 1.5 g. Once again the goal of using topology optimization on this part is not only to reduce weight, but to observe the limitations of this design process.

After redesigning the final part it is important to validate it in FEA. In figure 6.25 it is possible to observe the maximum displacement in the direction that occurs the maximum displacement for the different load cases. Figure 6.26 represents the Von Mises stress behaviour in the different load cases.

It is possible to observe that this final model do not suffer from considerable displacements, as such, this topology optimization present itself as good solution for the motor holder engine. It is important that this parts does not suffer from instability because the chosen actuators cannot handle many mounting flaws. It is possible to observe that the maximum stress will not be a

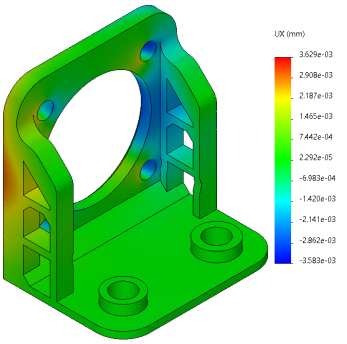

(a) Displacement for the maximum displacement direction for the 40 mm load case

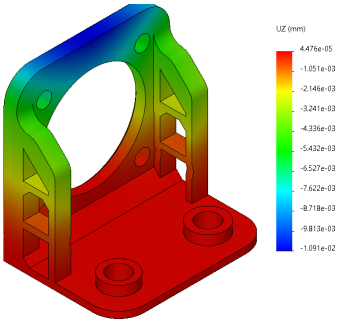

(b) Displacement for the maximum displacement direction for the 20 mm load case

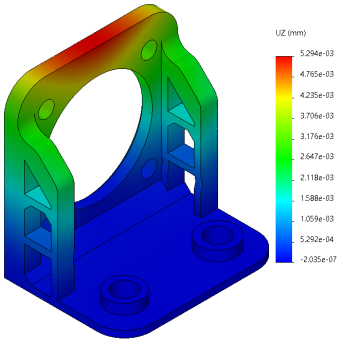

(c) Displacement for the maximum displacement direction for the Z-axis load case

Figure 6.25: Displacement for the 40 mm load case (a), 20 mm load case (b), and the Z-axis load case (c)

problem. Once again stress is focused in the fasteners that connect the wall mount with the parts itself.

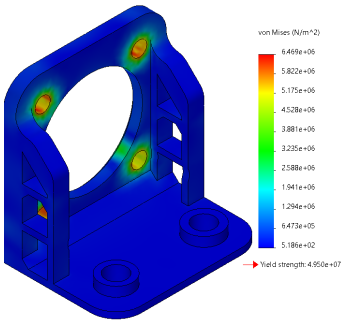

(a) Von Mises stress for the 40 mm load case

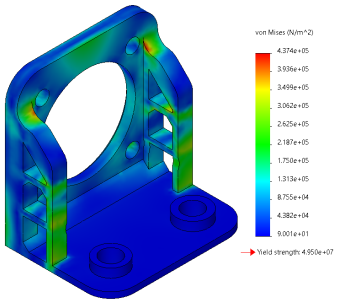

(b) Von Mises stress for the 20 mm load case

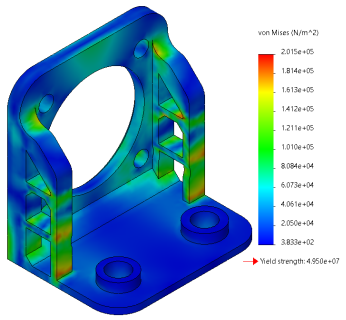

(c) Von Mises stress for the Z-axis load case

Figure 6.26: Von Mises stress for the 40 mm load case (a), 20 mm load case (b), and the Z-axis load case (c)

6.2.4 Dynamic validation

As final step of this chapter, dynamic validations were conducted. Even thought it is expected that the static load cases will have an conservative approximation to the real situation. Commonly, dynamic analysis is avoided so that it is not required complex models and extra computational power. Having a more accurate model and result will help reducing costs and improving parts for the simulation.

In the static simulation the inertial factor were approximated to the maximum thrust force that the engine could provide to the part. This is not accurate for two main reason: inertial factors and the working behaviour of the actuator. The first factor is the heaviest in the final accuracy of the results. It is not expected that all of the thrust force will be applied in the part as a force in a certain surface. The thrust force will be applied to body in study, proven by the second law of dynamics, as a given acceleration that it is dependent on the total inertia of the whole translating system. This means that the inertial factors that the body will suffer is not the maximum thrust force, but a rather lower $m_{part} \cdot a_{system}$. The mass of the part can be replaced by inertial matrix that will refer how mass is distributed along the body. The second main factor is that not only acceleration is time dependent but as well on the behaviour of the actuator. It is yet to be developed an engine that can in an instant apply the maximum thrust force to the system that is driving. Thus, the thrust force that is driving the system will probably reach the rated maximum thrust force of the engine, due to the small incremental nature of the mechanism.

In an linear static analysis the main driving equation of the system that will then be applied in the finite element analysis is:

$$[K]\{u\} = \{f\} \tag{6.1}$$

Where $[K]$ is the rigidity matrix, u is the displacement vector and the f is the resultant force vector [112]. This is the typical equation that static analysis use for the displacement of a cantilever beam, for example. In a linear dynamic analysis, the second law of dynamics it is applied and there will be inertial, damping and elastic factors [112]. As such, the equation taken in considerations in the finite element analysis is:

$$[M]\{\ddot{u}(t)\} + [C]\{\dot{u}(t)\} + [K]\{u(t)\} = \{f(t)\} \tag{6.2}$$

Where $[M]$ is a mass matrix of the body, $[C]$ is a damping matrix - typical in the presence of material with viscoeleastic properties - and $[K]$ is the rigidity matrix. It is important to notice that in a dynamic analysis displacement, $u(t)$ can vary with time and, as a consequence, force, $f(t)$ will to.

Polylactic acid is a biopolymer that due to a chain-like structure has a viscoelastic behaviour. Resembling other polymers, PLA is stable until the temperatures of around 60ºC, that it is the glass transition temperature. Above 65ºC PLA presents a significant loss in Young Modulus [113]. Having semi-cristally properties, PLA presents an visco-elastic behaviour over the glass transition temperature and a very brittle elastic behaviour under that temperature. This could be a problem if the whole system was not thermally stable. Due to the small usage of electronics and stable

actuators then ventilation is not required. Another solution would be to use a more thermally capable polymer in the additive manufacturing of the parts, such as PETg. Although, it is important to notice that creep occurs at ambient temperature. This is not expected to be a problem since loads are very small and temporary. As a conclusion, it is possible to consider PLA, in the dynamic model being created, as an elastic material. The differences will be negligible.

6.2.4.1 Cell Phone holder

This is probably the most critical part of the different case studies. This part will hold the user smartphone. It has to be lightweight and ensure that no harm happens to user's phone. Lightweight is extremely important to achieve the best velocity possible. The counter point of achieving higher velocities is higher inertial effects. Having a strong stiffness-to-weight ratio will also increase the natural frequency of the first mode of vibration which is important to avoid cyclic stress and parasitic noise.

For this model no global damping was considered. This means that if oscillations occurs, the body will keep oscillation without returning to the original position. Therefore, if the part is designed to withstand an "infinite" oscillation, then it can withstand anything else. The mesh used for this model can be observed in table 6.15. For exterior load it were considered two: the normal

Type of Mesh	Number of Nodes	Number of Elements	Element type	Element order
Blended Curvature based	77070	45985	Tetrahedron	Second Order

Table 6.15: Mesh used for the dynamical analysis of teh smartphone holder

force of the smartphone (10 Newton) and an uniform base excitation. The uniform base excitation was applied the known displacement, 5 mm, in a linear manner over the course of one second. It is expected that stress will be lower and displacement as well since it does not considers all of the thrust force on to the body. The observed dynamic stress and displacement can be observed in figure 6.27.

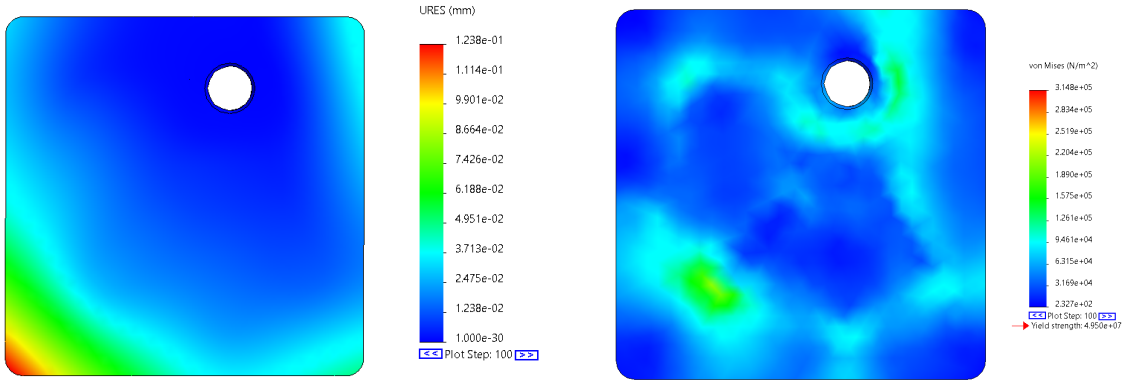

(a) Dynamic displacement of the part in study

(b) Dynamic stress of the part in study

Figure 6.27: Dynamic displacement (a) and stresses (b))

As expected initially, the better approximation would lead to more accurate results. Due to the really low density of PLA and the small weight of the smartphone, the maximum displacement and stress are lesser than the ones that this parts was designed to. As a consequence it is possible to safely guarantee the work-ability of the part. It is interesting to observe that the maximum displacement observed was only 128 μm. In the region where the smartphone will actually be applied it had a medium displacement of around 20 μm with a maximum stress of $0,115MPa$. As expected the values in the dynamical situation are exponentially lower, guaranteeing the definitive performance of the part.

To finally confirm this functioning of this part, the most accurate case was considered, a multi-body dynamical (MBD) model of the assembly. The final model of this part considers the assembly of the optic tube with the smart-phone holder. The optic tube was considered as a deformable body. To better register the load distribution of the smartphone on the part a partition was created with the dimension of 160 mm x 70 mm. A force of 10 Newtons was considered. Uniform base excitation was used to define gravity and a given displacement, 5 mm. A blended curvature-based mesh was used and a second order tetrahedron element. This can be seen in table 6.16.

Type of Mesh	Number of Nodes	Number of Elements	Element type	Element order
Blended Curvature based	43934	23825	Tetrahedron	Second Order

Table 6.16: Mesh used for the MBD

Between the two parts bonded contact sets were created since penetration between the bodies was not allowed. It is also expected that both bodies would displace themselves in unison. Being this the most accurate model, it is expected that displacement will occur mainly in the area where the forces are applied. Figure 6.28 shows the stress and displacement for this case.

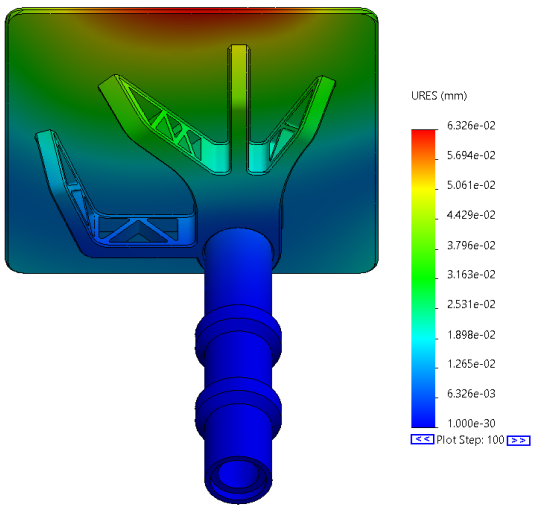

(a) Dynamic displacement of the assembly in study

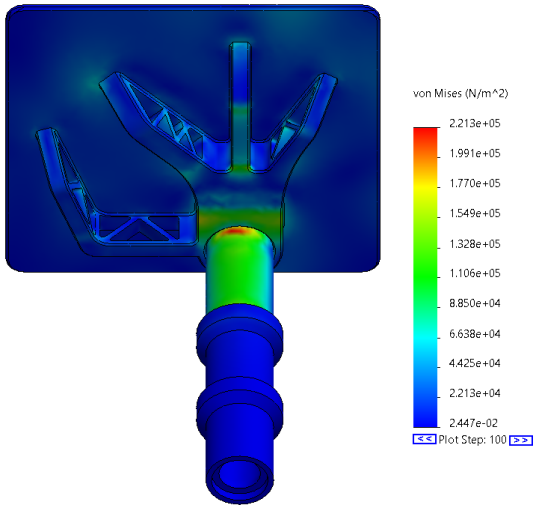

(b) Dynamic stresses of the assembly in study

Figure 6.28: Dynamic displacement (a) and stresses (b))

As expected, being this the most accurate model with the load applied only in the area that expected to participate, then them maximum displacement was considered in this part. The part has been designed with this consideration in mind, with the addition of an extra branch in the middle. This extra branch would add the strength required to stop excessive displacement to occur in the critical area where the smartphone is placed. As such the maximum displacement observed was on 63.3 microns, making this the smallest displacement observed. It is possible to assume, once more, that the body will perform as expected.

Two important conclusions are taken. The first is the fact that other areas, which have less support, don't suffer with the load of the smartphone. This creates a smaller displacement in regions that were once critical. The second important conclusion is that the optic tube does not suffer with displacement. The small load nature of the body does not create buckling even when having a more massive mass being displaced. It is possible to observe that displacement will occur in the axial direction of this body, thus there is no moment created by inertial factors. As such, the optic tube can be considered as a rigid body. It is possible to conclude that, the center of gravity of the assembly is on the axis of the optic tube near the interface of both bodies.

Finally, the vibrations modes of the body were observed as well. Figure 6.29 shows the different frequencies for the different modes of vibration. The first mode of vibration starts at 121 Hz. As a consequence it is important that the system does not achieve this kind of frequencies during the focusing process.

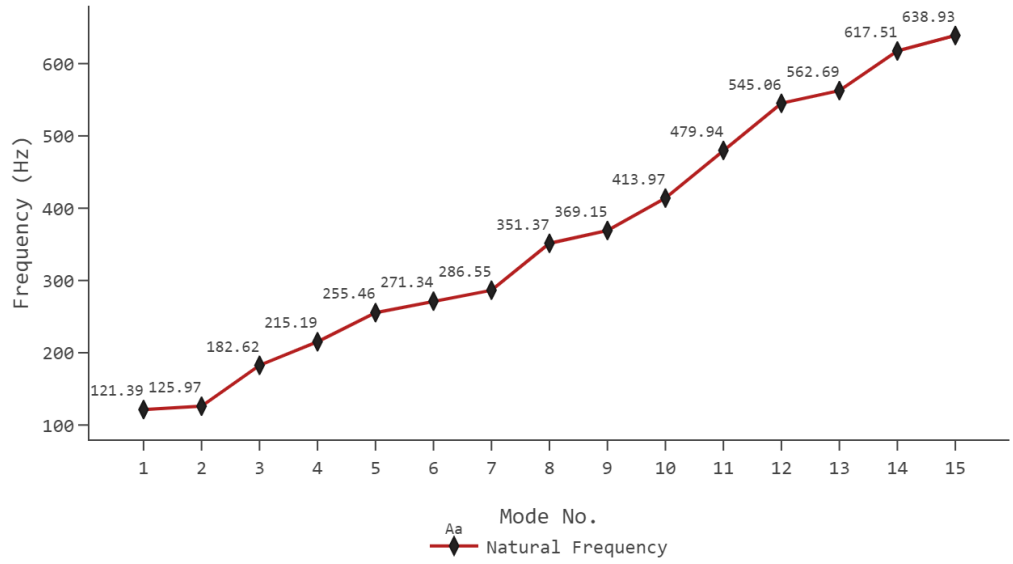

Figure 6.29: Modes of vibration

Finally, the effect of mass on the mode of vibration and direction was studies as well as it is possible to observe in figure 6.30. As expected the first mode of vibration is the one where mass will have higher dynamic response in the critical direction. With the increase of frequency the modes of vibration will have an higher influence in the other two critical direction. It is important

to take in consideration the eighth and ninth mode of vibration because it can lead side oscillations and lead to the misalignment of the smartphone as well. If this is presented as a problem, it is expected that a material with a minimized $\frac{E^{\frac{1}{3}}}{\rho}$ will have better dynamic responses [114].

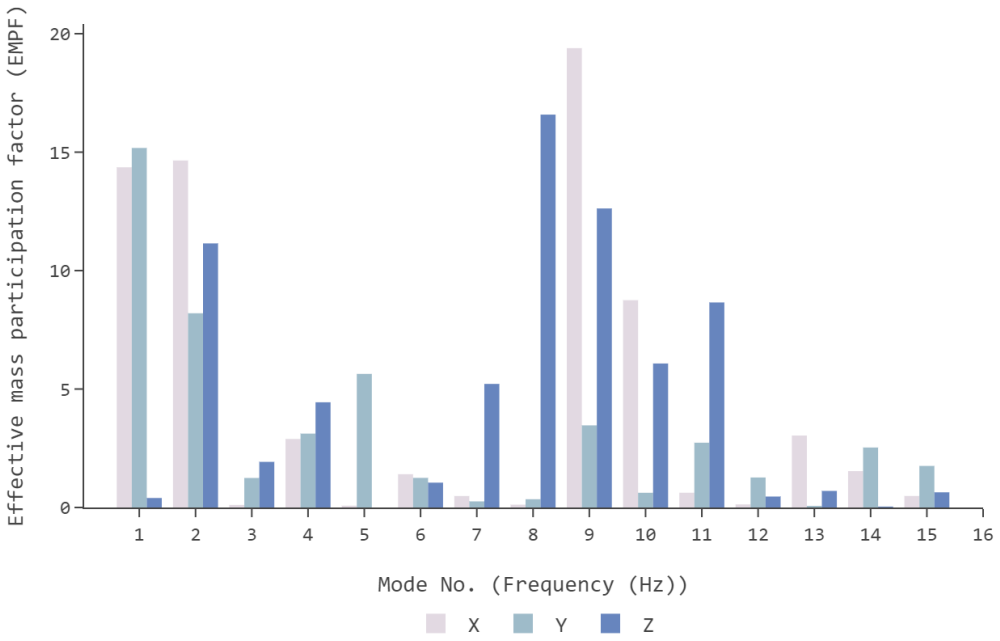

Figure 6.30: Modes of vibration vs Effective mass participation factor (EMPF)

6.2.4.2 Optic Tube Holder

This part only has to guarantee the displacement of the all the parts that will be displaced in the vertical direction. It is important for this part does not suffer possible radial with misalignment, otherwise it will lead to a defective focusing system.

For this model, no global damping was considered. Both load cases were considered, but only the one that suffer the most with stress and displacement will be presented. For external load, an base excitation was used for a given displacement and to define the gravitational acceleration. The mesh used was a very refined blended curvature-based mesh. The values of the mesh can be observed in table 6.17.

Type of Mesh	Number of Nodes	Number of Elements	Element type	Element order
Blended curvature based	90773	57353	Tetrahedron	Second Order

Table 6.17: Mesh used for the dynamical analysis of the optic tube holder

Since the result from static simulation were very satisfying, it is expected that this body will be very stable as well. The determined displacement and stress can be seen in figure 6.31.

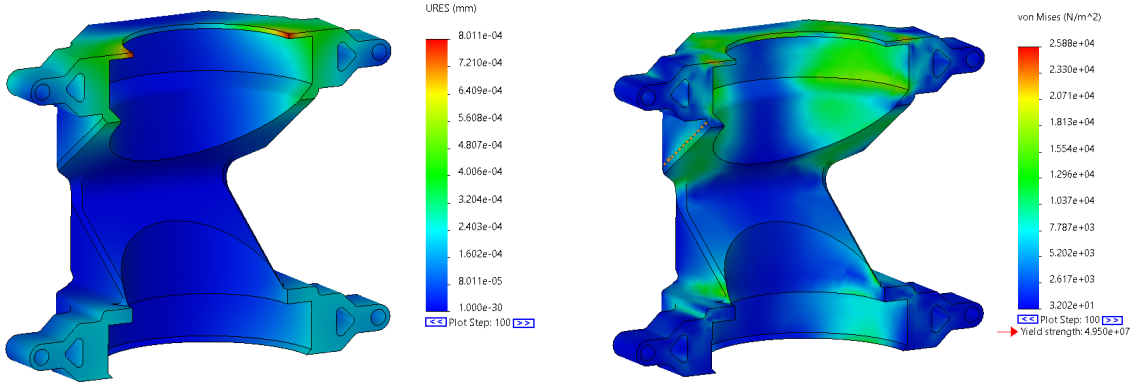

(a) Dynamic displacement of the body in study **(b)** Dynamic stresses of the body in study

Figure 6.31: Dynamic displacement (a) and stresses (b))

As observed, the maximum stress achieved is $0,02588MPa$ and the maximum displacement was $0,8$ microns. Once again the maximum values are very small. As expected this part is extremely stable and it can be guaranteed the correct functioning of this part. It is also interesting to observe that designing for an simplified static load case allows to achieve a design that will conform to the weight and safety constrains.

6.2.4.3 Engine Holder

The final part that will be validated with dynamic efforts will be engine hold mount. On this part there are two statics load case and one that suffer with dynamics efforts. This is the engine mount that will translate 20 mm over the smaller axis direction. This is a very small part and the total inertia of assembly of bodies is large. Thus, dynamic efforts on this part should be studied. The considered static situation of applying the 45 N of the thrust force where the interaction between the model and the actuator is not the most accurate case. The thrust force of the 45 N will be transformed into acceleration taking in account the mass of the whole assembly. The part in question will suffer from this acceleration in the whole case. This also means that the lighter the assembly the higher the acceleration that the body will suffer. Revolving to the second law of dynamics, higher acceleration in a body with a constant mass, the inertial efforts will increase.

For this model, it was considered a very refined blended curvature-based mesh with second order tetrahedron elements. This is possible to observe in table 6.18.

Type of Mesh	Number of Nodes	Number of Elements	Element type	Element order
Blended curvature based	154520	99919	Tetrahedron	Second Order

Table 6.18: Mesh used for the dynamic analysis of the engine holder

Base excitation was applied in one direction, for a given distance. The total step time was 1 second. Considering that the body will run 20 mm will create a more conservative mindset over the real effort. To represent the weight of the engine a remote load of 0.5 N was applied as well in the respective center of gravity. The stress distribution and the resultant displacement can be observed in figure 6.32.

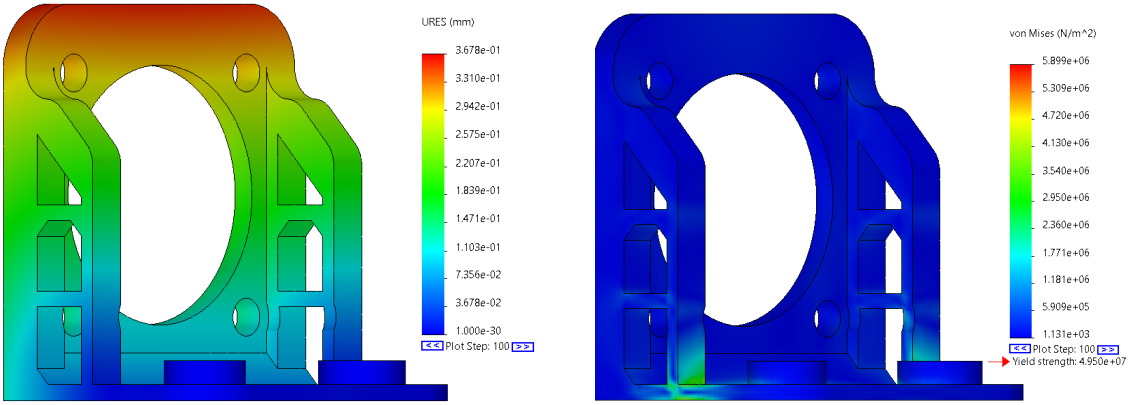

(a) Dynamic displacement of the body in study **(b)** Dynamic stresses of the body in study

Figure 6.32: Dynamic displacement (a) and stresses (b))

It is possible to observe that inertial efforts will have an high load case in this part. The maximum stress observed was $5,9MPa$ and the maximum displacement was $0,3678mm$. It is safe to say that this part does not hold for expectation required for the correct functioning of the actuator.

Thus, this part was remodeled in the critical area to increase rigidity at the expense of mass. The final mass of the part is 1.95 g. The stress and displacement of the new iteration was done for this new model as it can be seen in figure 6.33. It is possible to observe that with the addition of

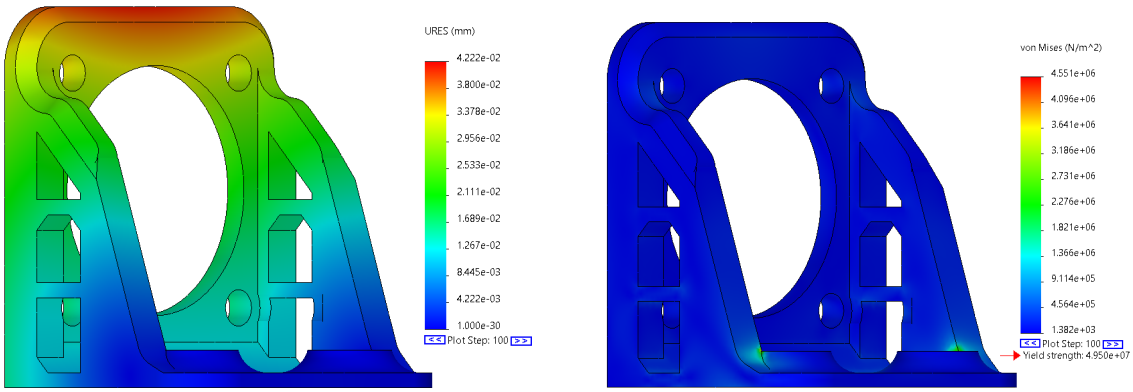

(a) Dynamic displacement of the body in study **(b)** Dynamic stresses of the body in study

Figure 6.33: Dynamic displacement (a) and stresses (b))

some new features the new maximum stress is $4,55MPa$ and the maximum displacement is $42,22$ microns. The expense of some mass allow to achieve better dynamic performance of the part. The final model can be observed in figure 6.34.

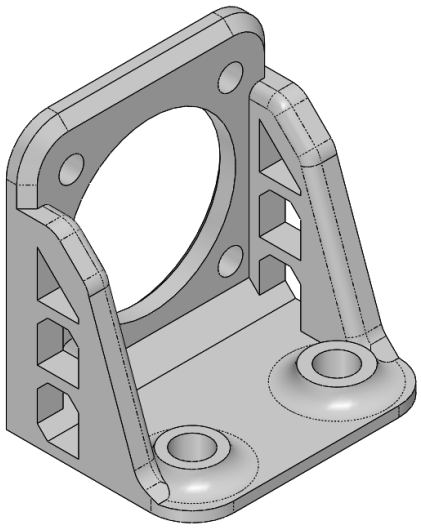

Figure 6.34: Final model obtained for the engine holder

Chapter 7

Results and discussion

After visualizing a engineering prototype it is important to actually create the required a physical prototype. Due to limitations on this dissertation will only be presented the prototyping of the work-alike prototype to guarantee the correct performance.

The main goal of this chapter is to assess the manufacturing, assembly cost and improvement opportunities of the current design.

In this chapter, it will be possible to observe an in depth analysis of the different difficulties of the manufacturers while working with the different parts of aluminium and Alucobond®. The easiness and flow of the assembly will be explored and explained.

Finally, a cost analysis will be done so that it is possible to correctly decide between the different presented solutions. With this it will be possible to observe how cost will have an effect on the performance of the final product. As a consequence, an it is possible to have an educated decision between the different prototypes.

7.1 Metallic Solution

Under this section, the assembly of both aluminium solutions will be explored. It is expected that these both solutions will have similar results since they are of a similar size and use similar parts. The main difference between these two solutions is the stage that will be used. The assembly of the stages and the conclusions observed will be covered as well.

7.1.1 Assembly of the chassis

Assembling the chassis is a component of the system that's constant in all of the presented solutions. Due to the easy availability of equipment for extruded aluminium profiles, assembly of the chassis was simple and effortless. The extruded aluminium profile were bought on *RatRig* at the cost of 7.50 € or 8.43 USD per meter.

Firstly, it was necessary to saw the long extruded aluminium profile in smaller ones that would fit the different necessary dimension for the chassis. Normally, sawing service can be done straight out of the shelf by a small extra fee. To save on cost and time of manufacturing the profiles were manually sawed and rectified. It is expected that with the increasing in production size, the cost of skilled sawing labour and the price per meter of aluminium extruded profile would decrease exponentially.

The second part when assembling the chassis was the addition of using of rubber feet. In addition of the rubber feet the top part of the structure needs as well the machining of internal threads. Internal M5 threads were manually done to the profiles. This process is extraneous and can be expensive, in particular, if done by hand. The top part is not fundamental for the correct functioning of the device. The rubber feet bring many advantages such as better calibration and reduced transmission of vibrations from the device to the working table. It also serves a way to fasten the lower base in the look-alike prototype for fast prototyping. As such, at least four different M5 internal thread need to be added to the aluminium profiles.

To join the profiles in different directions, natural cast brackets were used as corners. The main advantage of using this type of brackets is due to their low cost. Each bracket to be correctly assembled requires the use of a square rule and two different bolts. M5 bolts and T-nuts where used in all of the brackets. This process can take up quite of time, so it advised to use better cornet elements. For example, inside hidden corner brackets present different advantages. This type of corners don't requires extra t-nuts, reducing the amount of part count and simplifying assembly. Another advantages is that they go inside the profile so don't need to be squared. The larger section are allows as well to better restrain the two beams together without creating problems for calibrations. The main disadvantage is that this parts are almost double the cost. It is important to be noted that, with batch discounts and reduced assembly time this parts would turn profitable.

Finally, the chassis can be assembled. The assembly of the chassis took around 3 hours. All of the parts were squared to guarantee the best performance and calibration of the product. It was found later that the best way to assemble the body is by firstly assemble the different stages with

the respective bases and then bringing them together with brackets and the structural parts. Figure 7.1 shows and assembled chassis.

Figure 7.1: Assembled chassis

In beginning of the design for manufacturing it was decided to use only one plate thickness to ease production and assembly. As such, due to the difficulty of laser cutting aluminium it was decided on a general thickness of 2 mm. This is a recommended thickness for a small value that still presents good results without further studies on the influence of cutting properties on the aluminium plate.

The observed results of the aluminium plate from both suppliers were deemed as excellent. As expected there was no thermal deformation effects on the parts. As a consequence, it is possible to achieve less expensive, lighter product with great quality.

The quality of the cutting procedure is also extremely important. Not accurate cuts can lead to extra rectification procedures and to a longer and harder assembly. As a consequence, extra time and money is spent on the total product. It is also expected a worse performance due to flaws that come with non accurate cuts. Calibration tools can be added to better help overcome faulty parts such as rubber feet, that can be calibrated to compensate extra millimeters.

7.1.2 Structural elements & Z Frame assembly

The vertical frame is the one that will hold the the optic tube. Therefore, it is important to guarantee parallelism and perpendicularity between both columns and the optic tube. In the situation, where

this is not verified, it is expected misalignment of the optic tube.

Before starting the assembly it is important to thread the profiles with a tap. Doing this function beforehand will help having a faster assembly without major calibrations issues. Afterwards, in the assembly of the vertical axis, is necessary to guarantee the parallelism between the both major columns. As such, the first piece to be assemble is the back-plate. To correctly assemble this plate, it is important that all the four suggest fasteners be used. Each pair of two fasteners will guarantee the correct alignment of the vertical column in question.

The next step to finish the assembly of the two columns is the correct fastening of the rubber feet using two M5 fasteners and the top plate. The addition of rubber feet will help calibrating the height of each column in the situation of existing manufacturing issues. Finally the top place, also fastened with two M5 will guarantee even further the alignment of both columns. It is mandatory that both this columns are as perpendicularly as possible with the base and parallel between them both. If these conditions are not verified, the concentric relation between the optic tube and the illumination module should not be expected. Figure 7.2 shows the procedure to assemble the vertical module without the structural elements.

After having the main frame of the Z axis assembled, the two side walls are now assembled. Fixating these two side walls beforehand allow for easier alignment. These walls should fit correctly against the back-plate giving the first initial position where to assembly the plates. Two different M3 fasteners are used to correctly fixate this part in the initial frame.

Finally the Z stage can be assembled. First, the press-fit inserts are fitted in the polymer part that will hold the optic tube. It is important to be attentive to correct side of the plate in the assembly process. The next step is to fasten the part that holds the optic tube by press-fitting it. It was observed that the optic tube fits perfectly being the designed system ideal to correctly fix it.

After the stage is assembled with the two different plates fastened, then it can finally be assemble against the vertical frame in the desired position. The best way to fasten the stage is by laying down the frame on to the base. Only three M3 bolts are required to fasten the stage. To assemble all of the parts to the frame it was used T-Nuts and bolts.

The final step was to assemble the engine mount and the parts that hold the micro switches. M2 bolts were used with a nut and a washer to correctly fasten the micro switches. The vertical frame is now built.

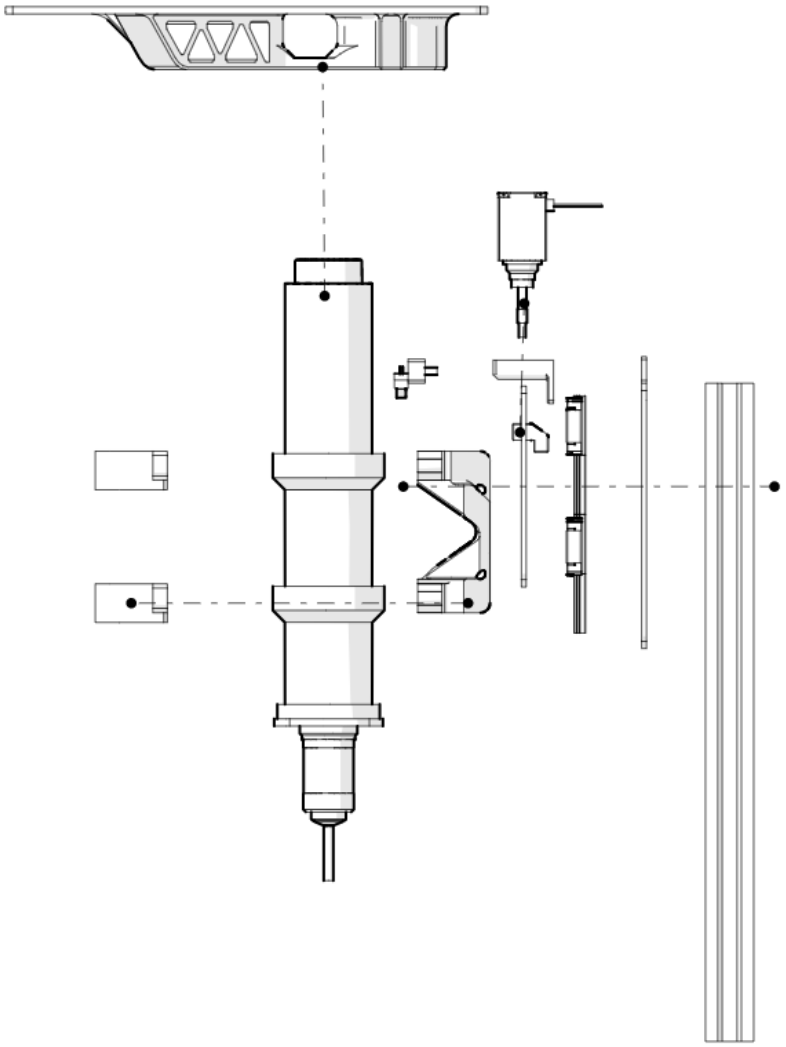

Figure 7.2: Vertical module assembly procedure

7.1.3 XY Box assembly

The XY box is the most important module of the device. This is the module that holds the illumination module, the XY stage, the sample and two actuators. Connecting this stage to the ground there are two extra legs and the vertical frame. After the correct assembly of this module, the engineering prototype is completed. The XY module assembly procedure is displayed in figure 7.3.

The first step of the module that takes the longest to assembly is to correctly orientate the base plate. The base plate will be the most important part in the whole product. This part will guarantee the correct performance of the focusing system, as well holding and guiding the base module. This plate will also hold the XY table.

The second step is to fasten a guide to the base plate. It is important to guarantee that the side of the extruded profile is flushed with the side of the base plate. This will guarantee that, afterwards, when assembling the legs, they will fit correctly.

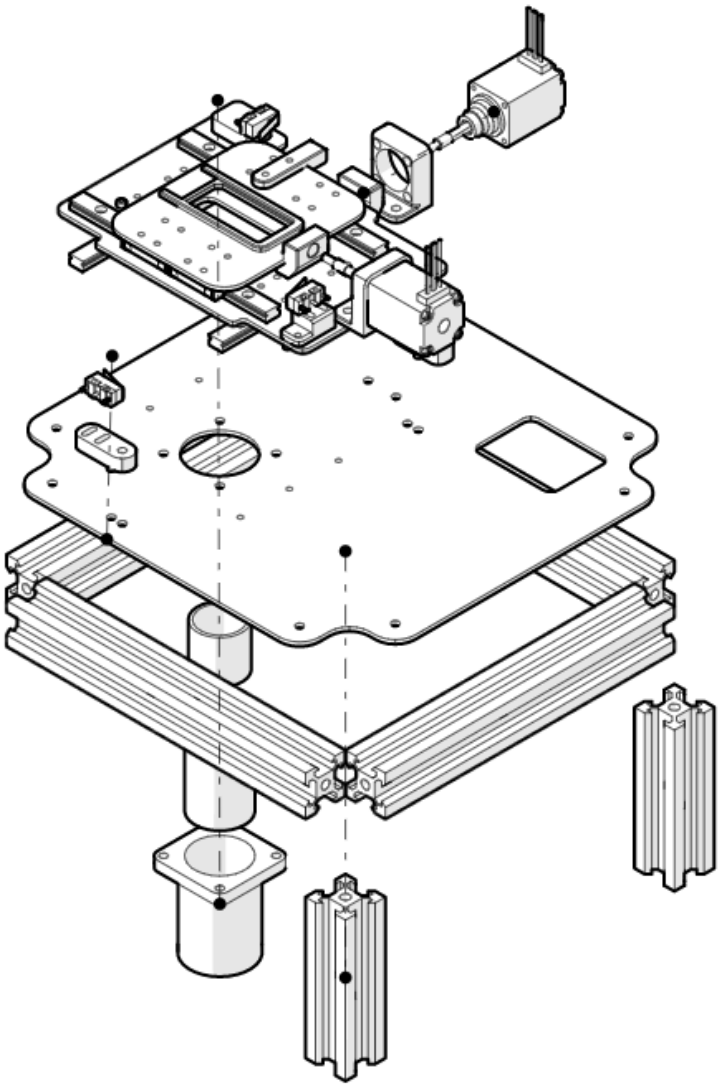

Figure 7.3: XY module assembly procedure

To correctly, advance on the assembly of the base plate, a perpendicular profile is mounted. With the usage of a square it is possible to guarantee the perpendicularity between both profiles and the distance that hey have between them. Once again it is important to wave the side of profile flushed with side of the base plate. After this profile is assembled, a bracket between the two assuring that it doesn't occur any misalignment.

It is important to understand that the correct alignment of the profiles in the base plate will guarantee the parallelism of the device as well. As such, in the end of the assembly, the device will be over-constrained leading to a well performed device without required extremely skilled machining and assembly.

These process should be repeated for the following profiles. Although it is important to observe that the micro-switch that it is embedded in the profile should be assembled before hand in the base

plate. In the end, the main box of the XY module is assembled.

The next step is to assemble the XY stage table and the rest of the parts needed for correct functioning of the device, such as the illumination module. With the XY stage assembled it is possible to jump to last step of assembling the XY table.

The final step of the base is to assemble the two front legs of the system. It was observed that mounting this two front legs can be extensive and take some time. The main difficulty in assembling this two legs it guarantee that both have the same height from the working table to the base. In this moment the assembler need to fasten the brackets holding the parts. The multi-tasking required in this process can lead to flaws and misalignment.

In this module it can be considered the fixation of the vertical frame with the XY base, as well. This process suffers a similar process to the assembly of the front legs. Although, now it is necessary to guarantee the correct level and balance of the table relative to the horizontal plane. Two brackets are fastened to hold the stage in place along with the front feet to the side walls as well. The product is now complete. Figure 7.4 shows the XY modules for the IGUS® stage and the PMI stage.

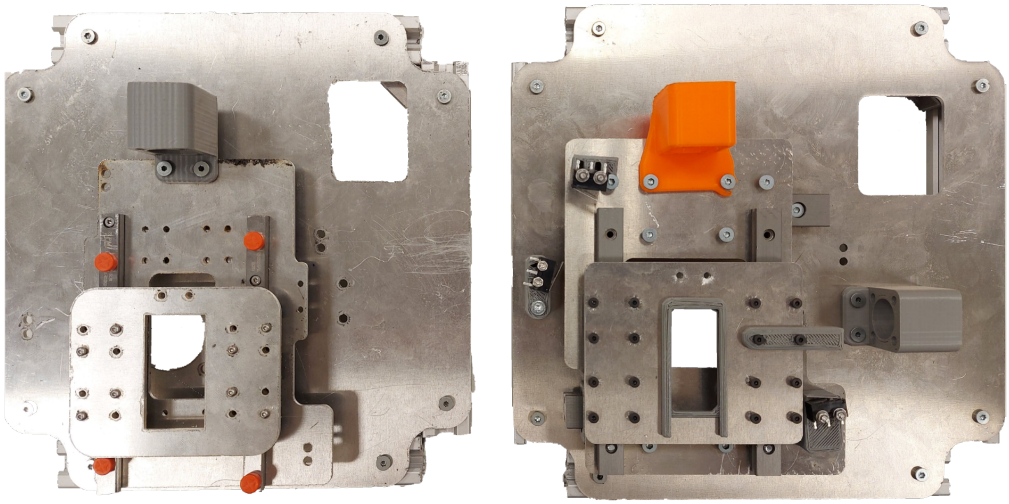

Figure 7.4: Both XY modules assembled

7.1.4 Stage assembly

In this subsection the assembly of the different stages will be observed and analysed. The stage requires extra attention when assembling. Flaws in the mounting process can lead to a faulty performance of the guiding hardware. Therefore, it is important to analyse this assembly in-depth.

The main flaws that can be observed by a faulty assembly of the stage is increased friction between the rolling elements and the guide and the worse life performance.

7.1.4.1 IGUS® assembly

When assembling the IGUS® stage, first it is necessary to observe how the different parts will interact together. For example, it is easily observable that in the rail, two carts will slide and this rail will be fastened over a base. Thus, the rail should be first component to be mounted.

The advantage of working with the selected IGUS® parts is the sturdiness to mistreatment and incorrect holding of the hardware. This means that the worker does not need to worry, as much, the way it holds the part due to the added robustness. For example, the usage of PTFE guides does not require a special treatment, whereas with the rolling elements counterpart it's mandatory to maintain the cart over a guide or a dummy guide, constantly, over the process of assembly. The consequence of this mistreatment, is the misalignment of the rolling elements and even risking damaging the cart itself.

The first step of assembling the stage is to fasten the rails to the base plate. It was observed that fastening the rails directly to the carts can be complicated and does not save significant amount of time. Another, important observation is the fact that having a threaded holes is easier for an assembly standpoint, requiring less fasteners and hardware parts. As such, this option should be considered while attending to the cost of the threading operation.

After the assembly of the rails, it can be assembled the plate that goes on top. Firstly, the carts are dragged to the rails and a verification acessing the sliding performance should be done. The next step is to firstly fasten one cart to the plate above with the correct bolt. Armed with a square, it is important to guarantee that the top plate is parallel to the bottom one. This will also guarantee that the plate is aligned with the translated direction not creating any unwanted misalignment that will create a flawed performance.

For the vertical stage these steps would be sufficient and calibration would proceed. For the XY stage, it is important now to mount the different components that will hold electronics, such as the engine mount and the mounts for the electrical end-stops.

Before proceeding to the final fastening of the XY table it is important to calibrate the rails, starting from the above axis first. In the case of IGUS® parts, due to the loose tolerances, they are auto calibrated. However, it was observed that a certain adjustment in parallelism of the rail might be required. To achieve this, parallelism should be tested with a jig or a comparator while testing the sliding tolerance. In the case of IGUS® parts, one of the guides should be loosen so that the carts can auto-adjust to it [115].

It was observed that IGUS® parts present a certain resistance to sliding. The four carts layout stopped any possible yaw moments from occurring due to extremely wide tolerance range. Another important regard is that it's not mandatory in the fasten completely the bolts of the carts that are over the loose guide. This will lead to a better sliding behaviour, therefore less resistance to the actuator. The assembly, process of the XY stage can be observed in figure 7.5.

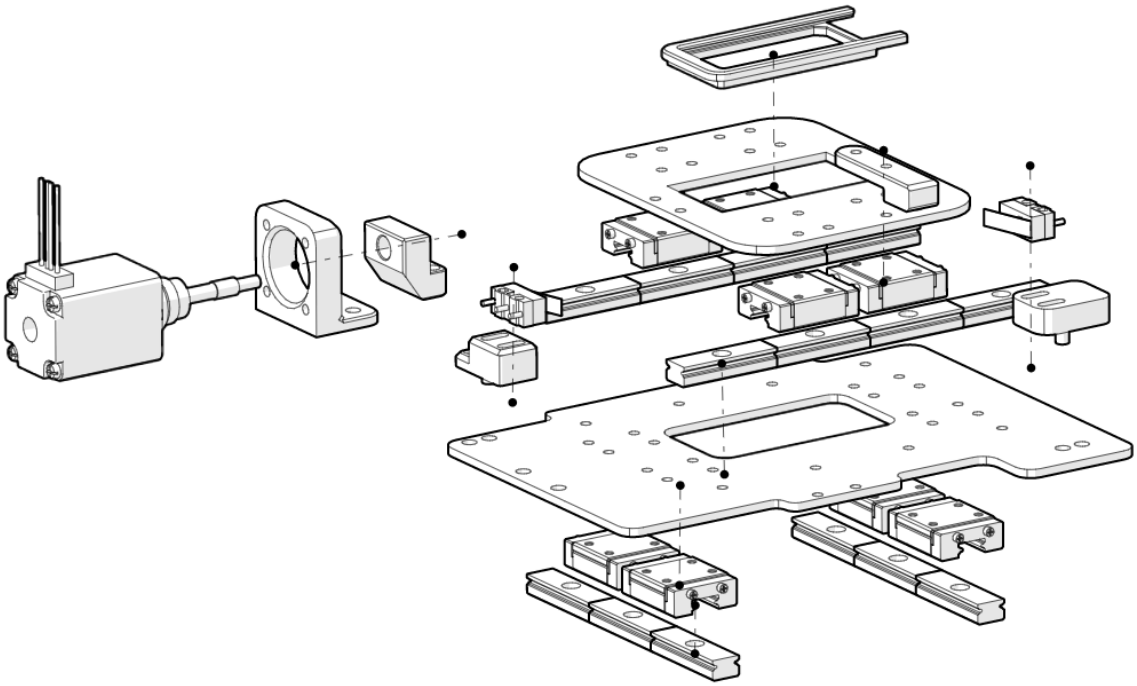

Figure 7.5: Assembly procedure of the XY stage

7.1.4.2 PMI assembly

The other situation in the suggested product is the situation where the assembly uses the PMI parts. The main difference between this two stages is mechanical solution that allows for better mechanical properties without compromising on weight and size.

The assembly process of using the PMI guides is similar to the IGUS® hardware . The main difference in the assembly is the calibration process and the observed final results. Another important factor to have in consideration is the carefulness required to assemble this hardware. Due to the usage of rolling elements, it is necessary to be attentive when working with these parts. It is required that the carts are over a guide at all moments to prevent that the rolling elements don't fall out of place. It is also required to guarantee that the working environment is cleaned before proceeding with the assembly of the hardware. Dust particles can significantly damage the performance of these parts.

Finally, it was observed that, due to the effect of the pre-loading, the parallelism error tolerances are very tight. This factor can lead to a worse performance of the stage. To achieve the parallelism error of 2-3 μm it is mandatory the usage of a comparator [116]. However, it was observed that sliding behaviour wise these guide don't suffer as much as the IGUS® ones. Even, with a non-tool assisted assembly, these parts present less sliding friction. This means that, performance is less prone to assembly error. It should be noted, that it will influence directly the long terms properties of the guides and a comparator or a very well studied jig should not be left unnoticed.

7.2 3D printed prototype

In this section the 3D printed solution will be explored to correctly observe the most common prototype. To print the necessary parts it was used an Ultimaker S3 and an Ultimaker S5.

The assembly of this solution was similar in terms of the metallic solution. The main difference between the two was that some parts suffered com polymeric contraction and it could be difficult to assemble some bolts. The solution for this problem is to over-scale 2-3% the part in the slicer software.

It was concluded that the XY base with the added thickness is extremely rigid and it's expected to hold to standard as seen in chapter 5. The main problem in this solution are the exterior structural elements. Due to the small thickness and large area they present a ductile behaviour making it difficult to achieve the correct alignment of the vertical frame. This problem can be passed over with the increase of thickness a few millimeters.

7.2.1 Choice of wall count and infill

The factors that will influence the most in final properties of part will be the shell perimeter wall count, the type of infill as well it's density. The main drawback of using high wall counts and infill densities is that fact that cost increases as well.

The chosen infill was the cubic infill. This infill has isotropic behaviour, being the one that required less time to manufacture, for the same density. This infill is isotropic therefore it tries to have similar properties in all directions. It is common to use the gyroid infill as it requires less material to achieve similar properties, but it comes with the expense of manufacturing time.

To understand the effect of the perimeter in the cost and ultimate tensile strength (UTS), 36 different samples were tested under the norm ISO 527 [117]. The tensile test machine used was the Mecmesin 2.5KN. The samples used was 1B. These in these samples it was tested the combination of different perimeters and infill densities. Three different samples were used for the same value. The densities tested were 25%, 50% , 75% and 100% and the wall count were 1,2 and 4. Wall count is the same for bottom layers, top layers and perimeter layers. The 3D printer to create the samples was the Ender 3 PRO modified with an auto-level sensor. The filament used was 1.75 mm, BQ PLA Gray Ash. Time of manufacturing and mass of each sample was measured as well. Figure 7.6 shows the different tested samples.

The main goal of this test was to understand how each factor influences each other, cost and UTS as well. The expected output of this study is a region of values that will give design insight on a near to optimum value of infill density and wall count. This values will then used when building the prototype.

Cost as the main factor of the study was projected as combination of two important factor: cost of material and cost of electrical power usage. To complement this equation importance factors can be added, to better represent situations where the build time is extremely important or filament usage is more important. For example, during the COVID19 pandemic, the PLA worldwide stock was down due too the efforts for the pandemic. Therefore, this is a situation where material cost

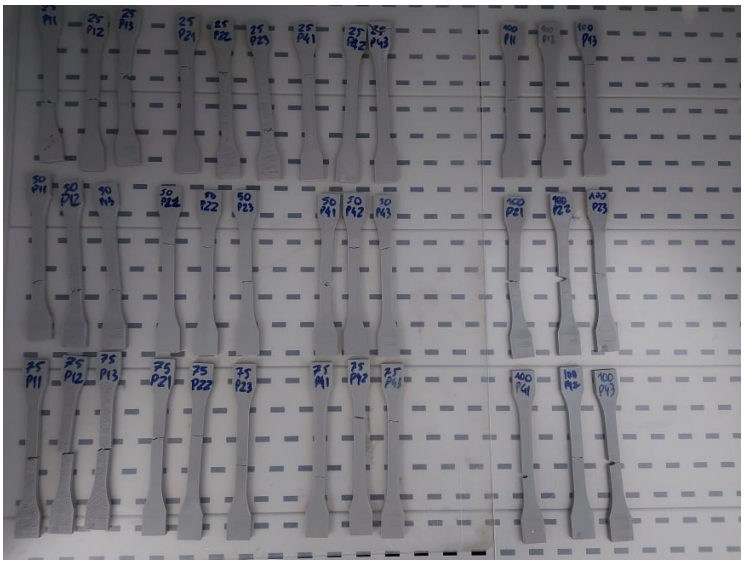

Figure 7.6: Tested samples

importance would be extremely important [118].

$$C_t = \alpha C_1 m + \beta C_2 t \tag{7.1}$$

Where α and β are the simplification factors of the mass and power usage, respectively. C_1 and C_2 are constants that relate the price per gram and the price per minute for an Ultimaker S3. For this study the value of α and β will be unitary for simplification purposes. C_1 the cost per gram, is $0.0253\frac{USD}{g}$ at the moment of research for the used filament. To determine the cost of C_2 it was considered the mean cost of KWh for USA's industry and half of maximum output of an Ultimaker S3, to consider peak usage - when heating the bed - as well normal usage, during printing. Thus C_2 is $0.00013375\frac{USD}{min}$. It is possible to conclude that the importance of manufacturing time would need to be 19 times higher of the material usage to surpass the cost of the material.

Another important factor to have in consideration is the resistant cross section area of the sample. Many studies have noticed that the main issue of studying infill density is the non constant area of the samples. Infill density will create voids, even piece that are 100% filled can have voids due to under extrusion and other calibration factors. Thus, it is proposed to create a model from the area by using CAD information [119] or through geometric measurement. In this study it was proposed and analytical geometric model that has in consideration the wall count and width as well the infill percentage. Some studies use the relevant density of the samples to find the number of voids per area [120]. Some studies have used the 100% as reference area. Thus it is possible to create a relation with:

$$C_s = A_s - A_i + (A_i * \%Infill) \tag{7.2}$$

Which can be written as:

$$C_t = A_s - A_i(1 - \%Infill) \tag{7.3}$$

Where A_s is the apparent section area of the sample and A_i is the are where there will be infill. A_i is given by:

$$A_i = t_i w_i \tag{7.4}$$

Where

$$t_i = t - 2w_c \cdot l_h \tag{7.5}$$

With W_c as the wall count, l_h as the layer height and t as the thickness.

$$w_i = w - 2w_c \cdot \phi_n \tag{7.6}$$

Where ϕ_n is the nozzle diameter that will define the perimeter wall thickness. This model will present a good approximation but there will be a small error to it, that it will not predict extrusion problems and the complexity of the geometry of the infill. Considering this the Young's module obtained for the different parameters can be seen in table 7.1 and the respective mean.

Young's Module [GPa]					
Infill	25%	50%	75%	100%	Mean Wall Count
1 w_c	2,8	2,7	2,5	3,0	2,7
2 w_c	3,0	3,3	3,2	3,3	3,2
4 w_c	3,2	3,2	3,2	3,3	3,2
Mean Infill	3,0	3,1	3,0	3,2	3,1

Table 7.1: Determined Young's Module [GPa]

Observing table 7.1 it is possible to conclude the geometric model of the area is a good representation of the final result, being the value close to the observed in the literature [120–123]. The maximum error is 17% that can be due possible under-extrusion of filament. The UTS can be seen in table 7.2. Firstly, before creating the relation between infill, wall count and UTS and Cost, it

UTS [MPa]					
Infill	25%	50%	75%	100%	Mean Wall Count
1 w_c	21.0	23.0	25.1	36.3	26.4
2 w_c	27.4	30.6	32.0	36.6	31.7
4 w_c	36.9	37.0	38.1	42.6	38.6
Mean Infill	28.5	30.2	31.7	38.5	32.2

Table 7.2: Determined UTS

is necessary to understand the effect of each factor in the cost and in the strength-to-weight ratio. The first will allow to understand each factor as more influence in the cost. Strength-to-weight ratio (or cost) is a great way to comprehend the behaviour that will give more strength per gram. As seen above, because the cost of material is 19 times above the cost of time, then in this case in particular strength-to-weight ratio can be considered strength-to-cost ratio as well. Figure 7.7a

show the evolution of strength-to-weight ratio by infill and wall count. Figure 7.7b show the effect on cost by infill and wall count. It is possible to observe in figure 7.7a that relative cost of

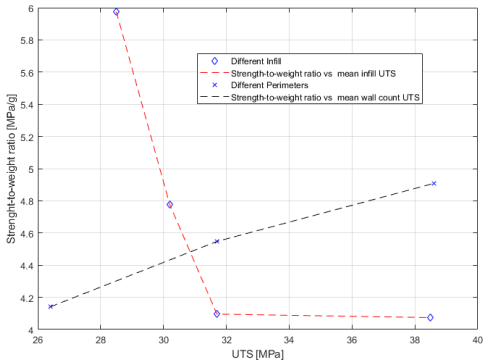

(a) Evolution of S/W ratio by infill and wall count.

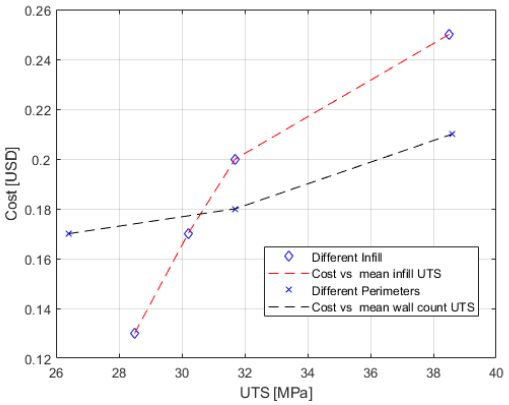

(b) Evolution of cost by infill and wall count.

Figure 7.7: Evolution of different metrics

part over 75% will very similar. Another conclusion that can be taken is that low infills have the tendency to value most the part. This goes is concurrent with the expected where topology is of utmost importance in mechanical factors. Thus, increasing infill will not take an high effect on the UTS. It is possible to conclude that it is not worth the increase between 75% and 100%, as it also possible to observe in literature [119]. This image also show the raising effect of wall count in the ratio. Once again, this proves the effect of the perimeter for an efficient design for additive manufacturing. Thus, to achieve an effective cost infill should be maintain to a minimum and wall count should be increased instead.

On another hand, figure 7.7b relates the cost with the achieved mean UTS for perimeter and wall count. This figure proves once again that infill is the one that mainly dominates cost over wall count.

MATLAB offers powerful tool-kits to create surfaces that closely fit the data set. A script was written to be able to apply a surface that correlates the UTS matrix with the other factors in study. The model surface was achieved by bi-cubic interpolation that closely fits the data set. Bi-cubic interpolations allow to use an third degree polynomial to do the interpolation in a grid like mesh. This polynomial is given by:

$$g(x,y) = \sum_{i=0}^{3}\sum_{j=0}^{3} a_{ij}x^i y^i \tag{7.7}$$

Where a_{ij} coefficient is given by the cubic interpolation polynomial. Being this method an interpolate method, it is expected and adjacent error. Another important factor is the mesh quality. Thus, more test from different points in the grid would be expected more accurate results.

Figure 7.9 relates the total cost of the sample with the infill percentage and wall count. Figure 7.8b relates the UTS with infill percentage and wall count. Finally, figure 7.8a relates the strength-to-cost ratio with infill percentage and wall count.

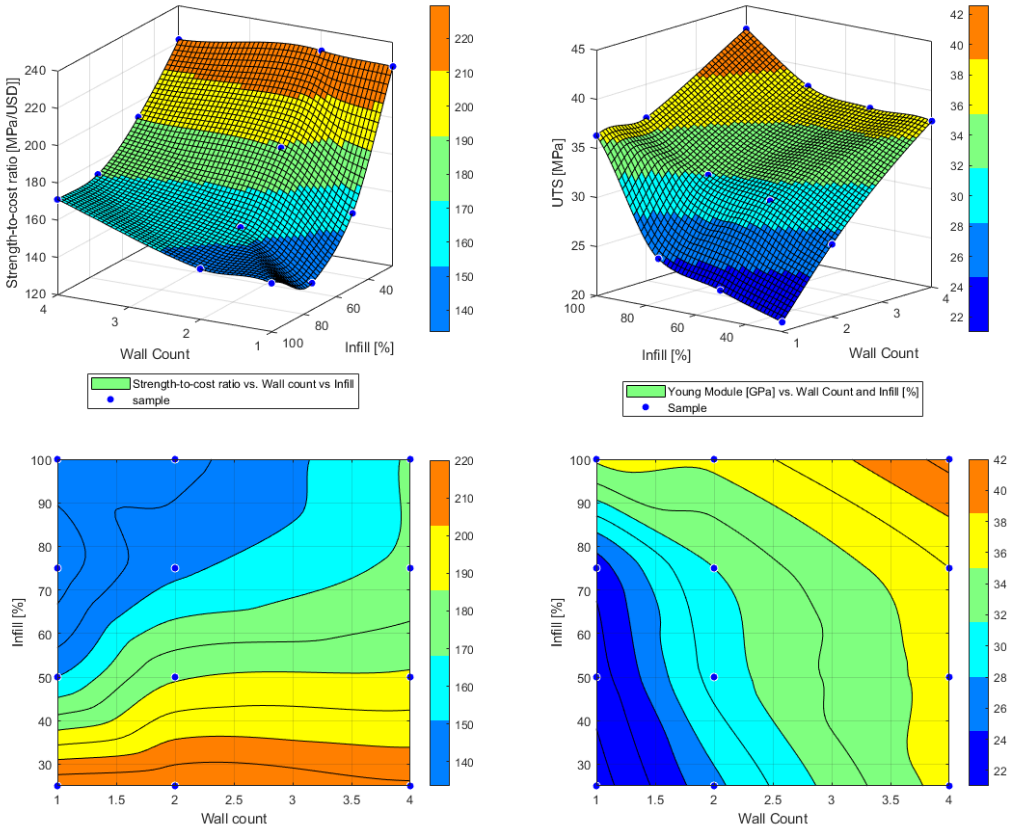

(a) Cost-Effectiveness ratio vs Infill vs Wall Count **(b)** UTS vs Infill vs Wall Count

Figure 7.8: Different surface and the correspondent contour plots created with the experimental results

These plots not only confirm what was expected, but they also function as decision contours. Thus, by observing these figures one can find the correct region of points in the data set to decide the best parameters that fit the inputs for the product in study.

Thus, in the case of the microscope in analysis, all parts that will be 3D manufactured, the main goals is to have the most cost-effective properties while using the most infill possible as way to improve strength. Thus, this can be seen in the contour plot of figure 7.8a. The orange color is the that mostly optimizes our cost. As such the values of perimeter that allow for the most infill while in the orange section is 2 and 3. This number of wall count is extremely cost optimal up to a max of 35% infill. This decision confronting with figure 7.8b shows how to decide the wall count. Two walls, 35% infill is in the light blue area between an UTS of 28-30 MPa. On the other hand, the contender three wall, 35% of infill is in the green area between 32 and 34 MPa. Even tough the decision seems obvious by now, it is important to observe the difference in total cost of the same part. As such, observing plot 7.9 it is possible to note that the difference between prices for a 2 or 3 wall count is not very much, being only two cents different. Having the product some

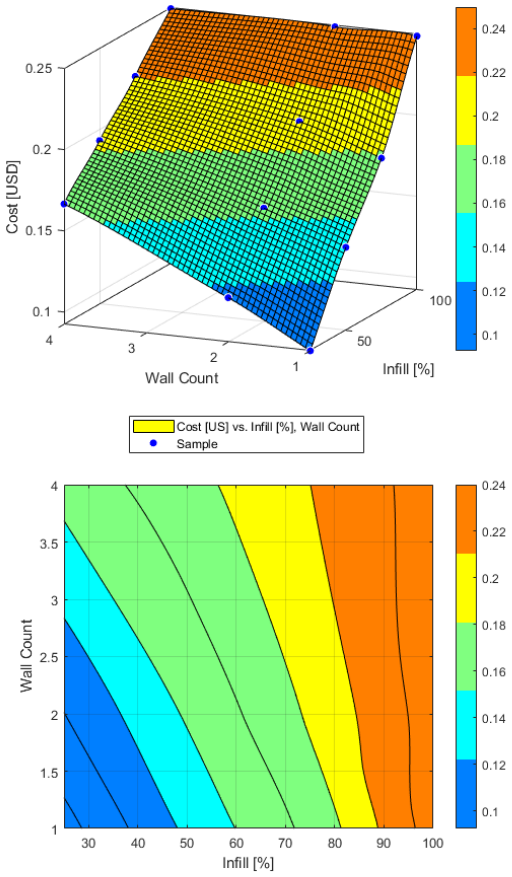

Figure 7.9: Cost vs Infill vs Wall Count

structural elements, then the small cost difference was sacrificed and the parameters chosen were 35% and 3 wall count.

7.2.2 Parts created for additive manufactured solution

To simplify the 3D printing solution and reduce the part count it was decided to remove the corner brackets. Each bracket requires the usage of two bolts, two t-nuts and each corner requires at least two different brackets. The total part count for the minimum case is fours bolts and two brackets. The addition of a 3D manufactured corner can easily simplify the number of parts needed. Each corner will only need three bolts and one 3D printed bracket.

Time of assembly will be reduced as well. The correct positioning of each bracket requires the use of a square to guarantee 90º between both profiles. Brackets will also slide, under extreme stress, causing misjudgements.

The developed corner bracket allows for the easy assembly of the three different profiles. It is a small, lightweight and it can be also created by more traditional method such as CNC milling. 3D manufacturing solves this problem by creating this small part, in-house, without the added extra cost. Figure 7.10 shows the CAD model of the part.

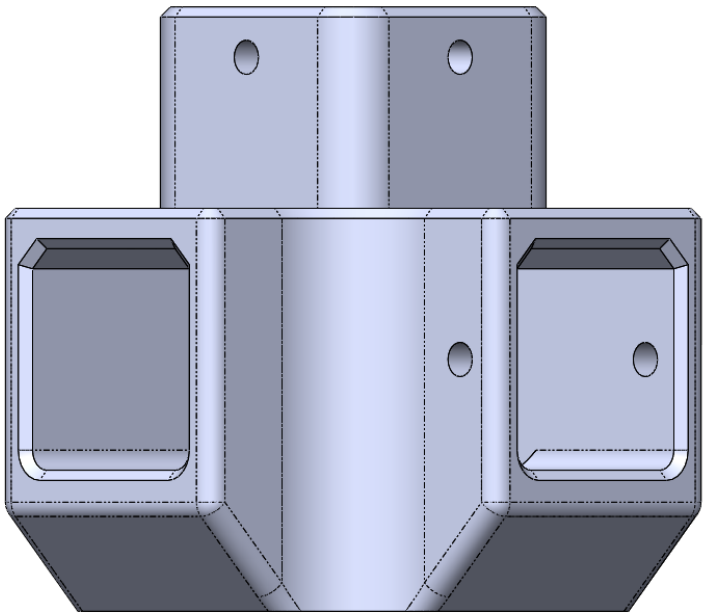

Figure 7.10: Developed 3D manufactured corner bracket

In addition to the corner brackets, additive manufacturing also appears not only as way to create structural elements but for the fast development of tooling, as well.This tool can be used to simplify assembly and calibration.

When mounting the guides, it is expected that parallelism error is minimized. The common process can be tedious and extraneous to guarantee the correct parallelism. It was created a jig that simplifies this process. The usage of a comparator should be used as well. With this part the assembler can easily mount a more precise parallelism when compared to the reference guide. This part also guarantees that only the a certain portion of the guide is being calibrated. When

used with a comparator the part observed in figure 7.11 can improve and facilitate calibration and reduce assembly time.

Figure 7.11: Jig created to facilitate assembly

It was observed when assembling the IGUS® guides that this system is perfect for the correct parallelism error. The applied process of going bold by bolt checking with the jig created.

This jig can be improved to better and easier allow the correct calibration of the guides. A good calibration device will improve assembly time considerably. This jig should be machined in some regions to guarantee the most accurate precision possible.

Another jig that was manufactuer to help the manual sawing of the profiles was a 3D printed guide for the blade. This part it is a common product that can be bought in an hardware store. Although with a FDM machine it is possible to create it without an elevated cost in the office space. The main advantage of FDM in this part is the fact that it doesn't require to go through the purchasing order process of the enterprise in consideration. The guide of the hand-saw that was printed can be observed in figure 7.12.

Figure 7.12: Jig created to facilitate manual sawing

7.3 Economic comparison

The purpose of creating a low-cost device is to offer a less expensive solution compare to the ones currently in the market. Applying DFM&A methodologies improved the number of parts required and the easiness of assembly. With these mindset it is possible to create a lower cost solution to the present in the marked. The main goal of this section is to do an economical analysis on the solutions built and compare between them and with the solutions in the market. Finally, it will be decided on a solution that should be explored to further production stages.

7.3.1 Solutions analysis

7.3.1.1 IGUS® solution analysis

The first solution to be analysed is the solution that uses IGUS® parts. This prototype is the bigger one and uses aluminium plates as structural solution.

It was observed that the net weight of the product is $2.086Kg$ and summing the IGUS® stage, the total final weight of the product is $2.63Kg$. The total volume of this product is 13.9 Liters. The assembly time took approximately a full day of work,8 hours. The hour rate for assembly that will be used is 15.82 USD or 13.94 €. This is the mean hourly rate of typical assembly line worker in the US [124].

After the sum of the different factors of this prototype, it is expected a total cost of 1016 €. This price is extremely lower of what it is observed in the market. The total cost of the product is almost half compared to a typical high-end motorized stage that were observed in chapter 3. In addition to this, the low cost solution for malaria, the Autoscope UW predicts that it can be produced at the lowest cost possible of 1500 USD. It is expected that the total cost of 1016 € can be reduced with increased production. It is possible to observe the advantage of using lower end parts and rethink the stage mechanism. Even tough it is important to use as many standardize parts as possible, in some cases, this might not be profitable. A complex automated stage created by, for example, ThorLabs would offer more than the minimum required for the necessary performance of the system. In contrast, a case that was proven successful by using standardize parts was the chassis. The addition of V-Slot extruded aluminium profile came at total material cost of 9.96 €. Using aluminium profiles is a solution that it hard to battle against. They are extremely cost-effective in creating a very rigid, easy to assemble structure.

This solution as 408,4 €/Kg and 73 €/L. This means that to buy a kilogram of this solution, one must spend at least 408.4 € and to spend at least 73 € for a liter. These two metrics give comparison factors that observe how well capital is being spent. The ratio of euro per liter gives a general sense on how well is space being used. In the situation where cost is similar, the one who is more compact will have a better usage of space. Therefore the higher this ratio the better. Weight ratio gives a better efficiency of weight. A lower ratio will lead to the conclusion that for the same weight one prototype is more expensive than the other. The lower the cost per kilogram the more efficient is the prototype, meaning that capital is more evenly spent around the components.

Assembly will be influenced by the total number of fasteners used. In this product, assembly consists mainly in the fixation of different parts together with the correct calibration. Thus, the number of bolts, nuts and washers will influence drastically the assembly cost. To correctly assemble this prototype it took 8 hours, which corresponds to a total of 111.52 €. In this assembly it exists 126 bolts, 81 nuts and 83 washers compiling the biggest portion of the total part count as it is possible to observe in figure 7.13. Since, most bolts, in this case use a washer and a nut as well, only the total number of bolts were considered.

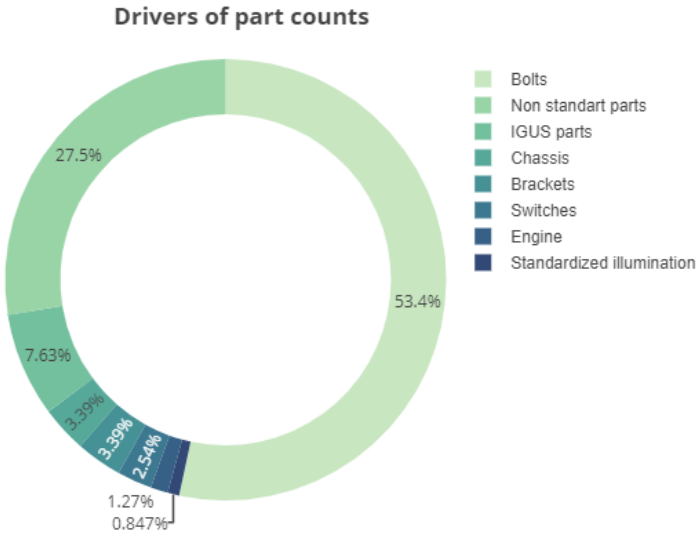

Figure 7.13: Part count drivers

Thus, the total cost of the assembly per the number of bolts is 0.89€ per bolts. This means that for each bolt added, a total of 90 cents will be added to the assembly cost. The time of assembly is not linear because it depends on multiple factors. However, this ratio gives an important insight on how much money is being spent in fastening bolts. One of the main goal of DFM&A mindsets is to reduce this ratio as much as possible. As such, by observing while assembling the part, at a first glance and assuming the use of the enclosure, 22 bolts can be discarded decreasing the total number of bolts needed to 104. This will increase the ratio to 1.072 as it is expected a reduction in assembly time. With this improvement the ratio of number of bolts per the total part count - bolts plus components - is the 0.945. This indicates that now, bolts are not the majority of the assembly. Finally, the cost per bolt of this solution is 8.07 € per bolt. The number of bolts per hour of assembly is 15.75. This means that, it is expected that reducing 16 bolts will save an hour of assembly time.

This solution presents a total of 110 components of which 41% are standardized. Reducing the total number of bolts will be a hard task since there are some that are mandatory due to the usage of carts and guides. An important factor to add is that most of the bolts in this assembly have similar heads and sizes. As a consequence, the time of switching tool head is reduced.

Finally, it is important to observe that the main driver of cost of the prototype are the linear high precision actuators, as it is possible to observe in figure 7.14. This indicates that, reducing the total cost will be difficult, since, 61% of the price tag is dominated by the actuators. The best way to save on total expenses is by reducing assembly and manufacturing cost. In this prototype, the total cost of manufacturing the aluminium plates was 30.87 €. It is expected that with an higher production and trade deals this price will be diminished exponentially. Finally, it is possible to conclude that the more, it is saved on actuators the less the total cost of the product will be.

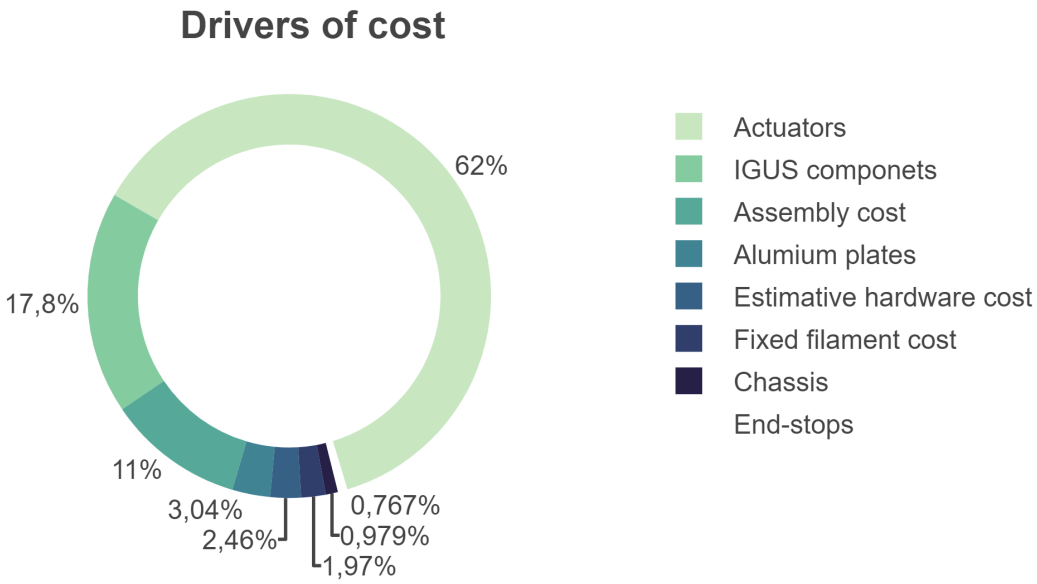

Figure 7.14: Cost drivers of the IGUS® solution

The total cost of the linear actuators is 5.65 times higher than the assembly cost. This means that, in the situation where a trade deal is able to reduce the total cost of the actuators, such as batch discounts, then the assembly cost becomes extremely more relevant. As a consequence, it is recommended a future iteration to explore more extensive design for assembly concepts. This will allow to develop a better product without throwing unnecessary capital to the product leading in the end to a more expensive design.

7.3.2 PMI hardware solution

The usage of PMI parts, and, as a consequence, a better stage led to an overall increase in performance and a more compact solution. The main difference by using a stage with parts from PMI is that performance, due to lightweight and a better build solution, is increased.

The overall assembly was also simplified. Firstly, the recirculating ball bearings, even though they have tougher mounting tolerances, for fool proofing has beem taken better in consideration. As such, assembly mistakes with PMI parts is not expected to affect performance of the part, damaging only the rated work life. Since, loads in this product are very small then, mounting errors will not affect, in a relevant manner, the total rated life of the stage. Another factor that

simplified manufacturing is that, by having a smaller parts, it allows to decrease the size of the aluminium plates that hold the stage. In addition to this, PMI parts only use on type of series - the 07 - allowing for better interchangeability of hardware between the different stages. This brought the total assembly time to 5 hours, at a cost of 69.7 €.

The lightweight of the smaller stage and the respective smaller chassis allowed for lighter frame with a total mass of 2.4 Kg and a total volume of a 12.05 L. The total cost per liter in this solution is 86.6 € per liter and the total cost per kilogram is 461.4 € per kilogram.

The total cost of this solution is around 1043 € with a chassis cost of 9.6 €. The cost of aluminium for this solution, even tough smaller, it costs 36.5 €. By observing figure 7.15 it is possible to observe that the linear actuators are still the most predominant relevant cost of the total cost. The decrease of assembly cost leveraged the increased cost of the new guides.

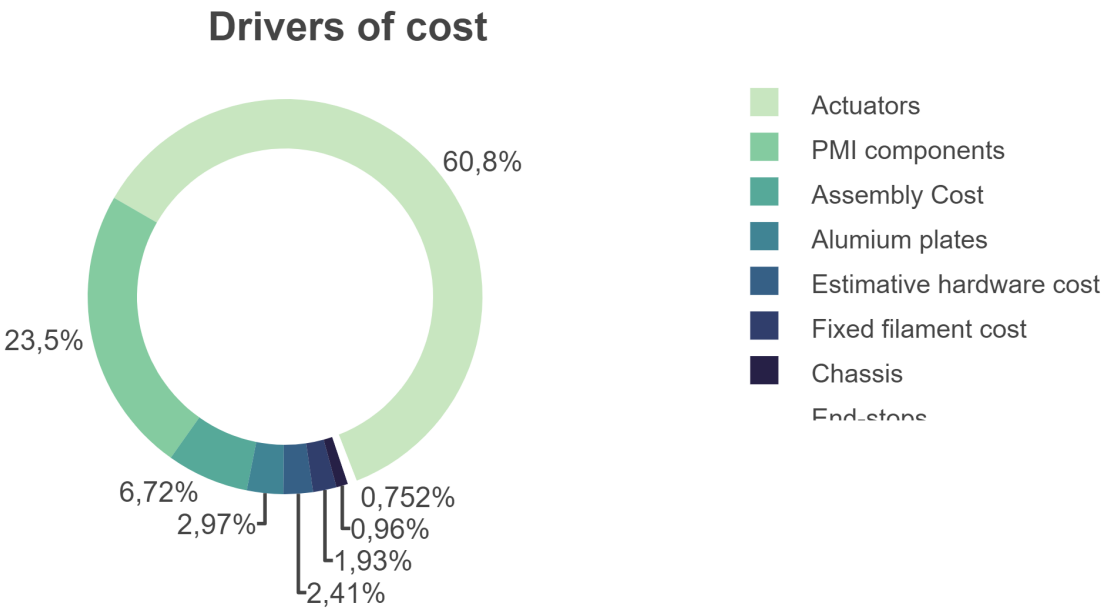

Figure 7.15: PMI hardware solution cost drivers

In term of the number of parts, this solution has the same amount of hardware being use. It is important to notice that the array of bolts sizes is smaller, leading to even less tool changes. The size of the bolts used have also a better mounting sequence as well due to a more uniform assembly. The determined cost of assembly per bolt is 0.55 € per bolt, decreasing the importance of having extra hardware.

7.3.3 3D printed solution

The next constructive solution was manufactured in a 3D printed technology, FDM. As a consequence, it is expected a reduce in part costs and in mass since, 3D manufacturing allows for the usage of cellular structures and uses polymers as material. This solution uses an IGUS® stage and therefore has similar dimensions to the respective solution.

Considering using 3D printed manufacturing extruded profiles reduces considerably the weight of the total product. In this solution the total mass is 1.781 kg. To better understand the final weight of the parts, it was considered the value given by the slicer when simulated for the defined parameters. The estimated total weight of filament being used is 993g, approximately a kilogram of filament. Since, it is necessary to buy a roll of filament in each prototype it was considered the full cost of a kilogram of filament. Past prototypes, only used around an estimate of 350 g, where this prototype uses a full kilogram. Thus, there will be a difference in the cost of material used. Since it is necessary to buy, at least, a full roll of filament, to simplify and have a conservative position, it was considered the full cost of a roll of filament in every solution.

The total volume of this solution is approximately 14 liters since the chassis is a few millimeters higher and parts are larger as well. The chassis cost in aluminium of this part is 4.14 € and the total assembly cost is 69,7 €. The decrease in price is due to the exterior structural elements such as aluminium plates and chassis parts are now included in the filament price tag.

The total cost per kilogram is 526.9 € per kilogram and the total cost per liter is 67 € per liter. The assembly took around 5 hours. The assembly time in this solution is justified by the usage of less part such as brackets and nuts.

The consequence of using 3D printed jigs and parts that can help in assembly or reduce the total number parts is the reduced number of bolts. For example, the total number of bolts in this solution is 118 and the necessary number of bolts is 98. The number of brackets is also now half. As such the bolt per part ratio in this solution is expected to be 1.11 bolts per component and the assembly cost per bolt is 0.59 € per bolt.

As it is possible to observe in figure 7.16 the value of actuators cost increased as the main driver. This is due the fact that now, most of the exterior components are under, a less expensive factor - PLA filament.

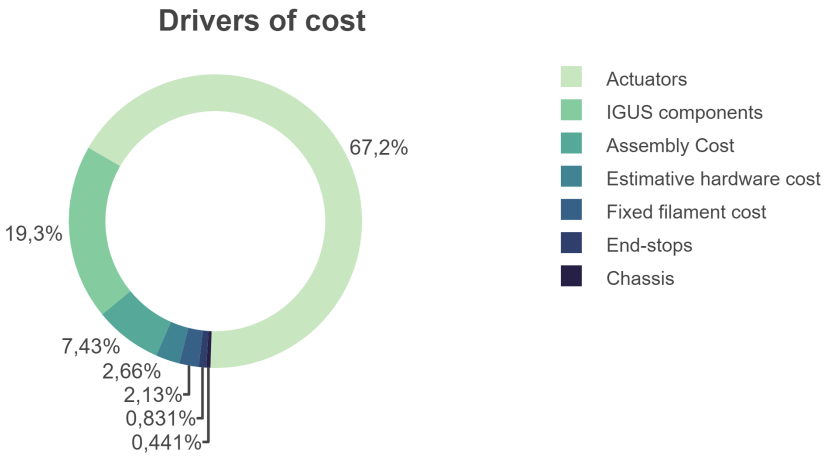

Figure 7.16: 3D printed solution drivers of cost

The 3D manufactured solution presented itself as the lightest and cheapest solution to creates. The easy of assembly and easy to get filament, make this a very good way to create prototypes.

In the situation where the combined cost of the chassis and the manufacturing of the aluminium sheet drop under the cost of a kilogram of filament, then this solution becomes obsolete.

7.3.4 Alucobond® solution

The final solution created was the one made with plates made in Alucobond®. The usage of this material not only improves flexural properties as well in terms of strength-to-weight ratio. The added thickness will also provide better rigidity and less deformations, as well. Alucobond® comes with the increase price of using a premium material. This section goal is to address the cost-effectiveness of this solution. Only the parts of the stages were created in Alucobond® to save down on total cost.

As expected this parts have a reduced weight due to the usage of PET as the core polymer. As a consequence the total weight of this solution is 2.35 Kg with a volume of 13.93 liters. As expected the volume is the same, with a smaller total weight. The weight, as expected, was reduced in particular in the XY-Z stage. This means that this reduction of weight is more relevant to performance than structural. As such, the weight reduction will effect directly performance and not overall product weight. The cost per kilogram of this solution is 506.7 € per kilogram and the cost per liter is 85.5 € per liter. The total cost of this solution is around 1190€ with a chassis cost similar to the IGUS® guides. Figure 7.17 shows the different cost drivers for this solution. As it is possible to observe, in this solution the engine cost do not cover more than half of the cost of the product. The usage of Alucobond® can turn reducing the total cost more difficult.

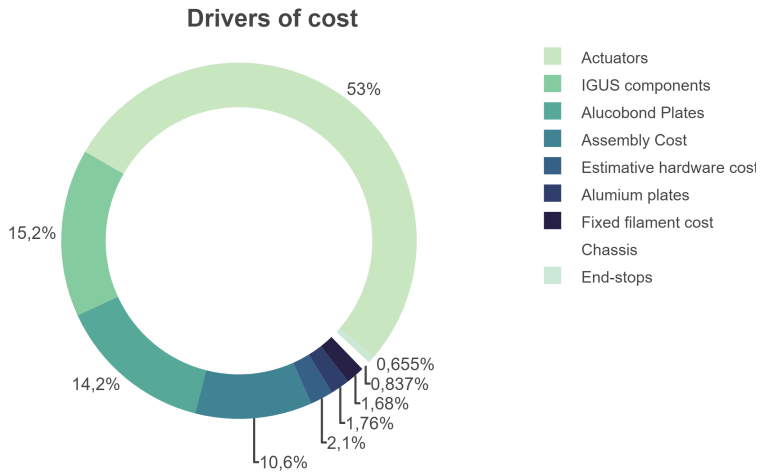

Figure 7.17: Alucobond® solution drivers of cost

In terms of the number of parts, this solution has a similar number of part to the IGUS® solution. The main difference is that the cost per component and the cost per bolt increased. Assembly time was similar to the assembly time of the IGUS® parts.

In this solution, the price of the Alucobond® plates had a total cost of 168.6€. It was observed that due to the exclusivity of this material it was necessary to buy at least a meter squared of sheet. It is expected that this material turns better profit when building the enclosure due to the faster

assembly and manufacturing. It is important to notice that it is expected that the material cost will be reduced as production increases.

As observed in 6.1.1.4 the aluminium plate Compared with the Alucobond® had a difference of 56g, a reduction of 30%. The displacement of Alucobond® is 18 μm lower, a reduction of 46%.

7.3.5 Summary and final comparisons

After all the metrics being displayed and explained, it now possible to compare the solutions between them. Table 7.3 shows different measurement of the different tested solutions. The main goal of this subsection is to compare all the solutions between them and decide what is the best solution to follow for final production.

Solution	Mass [Kg]	Volume [L]	Fastener	Components	Assembly time [h]	% of standard parts
IGUS® stage	2.49	13.93	126	110	8	41
PMI stage	2.26	12.05	126	110	5	41
3D printed	1.781	14	118	106	5	35
Alucobond®	2.35	13.93	126	110	8	41

Table 7.3: Measurements of the different tested solutions

As it is possible to observe, the 3D printed solution is the lightest prototype as well the one that uses less fasteners. On the other hand, the aluminium prototype with the IGUS® stage is the heaviest and the longest assembly time. Table 7.4 displays different cost metrics observed during the economical analysis of the different solutions.

Solution	Euro/Kg	Euro/L	Ass. Cost [euro]	Total cost [euro]	Ass. cost / Fastener	Chassis Cost [euro]
IGUS® stage	408,4	73	111.52	1017	0.885	9.96
PMI stage	461.4	86.5	69.7	1043	0.55	9.59
3D printed	526.9	67	69.7	938.4	0.59	4.14
Alucobond®	506.7	85.5	111.52	1174.948	0.885	9.96

Table 7.4: Cost metrics of the different tested solutions

In this table it is possible to conclude that the system that has the better weight for a certain cost is the IGUS® stage while the one that has a better performance in terms of volume per cost is the PMI solution.

IGUS® stage presents the lowest possible cost per kilogram. This means that for the same weight, then this solution presents the lowest cost in terms of overall components being used. It is interesting to observe that the 3D printed solution, even thought it is the lightest, presents the higher cost per kilogram. This is due to the cost still being reasonably high, while having less mass. It is possible to observe the heavy influence of the lightweight actuators on this metric.

In terms of euro per liter the PMI stage has been determined with the highest value. This means that for 1L liter of this solution, cost will be higher. This may mean that space is being

better used due to the increased of cost density over the product. On another hand, the 3D printed solution has a the biggest dimension while having a smaller cost. The cost density is not the most important metric, but it gives a good visualization of how compact the product is.

In terms of total cost the less expensive is the 3D printed prototype and the most expensive is the Alucobond® one. Being the 3D printed prototype the one that is reduces cost the most, this proves the feasibility of creating this device as with manufacturing parts. Although, with the increase in production it will become disadvantageous. As such, when creating a prototype, it should be done in 3D printing. Not only it will save time and cost, but it allows to jump over the pipeline required to submit purchase orders and working with third parties. These two factor are fundamental for project management and development.

It's interesting to observe that total cost do not have considerable difference between them. The medium value of cost between the four different solutions is 1045.7 euros with standard deviation of 93.25 euros. As such deciding between either solution will not take the product from the range of a low-cost product.

To conclude, all solutions are feasible. A more in-depth comparison between stages is required to settle on a final product. The 3D printed prototype is a good option in development stages and the PMI solution is another great option due to a good cost density and medium total cost. The PMI solution also saves extra in enclosure material due to a smaller size body.

7.3.6 Stages comparison

In this section both stages will have a more in depth analysis. This will help understand the effect that capital will have in performance and what to expect and to correctly decide if the investment on more expensive parts is actually a good investment.

In a low-cost device, capital investment relate to performance should be a very considerable factor. It is important to ask, how much value will be created by the extra cost.

As a consequence, it is important to analyse the economics behind selecting which stage to choose. PMI parts are clearly more expensive. However, they come with a notable performance increase.

Starting with the IGUS® solution, as expected this solution presents a lower cost being these products find themselves, despite having good quality, in the end of the spectrum of performance linear guides. The total cost of all the required parts for the XY-Z stage is 181.2 €. The mass of the rails is 98g and the mass of the carts is 306g. This is specifically high due to usage of series 12. Each cart of these series weighs about 34g. The total weight of IGUS® parts is 404g. Thus, the total cost per Kg is 448.6 €. It is observable that the lower this value the better because it means a lower cost.

In terms of the aluminium plates used in this XY stage, the largest plate weights 53 g and the small 24g. In addition to this, it is summed up the weight of the engine and other minor components, in a grand total of 0.140 Kg. The total cost of this plates was 2.06 € with a ratio of weight-to-cost of 0.037 Kg per euro. The higher this ratio is the cheaper was to manufacture the parts.

On the other end, PMI parts present a better and more notable performance. The PMI parts is good mid range solution for an affordable price. This solution also comes with an extensive documentation on the performance, geometric tolerances and assembly.

The total cost of PMI parts is 244 €. Due to the great mechanical properties of this part, only series 07 was used. The rail, being stainless steel is heavier than the IGUS® rails. The total mass of the rails is 0.180 Kg and the mass of the carts is 0.084 Kg. Each cart has a weight of 7g. The total weight of the system is 265 g. The total cost per kilogram is 921,5 € per kilogram.

Due to the smaller size, less rails can be used. Due to a minimum "rail size", it had to be bought at least 1 meter of rail even tough it was only necessary 550 mm. The large and small aluminium plates that are used in the XY stage, weighs 48g and 20g, respectively.

The total cost of the this two plates was 7.56 €, having the weight-per-cost ratio of 8.9 g per euro. The higher manufacturing cost depends on the manufacturer. The display of these different metrics can be found in table 7.5.

Solution	Mass [Kg]	Euro/Kg	Total Cost	Cost of the XY plates	Weight of the XY stage [Kg]
IGUS® stage	0.54	448.6	181.2	2.06	0.14
PMI stage	0.39	921.5	244	7.56	0.13

Table 7.5: Cost metrics of the different stages

The upgrade to the PMI stage would grant a 45% decrease in mass and a more compact and uniformed stage. In addition, to all these great factors, better guides would conferee a better life rating, rigidity, sliding tolerances, rail material and overall customer experience.

For the 7 series PMI carts the overall static life rating, C_0 is 1280 Newtons, while the same rating for the 12 series from IGUS® is 960 Newtons. This means that for the unit price of 13.9 €, the PMI cart as a 0.01 €/N. IGUS® cart, rated at 13.04 €, has a 0.013 €/N. This means that for the same rated life, the IGUS® cart is 0,3 cents more expensive.

It is important to notice that IGUS® series 12 is a very big cart at a total weight of 34g and the PMI series 7 cart weighs only 7g. As such, the cost per gram of the IGUS® cart is 0.38 while PMI is 1.98. The PMI rating is 5.17 times higher than the one from IGUS®. This rating means that for a cart with the same weight, it would cost almost 5.17 times more to buy a PMI cart.

Finally, the life-per-gram ratio of PMI is 128,85 N/g and IGUS® is only 28.3 N/g. That's an increase of 6.5 times of the initial value. This ratio gives a good impression of how better the PMI carts actually are. Despite being smaller and lighter, this hardware also presents better rated life. This rating divided by the cost of the cart will give a good impression of how more cost efficient are this parts. The PMI parts have a 13.15 N/g€ and IGUS® parts have 2.1 N/g€. As such, PMI parts are more efficient for the price.

Another important comparison is the geometric tolerances. The geometric tolerances between the cart and the rail for the PMI is 0.04 mm while IGUS® parts is 0.1 mm. The increased accuracy is observed not only in the running smoothness but in the assembly as well. Finally PMI guides

have the ability of being pre-loaded that increases exponentially the overall rigidity of the system, making it harder for displacement in the rolling direction.

As such it is important to understand what is the importance that it will be given to pre-loading, better tolerances and better documentation. How much is one willing to increse the budget for the linear guides to have these extra improved features. The total difference of cost between both stages is around 63 €, an increase in cost of 34% of the IGUS® stage. In total product cost the difference is 26.7 € an increase of 2.5% of the total product cost. Due to the great cost efficiency, smaller size, lighter weight, better life rating and other important factors, the increase of 2.5% in the product cost is advised.

7.4 Improvement opportunities

Development is an iterative process. This means that, evolution can only be done by creating different and improved versions of the same idea. Exploring an idea in-depth means that multiple iterations will be created to better optimize the choose metrics. The relevant importance of creating multiple prototypes to achieve the most effective product possible. As expected, after the assembling and analysing the different prototypes it is possible to observe different improvement opportunities that can be explored further with the goal to optimize the desired metrics.

Assembly improvement It was seen that using threaded holes will improve assembly time and the overall quality of the fasteners. Using threads instead of a typical washer and nut. This will reduce the total amount of hardware needed as well. The down-side is the increased manufacturing time due to the addition of this stage. It is believed that for higher production, threading will save essential time in assembly, in particular, when working with M2 hardware.

Material selection This model can have more hybrid approach if total weight is required to be saved. Some components of the XY base can switched with polymeric materials maintaining the structure of the product in more rigid material. This change it is expect to better improve the total weight of the device, making it more friendly for field practices.

Part Redesign While exploring the usage polymeric materials, it is suggested to better observe the behaviour of the 3D printed base. As such, this part from the XY could be redesigned to avoid using more extruded profiles, reducing the total number of components, while maintaining a reduced weight. The main disadvantage of this part is the creation of another part that will use more complex forms of manufacturing that can increase cost. This would also allow for added features such as the addition of a proper enclosure for electrical and optical hardware. Other features such as mounting shoulders and mounting boss can be added as well. This would improve the overall performance of the part and assembly. The suggest modification can be observed in figure 7.18

Assembly improvement It was observed that the created jig improved and accelerated the calibration of the parallelism error of the rails. This calibration is the main bottleneck of the assembly. As such, an improved and more in-depth jig that can accurately guarantee the necessary tolerance would reduce exponentially the assembly time, reducing the total cost as well. This would also reduce the necessity of a more skilled assembler.

Electronical Mounting It was observed that the mounting of the electrical end-switches could be difficult. It is suggested that further improvement to the part is done such as: the calibrating range and the distance between the pin and where the bold will be screwed.

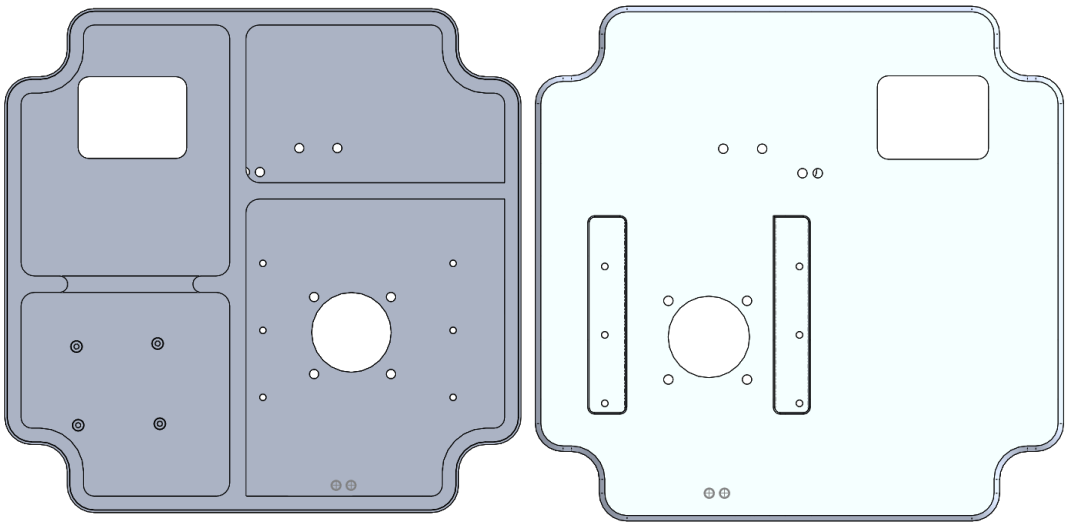

Figure 7.18: Suggested modification an improved XY base that would require more advance manufacturing technologies

Assembly improvement Adding calibration features to other important holes can be a time saver, improve the quality of the assembly at almost no extra cost. It would also be great if a decal could be added to correct side of the plate pointing to the top surface.

Structural improvement Assembling the front legs can be extremely difficult not only to calibrate but to guarantee the right level of the table. It was observed that this would be more efficient with the usage of only a total of three legs. In the situation, of leaving the four legs for better stability, then it is advised to add a front plate that connect both legs and guarantee parallelism and perpendicularity with the floor. This can save calibration time and the amount of brackets requires.

Assembly improvement It was observed that the device has too many bolts. It would be interesting to explore future way to use less complex fasteners in the product, improving as such the total time. It is also important to study the amount of fasteners required in each part, to reduce at the maximum possible the number of fasteners.

Assembly improvement A factor that should be explored further with the production of this prototype is to better improve cable design. When assembling electronics features for cable design is of highly importance for a fast assembly and a lean product.

Conceptual opportunity With the developed plan, this device and the design process could be explore to better considered the environmental footprint.

Conceptual opportunity In this dissertation, the device is clearly separated in three distinct modules. In eventual design for assembly improvements this concept could be explored further

to better improve the modularity. It is expected that a modular design will decrease cost and easy maintenance, assembly and disassembly.

Chapter 8

Conclusions and Future Work

The main goal of this dissertation was to improve and redesign an existing solution of the μSmartScope. In the end, it was developed a new solution with a stronger frame and a different layout. Novel simulation concepts armed with state of the art digital manufacturing technologies were used to better optimize different components. In the end, it was possible to obtain four different working solutions with varying degrees on cost and performance. It was concluded that the 3D printed solution is the one selected for prototyping . The solution with PMI stage is the one that should follow for mass manufacturing.

8.1 Results

This dissertation explored further the design process of creating a low-cost micro-stage with the application of DFM&A methodologies.

In the first pre-development stage, the first solution to the CLARE project developed by Fraunhofer AICOS was studied. It was observed that there was a vast array of improvement opportunities that would result in the desired performance for this product. The main flaws of this prototype were the overall high complexity of assembly, total part count, and the usage of different thicknesses in the chosen aluminum plates. This device was extremely heavy, is not user friendly for an on-field device. In addition to this, it was observed that only using two guides was not the ideal solution to a stable system. The chosen stage layout would lead to parasitic errors as well.

With this case, the conceptual phase were different ideas were explored where the main goal was to create a more stable and faster stage. To achieve this, it was decided to bring the XY stage that translates the sample to a base and uniform the vertical this axis. The goal of the concept of only moving the illumination module is to create a faster, more accurate, and better repeatability focusing mechanism. It was expected that this would improve the bottleneck of the overall product. After exploring different conceptual prototypes and ideas a proof-of-concept was observed.

In this iteration, it was suggested that instead of translating the illumination module, it would be the optic tube with the cellphone attached that would translate in the vertical direction. To achieve a fast and accurate mechanism it would be important to create light and stiff components.

Following this idea, it followed a more technical stage where it was studied the influence of the different load situation on the working behavior of the guides. The rated life of the linear guides was explored in-depth. Analytical dynamical models to comprehend the effect of inertia on the moving stage. In addition to this, an analytical structural analysis proceeds to test bending and buckling on the columns. This helped decide on how to design the chassis of the product with extruded aluminum profiles. It was observed that using aluminum profiles would be a cost-effective solution to achieve a light and rigid structure.

It was concluded that it was mandatory to better improve the product to a faster and easier assembly. As such different solutions were created to better help manufacturability and assembly as well.

It was also studied, the usage of PMI parts instead of using IGUS®. PMI parts were observed to be more cost-efficient having a better-rated life per gram, such as being a more lightweight and sturdy solution.

COVID19 proved a challenge to develop different prototypes due to lockdown policies. As such, it was asked what was the feasibility of manufacturing the complete stage in FDM while applying and DfAM mindset to better improve final results. Tensile tests were done to better observe the effects of infill and wall count on the cost-effectiveness of the 3D printed part. The best results achieved for a cubic infill was a density of 35% with 3 walls for the perimeter. Parts were manufactured having these values as a design insight.

To evolve the work-alike prototype to an engineering prototype it was thought on an enclosure. To manufacture this enclosure it was studied the effects of Alucobond®. This material is a sandwich structure with a PET core that has a great weight to rigidity ratio. It was observed that using fasteners directly in touch with the core material can lead to a loss of properties over-time. It was suggested to use an insert of a 3D printed part to stop this from happening.

ABAQUS was used to study the effect of the load on key structural components. Static situations were used to use less computational power and over-design the system. It was concluded that there won't be any significant structural problems with the current design. *Solidwork* was used as the CAE software to better improve on specific case studies. It was used solid elements with a novel blended curvature-based mesh to better represent complex geometries while maintaining a more constant aspect-ratio between all elements.

The design process started with the FEA validation of a simple version of the part. In the case of having a positive outcome, this part would suffer a multi-load case situation topology optimization algorithm under the *SolidWorks* framework. The next step would be the remodeling of the part and re-do the static simulations. As such, topology optimization was used as a design insight for the optimization of the parts. The most critical part was the part that requires holding the cellphone. It was possible to reduce the weight from 1223g to 245g. It is expected that by using cellular structures typical of 3D manufacturing it is possible to reduce this weight to 168g.

Dynamical simulations were done as well to the final parts to better comprehend the true behavior of the components. It was observed that in a more realistic load case, the studied results were smaller than the ones observed with the static validations, guaranteeing the correct performance of the parts.

Finally, a cost analysis was done to better observe the most efficient solution. It was concluded that the PMI stage offers the best cost-effective for performance tables. This is due to the smaller size of the hardware with the added rated life. These parts also include features such as pre-loading and better tolerances that greatly complement the extra cost compares to the IGUS® parts.

It was concluded that the main driver of cost in the state of the art actuators meaning that a trade deal would discount greatly in the total cost of the device. The total cost of the devices rounds around 1050€ making it a very low-cost solution compared to the ones observed in the market review. The usage of Alucobond®bond must be better explored because it can present a great, easy to assemble solution with the addition of the extra cost. It is expected that by increasing production, the usage of this premium material would become cost-effective.

8.2 Further Work

Further work addressing this dissertation would be essential to leading the different presented solutions to a product phase. As such, during the dissertation work I have observed the following areas that could still be explored:

- Address the improvement opportunities observed in chapter 7.4;
- In this regard, I advise another DFA iteration to better improve assembly and explore other easier fasteners;
- It would be interesting to work the professional of the are to obtain valuable feedback;
- Benchmark the product;
- To better apply this device in countries with more complex weather conditions it's mandatory to find a solution to stanch and protect the hardware;
- Finally, I advise to contact a manufacturer and take this solution from an engineering prototype to a complete final product.

References

[1] WHO. WHO | Cervical cancer. https://www.who.int/health-topics/cervical-cancer (visited on 30/05/2020), 2018.

[2] Luís Rosado, Paulo T. Silva, José Faria, João Oliveira, Maria João M. Vasconcelos, Dirk Elias, José M.Correia da Costa, and Jaime S. Cardoso. μSmartScope: Towards a Fully automated 3D-printed smartphone microscope with motorized stage. *Communications in Computer and Information Science*, 881:19–44, 2018.

[3] James A. DeRose and Michael Doppler. Guidelines for Understanding Magnification in the Modern Digital Microscope Era. *Microscopy Today*, 26(4):20–33, 7 2018.

[4] Martin Wilson. Microscope Resolution: Concepts, Factors and Calculation | Learn & Share | Leica Microsystems. https://www.leica-microsystems.com/science-lab/microscope-resolution-concepts-factors-and-calculation/ (visited on: 11/02/2020).

[5] Jianchao Yang and Thomas Huang. Image super-resolution: Historical overview and future challenges. In *Super-Resolution Imaging*, pages 1–33. CRC Press, 1 2017.

[6] Kenneth R. Spring and Michael W. Davison. Field of View | MicroscopyU. https://www.microscopyu.com/microscopy-basics (visited on 10/02/2020).

[7] Mustafa Turkmenogly, Orhan Sengul, and Levent Yalciner. MTF Measurements for the Imaging System Quality Analysis. *Gazi University Journal of Science*, 25:19–28, 2012.

[8] Marly G.F. Costa, Cícero F.F.Costa Filho, Juliana F. Sena, Julia Salem, and Mari O. De Lima. Automatic identification of mycobacterium tuberculosis with conventional light microscopy. In *Proceedings of the 30th Annual International Conference of the IEEE Engineering in Medicine and Biology Society, EMBS'08 - "Personalized Healthcare through Technology"*, pages 382–385, 2008.

[9] Steve M. Blevins, Ronald A. Greenfield, and Michael S. Bronze. Blood smear analysis in babesiosis, ehrlichiosis, relapsing fever, malaria, and Chagas disease, 2008.

[10] Steven E. Waggoner. Cervical cancer. *Lancet*, 361(9376), 6 2003.

[11] Ewert Bengtsson and Patrik Malm. Screening for Cervical Cancer Using Automated Analysis of PAP-Smears. 2014.

[12] C. Vargas and E. Romero. A low cost and efficient prototype of a motorized microscope. In *Proceedings - Electronics, Robotics and Automotive Mechanics Conference, CERMA 2006*, volume 1, pages 83–86, 2006.

[13] Edmon O. Fernandez, Nilo M. Arago, Jennifer O. Aquino, Jasmine P. Marie Bravo, Julie Anne S. Francisco, Claudine B. Vanessa Gaddi, and Cinderella A. Simbran. Microcontroller-Based Automated Microscope for Image Recognition of Four Urine Constituents. In *IEEE Region 10 Annual International Conference, Proceedings/TENCON*, volume 2018-October, pages 1689–1694. Institute of Electrical and Electronics Engineers Inc., 2 2019.

[14] C. J.R. Sheppard. Microscopy: Overview. In *Encyclopedia of Modern Optics, Five-Volume Set*, pages 61–69. Elsevier Inc., 1 2004.

[15] A.S. Holik. Optical Microscopy. *Encyclopedia of Materials: Science and Technology*, pages 6458–6463, 1 2001.

[16] H.Ernst Keller. Proper Alignment of the Microscope. In Leslie Wilson and Paul Matsudaira, editors, *Methods in Cell Biology*, volume 72, pages 45–55. Academic Press, 1 2003.

[17] Caitlin Smith and Michael Eisenstein. Automated imaging: Data as far as the eye can see. *Nature Methods*, 2(7):547–555, 7 2005.

[18] M Oheim. High-throughput microscopy must re-invent the microscope rather than speed up its functions. *British Journal of Pharmacology*, 152(1):1–4, 9 2007.

[19] Roy Wollman and Nico Stuurman. High throughput microscopy: From raw images to discoveries. *Journal of Cell Science*, 120(21):3715–3722, 11 2007.

[20] Michael E Dailey, Conly L. Rieder, Alexey Khodjakov, Paul D. Andrews, Jason R Swedlow, Jennifer C. Waters, Griffin. John D., Scott G. Olenych, Nathan S. Claxton, and Michael W Davidson. The Automatic Microscope | MicroscopyU.

[21] Prior Scientific. Prior Scientific. https://www.prior.com/ (visited on 20/02/2020), 2009.

[22] Thorlabs. Motion control. https://www.thorlabs.com (visited on 19/02/2020), 2020.

[23] Inc Leica. Microscopes and Imaging Systems | Leica Microsystems. https://www.leica-microsystems.com/ (visited on 20/02/2020), 2020.

[24] Inc Olympus. XC10 | Olympus Life Science. https://www.olympus-lifescience.com (visited on 20/02/2020), 2020.

[25] Inc Nikon. Nikon | Healthcare Products & Solutions (Microscope Solutions). https://www.nikon.com/products/microscope-solutions/ (visited on 20/02/2020).

[26] Microworld. Microscope Sales & Service | Shop Microscopes For Every Application. https://www.microscopeworld.com/ (visited on 20/02/2020), 2020.

[27] Charles B. Delahunt, Courosh Mehanian, Liming Hu, Shawn K. McGuire, Cary R. Champlin, Matthew P. Horning, Benjamin K. Wilson, and Clay M. Thompon. Automated microscopy and machine learning for expert-level malaria field diagnosis. In *Proceedings of the 5th IEEE Global Humanitarian Technology Conference, GHTC 2015*, pages 393–399. Institute of Electrical and Electronics Engineers Inc., 12 2015.

[28] University of Cambridge. OpenLabTools. http://www.openlabtools.org/ (visited on 15/03/2020), 2013.

[29] Robert A.A. Campbell, Robert W. Eifert, and Glenn C. Turner. Openstage: A low-cost motorized microscope stage with sub-micron positioning accuracy. *PLoS ONE*, 9(2):e88977, 2 2014.

[30] W. Jywe, Y. R. Jeng, C. H. Liu, Y. F. Teng, C. H. Wu, T. H. Hsieh, and L. L. Duan. Development of a middle-range six-degrees-of-freedom system. *Proceedings of the Institution of Mechanical Engineers, Part B: Journal of Engineering Manufacture*, 224(4):679–688, 2010.

[31] Bhaskar Dasgupta and T. S. Mruthyunjaya. Stewart platform manipulator: A review. *Mechanism and Machine Theory*, 2000.

[32] Junkang Guo, Zhigang Liu, Baotong Li, and Jun Hong. Optimal tolerance allocation for precision machine tools in consideration of measurement and adjustment processes in assembly. *International Journal of Advanced Manufacturing Technology*, 80(9-12):1625–1640, 10 2015.

[33] Klaus S. Sollmann, Musa Jouaneh, and David Lavender. Dynamic Modeling of a Two-Axis, Parallel, H-Frame-Type XY Positioning System. *IEEE/ASME Transactions on Mechatronics*, 15(2):280–290, 2010.

[34] CoreXY. CoreXY | Cartesian Motion Platform. http://www.corexy.com/index.html (visited on: 25/03/2020).

[35] PI. XY Stages – 2-Axis Motorized Precision Positioning Stages. https://www.pi-usa.us/en (visited on 24/02/2020), 2020.

[36] Seung Kook Ro and Jong Kweon Park. A compact ultra-precision air bearing stage with 3- DOF planar motions using electromagnetic motors. *International Journal of Precision Engineering and Manufacturing*, 12(1):115–119, 2 2011.

[37] Maneuf Serge, Thomas Patrick, and Franck Duquenoy. Motion Systems: An Overview of Linear, Air Bearing, and Piezo Stages. In *Three-Dimensional Microfabrication Using Two-Photon Polymerization: Fundamentals, Technology, and Applications*. 2016.

[38] Wu-Le Zhu, Zhiwei Zhu, Yi Shi, Xinwei Wang, Kaimin Guan, and Bing-Feng Ju. Design, modeling, analysis and testing of a novel piezo-actuated XY compliant mechanism for large workspace nano-positioning. *Smart Materials and Structures*, 25(11):115033, 10 2016.

[39] Shorya Awtar and Gaurav Parmar. Design of a large range XY nanopositioning system. *Journal of Mechanisms and Robotics*, 5(2), 3 2013.

[40] Guangbo Hao and Xianwen Kong. A novel large-range XY compliant parallel manipulator with enhanced out-of-plane stiffness. *Journal of Mechanical Design, Transactions of the ASME*, 134(6), 6 2012.

[41] Larry L. Howell, Spencer P. Magleby, and Brian M. Olsen. *Handbook of Compliant Mechanisms*. Wiley, 2 2013.

[42] Kee Bong Choi and Doo Hyeong Kim. Monolithic parallel linear compliant mechanism for two axes ultraprecision linear motion. *Review of Scientific Instruments*, 77(6):065106, 6 2006.

[43] Eric Coatanéa, Sarayut Nonsiri, Ricardo Roca, Faisal Mokammel, Juliane Kruck, and François Christophe. Systematic search for design contradictions in systems' architecture: Toward a computer aided analysis. *Journal of Integrated Design and Process Science*, 19(1):25–46, 6 2015.

[44] Toto. Air Bearings - Ceramics. https://jp.toto.com/products/ceramics/en/air/ (visited on 24/02/2020).

[45] Igus Inc. Igus Catalogue. www.igus.eu, 2013.

[46] Exlar Corporation: Exlar Corporation: Linear actuator | Packaging World. https://www.pakworld.com/machinery/ (visited on 24/03/2020), 2014.

[47] Richard Gordon Budynas and J. Keith Nisbet. *Shigley's Mechanical Engineering Design ,10th edition*, volume 1. McGraw-Hill Education, 10 edition edition, 2014.

[48] Y. Altintas, A. Verl, C. Brecher, L. Uriarte, and G. Pritschow. Machine tool feed drives. *CIRP Annals - Manufacturing Technology*, 60(2):779–796, 2011.

[49] Mei Yung Chen and Jian Shiun Lu. High-precision motion control for a linear permanent magnet iron core synchronous motor drive in position platform. *IEEE Transactions on Industrial Informatics*, 10(1):99–108, 2 2014.

[50] Alexander Slocum, Murat Basaran, Roger Cortesi, and Anastasios John Hart. Linear motion carriage with aerostatic bearings preloaded by inclined iron core linear electric motor. *Precision Engineering*, 27:382–394, 2003.

[51] Z. Ferková, M. Franko, J. Kuchta, and P. Rafajdus. Electromagnetic design of ironless permanent magnet synchronous linear motor. In *SPEEDAM 2008 - International Symposium on Power Electronics, Electrical Drives, Automation and Motion*, pages 721–726, 2008.

[52] Liyi Li, Donghua Pan, and Xuzhen Huang. Analysis and optimization of ironless permanent-magnet linear motor for improving thrust. *IEEE Transactions on Plasma Science*, 41(5):1188–1192, 2013.

[53] Ronald S. Fearing. 6. Micro-actuators for micro-robots: Electric and magnetic. In *Handbook of Sensors and Actuators*, volume 6, pages 161–179. Elsevier, 1 1998.

[54] Kenji Uchino. Ceramic Actuators. In Anthony Kelly and Carl Zweben, editors, *Comprehensive Composite Materials*, chapter 6.35, pages 663–671. Pergamon, 1 2000.

[55] Y.Q. Fu, J.K. Luo, A.J. Flewitt, and W.I. Milne. Smart microgrippers for bioMEMS applications. In *MEMS for Biomedical Applications*, pages 291–336. Elsevier, 1 2012.

[56] K. Uchino. Piezoelectric ceramics for transducers. In *Ultrasonic Transducers: Materials and Design for Sensors, Actuators and Medical Applications*, pages 70–116. Elsevier Inc., 1 2012.

[57] Sandra V. Kik, Claudia M. Denkinger, Pamela Chedore, and Madhukar Pai. Replacing smear microscopy for the diagnosis of tuberculosis: What is the market potential?, 6 2014.

[58] R. Dendere, N. Myburg, and Tania S. Douglas. A review of cellphone microscopy for disease detection. *Journal of Microscopy*, 260(3):248–259, 12 2015.

[59] Aydin Arpa, Gordon Wetzstein, Douglas Lanman, and Ramesh Raskar. Single lens off-chip cellphone microscopy. In *IEEE Computer Society Conference on Computer Vision and Pattern Recognition Workshops*, pages 23–28, 2012.

[60] Sungkyu Seo, Ting-Wei Su, Derek K Tseng, Anthony Erlinger, and Aydogan Ozcan. Lensfree holographic imaging for on-chip cytometry and diagnostics †. 2008.

[61] Derek Tseng, Onur Mudanyali, Cetin Oztoprak, Serhan O. Isikman, Ikbal Sencan, Oguzhan Yaglidere, and Aydogan Ozcan. Lensfree microscopy on a cellphone. *Lab on a Chip*, 10(14):1787–1792, 2010.

[62] D N Breslauer, R N Maamari, N A Switz, W A Lam, and D A Fletcher. Mobile Phone Based Clinical Microscopy for Global Health Applications. *PLoS ONE*, 4(7):6320, 2009.

[63] Bharat Bhushan and Matt Caspers. An overview of additive manufacturing (3D printing) for microfabrication. *Microsystem Technologies*, 23(4):1117–1124, 4 2017.

[64] Robert J. Morrison, Scott J. Hollister, Matthew F. Niedner, Maryam Ghadimi Mahani, Albert H. Park, Deepak K. Mehta, Richard G. Ohye, and Glenn E. Green. Mitigation of

tracheobronchomalacia with 3D-printed personalized medical devices in pediatric patients. *Science Translational Medicine*, 7(285), 4 2015.

[65] Kun Liang, Simone Carmone, Davide Brambilla, and Jean Christophe Leroux. 3D printing of a wearable personalized oral delivery device: A first-in-human study. *Science Advances*, 4(5):eaat2544, 5 2018.

[66] Mark H. Michalski and Joseph S. Ross. The shape of things to come: 3D printing in medicine, 12 2014.

[67] C. Lee Ventola. Medical applications for 3D printing: Current and projected uses. *P and T*, 39(10):704–711, 10 2014.

[68] Rob Davies. UK manufacturers to regear factories to build ventilators for NHS | Business | The Guardian. https://www.theguardian.com/business/2020/mar/17/uk-manufacturers-regear-factories-build-ventilators-nhs (visited on 21/03/2020), 2020.

[69] FDA. Technical Considerations for Additive Manufactured Medical Devices | FDA. Technical report, U.S. Department of Health and Human Services Food and Drug Administration, Rockville, MD, 12 2017.

[70] Rebecca Voelker. Regulatory Pathway for 3D Printing. *JAMA*, 319(3):220, 1 2018.

[71] William H Maisel. Medical Device Regulation: An Introduction for the Practicing Physician. Technical report, 2004.

[72] Cazacu Razvan and Grama Lucian. Overview of structural topology optimization methods for plane and solid structures. In *Annals of the University of Oradea*, page 7, Oradea, 12 2014. Fascicle of Management and Technological Engineering.

[73] Xiangyang Zhou, Liping Chen, and Zhengdong Huang. The SIMP-SRV Method for Stiffness Topology Optimization of Continuum Structures. *International Journal of CAD/CAM*, 7(1):41–49, 2007.

[74] Robin Larsson. Methodology for Topology and Shape Optimization: Application to a Rear Lower Control Arm. Technical report.

[75] Dassault Systemes. Structural Optimization | Tosca. https://www.3ds.com/products-services/simulia/products/tosca (visited on 23/03/2020), 2020.

[76] D Brackett, I Ashcroft, and R Hague. Topology optimization for additive manufacturing, 2011.

[77] Dassault Systemes. Design through analysis: improving product design and automating manufacturability with topology optimization. Technical report, Dassault Systèmes, 2018.

[78] M. David Anderson. *Design for manufacturability*. Taylo & Francis Group, 2014.

[79] David Stienstra. Introduction to Design for Manufacturing. http://me.gatech.edu/files/capstone/L071ME4182DFA.

[80] G. Boothroyd. *Assembly Automation and Product Design*. Number -. Taylo & Francis Group, 2nd edition, 2005.

[81] Anil Mital, Anoop Desai, Anand Subramanian, and Aashi Mital. Designing for Assembly and Disassembly. In *Product Development*, pages 159–202. Elsevier, 1 2014.

[82] Corrado Poli. Assembly. In *Design for Manufacturing: A Structured Approach*, pages 253–276. Elsevier, 1 2001.

[83] Z. Yoosufani and G. Boothroyd. Design for Manufacturability. Report Number 2. Design of Parts for Ease of Handling. | National Technical Reports Library - NTIS. Technical report, 1978.

[84] Bekir Sami Yilbas. Some applications of laser cutting. In *The Laser Cutting Process*, pages 205–297. Elsevier, 1 2018.

[85] D.A. Belforte and J.M. Jafferson. Laser Cutting. In *Reference Module in Materials Science and Materials Engineering*. Elsevier, 1 2016.

[86] W M Steen. Laser material processing—an overview. *Journal of Optics A: Pure and Applied Optics*, 5(4):S3, 6 2003.

[87] A. Riveiro, F. Quintero, and J. Pou. Laser Fusion Cutting of Difficult Materials. In *Advances in Laser Materials Processing*, pages 43–67. Elsevier, 1 2018.

[88] Zsolt Albert Barabas and Alexandru Morar. High Performance Microstepping Driver System based on Five-phase Stepper Motor (sine wave drive). *Procedia Technology*, 12:90–97, 2014.

[89] Haydon Kerk. Size 08 Hybrid Stepper Linear Actuators | 21000 series Linear Actuator. https://www.haydonkerkpittman.com/products/linear-actuators/hybrid-stepper/size-8 (visited on 10/03/2020), 2020.

[90] NSK. *Precision Machine Components - General Catalogs*. Number CAT No. E3161b. NSK, 1st edition, 2008.

[91] Simões Morais. *Desenho Técnico Básico 3*. Porto Editora, Porto, 2006.

[92] Bosch Rexroth. Rexroth - Linear Motion Technology. https://www.boschrexroth.com (visited on 16/03/2020), 2020.

[93] Schneeberger. MiniX product catalogue. www.schneeberger.com, 2019.

[94] Stephen P Timoshenko and Sergius Woinowsky-Krieger. *Theory of plates and shells*. McGraw-hill, 1959.

[95] University of Auckland. 6. Plate Theory. Retrived from http://homepages.engineering.auckland.ac.nz (visited on 17/04/2020).

[96] Ansel C. Ugural. *Stresses in Beams, Plates, and Shells*. CRC Press, 2010.

[97] John F. Stanton Josef C. Taylor. Friction Coefficients for Stainless Steel (PTFE) Teflon Bearings. (October):111, 2010.

[98] FP Beer, ER Johnston, and JT DeWolf. *Mechanics of materials, 5th SI Edition*. McGraw-hill, 7th edition, 2014.

[99] 3A Composites. Alucobond - Fascinating facades. Technical report, Singen.

[100] 3A Composites GmbH. ALUCOBOND ® Processing and Technical Data GB.

[101] Ben Redwood, Filemon Schffer, and Brian Garret. *The 3D printing handbook: technologies, design and applications*. 3D Hubs, 2017.

[102] Kunal Singh. Experimental study to prevent the warping of 3D models in fused deposition modeling. *International Journal of Plastics Technology*, 22(1):177–184, 6 2018.

[103] Mohammad S Alsoufi, Abdulrhman El-Sayed, and Abdulrhman E Elsayed. Warping Deformation of Desktop 3D Printed Parts Manufactured by Open Source Fused Deposition Modeling (FDM) System Environmental sustainability and energy conservation during machining processes View project Warping Deformation of Desktop 3D Printed Parts. Technical report, 2017.

[104] Dassault Systemes. ABAQUS 6.14, 2018.

[105] Engineering ToolBox. Metric Bolts - Minimum Ultimate Tensile and Proof Loads. https://www.engineeringtoolbox.com/metric-bolts-minimum-ultimate-tensile-proof-loads-d_2026.htm, 2018.

[106] J Davies M. *Lightweight Sandwich Construction*. Wiley-Blackwell, 0.

[107] Floriane Laverne, Frédéric Segonds, Nabil Anwer, and Marc Le Coq. DFAM in the design process: a proposal of classification to foste early design stages. In *CONFERE 2014 CROATIE*. Ecole Nationale Supérieure d'Arts et Métiers, 2014.

[108] A. W. Gebisa and H. G. Lemu. A case study on topology optimized design for additive manufacturing. In *IOP Conference Series: Materials Science and Engineering*, volume 276. Institute of Physics Publishing, 12 2017.

[109] Ultimaker. Mechanical properties* Injection molding 3D printing. Retrieved in ultimaker.com (visited on 18-05-2020), 2018.

[110] Solidworks. Solid Mesh. http://help.solidworks.com/2012/English/SolidWorks (visited on 23/04/2020), 2012.

[111] Solidworks. The New Blended Curvature-Based Meshing Algorithm. https://blogs.solidworks.com/tech/2016/ (visited on 04/06/2020), 2016.

[112] Dassault Systemes. SOLIDWORKS Help - Linear Static versus Linear Dynamic Analysis. http://help.solidworks.com/2018/english/SolidWorks/ (visited on 15/05/2020), 2018.

[113] Z W Muthui, P K Kamweru, F G Nderitu, S A Golicha Hussein, R Ngumbu, and G N Njoroge. Polylactic acid (PLA) viscoelastic properties and their degradation compared with those of polyethylene. *International Journal of Physical Sciences*, 10(21):568–575, 11 2015.

[114] Michael F Ashby. *Materials Selection in Mechanical Design*. Elsevier, Kidlington, Oxford, 4th edition, 2011.

[115] Matt Mowry. Five linear bearing mistakes you don't know you're making. *Inc, Igus*, page 4.

[116] PMI. PMI Catalogue - Linear Guideway. Retrieved from http://www.ampo.cz/produkty (visited on 18/04/2020), 2009.

[117] ISO. Plastics-Determination of tensile properties (ISO 527). Technical report, ISO, 2012.

[118] Khaled G. Mostafa, Carlo Montemagno, and Ahmed Jawad Qureshi. Strength to cost ratio analysis of FDM Nylon 12 3D Printed Parts. *Procedia Manufacturing*, 26:753–762, 2018.

[119] Liseli Baich, Manogharan G, and Marie H. Impact of Infill Design on Mechanical Strength and Production Cost in Material Extrusion Based Additive Manufacturing. 2016.

[120] Ala'aldin Alafaghani, Ala Qattawi, Buraaq Alrawi, and Arturo Guzman. Experimental Optimization of Fused Deposition Modelling Processing Parameters: A Design-for-Manufacturing Approach. *Procedia Manufacturing*, 10:791–803, 2017.

[121] J. M. Chacón, M. A. Caminero, E. García-Plaza, and P. J. Núñez. Additive manufacturing of PLA structures using fused deposition modelling: Effect of process parameters on mechanical properties and their optimal selection. *Materials and Design*, 124:143–157, 6 2017.

[122] Ana Pilar Valerga, Moisés Batista, Jorge Salguero, and Frank Girot. Influence of PLA filament conditions on characteristics of FDM parts. *Materials*, 11(8), 7 2018.

[123] Rafael Thiago Luiz Ferreira, Igor Cardoso Amatte, Thiago Assis Dutra, and Daniel Bürger. Experimental characterization and micrography of 3D printed PLA and PLA reinforced with short carbon fibers. *Composites Part B: Engineering*, 124(May):88–100, 2017.

[124] U.S. Bureau of labor Statistics. Occupational Employment and Wages, May 2017. https://www.bls.gov/oes/2017/may/oes519199.html (visited on 10/06/2020), 2018.

Appendix A

Appendix

A.1 Conceptual Art

In this section some conceptual art and sketches are presented to show the design process in the different types of prototypes and conceptual ideas as well.

Figure A.1 shows the different concept art related to the conceptualization phase of the design process. Figure A.2 shows the different concept art while working on the engineering design.

Figure A.3 shows the final concept art done for the look-alike prototype.

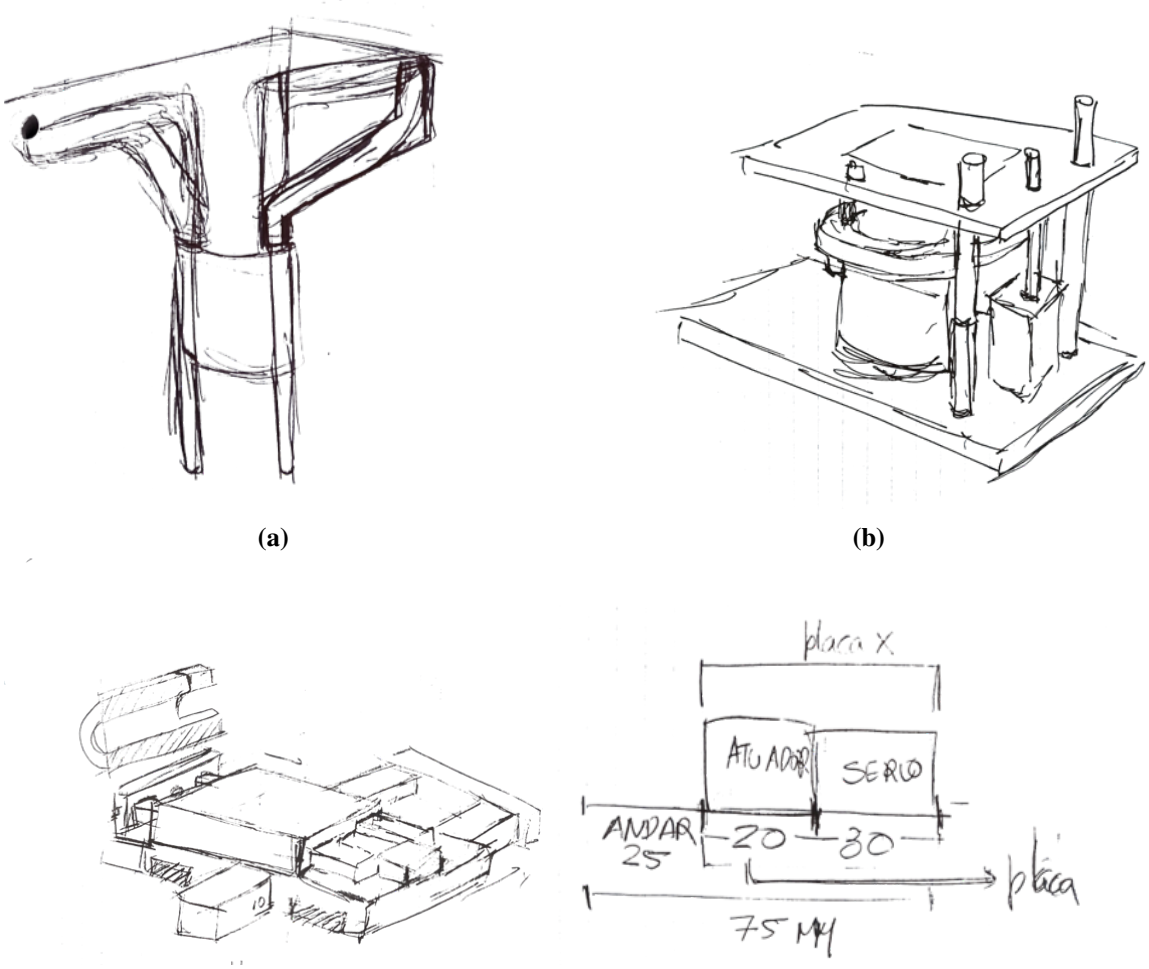

(a) **(b)**

(c) **(d)**

Figure A.1

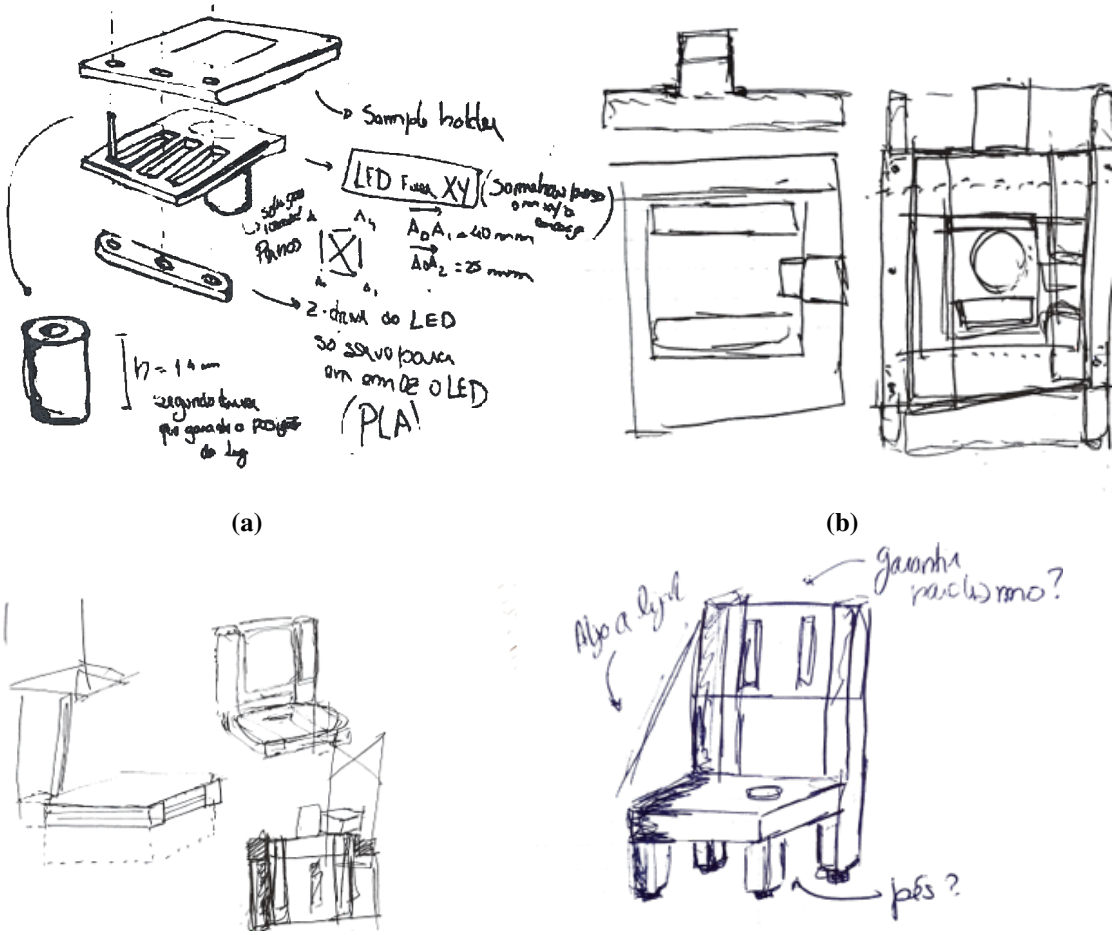

(a) **(b)**

(c) **(d)**

Figure A.2

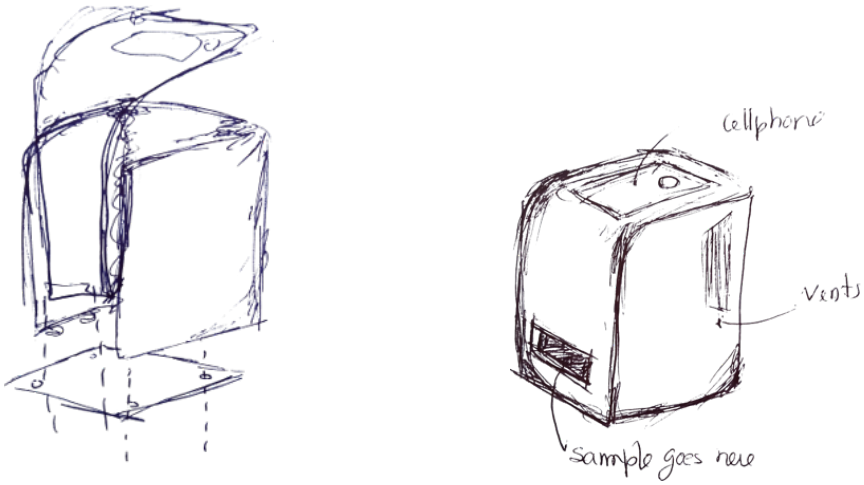

(a) **(b)**

Figure A.3

A.2 Render

This sections show the different ultra-realistic renders made in Solidworks visualize of the work-alike prototype, the look-alike prototype and the case studies. Figure A.4 shows the render of the work-alike prototype. Figure A.5 shows the render of the look alike prototype. Figure A.6 shows the render of the different case studies in their final iteration.

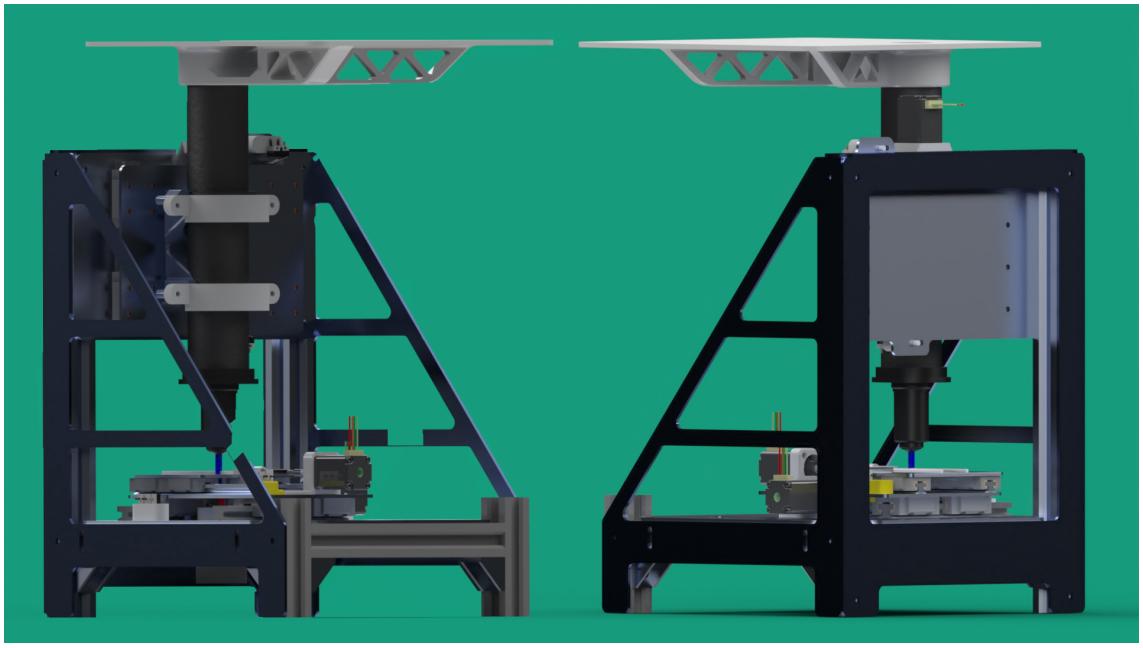

Figure A.4

Figure A.5

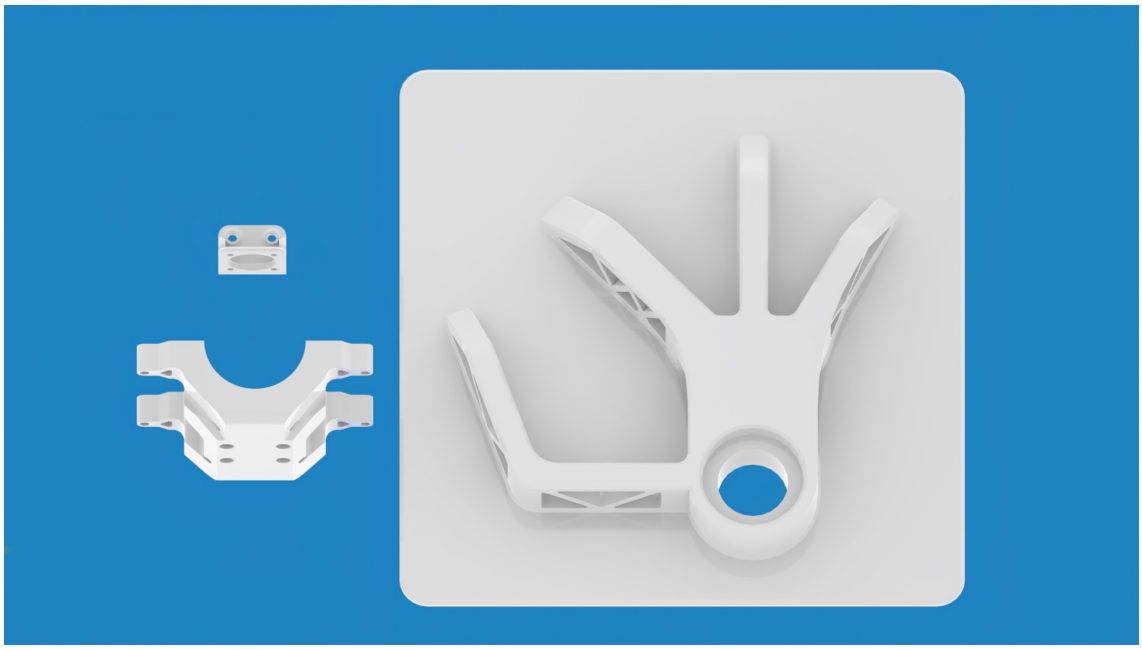

Figure A.6